Loading and Dynamic Response of Jacket Structures to Breaking and Non-breaking Waves

Von der
Fakultät Architektur, Bauingenieurwesen und Umweltwissenschaften
der Technischen Universität Carolo-Wilhelmina
zu Braunschweig

zur Erlangung des Grades eines
Doktoringenieurs (Dr.-Ing.)
genehmigte

Dissertation

von
Arash Khansari
geboren am 21.09.1986
aus Teheran, Iran

Eingereicht am: 23.05.2017
Disputation am: 16.10.2017

Berichterstatter: Prof. Dr. –Ing. Hocine Oumeraci
Prof. Dr. –Ing. Arndt Hildebrandt

2018

To my beloved family

Preface

Completing this PhD would not have been possible without the support and encouragement of many people.

I would like to express my sincere gratitude to my PhD supervisor Prof. Dr.-Ing. Hocine Oumeraci, for his continuous supports during my PhD study. I would like to thank him for his patience, motivation, and immense knowledge. His guidance helped me in all the time of research and writing of this thesis. I also greatly appreciate the effort of Professor Arndt Hildebrandt and Professor Klaus Thiele in reviewing the manuscript and providing me with valuable comments. I would like to appreciate the support of Dr. –Ing. Stefan Schimmel with providing valuable advices and writing evaluation reports for this research.

I appreciate the large wave flume GWK which made the data from WaveSlam project available. I would also like to acknowledge the scholarship provided by German Academic Exchange Service (DAAD) for pursuing my PhD in Germany. This support is gratefully acknowledged.

I would like to thank all my colleagues at LWI for their advices and collaborations at the various stages of this research and for the great moments spent together. I would especially like to acknowledge Mrs. Lara Stryjewski for her kind care and support in and outside of LWI. My special thanks goes to Ms. Gabriele Fournier for her supports during this study.

Finally, I would like to express my deepest gratitude to my parents, Qodratollah Khansari and Azam Farajollah-pour and my love, Parastoo Anbarafshan who always encouraged me and I have received their supports in different stages of my life even from miles away. I owe everything to them, without their everlasting love and support; I never would have completed this PhD.

Kurzfassung

Die Bemessung und der Bau von Gründungsstrukturen für Offshore Windkraftanlagen - insbesondere in größeren Wassertiefen stellen zwei der größten Herausforderungen im Bauingenieurwesen dar. Offshore Windparks werden zunehmend in tieferen Gewässern mit geschätzter Leistung von mehr als 5 MW der Windenergieanlagen eingesetzt, so dass gut-konzipierte Gründungskonstruktionen gebraucht werden. Obwohl sich Monopile-Gründungen im Flachwasser bewährt haben, ist die Umsetzbarkeit und Wettbewerbsfähigkeit dieser Konstruktionen in größeren Wassertiefen fraglich. Jacket-Bauwerke, welche vorwiegend in der Offshore-Öl- und Gas-Industrie eingesetzt werden, stellen eine der vielversprechendsten Alternativen für die Gründung von Windenergieanlagen in größeren Wassertiefen dar.
Unter den vielfältigen Belastungen, die auf die Jacket-Strukturen wirken, gefährden die Seeganglasten, insbesondere der Druckschlag brechender Wellen, die Standsicherheit der Konstruktion am stärksten. Daher ist eine verlässliche Abschätzung der Wellenbelastung entscheidend für die Bemessung der Jacket-Strukturen. Trotz der vitalen Bedeutung der Krafteinwirkung durch brechende Wellen liegen bisher in den Regelwerken und Normen für die Bemessung sowie in weiteren Publikationen noch keine Ansätze zur Abschätzung der Druckschlagbelastungen vor. Darüber hinaus sind die Auswirkungen solche extreme Wellenbelastungen sowie die einhergehenden Unsicherheiten im dynamischen Verhalten des gesamten Jacket-Bauwerkes, einschließlich des Verhaltens der Gründungspfähle, noch nicht vollständig erforscht.
Diese Arbeit zielt daher darauf ab, das Verständnis um die Interaktionsprozesse zwischen Wellen und Jacket-Strukturen zu verbessern und folglich Bemessungsformeln für die Belastung dieser Offshore-Bauwerke durch Wellendruckschlag zu entwickeln. Zunächst wird der Stand der Wissenschaft systematisch und kritisch analysiert, um die Interaktionsprozesse sowie die einhergehenden Wissenslücken und Modelleinschränkungen zu identifizieren. Anschließend werden die vorliegenden Daten früherer Versuchen an einer maßstäblichen Fachwerkskonstruktion im Großen Wellenkanal (GWK) in Hannover analysiert, die brechenden und nicht-brechenden Wellen ausgesetzt wurde. Hierdurch werden die relevanten Bemessungsparameter identifiziert und neue belastbare Berechungsansätze für den Druckschlag auf die Stützen und Streben einer Jacket-Struktur entwickelt. Unter Verwendung eines CFD-Modells zur Simulation der Wellen und eines CSD-Modells der Fachwerkstruktur werden die physikalischen Modellversuche im GWK numerisch nachgestellt und ein methodischer Ansatz zur Berechnung der Belastungen erarbeitet, die durch nahezu-brechende und brechende Wellen induziert werden. Dieser Ansatz, einschließlich der Formel zur Berechnung der Druckschlagbelastung, wird zur Berechnung der Gesamtbelastung einer Jacket-Struktur ohne Pfahlgründung im Naturmaßstab (OC4 Jacket) durch brechende Wellen angewandt. Das Finite Elemente (FE) Modell der OC4 Jacket wird um ein Modell der Pfahlgründung erweitert, so dass das Verhalten der gesamten Konstruktion numerisch mit dem Modell der Tragstruktur ohne Gründungselemente verglichen werden kann. Abschließend wird das dynamische Verhalten der OC4 Jacket mit Pfahlgründung unter der Belastung durch brechende Wellen systematisch analysiert und ein maßgeblich verbessertes Prozessverständnis der Interaktion zwischen Seegang und Jacket-Struktur erzielt.
Es wird nachgewiesen, dass die entwickelten Berechnungsansätze für die Druckschlagbelastung auf Jacket-Bauwerke allgemeingültig und physikalisch fundiert sind. Sie führen zu wesentlich kleineren Spitzenbelastungen bei gleichzeitig längerer Einwirkungsdauer als die Formeln, die für einzelne Pfähle entwickelt wurden. Es wird erwartet, dass die neuen Ansätze Anwendung in der Berechnung der durch brechende Wellen induzierten Wellenbelastung auf gesamte Jacket-Strukturen finden werden. Darüber hinaus werden im Rahmen der Arbeit neue Empfehlungen für den Entwurfsprozess von Jacket-Strukturen mit einem besonderen Schwerpunkt auf der Interaktion zwischen Gründungspfählen und Boden herausgearbeitet.

Abstract

The design and construction of support structures for offshore wind turbines represents one of the most challenging issues in civil engineering, especially in larger water depth. As offshore wind farms are increasingly deployed in deeper water and the rated output of wind turbine generators exceeds 5 MW, well-engineered foundation solutions are required. Despite the reported satisfactory performance of mono-pile support structures in shallower water, their feasibility and competitiveness becomes questionable in deeper water. Jacket-type structures, which have been the most commonly structures used in the offshore oil and gas industry, represent one of the most competitive alternative solutions for sub-structures in deeper water.

Among the diverse types of loads on jacket structures, wave loads, especially breaking wave loads, are the most likely to threat the stability of the structure; therefore, the correct estimation of the wave loading of an offshore jacket structure is crucial for the design of these structures. Despite the importance of the correct estimation of breaking wave induced forces on jacket structures, so far, no slamming formulae to predict these forces are available in the design standards and guidelines or in other publications. Moreover, the implications of such extreme wave load events and the associated uncertainties for the dynamic response of the entire jacket structure, including the response of the foundation piles, are still not fully clarified.

This PhD study attempts to improve the understanding of processes associated with the interaction of waves and jacket structures and to develop reliable wave slamming formulae for the prediction of breaking wave-induced loads on jacket structures. First, the present knowledge is analysed to identify the processes involved in the interaction as well as the related knowledge gaps. Second, the data available from previous tests performed on a truss structure under breaking and non-breaking waves in the Large Wave Flume (GWK tests) in Hannover are analysed to identify the most relevant influencing parameters and to provide reliable slamming formulae for breaking waves on legs and braces of jacket structures. Third, using a CFD model set-up for the waves generated in the large wave flume GWK and a CSD model for the truss structure tested in GWK, the laboratory tests are reproduced and a methodology is proposed to predict total forces induced by near-breaking and breaking waves on jacket structures. Finally, the proposed methodological approach including the slamming force formulae developed in this study is implemented to calculate total forces by breaking waves on a full-scale jacket structure (OC4 jacket). The Finite Element FE model of the OC4 jacket is extended by pile foundation model and the structural performance of the entire structure was examined by comparing the results by those of the numerical models developed for the same jacket structure. Finally, the dynamic response of the jacket structure with pile foundation to breaking waves is systematically analysed to achieve a substantially improved understanding of the processes involved in the wave-jacket-pile foundation interaction.

The analysis has resulted in several findings for breaking waves and jacket structure interaction. The new slamming formulae are proved to be generic and physically justified; they predict much lower peaks of the slamming force and much higher impact duration than those predicted by other similar formulae, initially developed for a single pile. The new slamming formulae are expected to be widely applied in calculating wave load induced by breaking waves on entire jacket structures. Moreover, new recommendations for the design of jacket structures with a particular focus on pile-soil interaction are provided.

Table of Contents

List of Figures

List of Tables

List of Notations and Symbols

A	Area on the structure which is assumed exposed to the slamming force (m^2)
A_{Si}	Shaft area of the pile in layer I (m^2)
c	Undrained shear strength for undisturbed clay soil (kPa)
C	Viscous damping coefficient
c_{str}	Damping of the structure
C_b	Breaking wave celerity
C_D	Drag coefficient
C_M	Inertia coefficient
C_S	Slamming coefficient
C_{sF}	Slamming coefficient on the front face of the truss structure
C_{sR}	Slamming coefficient on the rear face of the truss structure
c_{str}	Structural damping
d	Water depth far from the structure (m)
D	Diameter of the cylinder (m)
D_1	Leg diameter in the area of imact (m)
D_2	Bracer diameter in the area of impact (m)
D_{calc}	Total diameter of the cylinder considering marine growth (m)
E	Modulus of Elasticity $(N/m2)$
F_D	Drag force (N)
F_I	Impact force (N)
F_M	Inertia force (N)
f_{Si}	Average unit skin friction along the pile shaft in layer i $(\frac{N}{m^2})$
F_S	Slamming force (N)
F_{sF}	Slamming force on front face of jacket structure (N)
F_{sR}	Slamming force on rear face of jacket structure (N)
F_{Spr}	Force in springs connected to the pile foundation (N)
F_{Quasi}	Quasi-static component of the wave force (N)
F_{Total}	Total wave induced loads on the structure (N)
$F_{(t)}$	Line force time history (N)
g	Gravity acceleration $(\frac{m}{s^2})$
h	Water depth (m)
h	Soil depth from mudline (m)
h_{Str}	Water depth next to the structure (m)
H	Wave height (m)
H_0	Wave height in deep water (m)
H_b	Breaking wave height (m)
H_S	Significant wave height (m)
H_{Str}	Wave height at the front face of the truss structure (m)
$H(\omega)$	Transfer function
H_{Soil}	Soil depth from mudline (m)
I	Second moment of inertia of the pile cross-section (m^4)
J	Dimensionless empirical constant with values ranging from 0.25 to 0.5 for clay soil
k_{str}	Structural stiffness (N/m)
k	Surface roughness

$\boldsymbol{k}$ Turbulent kinetic energy per unit mass (J/Kg)
k_{soil} Initial modulus of subgrade reaction of soil ($\frac{kN}{m^3}$)
K_f Member effective length factor
$\vec{k}_m$ Unit direction vector of the master cylinder member axis
K_{Spr} Stiffness of springs connected to the pile foundation representing soil(N/m)
l_{br} Length of the brace (m)
l_e Effective length of the member (m)
l_1 Left bracer length in slamming area (m)
l_2 Right bracer length in slamming area (m)
l_{tot} Summation of jacket bracers and pile length in the area of impact (m)
L Wave length (m)
L_0 Wave length in deep water (m)
L_{St} Wave length next to the structure (m)
L_{us} Unsupported length of the compression member (m)
L_{Br} Braced length of the structure: the height of the jacket structure which is equipped with diagonal braces (m)
L_{UB} Unbraced length of the structure: the distance between jacket's mudmat to soil surface (m)
$L_{Impact-Area}$ Length of impact area on the instrumented legs of the GWK truss structure (m)
L_{Span} The distance between the front and the rear face of the jacket structure (m)
t_{Span} The required time for the broken wave, for traveling the distance between the front face to the rear face of the jacket structure (s)
m Mass of the structure (kg)
m_a Added mass
m_c Constant of proportionality
P Actual lateral resistance of soil (kPa)
P_u Ultimate unit bearing capacity of soil (kPa)
p^* Pressure in excess of the hydrostatic (pa)
q_T Unit end resistance ($\frac{N}{m^2}$)
Q Mobilized end bearing capacity (kN)
Q_p Total end bearing (kN)
r_0 Pile outer diameter (m)
R Radius of the member of the structure (m)
s Horizontal distance from the periphery on the wet side of the cylinder to the sloping water surface, measured in the direction of the wave propagation. (m)
$\boldsymbol{S}$ Strain rate tensor (m)
$S_f(\omega)$ Lineared spectrum of the signal
$S_F(\omega)$ Linear spectrum of the real impact load
S_L Local scour depth around each individual pile (m)
S_G Global scour depth around the entire structure (m)
S_T Total scour depth around pile (m)
$S_{wind,k}$ Characteristic wind load effect
t Time (s)
t_c Total duration of consecutive breaking wave-truss structure impacts (s)

t_{max} Maximum soil pile adhesion or unit skin friction capacity (kPa)
t_{MG} Thickness of marine growth (mm)
t_s Mobilized soil pile adhesion (kPa)
t_{Span} The required time for the broken wave, for traveling the distance between the front face to the rear face of the jacket structure (s)
T Wave period (s)
$T_{Breaking}$ Breaking wave – front face of the truss structre impact duration
T_{Broken} Broken wave – rear face of the truss structre impact duration
T_{FE} Simulation time in the FE software (s)
T_s Natural period of the structure (s)
T_{tot} Total breaking wave-truss structure impact duration (s)
u Velocity field in Cartesian coordinates$(\frac{m}{s})$
v Water particle velocity $(\frac{m}{s})$
v_f Water particle verlocity at front face of the truss structure $(\frac{m}{s})$
v_h Horizontal component of the water particle velocity $(\frac{m}{s})$
v_n Water particle velocity perpendicular to the member $(\frac{m}{s})$
v_r Water particle verlocity at rear face of the truss structure $(\frac{m}{s})$
v_{sb} Water particle verlocity at side braces of the truss structure $(\frac{m}{s})$
v_v Vertical component of the water particle velocity $(\frac{m}{s})$
V_b Broken wave celerity $(\frac{m}{s})$
x Cartesian coordinates $(= (x, y, z))$
$\dot{x}$ Horizontal wave induced velocity of water $(\frac{m}{s})$
$\ddot{x}$ Horizontal wave-induced acceleration of water $(\frac{m}{s^2})$
X Depth below soil surface (mm)
X_R Depth below soil surface to bottom of reduced resistance zone (mm)
y Actual lateral deflection of soil, (mm)
z Level measured from still water level (m)
z_p Axial pile tip deflection (mm)
z_s Depth below the sea-bed (m)
α Pitch angle of the cylinder (°)
ρ Density of water $(\frac{kg}{m^3})$
β Angle of breaker tongue with horizontal plane (°)
θ Roll angle of the member (°)
β Frequency parameter
η Water surface elevation (m)
η_b Maximum elevation of the breaking wave (m)
η_F Water surface elevation of the breaking wave at front face of truss structure (m)
η_R Water surface elevation of the breaking wave at rear face of truss structure (m)
λ Curling factor
λ_r Slenderness ratio
γ_s Effective unit weight of soil $(\frac{MN}{m^3})$

γ Angle between the direction of the motion of the mass of water and the axis normal to the cylinder (°)
γ_j Coefficient for re-scale breaking wave-jacket structure impact time
γ_D Dropping coefficient
γ_{sh} Sheltering coefficient
ω Forcing frequency on the structure (Hz)
ω_w Excitation wave frequency (Hz)
ω_n Natural frequency of the structure (Hz)
ω_d Damped frequency of the oscillation
ω_s Natural frequency of the structure (Hz)
ξ Damping coefficient
ξ_0 Iribarren index
ε_c Strain which occurs at one-half the maximum stress on laboratory undrained compression tests of undisturbed soil samples
$d\tau$ Differential time interval (s)
μ Dynamic molecular viscosity $(pa.s)$
φ' Angle of internal friction (deg)
φ_i Angle between aligned member and intersected member i (deg)
$d\tau$ Differential time interval (s)
ϑ Kinematic viscosity (m^2/s)
μ_t Dynamic eddy viscosity $(pa.s)$
$\boldsymbol{\tau}$ Specific Reynolds stress tensor (pa)
σ_T Surface tension coefficient $(\mathrm{kg/s^2})$
k_γ Surface curvature (m^{-1})
$\alpha_R(x_R)$ Relaxation function
Ψ Wake amplification factor
Ω Forcing ratio
ν Kinematic viscosity $(\frac{m^2}{s})$
ν Poisson's ratio
Δt_{CFD} Time step for data output in the CFD model (s)
Δt_{in} Time step for wave data generation using Morison Eq (input of the CSD model) (s)
Δt_{out} Time step for data output in the CSD model (s)
Δ_{Spr} Spring/Soil displacement (m)

List of Acronyms

ANSYS	Anaysis system
CFD	Computational fluid dynamics
CSD	Computational solid dynamics
DAF	Dynamic amplification factor
DFR	Dynamic force response of the structure
DOF	Degrees of freedom
FB	Fixed base model of the jacket structure
FEM	Finite element method
GWK	Großen Wellenkanal
GP	The model of the jacket's foundation considering pile group
LC	Load case
LC − B	Breaking wave load cases
LC − N	Non-breaking wave load cases
LC − W	Static (self-weight) load cases
LFEB	Linear-frame finite element beam model
LWI	Leichtweiß-Institut für Wasserbau
KC	Keulegan carpenter number
LF2	Front leg of the jacket structure in elevation 2
MBS	Multi-body system
MSL	Mean sea level
NREL	National renewable energy laboratory
OC3	Offshore Code Comparison Collaboration
OC4	Offshore Code Comparison Collaboration Continuation
PB	Bottom of the pile foundation (Pile Bottom)
PH	Head of the pile foundation (Pile Head)
PL1 − 9	Sensors placed on the pile foundation of the jacket structure
QSFR	Quasi-static force response
RNA	Rotors, nacelle & assembly
SB4	Side brace of the jacket structure in elevation 4
SP	The model of the jacket's foundation considering individual single piles
SPR	Springs connected to the pile foundation
SWL	Still water level
TFR	Total force response of the structure
TP	Transition piece
WT	Wind turbine
X4S2	Center of X-joint at the level of 2 on the front face of jacket structure

1 Introduction

1.1 Motivation

Wind farms are planned at a greater water depth with larger turbines, particularly in Germany. This new direction will require new concepts of foundation, specifically jacket or tripod foundations. Among different types of substructures, jacket structures have been the most widely used type of structures in oil and gas industries. They are also increasingly becoming competitive, especially in terms of both costs and response to environmental loads, as support structures of wind turbines, which are generally built in intermediate to large water depths.

Even when jacket structures are built in larger water depth, they are frequently subject to significant breaking and near-breaking waves. (Figure 1-1).

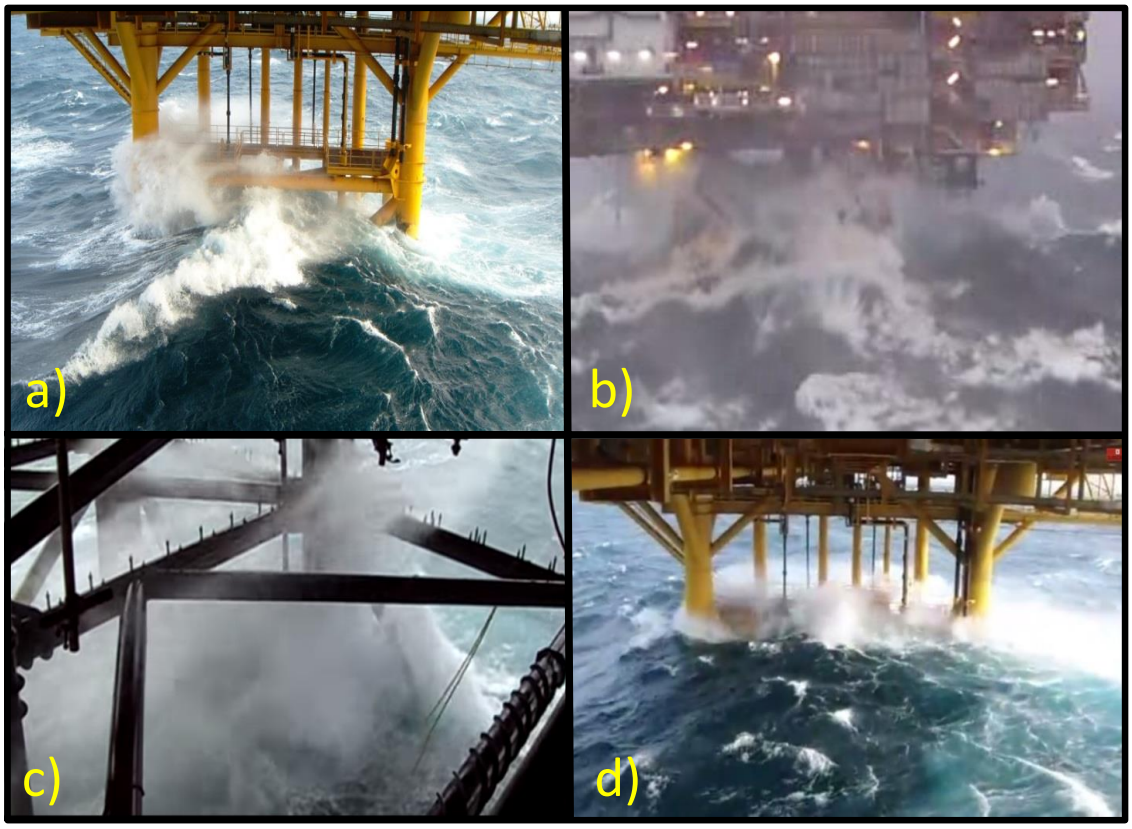

Figure 1-1. Breaking and near breaking waves on jacket structure a) near-breaking wave approaching the rear face; b) breaking wave on the front face c) breaking wave on a leg of the structure; d) near-breaking wave on the structure (snapshots from videos on https://www.youtube.com/)

The design of offshore structures in general and of jacket substructure of offshore wind turbines in particular, strongly depends on the expected extreme loads on the structure. Among the diverse types of loads on offshore structures, wave loads, especially breaking wave loads, are the most likely to threat the stability of offshore structures. Although the loads induced by

breaking waves may cause considerable damage to the structure members and endanger the overall stability of the jacket structure, the available guidelines and standards fail to provide formulae to predict the slamming forces by breaking waves on jacket structures. In fact, the slamming formulae developed conceptually for mono-pile structures are also used for the calculation of breaking wave loads on jacket structures. However, considerable uncertainties in the obtained extreme wave loads might result when applying such an approach. Moreover, the implications of such extreme wave load events and the associated uncertainties for the dynamic response of the entire jacket structure, including the response of the foundation piles, are still not fully clarified. This latter issue is even more crucial as the foundation piles of jacket structures for wind turbines are significantly shorter (i.e. with a basically different behaviour) than those commonly found in jacket structures supporting oil and gas offshore platforms for which a large experience is available.

These and further differences related to the structure itself make it difficult to readily and fully use the considerable experience, knowledge and modelling tools available from more than 4000 jacket platforms built for the oil and gas industries. Therefore, new knowledge and modelling techniques need to be generated, especially for the dynamic response to breaking wave loads. Indeed, it is crucial for both design and safety assessments to develop an improved understanding of the process involved in breaking and non-breaking waves on jacket structures and to enhance numerical approaches to predict the dynamic response of jacket structures to extreme wave loads.

1.2 Objectives

The *primary objective* of this PhD study is to improve the understanding of the processes involved in breaking and near-breaking waves and jacket structures interaction, and the associated dynamic response of jacket structures with pile foundation in sand and clay including a more precise and systematic identification of the key hydrodynamic, structural and geotechnical parameters influencing the dynamic response.

Based on this prospective knowledge, the *ultimate objectives* of the proposed research are:

i. Development of new formulae for the calculation of maximum breaking/broken wave impact loads on the braces and legs of the jacket structure as well as the total force on the entire structure. Since the formulae will be developed for a generic jacket structure subject to non-breaking, breaking and broken waves, they will be applicable for a wide range of hydrodynamic conditions and structure geometries.
ii. Computation of the dynamic response of jacket structures with pile foundation and identification of relevant parameters affecting the dynamic response of jacket structure to extreme load events induced by non-breaking to breaking waves.

1.3 Methodology

The methodology of the entire PhD thesis is summarized in Figure 1-2. This methodology will be specified precisely in Section 2.5 based on the results of the analysis of the current knowledge.

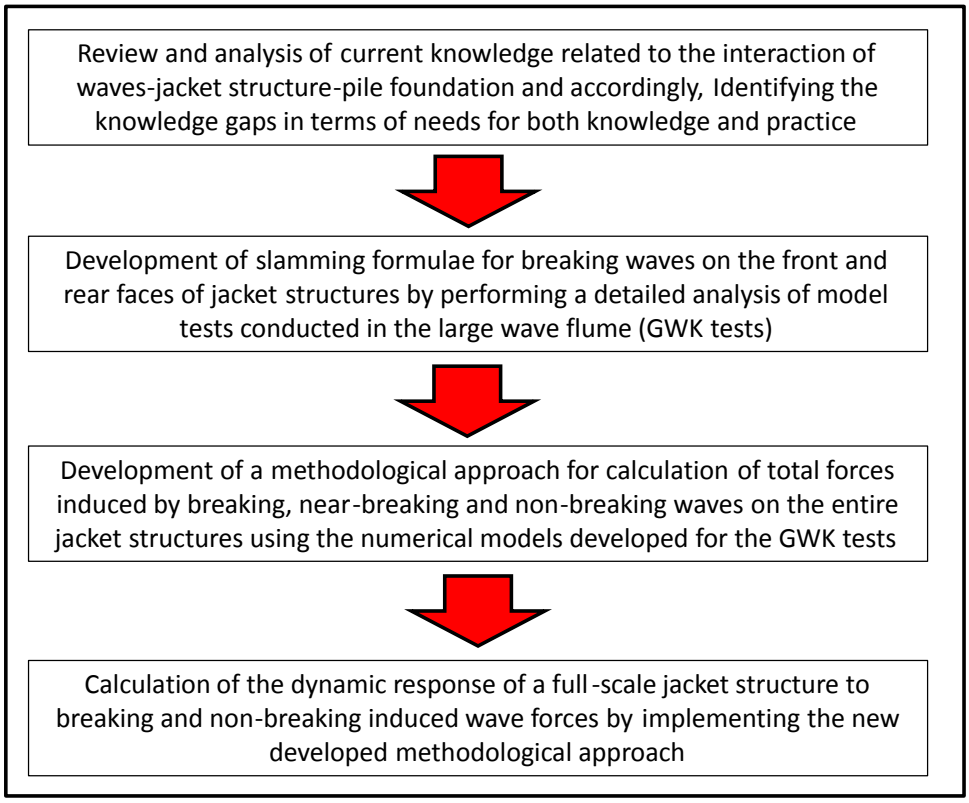

Figure 1-2. Tentative methodology of the PhD study

First, a comprehensive review and analysis of the current knowledge and models is performed. A particular emphasis will be put on the investigation of the process involved in waves-jacket structure-pile foundation interactions and the identification of the existing gaps in knowledge and practice (Chapter 2).

Second, new prediction formulae for the slamming force and its duration on the front and rear legs and braces of the jacket structure are proposed based on the large scale experiments performed in Hannover (Chapter 3).

Third, the total non-breaking, near-breaking and breaking wave forces on the truss structure and the corresponding total force responses are calculated using the CFD and CSD models set-up for the large scale experiments performed in Hannover (Chapter 4).

Finally, CFD and CSD models are set-up for a full-scale jacket structure, the so called 'OC4 jacket' with and without pile foundation. Breaking and non-breaking wave forces are simulated on the structure according to the methodological approach proposed in 2nd and 3rd phases of the PhD study. A systematic parameter and comparative studies are performed using the vali-

dated numerical model in order to identify most relevant parameters and modelling techniques affecting the dynamic response (Chapter 5).

The key results, achievements, limitations and recommendations for further studies are drawn in Chapter 6 of the present thesis.

2 Review and analysis of current knowledge

In this chapter, a comprehensive review and analysis of the current knowledge in academia and practice is performed. This includes analytical, numerical and physical modelling of the dynamic response of jacket structures to breaking and non-breaking waves, with a particular focus on impact loads and pile-soil interaction. The knowledge gaps related to the processes and parameters involved in the loading and the dynamic response of jacket structures are identified.

The position of the problem with respect to the current applications of jacket structures in the industry and the system approach is discussed in section 2.1. The previous analytical, experimental and numerical studies for the prediction of breaking wave loads on single pile structures are reviewed in section 2.2. The available pile foundation modelling approaches with different levels of complexity applied for fixed-bottom offshore structures are examined in section 2.3. Based on the results of the review of these studies, the most relevant parameters affecting the dynamic response of jacket structures as well as the knowledge gaps and model weaknesses are identified, so that the objectives and methodology of the PhD thesis are finally specified in section 2.5.

2.1 Position of the problem

2.1.1 Current development of fixed-bottom offshore structures

Offshore wind turbines have been installed in increasingly larger water depths using different concept of fixed-bottom structures over the last years. Among different types of fixed-bottom structures, mono-pile and gravity based foundations are successfully used for lower water depths in many wind energy projects in Europe (see Figure 2-2). However, the trend toward larger water depth has reached a level which makes the application of mono-pile and gravity structures impractical. Therefore, besides floating structures, new concept of fixed-bottom support structures such as tripod and jacket substructures are replacing the conventional mono-pile and gravity based structures.

A comparative analysis of the dynamic response of different fixed-bottom offshore structures under non-breaking waves was performed by Føreland et al. (2012) in order to identify the most appropriate solution for larger water depths. Finite element models (FEM) were set-up for different types of fixed-bottom offshore structures such as mono-pile, gravity, jacket and tri-piles for 2.5MW, 5MW and 10 MW wind turbines subject to non-breaking waves in the North Sea. Fabrication cost, dynamic response and water depth were analysed in order to identify the most promising solution for water depths ranged between 20 to 60m (see Figure 2-1). Results showed that, conventional mono-pile structures can be used efficiently in lower water depth (<30m). However, the application of mono-pile and tri-pile structures for higher water depths (40-60m) is hardly feasible due to their inappropriate dynamic response and excessive costs. Furthermore, as the installation and transportation of gravity based foun-

dation in larger water depths is very complex and highly dependent on the geotechnical properties of the site, they become impractical in intermediate depths to deep water. In fact, jacket structures are identified the best solution among the considered fixed-bottom structures in terms of both cost and dynamic response for supporting wind turbines in larger water depth (Figure 2-1)

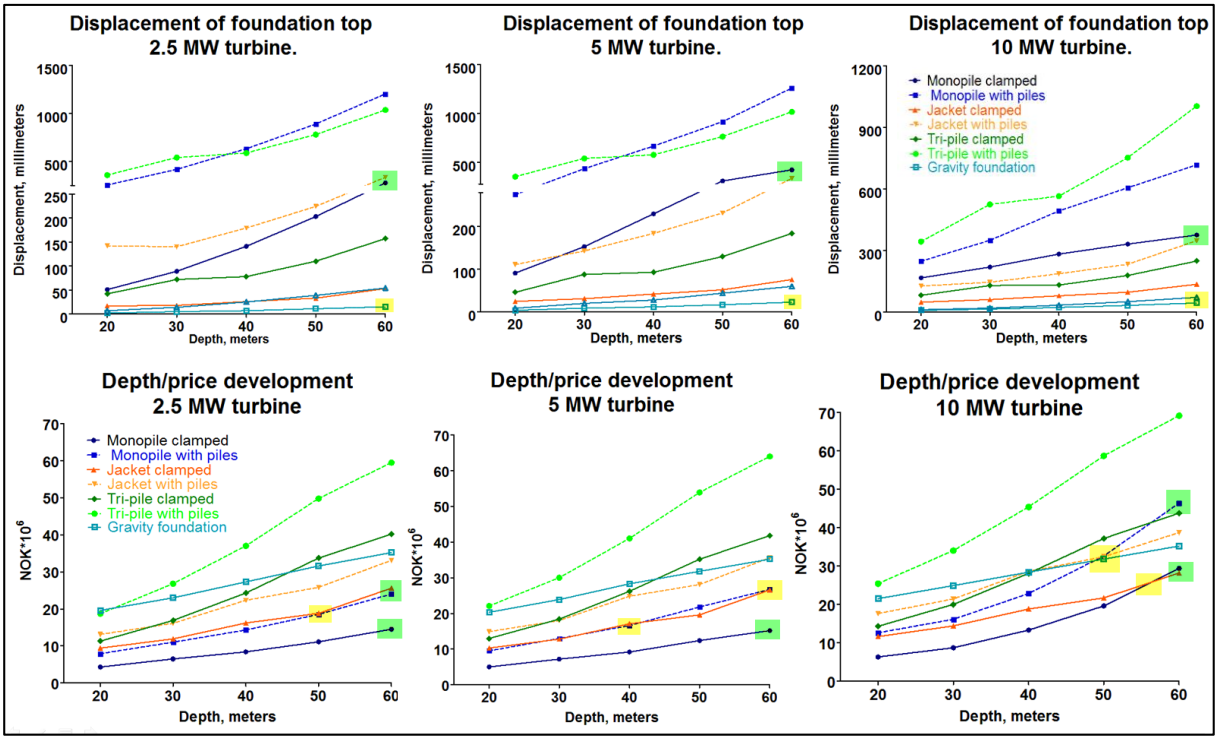

Figure 2-1. Dynamic response and cost analysis of fixed-bottom offshore structures located in different water depth (Føreland et al., 2012)

According to steel structure companies that are also manufacturer in the offshore oil and gas industry, the demand for jacket foundation for offshore wind turbine will increase, but the competition will also increase due to new companies entering the market and re-directing their activities toward substructures for wind turbines. For instance, several wind turbine manufacturer (e.g. DONG Energy, Ramboll IMS., Norse Energy, BiFab), which activities were previously focused on offshore oil and gas industry, have recently improved their equipment and human resources to manufacture jacket substructures for wind turbines. Further, a Scottish company called BiFab planned to offer complete EPC solutions for up to 150 jackets annually, over four years starting from 2012 (Higgins and Foley, 2012).

Basically, four major phases are required to build offshore wind farms: feasibility phase, development phase, installation phase and operation phase (Wiersma et al, 2011). The developed offshore wind farms in the recent years possess different types of substructures which have been selected and designed according to environmental loads and soil properties of the intended site. The information for the selected offshore wind farms in Europe including the duration of the aforementioned phases is summarized in Figure 2-2. These projects were chosen because they incorporate a wide range of conditions in six different countries which are all

commissioned, some being pilot projects of a few wind turbines and some among the largest offshore wind farm built to-date. For these wind farm projects, the distance to the shoreline ranges from 2.5 to 45 km in water depths varying from 0 to 45 m. As shown in Figure 2-2, the interest of offshore companies to develop wind farms in larger water depths and consequently, the application of jacket structures in such water depths is growing constantly, from 1997 to the present.

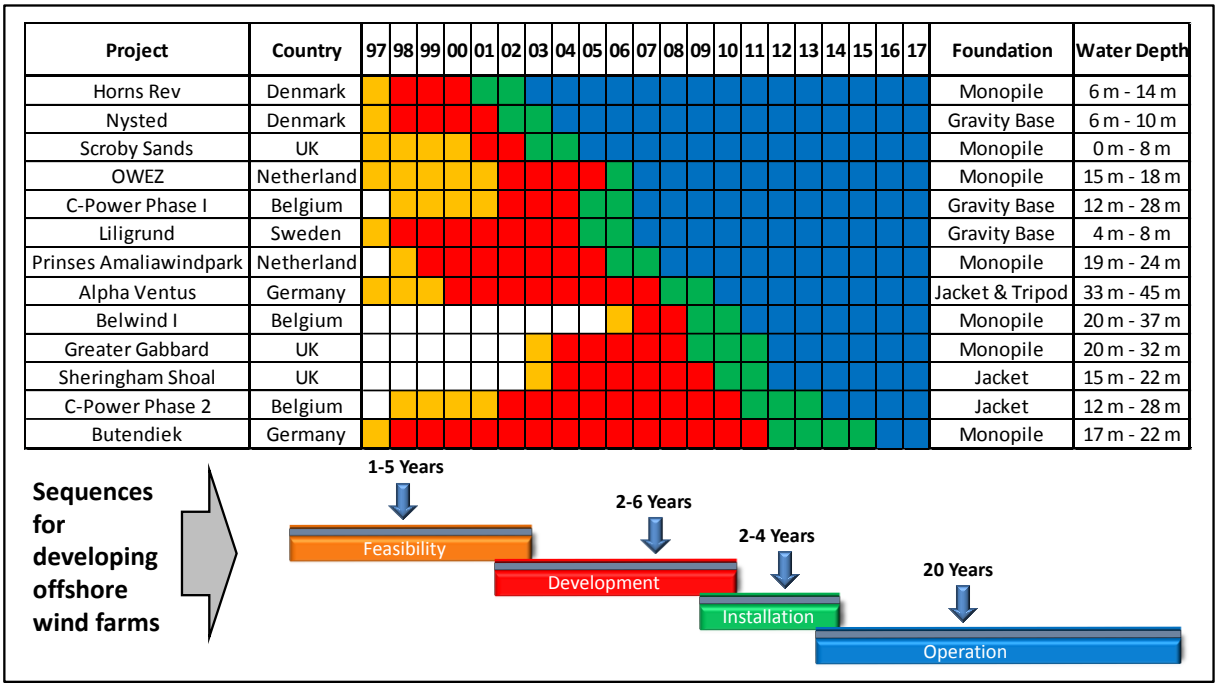

Figure 2-2. The progress sequences of several wind farm projects in Europe

The transportation of jacket structures from fabrication site to the operating site is very challenging. In general, the transportation may take several weeks. During the transportation, while the jacket structure is on top of a barge a damaged may be occurred due to a severe storm. Therefore, both the naval and structural behaviour should be analysed in order to avoid any unexpected problem.

Jacket structures supporting offshore platforms have been widely applied in oil and gas industry and as a result an extensive experience including the wave loading of the jacket structure and the dynamic response of the structure with pile foundation is already gained for the design process of jacket structures. However, there are several uncertainties for the application of the available experience for jacket wind turbines. The uncertainties come from the following issues:

(i) The pile foundation of offshore wind turbines is relatively shorter than those foundations for jacket platforms.
(ii) The geometry of jacket wind turbines is moderately different with jacket platforms (e.g. diameter of members, number of legs, type of braces)

(iii) The structural behaviour of jacket wind turbines is much more flexible than jacket platforms. This is due to the long tower on the top side, wind turbine on the tower and the lower stiffness of the jacket structure.

These and further differences related to the structure itself make it difficult to readily and fully use the considerable experience, knowledge and modelling tools available from more than 4000 Jackets built for the oil and gas industries. Therefore, new knowledge and modelling tools need to be generated, especially for the dynamic response to breaking wave loads which applies the largest environmental force on the structure.

2.1.2 Modelling techniques for the analysis and design of jacket structures

As the demand for the application of jacket structure in offshore wind industry is rapidly increasing, it is crucial to investigate the currently applied methods and techniques in the design practice of these structures. For this purpose, it is attempt in this section to review and analyse:

(i) the extended reports by several oil and gas companies for the design and analysis of a few jacket platforms located in Persian Gulf and Cyprus fields (e.g. NIOC, 2009; NIOC, 2011);
(ii) the international guidelines and standards (IEC 61400-3, 2009; DNV, 2010; DNV, 2013; ISO 21650, 2007; ABS, 2010; ABS, 2011; API RP 2A-WSD, 2007; ISO 19902, 2007; GL, 2005) and
(iii) the capabilities of the available tools which are currently applied for the analysis of jacket sub-structure of wind turbines (e.g. Bladed, FastCode).

Jacket structures should withstand various external loads during their lifetime and, as summarised for instance in Table 2-1, several types of analyses are generally required to ensure a reliable and safe design over life time (Sadeghi 2001).

Table 2-1. The main analyses performed commonly in practice to design jacket structures

Type of analysis	***Description***
In-place analysis	In-place analysis is conducted to evaluate the behaviour of jacket structures to the most extreme environmental loads induced by waves, winds, current and etc. during their service life time. This analysis is required to check the global integrity of the structure against premature failure. In a linear structural analysis with respect to ultimate limit state design (ULS), the characteristic capacity is normally taken as first yield or first component buckling. If tubular members of a jacket do not satisfy the ultimate strength requirements, resulting in yielding or buckling, it is assumed that the tubular member is not fit for the purpose. (Faseela and Jayalekshmi, 2015)
Earthquake analysis	Earthquake or seismic analysis is a subset of structural analysis which involves the calculation of the response of jacket structures subject to earthquake and is carried out to evaluate the performance of the struc-

	ture under earthquake excitation
Fatigue analysis	Fatigue analysis is performed to evaluate the long-term performance of jacket structures to cyclic loads. Fatigue is characterised by weakening of a material caused by repeatedly applied loads and it is characterised by the progressive and localized damage that happens commonly in connections of jacket structures
Impact analysis (vessel, ice, equipment and etc.)	Impact analysis is performed to predict the dynamic response of jacket structures to impact loads induced by ice, vessels and dropping of equipment on the structural members.
Load out analysis	Load out analysis is performed to evaluate the process of moving a jacket structure from a set of skid ways on the land to a cargo barge
Transportation analysis	This analysis is conducted to achieve a safer and more efficient transportation of jacket structures to the intended site.
Appurtenance analysis	This analysis is done to design the appurtenances of jacket structures such as anodes, fenders and etc.
Lift/Launch and upending analysis	In this analysis, the process of lifting and launching of jacket structures for the installation phase will be evaluated
Pile and conductor pipe drivability analysis	In this analysis, the static bearing capacity of the pile during pile driving is calculated. The maximum stress in the pile is computed and the efficiency of the driving system will be determined
Cathodic protection analysis	Using this analysis, the cathodic elements which protect the members of the jacket structure from corrosion and therefore, extend the operating life of the members are designed.

The aforementioned analyses are crucial to achieve a safe and reliable design of jacket structures. Among these analyses, the in-place analysis is the most challenging one because in this analysis:

(i) Several complex physical processes and interactions such as pile-soil and wave-structure interactions should be considered;

(ii) The extreme load events caused by different environmental loads (e.g. wind, wave, current, ice) on the structure should be properly modelled and predicted by accurate approaches;

(iii) The dynamic response of jacket structures with pile foundation should also be considered for extreme loads.

Therefore, the main focus of this section is to identify the current approaches applied in practice for performing in-place analysis. For this purpose, a comprehensive review and analysis of the current techniques and models used for the prediction of the dynamic response of jacket structures to breaking and non-breaking waves is performed with a particular focus on pile-soil interaction. This has been conducted through the review of several reports prepared by companies responsible for the design and analysis of jacket structures located in Persian Gulf and Cyprus. Moreover, several standard and guidelines are reviewed to find out the most common techniques which are being used by offshore companies to model jacket structures and the results are briefly summarised in Table 2-2.

Table 2-2. Current approaches applied by offshore companies for load assessment and analysis of jacket structures

Type of problem and analysis	***Method applied in practice***
Non-breaking wave loads	For non-breaking wave loads on jacket structures, the Morison's equation is commonly applied using the flow velocity and acceleration recognised considering the water depth, wave height and wave period in the site. The effect of the wave phase-lag on the different members of the structure is usually ignored by the tools used in practice, meaning that the incident wave on legs and braces of the structure is applied with the same phase. Moreover, instead of assigning different values of drag and inertia coefficients to members of the structure (considering the relevant KC numbers), average values of drag and inertia coefficients are used.
Breaking wave loads	There are several prediction formulae for the calculation of slamming force and duration by breaking waves on single piles (see Table 2-6), but no formulae are available for the prediction of breaking wave impact forces on truss-type structures. Currently, the slamming models conceptually developed for mono-pile structures are adopted for jacket structures to calculate breaking waves induced impact forces and their associated duration on jacket structure. (IEC 61400-3, 2009; DNV, 2010; DNV, 2013; ISO 21650, 2007; ABS, 2011; API RP 2A-WSD, 2007; ISO 19902, 2007)
Water level and currents	Two water levels with the return period of 50 years are considered to predict the wave loads on the structure: (i) the highest water level implying higher hydrostatic loads and current loads on the structure and (ii) the lowest water level which might lead to higher hydrodynamic loads on the structure. Three types of currents are considered for the calculation of total hydrodynamic loads: (i) Tidal currents (associated with astronomical tides), (ii) circulational currents (associated with oceanic-scale circulation patterns), and (iii) wind-generated currents. Loads induced by currents on a structure are generally considered by replacing the total water particle velocity (obtained from the superposition of the current velocity and the wave velocity) in the drag term of the Morison formula.
Wave direction	The design procedure is performed by varying the direction of wave incidence. Detail design analysis is usually performed based on minimum eight wave approach directions (0º, 50°, 90º, 130°, 180º, 230º, 270º, 310º).
Wind loads	Wind loads are generally calculated using blade element momentum theory (BEM) for return periods of 1-year and 100-years. Wind load is applied on area above still water level and orthogonal to the wind direction
Marine growth	The marine growth effects are usually considered by: (i) increasing the outer diameter of the member; (ii) considering an additional non-structural mass which reduces the natural frequency of the structure; (iii) increasing the surface roughness of the members and consequently, applying modified drag and inertia coefficients. The thickness of the marine growth depends on the type and location of the sea site as well as on the depth below still water level; recommendations are provided in several guidelines (e.g. DNV, 2013)
Foundation and soil modelling	Although modelling the pile foundation of jacket structures might strongly change the natural frequency of the structure, it is ignored in several industry and research projects. The most promising approach provided so far, is the non-linear load-deflection (p-y)

	approach with a proper linearization which is recommended in most of guidelines such as API (2005), GL (2005) and DNV (2013). However, even the application of this method for fixed-bottom offshore structures is still questionable (Lombardi et al, 2013). The pile foundation of numerous jacket structures installed in Persian Gulf and Gulf of Mexico are designed by implementing the very simplified models for the pile foundation modelling such as apparent fixity length model. As will be explained in section 2.3, the application of apparent fixity length approach might miscalculate the first and second natural frequency of the structure and therefore, should be avoided for jacket substructure of wind turbines.
Type of analysis for jacket substructure of oil and gas platforms	Linear dynamic analysis using a set-up Finite Element model is commonly used to compute the time-dependent global and local responses of jacket structures The analysis is normally based on modal superposition, as this type of analysis is much less time consuming than a full time dependent analysis. The magnitude of the inertial action which is established by a global dynamic analysis, can be a direct result of the global dynamic analysis, or can be derived from the quasi-static analysis and considering the Dynamic Amplification Factor (DAF) from the global dynamic analysis (as conducted for SP17 and SPD22 jackets in Persian Gulf).
Type of analysis for jacket substructure of wind turbines	There are two approaches for the analysis of jacket support structure of wind turbines (DNV, 2013): a) *Linear combinations of wind load and wave load effects*: In this approach the combined load effect in the structure due to concurrent wind and wave loads may be calculated by combining the separately calculated wind load effect and the separately calculated wave load effect by linear superposition. b) *Combination of wind load and wave load by simulation in the time domain:* In this approach, the combined load effect on the structure due to concurrent wind and wave loads may alternatively be calculated by direct simulation. This approach is based on structural analysis in the time domain for simultaneously applied (simulated) time series of the wind load and the wave load. By this approach, (simulated) time series of the combined load effect results, from which the characteristic combined load effect is interpreted. The dynamic analysis using this approach is also called "*coupled aero-servo-hydro-elastic"* method.

As described in Table 2-2, for jacket sub-structure of wind turbines subject to combined wave and wind loads, a type of analysis called *'coupled aero-servo-hydro-elastic'* is commonly performed to calculate the dynamic response of the system. Aero-servo-hydro-elastic load simulations mean that:

(i) The wind induced loads on the blades and tower are computed considering the flexible behaviour of the structural component (aero),

(ii) The hydrodynamics loads induced by waves and currents on the jacket structure considering that the flexibility and motion of the structure and its members do not affect the loads (hydro),

(iii) The control system is modelled (servo) and

(iv) The structure is modelled as flexible using structural dynamic models such as finite element or multi-body formulation models (elastic). During these simulations, the focus does not lie on a particular part of the turbine, but on determining the global loads and consequently, the global response of the entire system (Nygaard

et al, 2016). Table 2-3 provides a list of available aero-servo-hydro-elastic tools and briefly summarizes the hydrodynamic model used by each tool for the calculation of non-breaking wave loads on jacket structures.

Table 2-3. List of available tools for the aero-servo-hydro-elastic analysis of jacket structure of wind turbines and hydrodynamic models for the calculation of non-breaking wave forces on jacket structures

Code	***Applied Wave Theory***	***Hydrodynamic Model***
3DFloat	Linear wave theory (Airy), user defined subroutine, stream function theory	Morison Eq
ADAMS + AeroDyn	Airy, user defined subroutine, stream function theory	Morison Eq
ADCoS-Offshore	Airy, user defined subroutine, stream function theory	Morison Eq
ASHES	Airy	Morison Eq
Bladed V3.8X	Airy, user defined subroutine, stream function theory	Morison Eq
Bladed V4 Multibody	Airy, user defined subroutine, stream function	Morison Eq
FAST-ANSYS	Airy, user defined	Morison Eq
FEDEM WindPower	Airy, stream function theory	Morison Eq
Flex-ASAS	Airy, user defined subroutine	Morison Eq
GAST	Airy + potential flow or stream function theory	Morison Eq
HAWC2	Airy, user defined subroutine, stream function theory	Morison Eq
OneWind	Airy, user defined subroutine	Morison Eq
USFOS-vpOne	Airy, Stokes 5th, stream function theory	Morison Eq

As shown in Table 2-3, all of the aero-servo-hydro-elastic tools apply the Morison equation where velocity and acceleration are calculated by wave theories. For small waves in deep waters, the simplest linear wave theory (Airy) is of sufficient accuracy. However, as wave heights increases relative to the water depth (H/h) and wave length (H/L), this is not more the case, so that non-linear wave theories of increasing order would be required to model the wave kinematics and the induced flow with sufficient accuracy. As it comes to near-breaking waves, application of wave theories may underestimate the wave kinematics and this might be even more critical when breaking waves are considered. Although extreme loads on a jacket

structure might be induced by breaking waves, no theoretical or empirical model is proposed to predict the wave kinematics of breaking waves. Moreover, the location of the incipient wave breaking location and the process of wave transition from breaking to broken is not yet identified. For this purpose, CFD models which are computationally expensive and complicated to use can be applied. According to the author's knowledge, the CFD models have not yet been used for any industry project to simulate flow fields of near-breaking, breaking and broken waves.

The position of the problem is identified based on the detailed analysis of the annual reports published by offshore wind energy organisations, the reports prepared by offshore companies for the design and analysis of jacket structures, the current design guidelines and standards and the design tools available for the analysis of fixed-bottom support structures of offshore wind turbines. The results showed that the available models and techniques for the prediction of the dynamic response of jacket structures subject to extreme loads induced by breaking and near-breaking waves are inadequate. The most important uncertainties in the design practice arise from:

(i) The lack of reliable formulae for the prediction of breaking/broken wave-induced forces on the different members of jacket structures, and more importantly the lack of a methodological approach for the calculation of the total wave force on an entire jacket structure.

(ii) Insufficient understanding of the pile-soil interaction, including a precise identification of the most relevant parameters for the effect of pile foundation on the global dynamic response of jacket structures.

In this study, an attempt will therefore be made to improve the understanding of the processes associated with near-breaking and breaking wave loads on jacket structures, including a more precise and systematic identification of the most relevant hydrodynamic and geotechnical parameters as well as their relative importance for the total wave-induced forces and the associated dynamic response of jackets applied as support structures for offshore wind turbines. Based on this improved understanding, the current approaches for the prediction of the aforementioned wave loads will be enhanced, including the models for pile foundation and the identification of the parameters affecting the dynamic response of jacket structures.

2.2 Wave loads on jacket structures

2.2.1 Analytical studies on non-breaking wave on jacket structures

Jacket structures are subject to diverse environmental loads during their life time. Sea waves, as the most environmental important loads, can be non-breaking, near-breaking, breaking, broken and post-breaking. These waves can be described by deterministic and stochastic approaches. Currently, deterministic approaches are preferred to describe extreme wave events of a given return period. However, in some cases (e.g. fatigue analysis), stochastic wave approaches should be applied.

There are several approaches for the calculation of wave loads on fixed-bottom offshore structures. Table 2-4 compares the current approaches for the calculation of wave loads on offshore structures. In general, the Morison formula and CFD models may be applied for the prediction of non-breaking wave induced forces on multi-member offshore structures. Among these methods, the Morison equation is the most applied approach because of its simplicity and accuracy for non-breaking waves. Moreover, using the Morison equation, it is possible to consider water added mass effects due to the relative motion of the structure. However, the application of the Morison equation for non-slender structures such as gravity based structures may yield unreliable results as it cannot consider the effect of the structure on the wave field. Both Froude-Krylov-based approaches and CFD methods can also be used to predict hydrodynamic loads on offshore structures. However, so far, they have been in minor relevance for jacket structures as their application is very complex and computationally demanding.

Table 2-4. Current approaches for the calculation of wave loads on offshore structures and their applicability for jacket structures

		Morison formula	***Diffraction theory***	***Froude-Krylov approximation***	***CFD modelling***
Time/Frequency Domain		TD & FD	FD	TD	TD
Type of loading		Force	Pressure	Pressure	Pressure
Wave type		NoBr	NoBr	NoBr	NoBr, NeBr, Br
Structure type	***Non-slender***	No	Yes	Yes	Yes
	Slender	Yes	No	No	Yes
Applicability to jacket structures		Good	Mediocre	Good	Very Good
Computational efficiency		Good	Mediocre	Mediocre	low

TD= Time domain; FD= Frequency domain; NoBr =Non-breaking waves; NeBr =Near-breaking waves; Br =Breaking waves; N.A= Not applicable

Several studies have been recently performed on the calculation of wave loads on multi-member structures and the associated dynamic response of the structure (see Table 2-5) in which, different hydrodynamic models are implemented for the computation of wave induced loads on the structure. A tentative list of the selected recent studies including the research focus and the implemented methods for the calculation of wave loads on the structures is given in Table 2-5. As can be seen, most of the recent studies have applied Morison formula to model hydrodynamic loads on jacket structures. In some studies, CFD methods are used to validate the hydrodynamic results with Morison equation such as Robertson et al. (2013) which have used a CFD model to verify the results of the HydroDyn module in the FAST code. Overall, from the reviewed recent studies in this section, which are partly summarised in Table 2-5, it can be inferred that CFD models are particularly suitable for studies, which are mainly focused on hydrodynamics of multi-member support structures and when the dynamic response of the structure is of minor importance. This is for instance the cases for studies such

as those performed by Fuchs et al. (2012) and Hildebrandt (2012) that solely focused on the wave load of mono-pile and tripod structures, respectively, without consideration of the dynamic response. In general, when the focus is laid on the dynamic response of a full-scale jacket structure, the application of CFD models for the prediction of wave loads is currently hardly feasible in the design practice due to the excessive computational time and efforts required.

Table 2-5. Hydrodynamic models implemented in recent studies for the calculation of wave loads on jacket substructure of wind turbines

Authors	***Hydrodynamic model***	***Focus of the research study***
Jose and Choi (2017)	CFD model (RANS-VOF)	Wave loads induced by breaking waves on jacket structures
Barahona et al. (2015)	Morison Eq & CFD model (RANS-VOF)	Hydrodynamic of jacket substructures in FAST code
Shi et al (2015)	Morison Eq.	Pile foundation modelling of jacket structures
Shi et al (2013)	Morison Eq.	Parameter study for the dynamic response of a jacket substructure to non-breaking waves
Leschka et al (2014)	CFD model (RANS-VOF)	Wave-induced forces on a slender pile within a group of piles
Haselbach et al (2013)	Morison Eq.	Coupled and uncoupled analysis of jacket substructure
Jonkman et al (2012)	Morison Eq	Dynamic response of jacket structures to non-breaking waves: Comparison of the results of different codes
Fuchs et al. (2012)	CFD (RANS-VOF)	Impact loads induced by breaking waves on mono-pile structures
Hilderbrandt (2012)	CFD (RANS-VOF)	Impact loads induced by breaking waves on tripod structures
Larsen & Kim (2011)	Morison Eq.	Dynamic response of jacket structures considering the effect of wave non-linearity
van Gerven (2011)	Morison Eq.	Design and optimization of the jacket substructures
Fevåg (2011)	Morison Eq.	Influence of Marine Growth on the dynamic response of lattice substructures
Moll et al (2010)	Morison Eq.	Effect of added mass on the dynamic response of jacket structures
Peng Li (2010)	Morison Eq.	Analysis and design of jacket substructures of wind turbines
Henderson & Zaiijer (2008)	Morison Eq. & Froude-Kylov	Hydrodynamic loading of fixed-bottom offshore substructure of wind turbines

In fact, the quasi-static force including both drag and inertia components on the legs and braces of jacket structures, is commonly calculated by the well-known Morison equation (Morison et al., 1950). Wave forces on slender structural members submerged in water can be predicted by the Morison equation which is applied by almost all design tools used in the industry to calculate wave loads on jacket structures (see Table 2-3). The wave force on a small section of cylinder as shown in Figure 2-3 can be calculated by the Morison equation as follows

$$dF = dF_D + dF_M = \frac{1}{2}\rho_w C_D D|u|udz + \rho_w C_M \frac{\pi D^2}{4}\frac{\partial u}{\partial t}dz \qquad (2\text{-}1)$$

where F_D is drag force, F_M is inertia force, C_D is drag coefficient, C_M is inertia coefficient, D is pile diameter and u is horizontal wave-induced flow velocity.

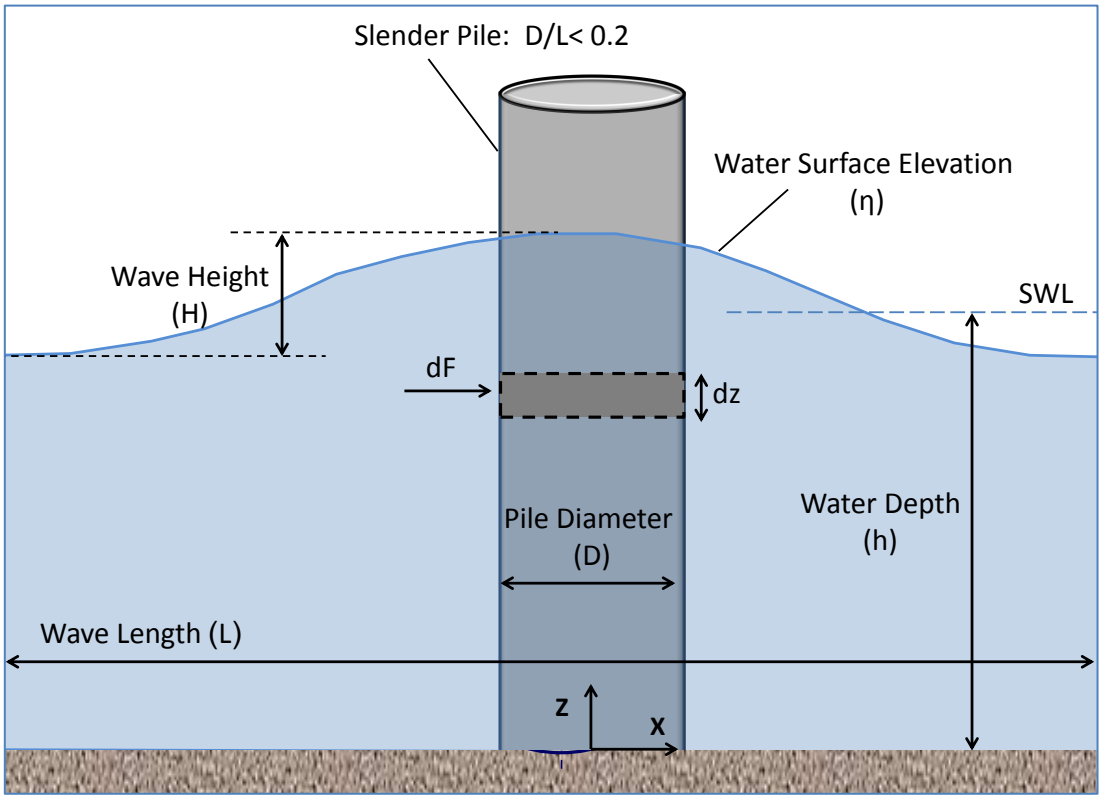

Figure 2-3: Definition sketch for wave forces on slender cylinder (Modified from Bonakdar, 2014)

By integrating Eq. 2-1 over the entire column at the cylinder, the total in-line force F on the cylinder may be obtained as follows (see Figure 2-3):

$$F = F_D + F_M = \int_{-h}^{\eta} \frac{1}{2}\rho_w C_D D|u|udz + \int_{-h}^{\eta} \rho_w C_M \frac{\pi D^2}{4}\frac{\partial u}{\partial t}dz \qquad (2\text{-}2)$$

where h is water depth and η is water surface elevation. Drag C_D and inertia C_M coefficients are experimentally determined over a range of the governing parameters (e.g. KC number $KC=u_{max}T/D$ or Reynolds number $Re=u_{max}D/\nu$). For a fixed pile in a fluid, the characteristic

length-scale is the diameter of the pile and the characteristic velocity is that of the fluid some distance away from the pile (undisturbed flow velocity).

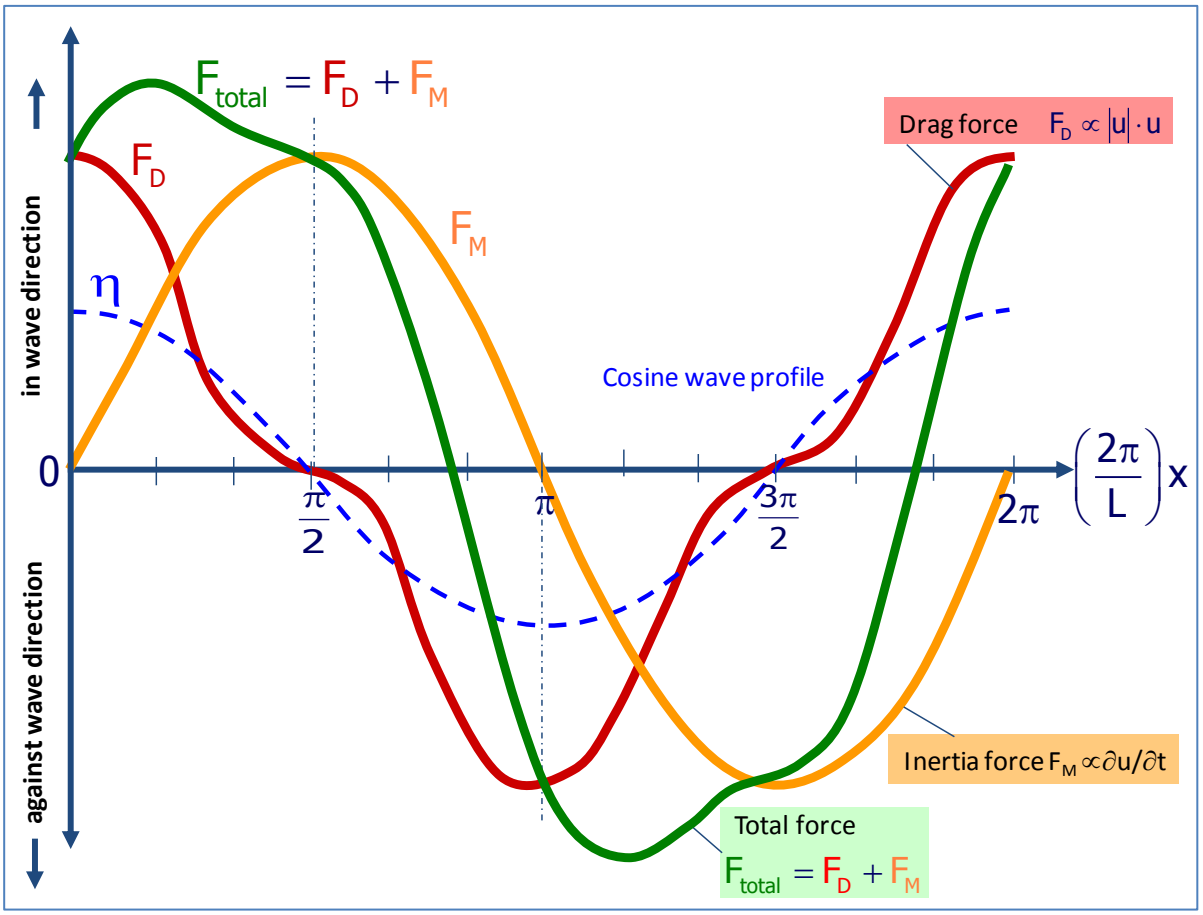

Figure 2-3: Graphical description of drag and inertia forces induced by a cosine wave (Oumeraci, 2008)

2.2.2 Analytical studies on breaking waves on jacket structures

Breaking waves on offshore structures may apply a significant force that might result in an impact load which is rather localised in space and of much shorter duration than those generated by non-breaking waves. Several studies have revealed that the Morison Equation underestimates the loads induced by near-breaking and breaking waves on slender cylindrical structures (e.g. Goda, 1966; Armand-Cointe, 1986; Wienke & Oumeraci, 2005; Irschik et al, 2004). The total breaking wave force on a slender pile, as illustrated by Fig. 2.5 and described by Eq. 2-3, is a summation of

(i) a quasi-static force consisting of a drag component (F_D) and an inertia component (F_M), commonly calculated by the well-known Morison formula (Eq 2.2), and

(ii) a slamming force (F_S) with a much shorter duration than that of the quasi-static force ($t_d << t_{Total}$)

$$F_{Total} = F_D + F_M + F_S \qquad (2\text{-}3)$$

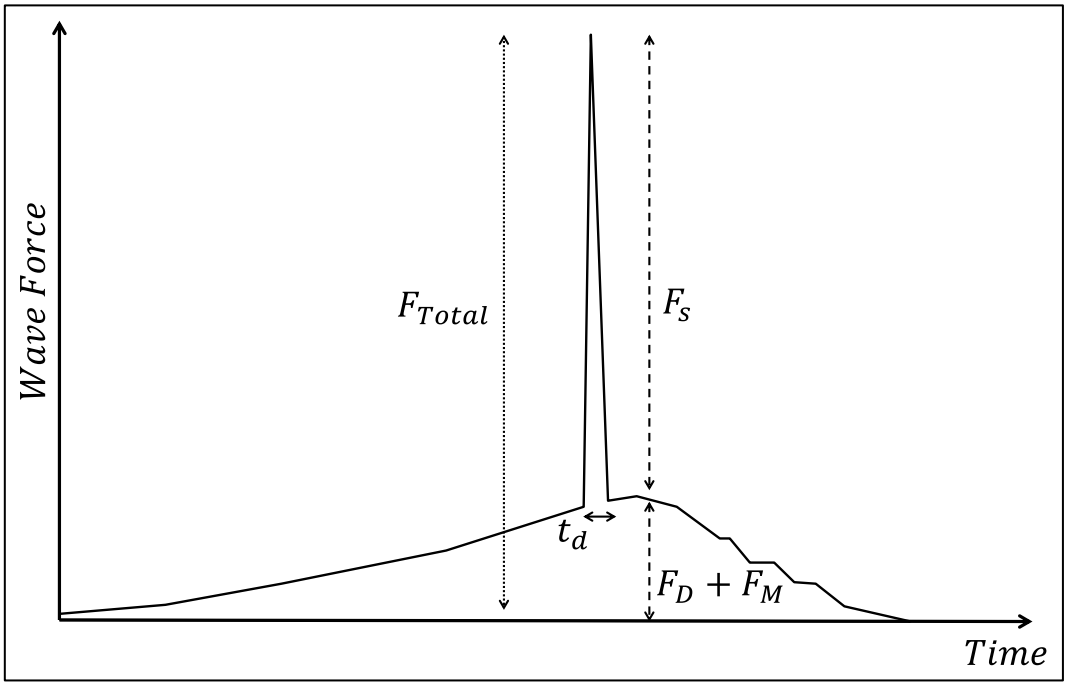

Figure 2-4. Quasi-static and slamming components of breaking wave force on a slender pile (Definition sketch)

The slamming force induced by a breaking wave on a slender pile is more difficult to analyse and predict, due to its highly transient and stochastic nature as well as to its extremely short duration. Therefore, diverse prediction models have been proposed, which are generally based on either *von Karman's impact theory* (von Karman, 1929) or on *Wagner's impact theory* (Wagner, 1932).

(i) The theory of *von Karman (1929)* is based on momentum conservation and the approximation of the cylinder with radius *R* by a flat plate with a width equal to the width 2c (t) of the immersed part of the cylinder at each instant of the impact as shown in Figure 2-5a. The maximum impact line force f_S is obtained as a function of the impact velocity V (see Figure 2-5a) :

$$f_S = \pi \rho_w R V^2 \qquad (2\text{-}4)$$

(ii) The theory of *Wagner (1932)* is also based on momentum conservation and the same assumption like that of von Karman. In addition, however, the flow beside the flat plate, which results in the so-called *pile-up effect*, is also considered. The latter is a deformation of the water surface as shown in Figure 2-5b. Due to this effect, the immersion of the cylinder occurs earlier, meaning that the duration of the impact becomes shorter and the maximum line impact force f_S becomes twice higher as compared to those obtained from von Karman's model. According to Wagner's theory, the maximum slamming force occurs at $t = 0$ and can be calculated as follows:

$$f_S = 2\pi \rho_w R V^2 \tag{2-5}$$

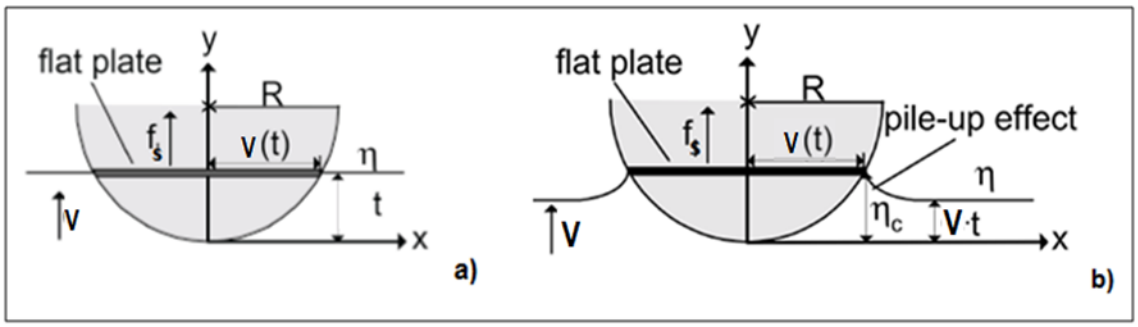

Figure 2-5. Definition sketches of 2D-impact models of a) von Karman (1929) and b) Wagner (1932)

Goda (1966) developed a time dependent slamming force formula, based on von Karman's theory and the assumptions that

(i) the breaker front over the impact height ($\lambda\eta_b$) is vertical and moves with wave celerity C_b (see definition sketch in Figure 2-6), and

(ii) the impact (line) force is uniformly distributed along the impact height as follows:

$$F_S(t) = \pi \rho_w R C_b^2 \lambda \eta_b \left(1 - \frac{C_b}{R} t\right) \tag{2-6}$$

Based on Eq. 2-6, the impact line force f_s is proportional to the term $\rho_w R\ C_b^2$, so that a time dependent slamming factor C_s can be defined:

$$C_S = \pi \left(1 - \frac{C_b}{R} t\right) \tag{2-7}$$

At the beginning of the impact (t=0), Eq.2-7 yields $C_s = \pi$ so that the maximum line force corresponds to that provided by the theory of von Karman in Eq.2-4.

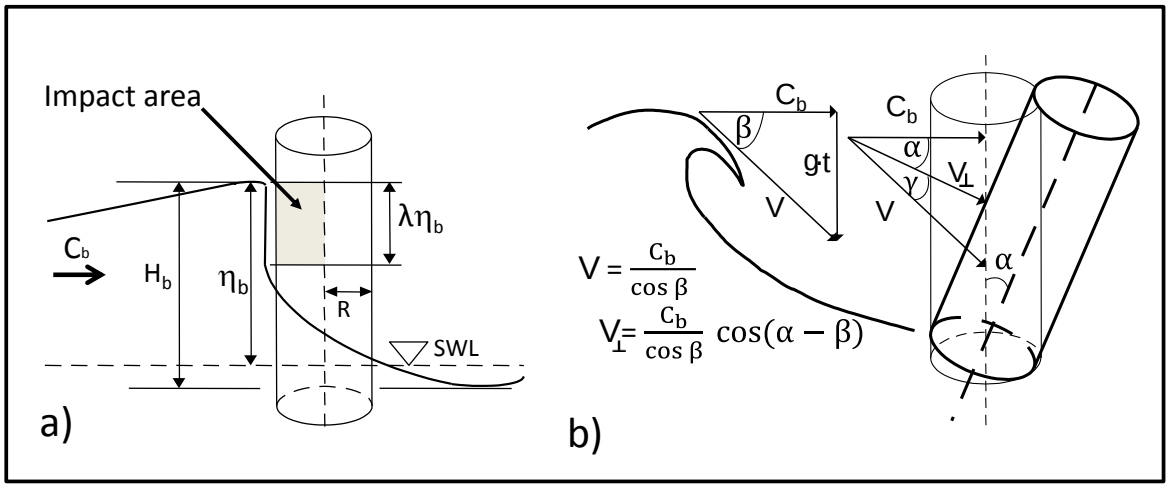

Figure 2-6. Definition sketches for a) slamming induced by a breaking wave on a vertical slender pile: curling factor λ and impact area ($\lambda\ \eta_b$) and b) inclined slender pile: angle γ between the direction of impact velocity V and the normal to the pile (Wienke, 2001)

One of the most recent studies on wave slamming forces on vertical and inclined slender cylindrical piles was conducted by Wienke and Oumeraci (2005), for which large-scale tests were performed in the large wave flume (GWK) in Hannover, Germany. Based on the experimental results and the Wagner model, a 3D description of impact force F_s was developed for vertical piles as well as for inclined piles by considering the angle γ between the direction of the so-called impact velocity V and the normal to the pile (see definition sketches in Figure 2-6):

$$F_{(t)} = \lambda\,\eta_b\,\rho_w\,R\,V^2\,\cos\Upsilon\,\left(2\pi\cos\Upsilon - 2\sqrt{\cos\Upsilon\frac{V}{R}t}\,.\operatorname{arctanh}\sqrt{1-\frac{1}{4}\frac{1}{\cos\Upsilon}\frac{V}{R}t}\right) \qquad (2\text{-}8)$$

When $0 \le t \le \frac{1}{8}\frac{1}{\cos\Upsilon}\frac{R}{V}$

$$F_{(t)} = \lambda\,\eta_b\,\rho\,R\,V^2\,\cos\Upsilon\,\left(\pi\sqrt{\frac{1}{6}\cos\Upsilon\frac{1}{\frac{V}{R}\acute{t}}} - \sqrt[4]{\frac{8}{3}\cos\Upsilon.\frac{V}{R}\acute{t}}\,.\operatorname{arctanh}\sqrt{1-\frac{V}{R}\acute{t}\sqrt{\frac{6}{\cos\Upsilon}\frac{V}{R}\acute{t}}}\right) \qquad (2\text{-}9)$$

When $\frac{3}{32}\frac{1}{\cos\Upsilon}\frac{R}{V} \le \acute{t} \le \frac{12}{32}\frac{1}{\cos\Upsilon}\frac{R}{V}$

The total duration of the impact force can be calculated by the following formula developed by Wienke and Oumeraci (2005):

$$t_d = \frac{13}{32}\frac{R}{V\ \cos\gamma} \qquad (2\text{-}10)$$

It should be stressed that the breaking wave impact is a dynamic force. Therefore, time is an important parameter to be considered in any prediction formulae for impact loads. Based on the previous studies performed on breaking waves on single piles, different formulae for impact duration (t_d), slamming coefficient (C_s) and values for curling factor (λ) were proposed.

For each model, generally based on either Karman's model or Wagner's model, the time dependent wave slamming force may be obtained from Eq. 2-11 by considering the respective slamming coefficient C_s and curling factor λ in Table 2-6. The impact duration t_d as defined in Figure 2-4 and the assumed vertical pressure distribution over the impact area are also indicated for each model.

$$F_s = C_s \, \rho_w \, R \;\; {C_b}^2 \lambda \, \eta_b \qquad (2\text{-}11)$$

Table 2-6. Available formulae based either von Karman's model or Wagner's model for impact force induced by breaking waves on vertical slender cylindrical piles with radius R

Study	***Slamming coefficient C_S***	***Curling factor λ***	***Vertical pressure distribution over impact area***	***Impact duration t_d***
(*) Goda (1966)	$\pi(1-\frac{C_b}{R}t)$	0.4	Uniform	$\frac{R}{C_b}$
(*) Tanimoto et al. (1986)	$\pi(1-\frac{C_b}{4\,R}t)$	0.5	Triangular	$\frac{R}{4\,C_b}$
(**) Wienke and Oumeraci (2005)	$(2\pi\cos\Upsilon - 2\sqrt{\cos\Upsilon\frac{V}{R}t}\,.\operatorname{arctanh}\sqrt{1-\frac{1}{4}\frac{1}{\cos\Upsilon}\frac{V}{R}t})$ $0 \le t \le \frac{1}{8}\frac{1}{\cos\Upsilon}\frac{R}{V}$; $(\pi\sqrt{\frac{1}{6}\cos\Upsilon\frac{1}{\frac{V}{R}\acute{t}}} - \sqrt[4]{\frac{8}{3}\cos\Upsilon}.\frac{V}{R}\acute{t}\,.\operatorname{arctanh}\sqrt{1-\frac{V}{R}\acute{t}\sqrt{\frac{6}{\cos\Upsilon}\frac{V}{R}}}$ $\frac{3}{32}\frac{1}{\cos\Upsilon}\frac{R}{V} \le \acute{t} \le \frac{12}{32}\frac{1}{\cos\Upsilon}\frac{R}{V}$	0.46	Uniform	$\frac{13\,R}{32\,V\,\cos\gamma}$
(**) Armand-Cointe Model (1986)	$2\pi - (4.72 - \ln\left(\frac{C_b}{R}t\right))\sqrt{\frac{C_b}{R}t}$	not defined	Uniform	$3.02\,\frac{R}{C_b}$
(**) Campbell-Weynberg (1980)	$5.15(\frac{2R}{2R+19\,C_b t}+\frac{0.107\,C_b t}{2R})$	not defined	Uniform	$\frac{13\,R}{32\,C_b}$

(*) von Karman's model; (**) Wagner's model

As shown in Table 2-6, already for the simple case of a single pile, the available models lead to different values of the impact duration (t), slamming coefficient (C_S) and impact area ($\lambda\eta_b$). Therefore, it is not difficult to imagine how complicated it would be to correctly predict the time history of the total wave force on much more complex multi-members structures such as jacket structures. While several design guidelines provide methods and formulae for the prediction of design impact loads induced by breaking waves on vertical slender piles, no guid-

ance is available for the assessment of design impact forces on truss structures in design guidelines and standards such as GL, 2005; IEC, 2009; ISO, 2007; DNV, 2013. Currently, Eq. 2-12 is adopted for the calculation of the maximum slamming force on the front face of jacket structures, in which the total maximum wave slamming force on the front face might be predicted by summation of slamming forces on each cylindrical member of the structure within the impact area shown in Figure 2-7. Therefore, the maximum slamming force on the front face of a jacket structure with only two legs, two x-type braces as well as the related impact areas (see Figure 2-8), is calculated according to the following formula (Aashamar, 2012)

$$F_s = 2\left(\frac{\pi}{2}\,\rho_w\,D_1\,C_b^2\,\lambda\,\eta_b\right) + \frac{\pi}{2}\rho_w\,D_2\,C_b^2(l_1 + l_2) \qquad (2\text{-}12)$$

, and the impact duration is commonly considered based on the slamming model proposed by Wienke and Oumeraci (2005) as follows:

$$t_d = \frac{13\ D}{64\ V\ \cos\gamma} \qquad (2\text{-}13)$$

Where $\boldsymbol{l_1 + l_2}$ is the total length of the braces directly exposed to the impact force, $\boldsymbol{D_1}$ is the leg diameter, $\boldsymbol{D_2}$ is the brace diameter, (see Figure 2-8) and *D* is considered the maximum value of $\boldsymbol{D_1}$ and $\boldsymbol{D_2}$. The first term of Eq.2-12 represents the impact load on the front legs of a truss structure and the second term describes the breaking wave loads on the braces.

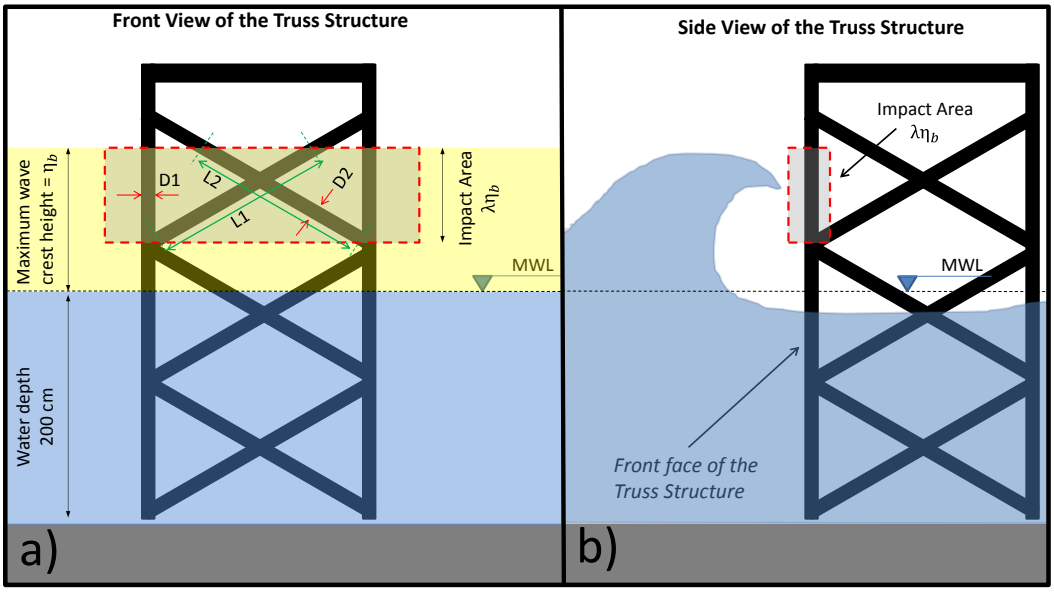

Figure 2-7. Front view (a) and side view (b) of the impact area on the front face of a generic truss structure

2.2.3 Experimental studies on breaking waves on jacket structures

Based on the current limitations for the prediction of breaking wave loads on jacket-type structures, only very few experimental studies have been recently performed on breaking wave loads on jacket-type structures. Aashmar (2012) set-up small-scale model tests (model scale 1:50) for a 3D truss structure under breaking waves at Norwegian University of Science

and Technology (see Figure 2-8a). The investigation by Aashmar resulted in a maximum slamming coefficient of 4.77. She stated that, the maximum response of the truss structure occurs for waves breaking at some distance before the truss structure and not for those waves breaking directly at the structure.

Navartnam (2013) set-up a 2D model of a truss structure with the scale of 1:50 under different breaker types (see Figure 2-8b). The results of his study showed that, the actual slamming forces on truss structures are much less than the values predicted by available slamming formulae initially developed for mono-piles. Woo et at. (2017) analysed numerically the dynamic response of 3D truss structures subject to slamming forces by extreme breaking waves. The structures were modelled using multiple lumped masses for the vertical projections of each member, and the slamming forces from the breaking waves were calculated and concentrated on the lumped masses. A numerical algorithm was developed to incorporate the slamming forces and to numerically compute the structural responses. The validity of the numerical analysis was verified by comparing the results with the experiments performed by Navartnam (2013).

The most comprehensive and reliable experiments so far, were performed in 2013 in Hannover in the frame of the WaveSlam project (Arnsten & Gudmestad, 2013). A set of large-scale experiments (scale factor of 1:8) were performed in the large wave flume (GWK) and non-breaking and breaking wave loads on jacket-type structures were investigated (see ure 2-8c). The objective of these large-scale experiments was to improve the available methods applied for the calculation of the breaking and broken wave loads on jacket-type offshore structures.

a) A 3D jacket structure under breaking waves (Aashmar, 2012)	b) A 2D jacket structure under breaking waves (Navartnam , 2013)	c) Large scale model tests in the frame of the WaveSlam project (Obhrai, 2015)

Figure 2-8. Recent experimental studies on breaking waves on jacket structures

Based on the unique large scale experiments performed in GWK, several research studies were conducted on breaking wave loads on truss structures (e.g. Chella, 2012; Choi et al, 2013; Jose & Podrazka, 2014; Navaratnam et al, 2013; Navaratnam, 2013; Rausa , 2014; Rausa et al, 2015;).

Chella et al. (2012) analysed the previous studies on wave impact forces and the key issues pertaining to these forces on jacket structures. They concluded that, considerable uncertainties in the estimation of hydrodynamic loads are caused by breaking waves on fixed offshore

structures and therefore, the design methods and guidelines for the prediction of breaking wave induced forces on offshore structures need to be enhanced.

Navaratnam et al, (2013), Navaratnam (2013) and Obhrai (2014) performed a preliminary analysis of the data from the WaveSlam project and compared the maximum measured slamming forces on the front face of the jacket structure with those slamming forces obtained by the application of wave slamming formulae developed basically for mono-pile structures. The results showed that the available formulae overestimate the peak of the slamming force, considerably. The associated impact duration was however not determined from the tests; instead, the slamming duration formulae proposed by Wienke and Oumeraci (2005) was considered as impact duration.

Rausa (2014) and Rausa et al. (2015) used the measurements in GWK tests to estimate the respective slamming factors on the front face of jacket structures. They set-up a Finite Element model in ANSYS and applied a triangular slamming force time history as uniform loads along the bracings of the front face and compared the response of the structure with measurements. Using this analysis, they obtained a slamming factor of 4.78 for the slamming force on the front bracings. However, the assumption that the shape of the slamming force time function is triangular was not supported by any data/results in their study.

Jose & Choi (2017) recently studied the slamming coefficients on local members of the GWK jacket structure under plunging breaker using a 3D CFD (Computational Fluid Dynamics) model set-up for the experiments (Figure 2-9b). They implemented the Empirical Mode Decomposition (EMD) approach to quantitatively compare the results of the CFD model and those from the laboratory tests. They concluded that the distribution of impact pressures on the local members over the impact area exhibits a triangular shape, unlike the slamming models proposed by Goda et al. (1966) and Wienke and Oumeraci (2005) which consider a uniform pressure distribution.

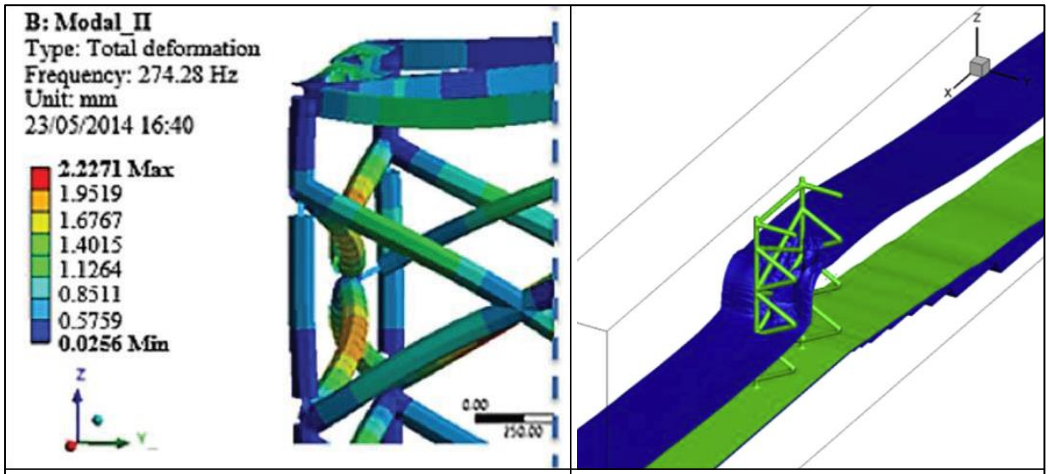

a) A CSD model set-up for the GWK truss structure in ANSYS (Rausa et al, 2015)

b) A CFD model set-up for breaking waves on the GWK truss structure (Jose and Chai, 2017)

Figure 2-9. Numerical models set-up for the GWK model tests

The investigations performed so far, on the GWK experiments have mainly resulted in different values of maximum wave slamming coefficient and curling factor considering the highest Dynamic Force Response (DFR) of the structure. Although these studies have significantly contributed to enhance the knowledge about the interaction between waves and truss structure, several gaps still remain which should be overcome to achieve a reliable prediction of breaking wave induced forces on truss structures and, consequently, a safe design of these complex structures:

(i) No slamming formulae are proposed to predict time series of the slamming force on the entire truss structure. In fact, none of the aforementioned studies has resulted in reliable and process based model to predict the total slamming force and duration induced by breaking waves on truss-type structures and

(ii) Impact duration which is an inseparable part of the impact force on the structure has not been investigated. The aforementioned studies have mainly considered the available impact duration formulae proposed for breaking waves on single piles (e.g. Wienke and Oumeraci, 2005; Goda,1966)

(iii) The slamming force by broken waves on the rear face of the truss structure was not considered. In fact, none of the reviewed studies has focused on impact forces induced by broken waves on the rear face of truss structures. However, the investigation in the present study revealed that these forces are considerable and cannot be neglected (see section 3.5).

2.2.4 Numerical studies on breaking waves on fixed-bottom offshore structures

Besides analytical and experimental investigations on wave loads on pile structures, few 3D numerical studies on modelling wave loads on single piles were published in the last years. Based on large eddy simulation (LES) method, Li and Lin (2001) developed a 3D numerical model to simulate non-breaking waves on a square cylinder. They stated that, the simulated non-breaking wave forces acting on the square cylinder are in a good agreement with those calculated by the Morison equation. Lin and Li (2003) also developed a 3D numerical model to investigate wave-current-structure interactions. Turbulent flow was simulated by a sub-grid-scale (SGS) model by using the concept of large eddy simulation (LES). However, the numerical results were not compared with laboratory measurements.

Morgan and Zang (2010) used an open source CFD code named OpenFOAM to numerically simulate wave run-up on a single pile with modelling only the laminar flow and simulating the free-surface motions by the Volume of Fluid (VOF) approach. The applied code is capable to solve the Navier-Stokes equations using the “Pressure Implicit with Splitting of Operators” (PISO) algorithm introduced by Issa (1986). The results of the numerical model were compared with the measured data. The authors found out that the main peak of the wave group was underestimated by the numerical model. Based on the open source CFD code, OpenFOAM, a 3D-flow model with a k-ω-SST turbulence model was developed by Leschka et al. (2014) to simulate the effect of large roughness elements (both submerged and surface piercing obstacles of different shapes and in different arrangements) on tsunami propagation. Their

model was well-validated using the laboratory experiments performed at Leichtweiß-Institute (LWI) by Bonakdar (2014).

One of the most critical issues of 3D numerical models is that they are computationally expensive, especially when a large number of tests are required (e.g. for systematic parameter study). This issue is even more problematic in the case of structures exposed to breaking waves because the complete numerical wave flume including the far field and near field needs to be simulated. To overcome this problem, a hybrid (2D-3D) CFD model system was developed and validated by El Safti et al. (2014). While the 2D model allows simulating efficiently the wave development and wave-wave interactions along large distances without any structure, the 3D model is considered for a smaller 3D domain in the near field around the structure. The outline and concept of the hybrid (2D-3D) CFD model system is briefly described in Figure 2-10.

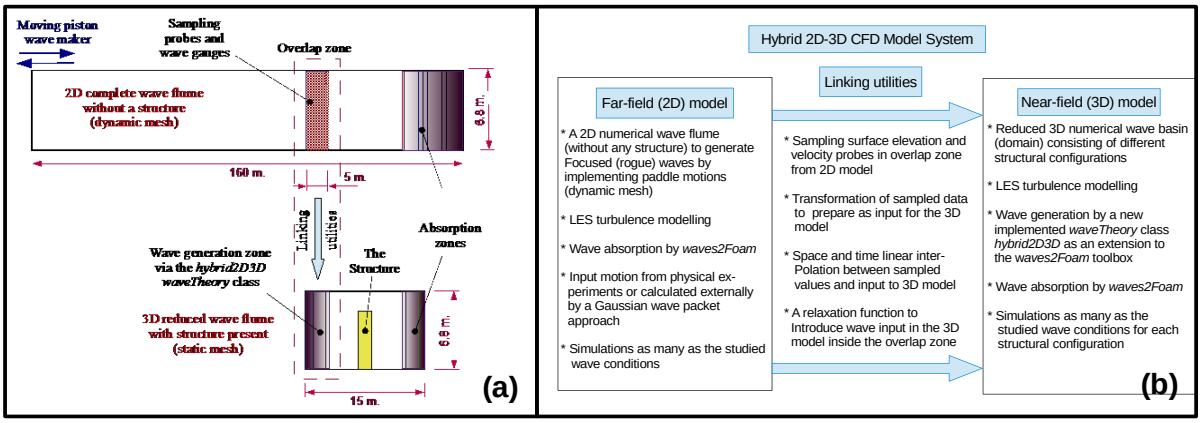

Figure 2-10. Hybrid (2D-3D) CFD model system: (a) concept of dual domain and (b) outline of model system (El Safti et al., 2014)

Recently, several CFD models have been applied for the calculation of extreme wave loads on fixed-bottom structures, including mono-piles. Several studies (e.g. Corte and Grilli, 2006; Zhou, 2010; Leschka et al., 2014; El Safti et al.,2014; Choi et al, 2014 & etc.) have addressed different problems associated with the wave loading of rigid mono-piles as well as wave run-up, pile group effects, focused waves on piles by the development of 3D numerical models using the Reynolds Averaged Navier Stokes (RANS) equations based on NS models (Figure 2-11 c & d). Advanced application of CFD models for mono-pile structures can be seen in the very recent studies performed by Sagar et al. (2015), El Moctar & Ley (2016) and Horn et al. (2016) on which Finite-Element Models (FEM) for solving structural equation of motion were coupled with flow simulations based on Reynolds-Averaged Navier-Stokes equations in order to investigate the influence of the structural flexibility and the structure vibrations on the resulting hydrodynamic forces on the structure (Figure 2-11b).

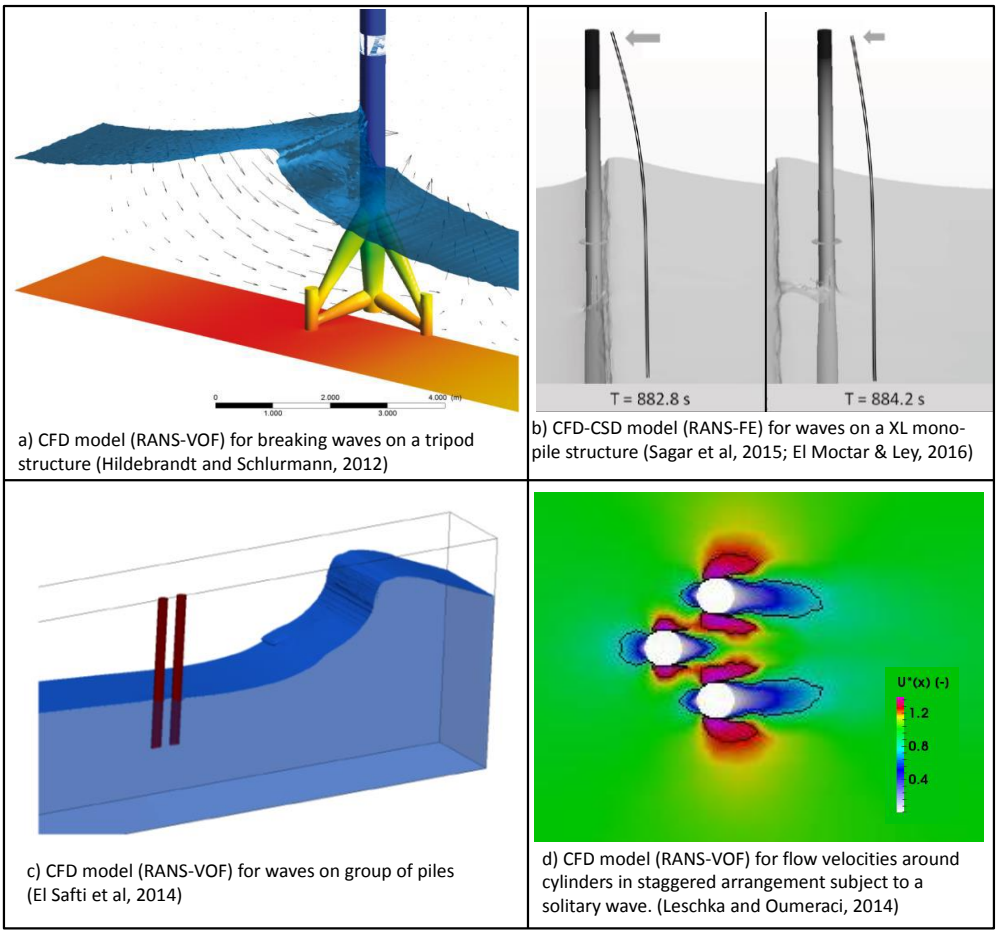

a) CFD model (RANS-VOF) for breaking waves on a tripod structure (Hildebrandt and Schlurmann, 2012)

b) CFD-CSD model (RANS-FE) for waves on a XL mono-pile structure (Sagar et al, 2015; El Moctar & Ley, 2016)

c) CFD model (RANS-VOF) for waves on group of piles (El Safti et al, 2014)

d) CFD model (RANS-VOF) for flow velocities around cylinders in staggered arrangement subject to a solitary wave. (Leschka and Oumeraci, 2014)

Figure 2-11. Numerical models developed for extreme waves on fixed-bottom offshore structures

Unlike for the case of mono-piles, where several CFD or CFD-CSD models have been developed for the prediction of extreme wave loads on rigid or flexible mono-pile structures, less attention has been paid for the development of CFD or CFD-CSD models for tripod or jacket structures. Hilderbrandt et al (2012) set-up a three dimensional CFD model based on volume of fluid (VOF) for a tripod structure under breaking and non-breaking waves which was tested in the large wave flume of Hannover (Figure 2-11a). The maximum slamming coefficients calculated in this study (Cs=3.5) was significantly lower than those provided by guidelines and standards (mostly around 2π). The impact duration however, was not addressed in this study. Recently, Lin et al (2017) simulated the wave run-up heights and wave loads on three types of wind turbine foundations, i.e. monopile, gravity-based and tripod support structures using a RANS solver and by employing k-ε turbulent closure.

Although the available numerical studies discussed in this section are based on simplifying assumptions, the results indicate that the numerical methods based on LES and RANS can simulate the wave loads on pile structures with an acceptable degree of accuracy. Overall, despite the recent achievements of the last years in the field of numerical modelling, no 3D numerical model is readily available to reliably simulate breaking and broken wave loads on a jacket structure except the recently performed study by Jose and Choi (2017) in which a CFD

model for breaking waves on a truss structure (GWK truss) was set-up and a tentative analysis of the forces on the legs and braces of the structure were investigated (see Figure 2-9b).

A detailed analysis of the available methods for the calculation of wave induced loads on jacket structures is performed including: i) analytical models developed for non-breaking waves on single piles, ii) analytical formulae developed for breaking waves on single piles, iii) laboratory tests performed recently for truss-type structures under breaking waves and iv) numerical models developed for breaking waves on fixed-bottom offshore structures. Overall, the previous studies have contributed to an improved understanding of wave-jacket structure interaction. However, several knowledge gaps are identified such as:

(a) the lack of a proper understanding of the validity range and the applicability of the Morison's equation for jacket structures,

(b) the lack of slamming force formulae for breaking/broken waves on the front/rear faces of jacket structures,

(c) the lack of a proper understanding of the effect of neighbouring members on the wave loading of a member of the jacket structure, and

(d) the lack of proper understanding of the processes associated with the propagation of the waves through the structure (e.g. water particle velocity changes, wave crest deformation), for instance how a breaking wave at the front face develops to a broken wave at the rear face of the structure.

Therefore, one of the focuses of this study should be a better understanding of the aforementioned processes in order to fill some of the identified knowledge gaps by using the available data from the GWK tests as well as CFD and CSD models validated by the GWK tests.

2.3 Pile foundation models for fixed-bottom offshore structures

The pile foundation of a fixed-bottom offshore structure should be capable to cope with all applied static, cyclic and transient loads during its life time. Cyclic shear loads on piles induce cyclic shear stresses in soil that may result in a gradual increase of pore pressure. Higher pore pressure may lead to an increase of the residual shear strains, thus reducing the shear strength of the soil; i.e. the evaluation of the structural dynamics will strongly be affected by the soil behaviour, thus requiring an integrated analysis of the soil-structure system. The analysis should be performed considering realistic assumptions for the stiffness and damping of both soil and piles. Several approaches with different levels of complexity may be utilized to determine pile-soil interaction for the foundation of jacket structures. In terms of complexity, these models are respectively classified as:

(i) simplified models representing the pile foundation,
(ii) load-deflection (p-y) models, and
(iii) complex 3D numerical models.

In this section, the aforementioned common approaches, their strengths and limitations are briefly discussed.

2.3.1 Simplified models representing the pile foundation

Several studies (e.g. Zaaijer, 2002; Zaaijer, 2006) have revealed that, the characteristics of the pile foundation will strongly affect the natural frequency of the fixed-bottom offshore structures and therefore, have to be properly modelled to predict the dynamic performance of the structure.

The study performed by Shi et al. (2015) showed that modelling the pile foundation might change the natural frequency of jacket structures up to 40% depending on the penetration depth of the pile foundation and the soil type. The dynamic response of jacket structures supporting wind turbines is much more complex to calculate than that of jacket structures for oil and gas offshore platforms because several interactions such as wind-turbine, wave-jacket, pile-soil should be simultaneously considered in the analysis. Therefore, it is necessary to simplify the model of the pile foundation while maintaining sufficient accuracy in order to achieve a higher computational efficiency. In addition, for some analyses (excluding extreme loads) such as fatigue in which the soil behaviour remains linear, there is no need to use complex foundation modelling techniques including the non-linear behaviour of the soil. For such analysis, the application of simplified models representing the pile foundation of jacket structures is adequate. In this section, the commonly applied simplified models are briefly summarised.

Effective fixity length

This approach has been widely used in practice to model the pile foundation of jacket structures designed for oil and gas platforms (e.g. NIOC, 2009 & NIOC, 2011). In this approach, the pile foundation is replaced by a rigid clamping of the pile at a specific depth below the mudline (see Figure 2-12a). In other words, the stiffness and damping of the soil are modelled with an equivalent tubular slender member with the same stiffness and damping characteristics. The length of this member is a function of the soil type and the pile diameter. Barltrop et al, (1991) investigate different soil types and recommended the fixity length of 3.5 to 8 times the pile diameter depending on the soil type. The stiffness matrix is defined as below for a pile with an effective length of L:

$$K = \frac{2EI}{L^3}\begin{bmatrix} 6 & -3L & 0 \\ -3L & 2L^2 & 0 \\ 0 & 0 & \frac{AL^2}{2L} \end{bmatrix} \quad (2\text{-}14)$$

The great advantages of this method are that it is very easy to implement this method for different types of fixed-bottom offshore structures and that very little information about soil properties are required to use apparent fixity length approach. However, since a wide range of total length of the equivalent member (from 2D to 8D) is suggested, the behaviour of the entire structure is very sensitive. In fact, the application of apparent fixity length may result in

different structural behaviour and therefore, is only recommended for a preliminary design procedure.

Stiffness matrix using a reference model

Using this approach, the stiffness matrix of the pile foundation system is predicted in the seabed. In order to determine the unknown elements of the stiffness matrix, a reference model is required. These elements can be obtained by performing a static analysis using the reference model. This matrix provides forces F, and moments M, for pile-head's displacements and rotations. Horizontal transition of u and the rotation of Θ are defined as laterally loaded degrees of freedom of the pile foundation. For this case the stiffness matrix is defined as follows:

$$F = Ku \tag{2-15}$$

$$\begin{bmatrix} F \\ M \end{bmatrix} = \begin{bmatrix} k_{xx} & k_{x\theta} \\ k_{\theta x} & k_{\theta\theta} \end{bmatrix} . \begin{bmatrix} u \\ \theta \end{bmatrix} \tag{2-16}$$

$$\begin{bmatrix} F_x \\ M \\ F_z \end{bmatrix} = \begin{bmatrix} k_{xx} & k_{x\theta} & 0 \\ k_{\theta x} & k_{\theta\theta} & 0 \\ 0 & 0 & k_z \end{bmatrix} \begin{bmatrix} x_s \\ \theta \\ z_s \end{bmatrix} \tag{2-17}$$

Where $k_{x\theta} = k_{\theta x}$;

Using stiffness matrix approach, the entire properties of the pile foundation are considered in a single matrix. Therefore, any kind of modification in the soil characteristics can be performed very simple and fast and as a result this method can be practically used to study the affective parameters of the soil on the entire response of the structure. The drawback of this model is its independency to a reference model.

Stiffness matrix using Randolph's elastic continuum model

The Randolph's elastic continuum model is an alternative approach for the calculation of the stiffness matrix which is independent of a reference model and can be derived directly from the soil properties. Randolph (1981) obtained the flexibility of the pile foundation through conducting a sensitivity and parameter analyses for a pile foundation with different geometries. The elements in the stiffness matrix in Eq. 2-17 are determined as follows:

$$k_{xx} = 4.52\, m^* r_0^2 \left[\frac{E_p}{m^* r_0}\right]^{\frac{1}{3}} \tag{2-18}$$

$$k_{\theta x} = k_{x\theta} = -2.4\ m^* r_0^3 \left[\frac{E_p}{m^* r_0}\right]^{\frac{5}{9}} \tag{2-19}$$

$$k_{\theta\theta} = 2.16\ m^* r_0^4 \left[\frac{E_p}{m^* r_0}\right]^{\frac{7}{9}} \tag{2-20}$$

And $E_p = \frac{EI}{\frac{1}{64}\pi D^4}$

$$m^* = m_c\,(1 + \tfrac{3}{4}\nu) \tag{2-21}$$

Where E is the modulus of elasticity of the pile, ν is Poisson's ratio, I is the second moment of inertia of the pile cross-section, r_0 is the outer diameter of the pile and m_c is the constant of proportionality and can be calculated using the following equation:

$$m_c = \frac{2}{L_c^2}\int_0^{L_c} G(z_s)dz \tag{2-22}$$

$$\text{And} \quad L_c = 2\,r_0\,[\frac{E_p}{m^*\,r_0}]^{\frac{2}{9}} \quad \& \quad G(z_s) = m_c\,.\,z_s \tag{2-23}$$

Where z_s is depth bellow the seabed and G is shear modulus of soil in different layers. Aforementioned integral should be solved iteratively and the relative values should be replaced in Eq. 2-23 to determine critical pile length L_c.

The main advantage of this approach is that, all relevant properties of the pile foundation are considered in a single matrix. This allows a simple modification of the soil information in the model. Both FUGRO and JBH companies adopted this method to transfer information for their foundation analysis. A further important advantage is that the Randolph stiffness matrix is independent of any reference model and can be directly generated considering the soil and pile characteristics.

Uncoupled springs

In this approach, the stiffness of the pile foundation is simplified using two uncoupled springs. One spring has lateral stiffness and the other one has rotational stiffness (Figure 2-12c). Hence, there are usually two degrees of freedom correspond to the lateral and rotational displacements of the pile foundation. When heave motion of the structure is important, the vertical degree of the freedom can be considered and the stiffness matrix of pile foundation at the mudline can be combined with a spring with vertical stiffness (Gazetas, 1991).

The stiffness of the uncoupled springs can be determined either with force methods or with displacement methods using the matrices in Eq.2-24 and Eq.2-25 as follows:

For force method (Figure 2-12d):

$$K = \begin{bmatrix} k_{xx} - \frac{{k_{x\theta}}^2}{k_{\theta\theta}} & 0 & 0 \\ 0 & k_{\theta\theta} - \frac{{k_{x\theta}}^2}{k_{xx}} & 0 \\ 0 & 0 & k_z \end{bmatrix} \tag{2-24}$$

For displacement method (Figure 2-12e):

$$K = \begin{bmatrix} k_{xx} & 0 & 0 \\ 0 & k_{\theta\theta} & 0 \\ 0 & 0 & k_z \end{bmatrix} \tag{2-25}$$

Figure 2-12 shows a definition sketch for the simplified approaches for modelling the foundation of the offshore wind turbines.

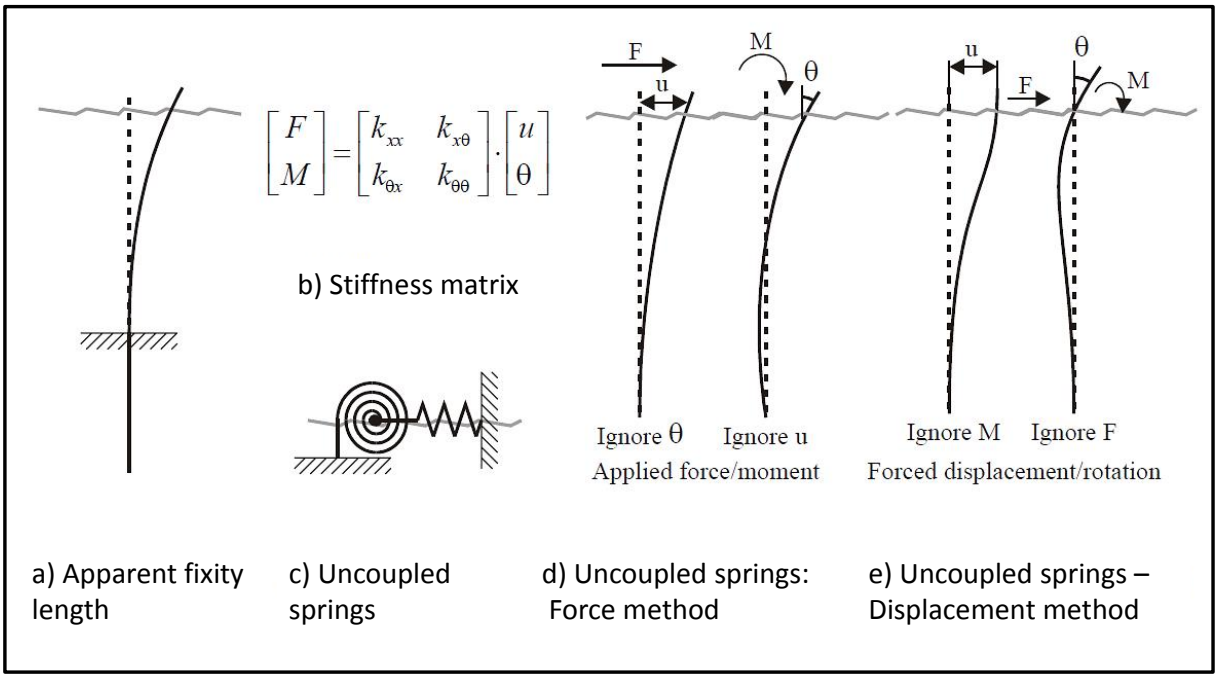

Figure 2-12. Foundation models for piled structures (Zaiijer, 2006)

Zaiijer (2006) performed a comparative analysis of the dynamic behaviour of fixed-bottom offshore structures for different simplified pile foundation models including the apparent fixity length, the stiffness matrix, the uncoupled springs and a finite element model as a reference model with distributed springs representing the soil stiffness (Figure 2-12). He computed the natural frequency of the structure with different pile foundations, modelled by the aforementioned simplified approaches. The results were compared with the natural frequency of the reference model and the most appropriate simplified technique to model pile foundation of fixed-bottom offshore structures was identified (Figure 2-13). The mentioned analysis was performed for a mono-pile structure, a tripod structure and a lattice structure supporting a 3MW wind turbine, all located in similar environmental conditions in the North Sea.

The results showed that, the first and second natural frequencies obtained with a stiffness matrix with coupled lateral behaviour corresponding very well to the reference finite element foundation model for different support structure types and the difference is less than the expected uncertainties in foundation behaviour (2% for the 1st natural frequency and 6% for the 2nd natural frequency). Moreover, the stiffness matrix has less degrees of freedom compared to the reference finite element model and will, therefore, reduce the computational complexities.

The application of uncoupled springs, however, results in larger deviations, which can exceed the expected errors. Moreover, using the uncoupled spring method, no significant reduction of degrees-of-freedom is obtained.

The application of the effective fixity length approach with different values of the equivalent pile penetration depth (2D, 4D, 6D & 8D) provides a wide range of results. Due to the large sensitivity of the predicted natural frequency to the effective fixity depth, the results of this model are not reliable to be considered for the final design. An effective fixity depth could be determined from a reference model or from measurements to reduce the complexity of the foundation model. However, a sensitivity study is always recommended when this model is applied.

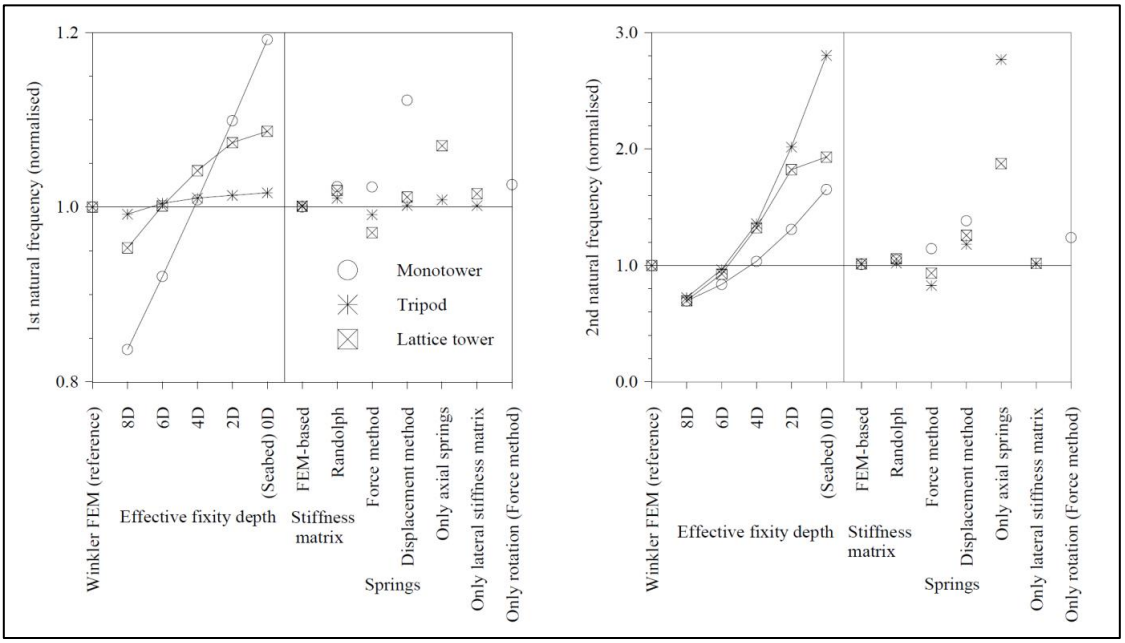

Figure 2-13. Normalized 1st and 2nd natural frequencies of the structures with different pile foundation models (Zaiijer, 2006)

2.3.2 Load-deflection (p-y) models

For fixed-bottom substructure of offshore wind turbines, the lateral pile-soil interaction modelling (lateral springs) dictates the piles head horizontal displacement and significantly influence the structural response. Therefore, usually for jacket structures, only the lateral soil stiffness is considered (e.g. Shi et al, 2015) when the dynamic response of jacket structures to lateral loads is the main focus. In fact, commonly no vertical soil modelling is included, i.e., no springs are considered for the shaft friction and no stiffness are considered for the pile tip resistance.

The most well-known pile-soil modelling approach implemented for fixed-bottom offshore structures is based on p-y curves developed in a research programme on laterally loaded piles for offshore structures including laboratory model testing and field tests with an instrument pile. That research was sponsored by a group of five oil companies (Matlock, 1970; O'Neill & Murchinson, 1983). The non-linear p-y approach with a proper linearization, which is recommended in most guidelines such as API (2005), GL (2005) and DNV (2013), has indeed provided relatively good results for fixed-bottom offshore platforms. The method for the extension of non-linear p-y curves for both clay and sandy soils are described below.

Clay

Figure 2-14 shows the typical non-linear response of clay to static and cyclic loading. Under cyclic loading, the lateral resistance of clay soil increases rapidly and reaches a maximum value at a certain displacement (y3), referred to as the 'critical movement'. Afterwards, clay starts losing resistance beyond a break point (p3, y3) while under static load the resistance increases reaching a constant value.

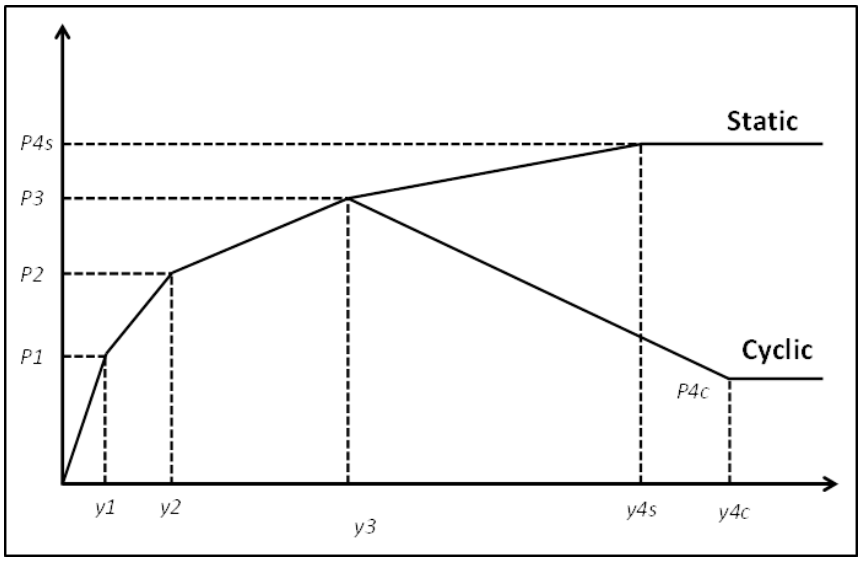

Figure 2-14. Clay behaviour under static and cyclic loading

As shown in Figure 2-14, the lateral soil resistance of clay soil is significantly non-linear and p-y curves can be derived from Table 2-7.

Table 2-7. Definition of p-y curves for the clay soil under cyclic loading. (API, 2005)

$X < X_R$		$X \geq X_R$	
p/p_u	y/y_c	p/p_u	y/y_c
0.00	0.00	0.00	0.00
0.50	1.00	0.50	1.00
0.72	3.00	0.72	3.00
0.72	∞	$0.72\ X/X_R$	15
		$0.72\ X/X_R$	∞

Where, p is actual lateral resistance, (kPa), y is the actual lateral deflection, (mm) and y_c can be calculated using the following expression:

y_c = 2.5 ε_c D, (mm) (2-26)

Here, D is the pile diameter (mm), ε_c is the strain which occurs at one-half the maximum stress on laboratory undrained compression tests of undisturbed soil samples and P_u is ultimate unit bearing capacity (ultimate resistance) that should be considered the minimum value of P_u obtained from Eq.2-27 and Eq.2-28.

$$p_u = 3c + \gamma_s X + J\frac{cX}{D} \quad \text{(kPa)} \tag{2-27}$$

And,

$$p_u = 9c \quad \text{(kPa)} \quad for \qquad X \geq X_R \tag{2-28}$$

Where c is an undrained shear strength for undisturbed clay soil samples (kPa), γ_s is an effective unit weight of soil (MN/m3), J is a dimensionless empirical constant with values ranging from 0.25 to 0.5 and might be determined by field testing. X is the depth below soil surface (mm) and X_R is the depth below soil surface to bottom of reduced resistance zone (mm) which can be expressed by Eq. 3-29.

$$X_R = \frac{6D}{\frac{\gamma_s D}{c} + J} \tag{2-29}$$

Sand

The resistance-deflection curve of sandy soil is nonlinear but basically different for cyclic loads in comparison to clay. While the ultimate capacity of sand under cyclic loading increases rapidly and reaches to a constant value (p3c in Figure 2-15), the ultimate capacity of clay drops after reaching its maximum value (p3 to p4c in Figure 2-14). Figure 2-15, shows a typical shape of the curve illustrates the nonlinear behaviour of sandy soil under static and cyclic loading.

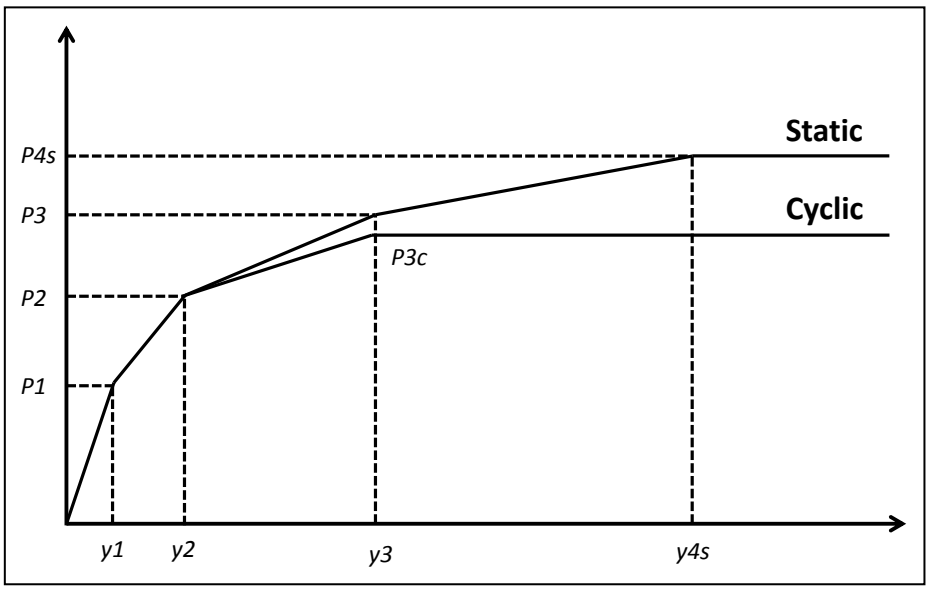

Figure 2-15. Sand behaviour under static and cyclic loading

The lateral resistance-deflection (p-y) relationships of sand soil can be approximated at any specific soil depth h_s, by the following expression:

$$p = A_s\, p_u\, \tanh\left[\frac{k\, h_s}{A_s\, P_u}\, y\right] \qquad (2\text{-}30)$$

Where, y is the actual lateral deflection (m), p_u is the actual lateral resistance (kN/m), A_s is a factor to account for cyclic or static loading (0.9 for cyclic loading), h_s is the soil depth from mudline (m) and k_{soil} is the initial modulus of subgrade reaction (kN/m^3) which can be determined using Figure 2-16a.

For a sandy soil, p_u can be considered by the smallest value of p_{us} and p_{ud} obtained from Eq.3.6 and Eq.3.7.

$$p_{us} = (C_1\, H_{soil} + C_2\, D)\, \gamma_s\, H_{soil} \qquad (2\text{-}31)$$

$$p_{ud} = C_3\, H_{soil}\, \gamma_s\, D \qquad (2\text{-}32)$$

where coefficients C1, C2 and C3 can be determined as a function of the internal friction angle from Figure 2-16b.

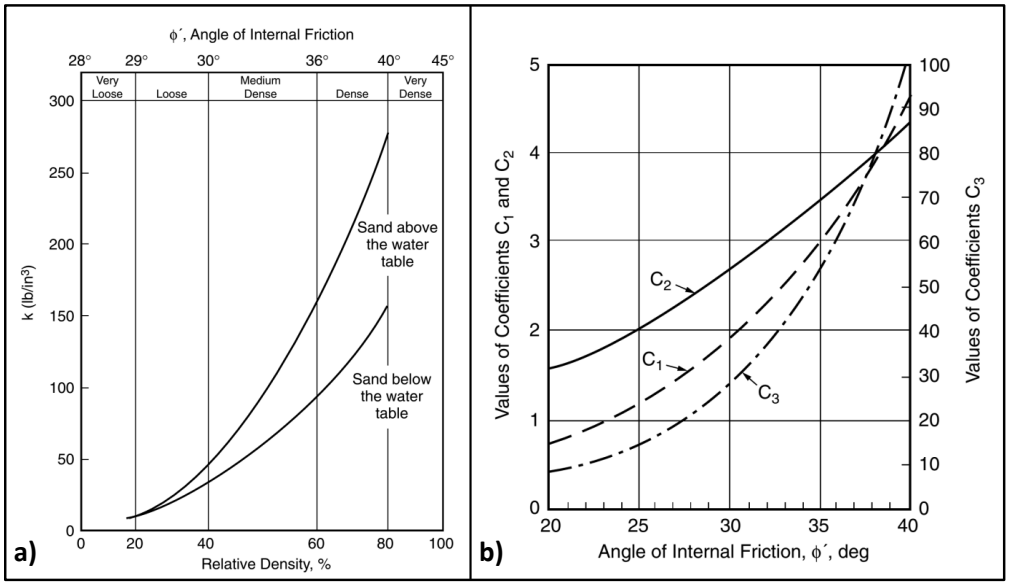

Figure 2-16. Determination of: a) Initial modulus of subgrade reaction (in Eq.2-30) and; b) coefficients of C1, C2 & C3 (in Eq.2-31 and Eq.2-32) for sandy soils (API, 2005)

The aforementioned approach is implemented to model the pile foundation of several fixed-bottom structures in research studies as well as practical industry projects.

API code p-y curves are empirically developed for long slender piles where the pile behaves flexibly i.e. the pile snakes and therefore, they provide reliable results for flexible foundations. When the pile foundation of the structure exhibits rigid body rotation and there is negligible bending in the pile, the provided p-y curves in API, GL and DNV will not estimate accurate results because they may predict conservative or non-conservative results. Furthermore, for

any application of p-y method for the foundation of jacket structures, the damping contributions of the pile foundation should be considered.

2.3.3 Complex 3D numerical models

The complex 3D numerical models for the consideration of pile-soil interaction, consists of several structural elements for foundation and environmental modelling of soil. The boundary conditions at soil-structure interface are used to formulate the constraints for coupling structural element via soil element.

Since the dimensions of soil are much larger than structural dimensions, some criteria should be defined for elements. For static analysis, a simple assumption can be considered, namely that soil elements are connected to a rigid plate. However, for dynamic analysis under cyclic loads, suppression of the reflection of the radiation effects must be considered. In this case, the model incorporates many DOFs (degrees of freedom) which increase the computational complexity. Figure 2-17 shows the recent 3D numerical models for single and group pile foundations under static and cyclic loads.

Although the comprehensive 3D numerical models are accurate and able to properly consider pile and soil interactions, they may not fit the complex models for offshore structures under waves because strong computational tools might be required to simulate the response of such complicated systems.

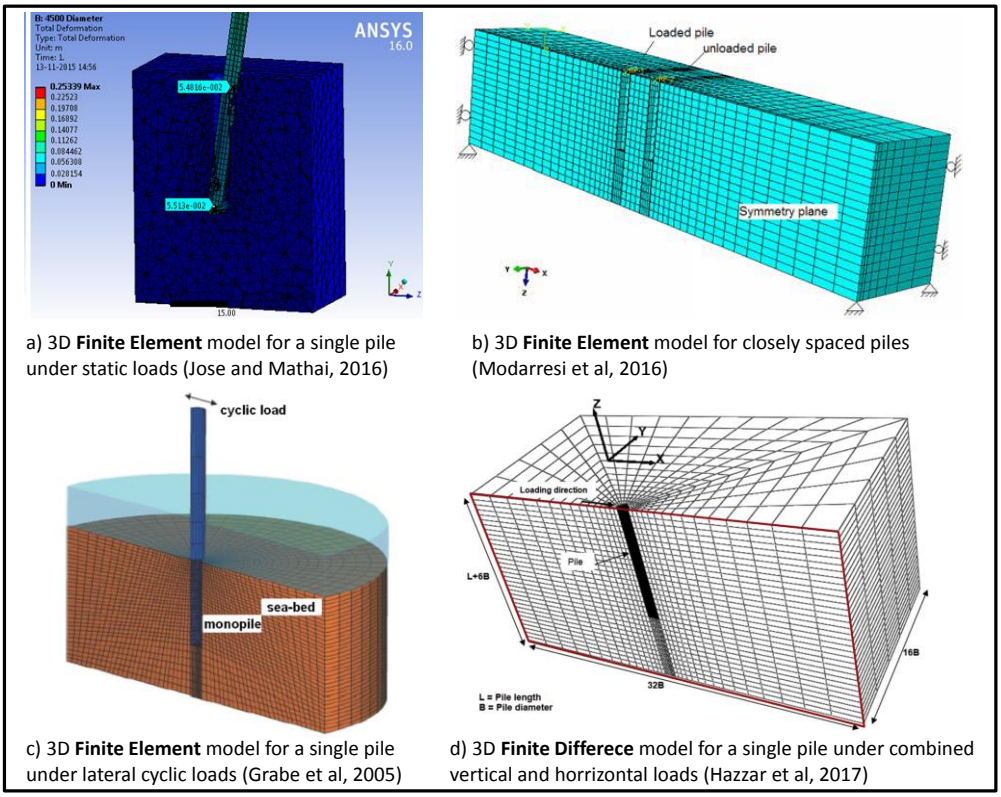

a) 3D **Finite Element** model for a single pile under static loads (Jose and Mathai, 2016)

b) 3D **Finite Element** model for closely spaced piles (Modarresi et al, 2016)

c) 3D **Finite Element** model for a single pile under lateral cyclic loads (Grabe et al, 2005)

d) 3D **Finite Differece** model for a single pile under combined vertical and horrizontal loads (Hazzar et al, 2017)

Figure 2-17. Selected recent studies on pile-soil interactions using complex 3D numerical models

Commonly, the complex 3D numerical methods are applied to model pile foundation of offshore structures, when only the process associated with pile and soil interaction is the main focus of the study and no concentration is laid on the other processes/interactions such as wave-structure and wind-turbine. Otherwise, the application of these models requires high computational demand. In addition, they need much more information about soil characteristics that makes them impractical as design tools for offshore wind turbines.

The analysis of the available methods for modelling pile foundation of fixed-bottom offshore structures has generally shown that most of the design guidelines (e.g. DNV, 2013; DNV; 2010; API, 2005; GL, 2005) recommend to use fully non-linear force-deflection model (p-y) for modelling the pile foundation of jacket structures under extreme wave loads. For load events caused by moderate waves on jacket structures (e.g. for fatigue analysis) the full complexity of the non-linear system is usually not required since soil reactions generally remain in the linear elastic range.

Although, the complex 3D numerical models with soil elements are more accurate to calculate soil-pile interactions, they may not fit the complex substructure models appropriately because these models are very complicated, may require much more sophisticated and more computationally demanding tools to calculate the dynamic response as well as more and detailed soil data.

Therefore, for this study, the fully non-linear force-deflection model (p-y) is identified as the most feasible and appropriate approach to model the pile foundation of a full-scale jacket structure (called 'OC4 jacket'), which has already been considered in different studies (see section 5.3)

2.4 Parameters affecting the dynamic response of jacket structures

So far, several studies have been performed to identify the most important parameters influencing the dynamic response of jacket structures. Cordle et al. (2011) performed a comparative analysis of the dynamic response of jacket structures with and without joint can model and showed that, considering or neglecting joint cans may not affect the behaviour of jacket structures (Figure 2-18a). Investigations performed by Kaufer et al (2010) and Kunho Kim et al, (2013) revealed that the effect of overlapped members should be considered for jacket structures, otherwise, the total mass of the structure will be overestimated up to 10 %. Moreover, ignoring the overlapped members, the total length of the legs and braces increases and consequently, the base shear forces and the overturning moments caused by wave loads on the structure will be overestimated (Figure 2-18b).

Moll et al, (2010) and Shi et al, (2013) studied the effect of hydrodynamic added mass and the effect of member flooding on jacket structures, and showed that both effects should be considered as they might significantly change the mass and natural frequency of the structure. (Figure 2-18c).

The investigation by Fevåg (2012) showed that, marine growth considerable affects the dynamic response of truss-type structures since it increases the hydrodynamic loads and the total mass of the structure. While a strong effect of marine growth was found on the third fore-aft and side-to-side frequencies of the jacket support structure, this effect for the first fore-aft and side-to-side frequencies of the support structure was small. (Shi et al, 2012).

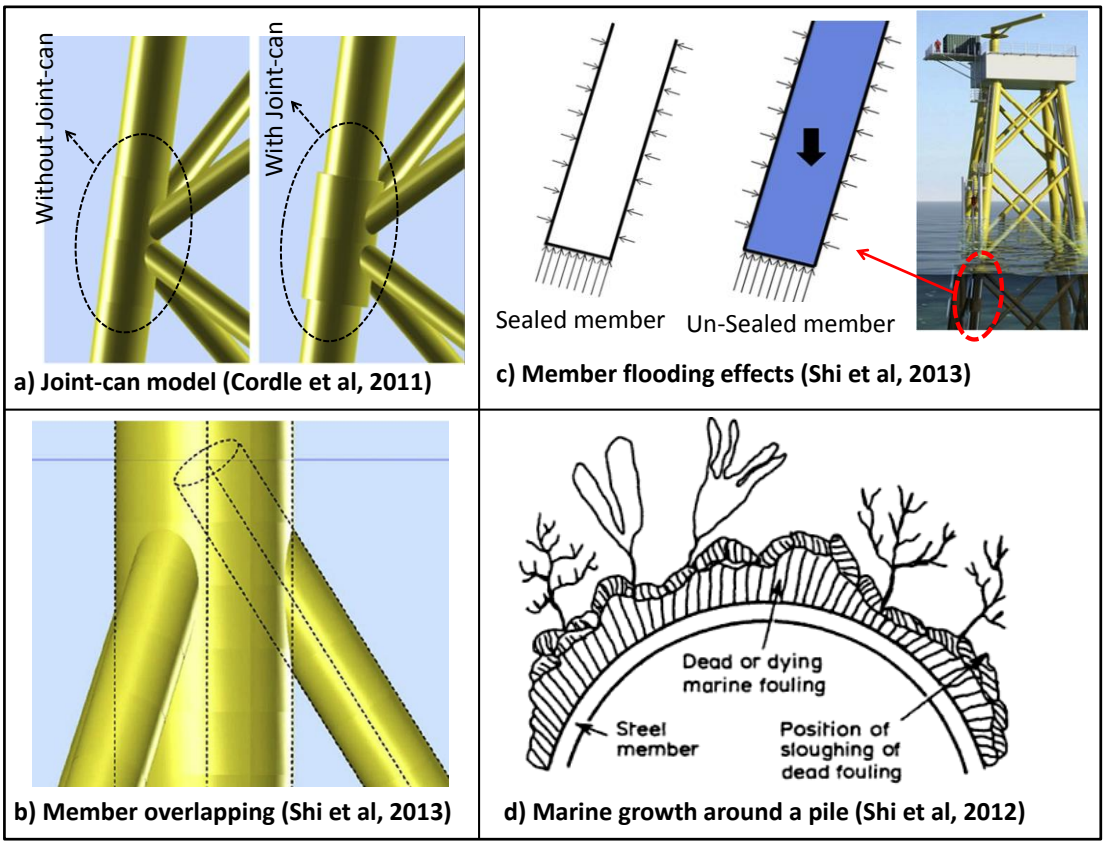

Figure 2-18. Identification of parameters affecting the dynamic response of jacket structures

Diamanti et al (2013) showed that the linear dynamic analysis provides reliable results for multi-member substructure of wind turbines. They investigated the non-linear effects due to large displacements, axial shortening caused by bending, cross-sectional transverse shear effects and etc., by performing aero-servo-hydro-elastic analysis. Diamanti et al (2013) compared the results of finite element codes which can capture nonlinear effects with output of the new linear module SubDyn, which was released by NREL (Popko et al, 2012). Results showed that the difference for the tower-top deflection and the deck displacement is less than 3%.

The "ringing" phenomenon which may occur while calculating the response of jacket structure under extreme waves was investigated by Larsen and Kim (2011). Ringing occurs normally when a large wave passes the structure causing single large impulse force which excites both low and high frequent vibrations of the structuure. They showed that the probability of ringing will increase when the incident wave period get closer to the natural frequency of the structure.

Pile-soil interactions in the foundation of jacket structures will significantly influence the natural frequency of the structure and consequently the dynamic response. For pile foundation modelling of fixed-bottom offshore structures, the non-linear behaviour of the soil become important when the structure is subject to extreme wave loads. However, in some cases, performing a non-linear analysis might decrease the computational efficiency without providing any excessive additional accuracy (e.g. long-term performance analysis). In order to achieve high computational efficiency, the following procedure can be followed for modelling of the pile foundation of fixed-bottom offshore structures:

(i) The pile foundation will be modelled linearly meaning that, the soil nonlinear effects will be initially ignored.
(ii) The maximum displacements of the linear pile foundation under extreme loads will be computed and it will be checked whether they are in the linear range.
(iii) If the maximum displacements exceed the threshold between linear and non-linear soil behaviour, nonlinear effects have to be considered to the model.

Figure 2-19 shows the key parameters for modelling of jacket substructure of wind turbines. The parameters in green colour will be considered in the model. The parameters in red will be neglected since they do not significantly influence the dynamic response of jacket structures.

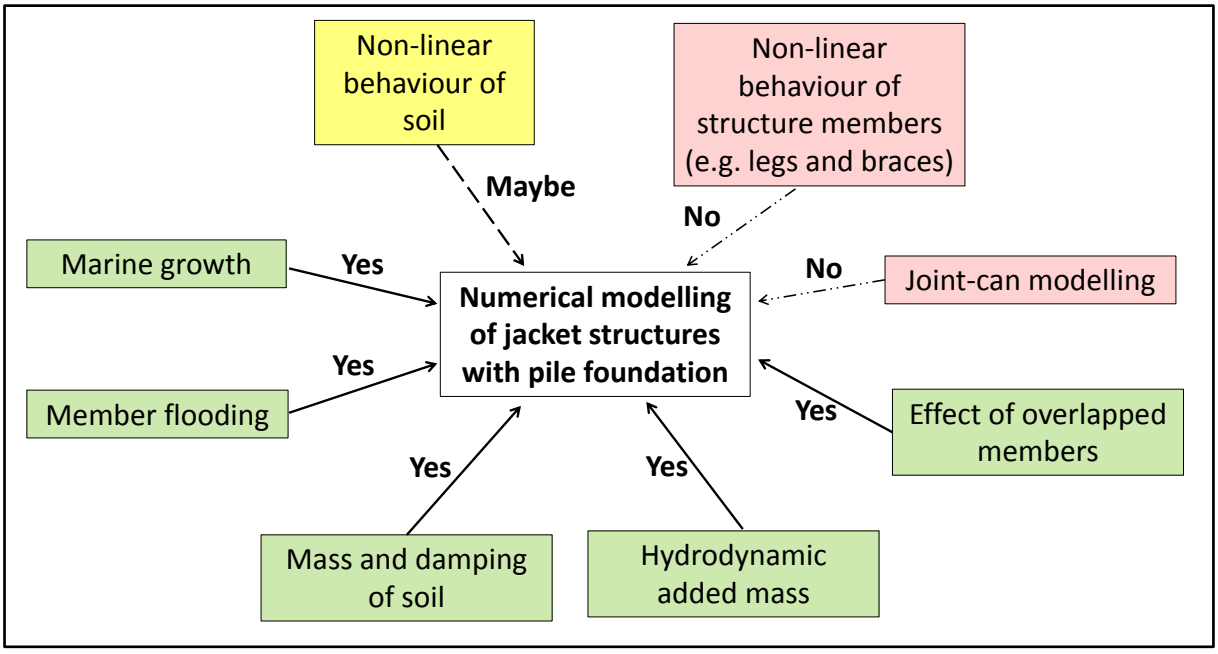

Figure 2-19. Influencing parameters for numerical modelling of jacket structures with pile foundation

2.5 Specification of objectives and methodology

Based on the results of the state of the art review and those obtained from the preliminary analysis of the available large scale experiments performed in GWK, the objectives of the PhD study tentatively formulated in Chapter 1 are specified more precisely as follows:

i. Development of physically-based and generic formulae for the prediction of slamming forces and duration due to breaking waves on jacket structures as a function of the most influencing hydrodynamic and structural parameters.
ii. Development of an approach for the calculation of total wave loads induced by near-breaking and breaking waves on jacket structures by implementing the aforementioned wave slamming formulae and the Morison equation with the wave kinematics calculated by a CFD model.
iii. Identification of the most important parameters related to the wave, structure and pile foundation affecting the dynamic response of jacket structures to extreme loads induced by breaking waves.

Figure 2-20 shows an overview of the specified methodology adopted in this study with four phases:

- *Phase 1:* As shown in this chapter, a comprehensive review and analysis of the current knowledge and models is performed in order to identify the knowledge gaps and shortcomings of the previous studies. This also includes the preliminary analysis of available large-scale tests carried out in GWK as a basis for the understanding of process involved in the interaction of waves and truss structures.
- *Phase 2:* Based on the results obtained from the analysis of the available knowledge, the necessity of proposing prediction formulae for wave slamming force on truss structures is determined. New prediction formulae for the slamming force and its duration on the front and rear legs and braces of the jacket structure will be proposed by conducting a detailed analysis of the GWK tests.
- *Phase 3:* Based on the knowledge gaps identified in Phase1, the importance of developing a technique for the calculation of total forces induced by very steep waves on truss structures is highlighted. An approach for the calculation of total near-breaking and breaking wave forces on truss structures and the corresponding total force response will be provided,
- *Phase 4:* A CFD model based on OpenFOAM will be set-up for a full scale jacket structure called ‘OC4 jacket’. The CSD model of the OC4 jacket structure will be first set-up without pile foundation, will then be extended by linear pile foundation model and finally improved by applying a non-linear soil model to the foundation. Breaking and non-breaking wave forces will be simulated on the structure according to the approach proposed in 2nd and 3rd phases. A systematic parameter study will finally be performed to identify the effect of wave, structure and pile foundation parameters on the dynamic response.

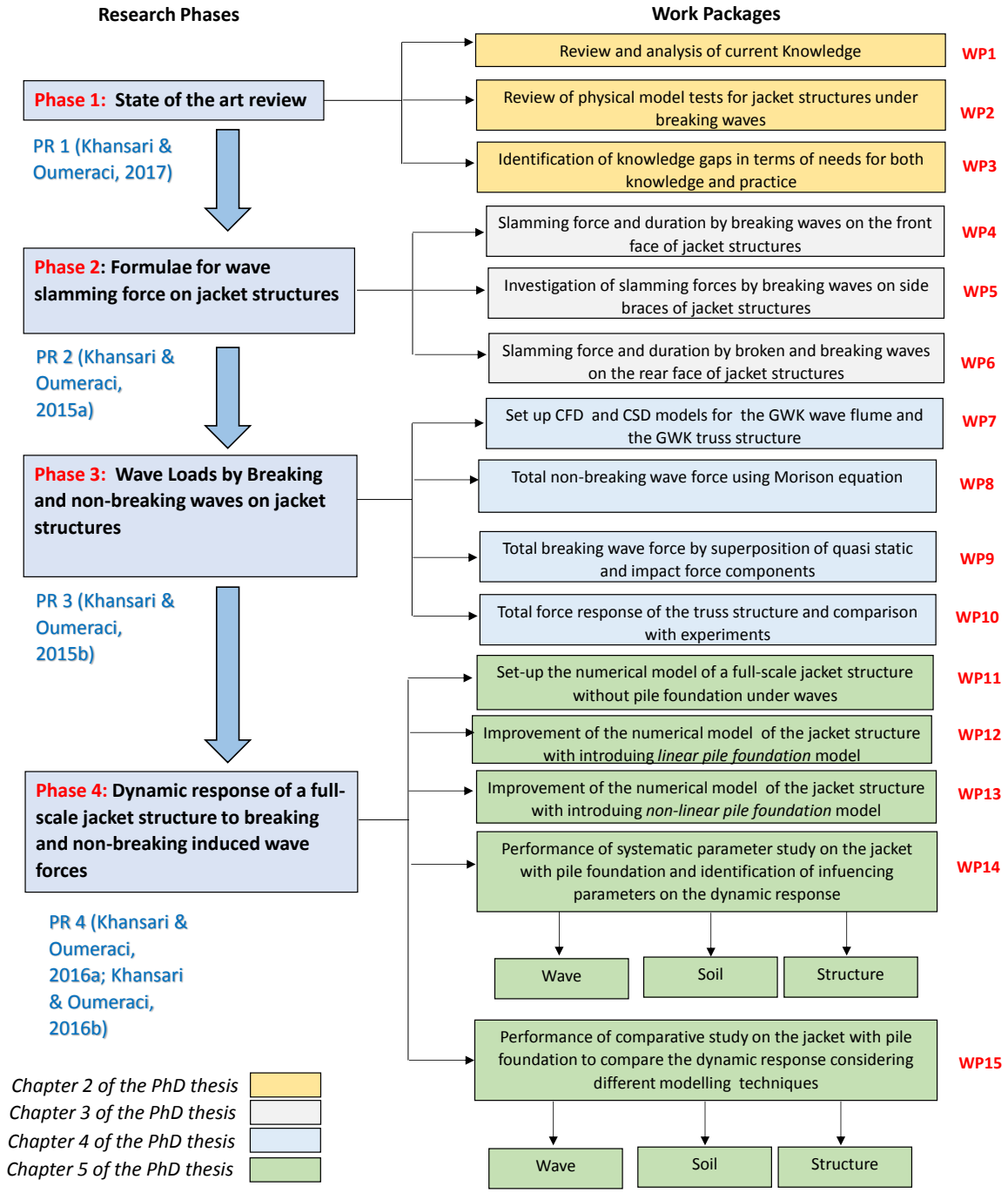

Figure 2-20. Specified methodology of the PhD study, including progress Reports PR1-PR4 for more details

3 Formulae for wave slamming force on jacket structures

While several design guidelines provide methods and formulae for the prediction of design impact loads induced by breaking waves on vertical slender piles, no guidance is available for the assessment of design impact forces on truss-type structures (e.g. GL, 2005; IEC, 2009; ISO, 2007; DNV, 2013). The investigations on breaking waves on truss structures are limited to very few small scale laboratory tests (e.g. Chella, 2012; Choi et al, 2013; Jose & Podrazka, 2014; Navaratnam et al, 2013; Navaratnam, 2013; Rausa , 2014) and none has resulted in reliable and process based model to predict the total slamming force induced by breaking waves on truss structures. The limitations of the aforementioned studies, which are related to the model set-up itself as well as to the measuring technics and the testing programme, have been recognised. To overcome these limitations new laboratory tests were performed in the large wave flume (GWK) by Arnsten & Gudmestad (2013), called hereafter "GWK tests". Based on the analysis of the data of these tests, time histories of the total impact force induced by breaking waves on the front face, the lateral faces and the rear face of jacket structures are analysed and formulae are proposed for the approximate calculation of the total force on the front face, the lateral face and on the entire jacket structure (see Figure 3-1). An investigation of the processes associated with breaking wave loads on jacket structures is performed with a particular focus on those processes involved in the interaction of a breaking wave with different structure members.

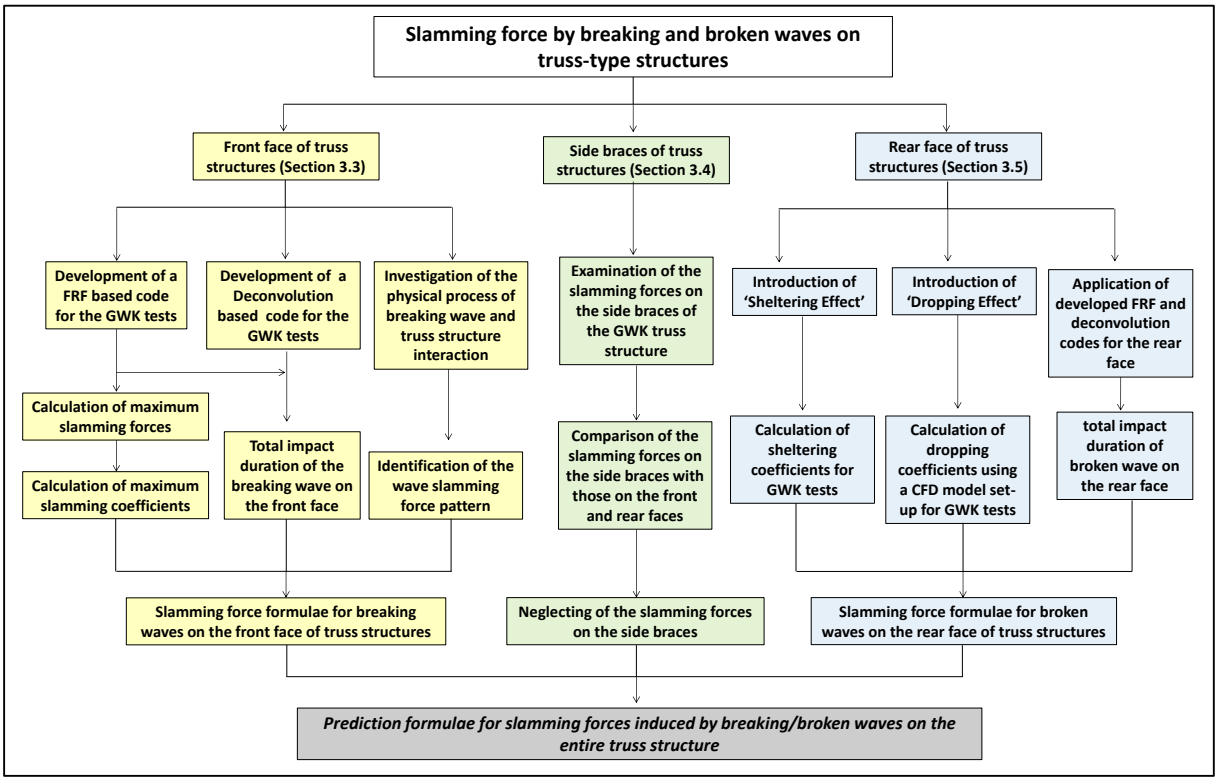

Figure 3-1. Methodology used for the development of new slamming formulae for breaking waves on truss-type structures

First, the GWK tests as well as the model set-up and the approaches for data analysis are introduced. Second, the types of wave breaking on truss structures are classified in 5 load cases according to the measurements in GWK. Third, formulae for the prediction of the impact force and duration on the front face of the truss structure are developed using a new approach by combining FRF and Duhamel's integral methods. Fourth, the slamming forces caused by breaking/broken waves on the side braces of the structure are investigated. Fifth, formulae for broken wave forces on the rear face of the truss structure are provided by introducing so-called 'dropping' and 'sheltering' coefficients. Finally, the new formulae for the total slamming force and Duhamel's integral approach are applied to reproduce selected GWK tests.

3.1 Laboratory tests in the large wave flume GWK

3.1.1 Model set-up and measuring techniques

In the previous experiments conducted in small-scale wave flumes to study breaking wave on jacket structures, several phenomena such as scale effect might significantly influence the accuracy of the experimental results as mentioned by Aashmar (2012) and Navaratnam (2013). Therefore, further experiments were performed on a jacket structure in the large wave flume (GWK) by Norwegian University of Technology NTNU and University of Stavanger (Arnsten & Gudmestad, 2013) in the frame of the WaveSlam project within the EU-HYDRALAB-programme. The main objective of these experiments on a typical jacket structure is to develop conceptual models for the prediction of the forces induced by breaking waves on jacket-type structures. The model setup of the laboratory tests performed on a jacket structure with X-braces tested in GWK is shown in Figure 3-2.

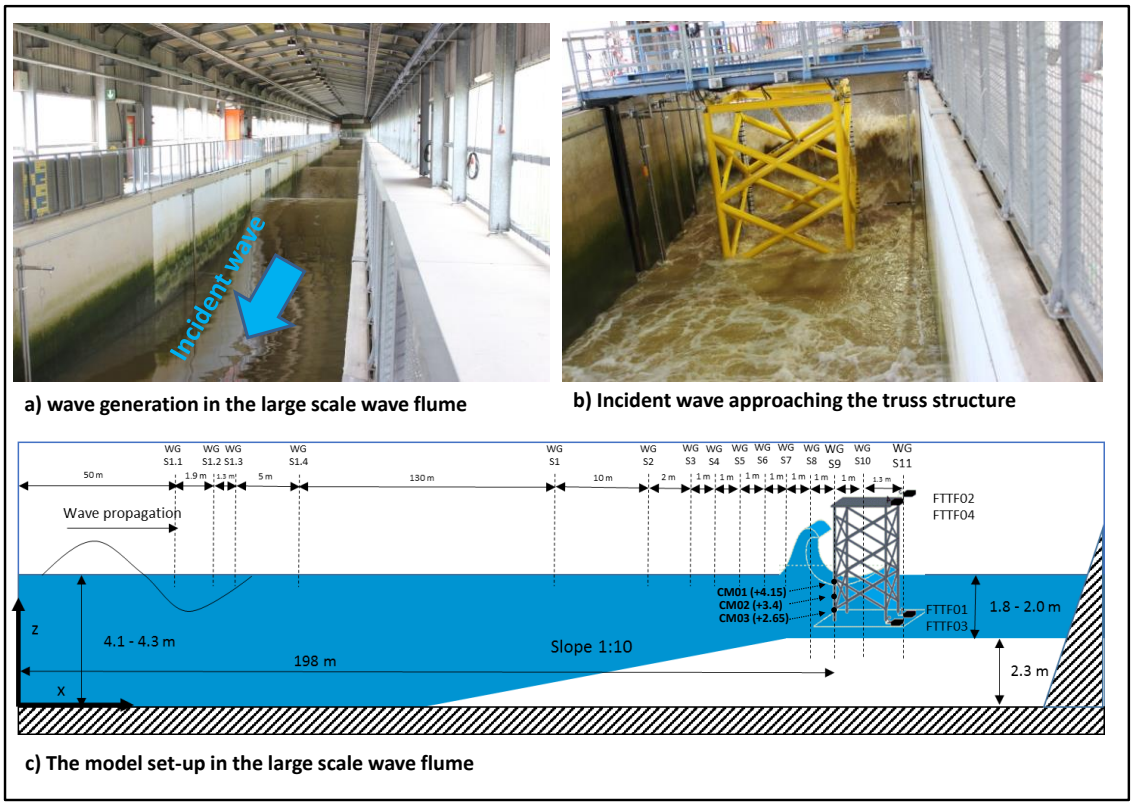

Figure 3-2. The laboratory tests performed on a truss structure in the large wave flume GWK

The large wave flume is approximately 300 m long, 5 m wide and 7 m deep. A model scale 1:8 was selected to reproduce water depths of approximately 16 m in prototype. The jacket structure was tested under irregular waves, regular non-breaking waves, plunging breakers and focused waves (breaking wave height up to 2 m and wave periods up to 6 s). 21 wave gauges were installed along the large wave flume. Since the incipient wave breaking location relative to the structure front is an important parameter affecting the slamming forces induced by breaking waves on the jacket structure, 10 closely spaced wave gauges were installed in front and next to the GWK jacket structure (WG2 to WG11 in Figure 3-2). Three velocity-meters are located at the front face of the structure in different water depths.

During the tests, a high speed camera (200 fps) and a normal camera (25fps) were used to capture the slamming events on the structure members. Both videos are synchronized with the data acquisition.

The truss structure consists of tubular members with legs and braces diameter of 0.14 meter. The connections of the members of the truss structure are rigid using penetration welding procedure. The structure is instrumented with 4 total force transducers (two at top (FTTF02 & 04) and two at the bottom (FTTF01 & 03) of the structure as can be seen in Figure 3-13d & Figure 3-2c), 10 local force transducers at the front legs and 12 XY force transducers on six different diagonal braces are installed to measure wave loads (Figure 3-3).

The jacket structure consists of tubular members with legs and braces with a diameter of 0.14 m. The connections of the members of the jacket structure are rigid using penetration welding

procedure. The structure is instrumented with 4 total force transducers (two at top (FTTF02 & 04) and two at the bottom (FTTF01 & 03) of the structure as shown in Figure 3-2 and Figure 3-3) to measure the wave force on the entire structure, and 10 local force transducers at the front legs (black sensors in Figure 3-3) and 12 XY force transducers on six different diagonal braces are installed to measure the wave forces on the individual structure members (blue in Figure 3-3).

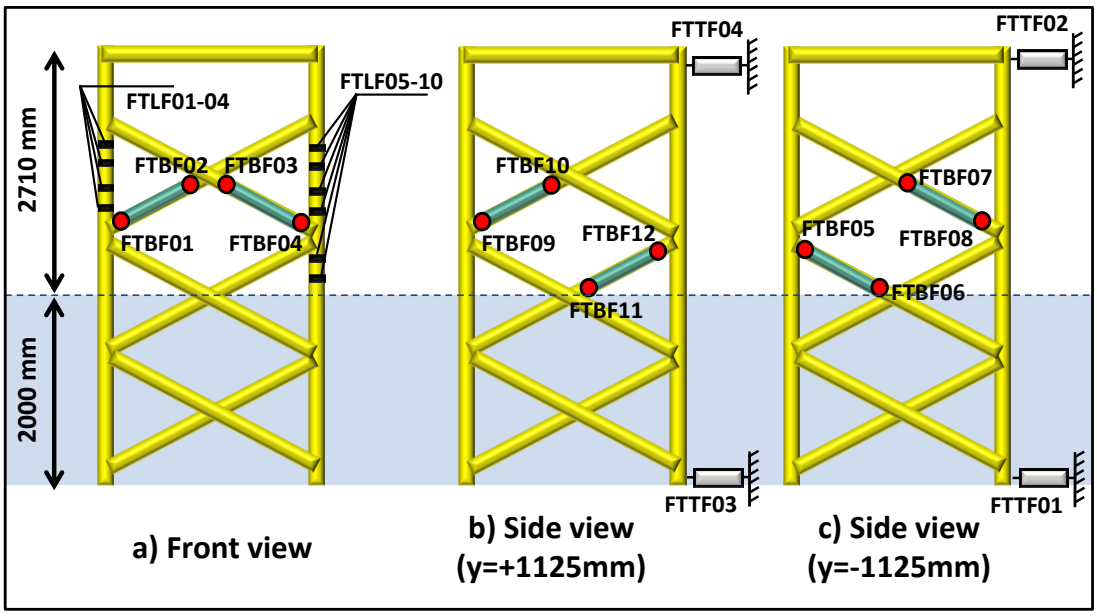

Figure 3-3. Instrumented members of the GWK jacket structure (FTBF: force transducers in braces; FTLF: force transducers in legs; FTTF: total force transducers)

The force transducers for the total force and inside the front legs were of the type S9M as shown in Figure 3-4 and Table 3-1 (total force: 20 kN at the bottom and 50 kN at the top of the truss structure).

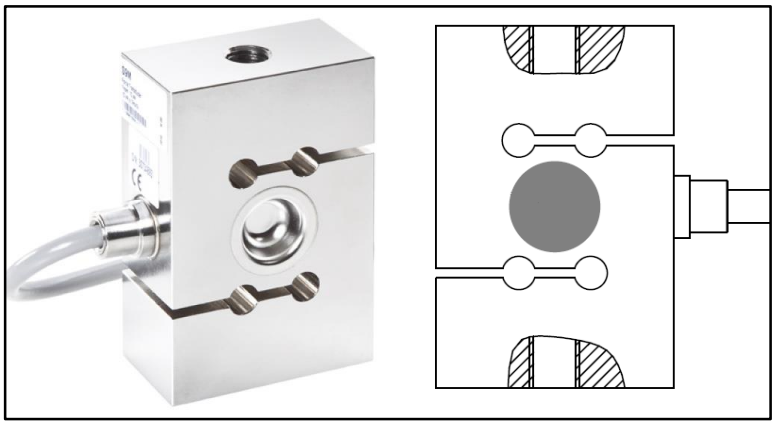

Figure 3-4. Total force transducer type S9M installed at the bottom and top of the truss structure (HBM, 2001), The transducers characteristics are given in Table 3.1.

These force transducers are suitable for measuring accurately both static/dynamic tensile and pressure forces. Table 3-1 summarizes the overall properties of the top and bottom force transducers.

Table 3-1. Total force transducers characteristics (Type of S9M)

Force transducer	*Nominal force (kN)*	*Nominal displacement (mm)*	*Accuracy class*	*Fundamental resonance frequency(kHz)*	*Maximum operational force %*	*Weight (kg)*
2 x Bottom	20	0.2	0.2	2.3	150	1.7
2 x Top	50	0.4	0.2	2.5	150	2.2

The 2D transducers for measuring the orthogonal forces on selected diagonal braces of the truss structure are special multi-component force transducers developed by Hottinger Baldwin Messtechnik GmbH. (see Figure 3-5)

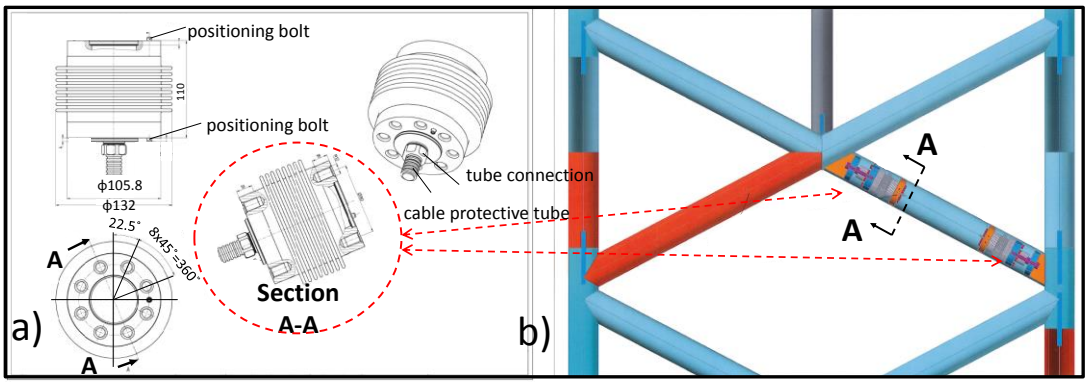

Figure 3-5. The force transducer installed in the braces of the GWK truss structure. a) Details of force transducers b) brace instrumented by the 2D orthogonal force transducer (Modified from: Vierath, 2011)

The extraction of the impact forces from the force response data measured in the lab for a truss structure is more complex than a single pile. Therefore, a new test called hereafter 'hammer test' is applied to determine a linear transfer functions in order to recover the impact forces induced by breaking waves on the truss structure. The hammer tests are carried out using two types of hammer hit on specific points on the GWK truss structure (see Figure 3-6): (i) the 1.5 kg hammer hit on the whole structure to measure the force response of the entire structure; (ii) the 0.1kg hammer hit on the local force transducers on the front face to measure the force response of each ring transducers.

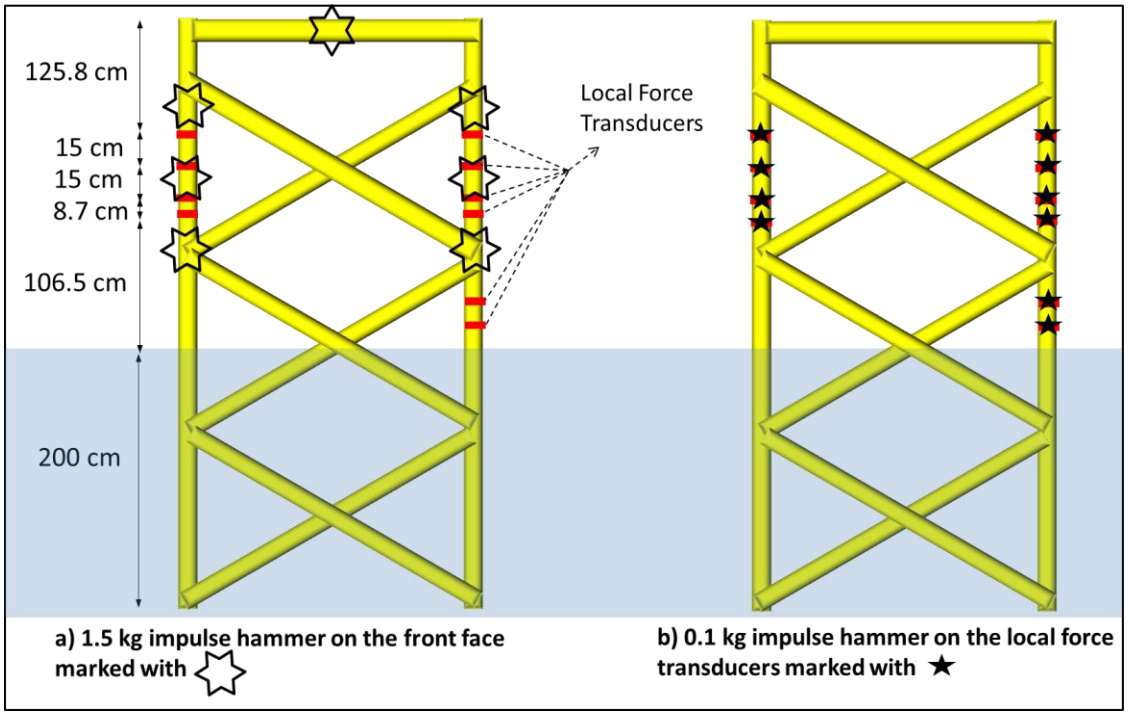

Figure 3-6. The approximate location of points on the front face of the truss structure subject to the 1.5kg and 0.1 kg hammers

3.1.2 Selected wave tests

For a proper analysis of the GWK tests and the development of a reliable generic model to predict the extreme loads induced by breaking waves on jacket structures, a broad range of wave conditions are considered. For the preliminary analysis, all wave tests conducted in the WaveSlam project are taken into account. For the ultimate detailed analysis, however, the regular wave tests in Table 3-2 are selected which might be representative for the hydrodynamic conditions tested for breaking and broken waves on the GWK jacket structure. Latter, the wave tests are classified considering the distance between the incipient wave breaking location and the jacket structure (see Figure 3-11).

Table 3-2. Selected regular wave tests for the detailed analysis to develop the total breaking wave force formulae in this study

Test No	***Wave height (H) [m]***	***Wave period (T) [s]***	***Water depth (h) [m]***	***Wave breaking location***
2013061408	1.75	4.6	4.3	*Wave breaks far in front of the structure: more than 4 m (See LC1 in Figure 3-11)*
2013061416	1.8	4.9	4.3	
2013061420	1.6	5.2	4.3	
2013061421	1.7	5.2	4.3	
2013061425	1.8	5.55	4.3	

2013061706	1.65	4.9	4.3	
2013061708	1.7	4.6	4.3	
2013061312	1.65	4	4.3	*Wave breaks far in front of the structure: between 1 to 4 m (See LC2 in Figure 3-11)*
2013061405	1.65	4.6	4.3	
2013061406	1.7	4.6	4.3	
2013061407	1.7	4.6	4.3	
2013061413	1.6	4.9	4.3	
2013061414	1.7	4.9	4.3	
2013061415	1.75	4.9	4.3	
2013061419	1.5	5.2	4.3	
2013061422	1.8	5.2	4.3	
2013061424	1.7	5.55	4.3	
2013061703	1.65	4	4.3	
2013061704	1.7	5.55	4.3	
2013061705	1.7	5.2	4.3	
2013061709	1.7	5.2	4.3	
2013061309	1.35	4	4.3	*Wave breaks at the front face of the structure (See LC3 in Figure 3-11)*
2013061310	1.45	4	4.3	
2013061311	1.55	4	4.3	
2013061313	1.6	4	4.3	
2013061402	1.5	4.6	4.3	
2013061404	1.6	4.6	4.3	
2013061423	1.6	5.55	4.3	
2013061701	1.45	4	4.3	
2013061702	1.55	4	4.3	
2013061401	1.4	4.6	4.3	*Wave breaks in the middle of the structure (See LC4 in Figure 3-11)*
2013061409	1.45	4.9	4.3	
2013061411	1.4	4.9	4.3	
2013061412	1.5	4.9	4.3	
2013061417	1.4	5.2	4.3	
2013061403	1.3	4.6	4.3	*Wave breaks behind the structure (See LC5 in Figure 3-11)*
2013061409	1.3	4.9	4.3	
2013061418	1.3	5.2	4.3	

3.1.3 Data analysis methods

The total breaking wave force (F_{Total}) including the slamming component (Figure 3-7) applied on the jacket structure is highly dynamic and can thus not be measured directly by force transducers. In fact, the recorded signals describe the dynamic response of the entire loaded system (structure with fixations and surrounding media) and might substantially differ from the actual wave load, depending on the dynamic characteristics of the loads (e,g. rise time and duration) and those of the loaded system (e,g. eigen- frequency).

For quasi-static forces ($F_D + F_M$) induced by non-breaking waves on a structure, the elastic deformation/motion at any point of the structure is proportional to the applied force. In this case, the quasi-static forces can be directly obtained by measuring the deformation/motion by strain gauges; i.e. the directly measured forces represent the actual wave loads.

For impact forces (F_S) induced by breaking waves on a structure, however, this approach does not apply. In fact, the propagation of internal stress waves within the structure must be considered, because the changes of the deformation/motion at any point of the structure differ from those of the applied impact force. Therefore, unlike in the quasi-static case, the direct measurement of the impact forces is not possible and the measured time series recorded by strain gauge-based force transducers does not represent the actual total breaking wave force ($F_{Total} = F_D + F_M + F_S$) but rather the response of the structure (with fixation and surrounding media) to F_{Total}, called hereafter "Total Force Response" (TFR) (see definition in Figure 3-7). To recover the applied impact F_S from the measured TFR, the response of the structure to the impact load, called hereafter "Dynamic Force Response" (DFR), should be extracted from the TFR. Finally, inverse analysis approaches/techniques can be applied (e.g. deconvolution technique, frequency response function, empirical mode decomposition) to recover the actual slamming force on the structure.

In this study, two inverse analysis approaches are used to recover the slamming force from the dynamic force response (DFR). The so called 'Frequency Response Function FRF' approach, which was proposed by Määtänen (1981) and used for ice impact on jacket structures, is applied here to recover the actual wave slamming force on the structure (see section 3.3.2).

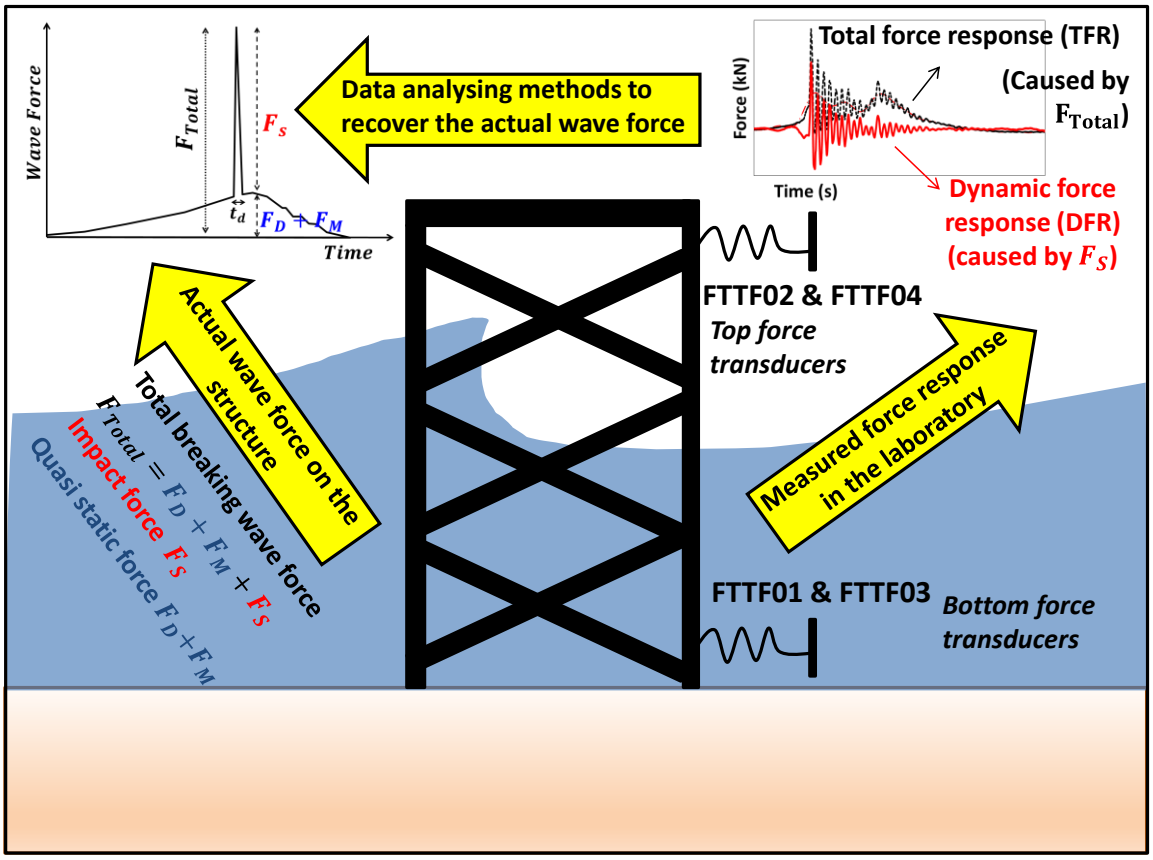

Figure 3-7. Indirect measurement of wave forces on the truss structure in the large wave flume GWK

The convolution (or Duhamel) integral method, which was previously used for single piles (e.g. Wiencke & Oumeraci, 2005), is applied to calculate the dynamic force response DFR of the truss structure (see section 3.3.1). Later, both approaches are combined in order to calculate the total duration of the impact force (see 3.3.4).

Laboratory tests on a truss structure subject to breaking and non-breaking waves in the large wave flume GWK are used. The structure is instrumented with 12 two-dimensional force transducers to measure the orthogonal forces in the front and side braces, 10 local force transducers to measure wave induced forces at the front legs and 4 total force transducers to measure the total force response TFR of the structure to breaking and non-breaking waves. Hammer test is performed to obtain the natural frequency of the structure and to determine a linear transfer function. The actual slamming force (time series) caused by breaking waves on the GWK truss structure will be recovered from the measured TFR in the laboratory using two inverse analysis approaches: (i) Convolution integral method; (ii) Frequency Response Function FRF method.

3.2 Classification of wave loads on jacket structures

In the analysis of the data from the GWK tests on a truss structure under breaking, near breaking and non-breaking waves, a brief examination of the results revealed that the slamming wave force applies not only on the front face of the truss structure but also on its rear face.

The slamming force on both faces is significantly affected by the distance between the location of incipient wave breaking and the truss structure. In order to roughly estimate the location of incipient wave breaking, the records from the wave gauges just in front of, at and inside the truss structure in Figure 3-8 are comparatively examined. The structure is supported by four force transducers (strain gauges) two at the top (FTTF02&04) and two at the bottom (FTTF01&03) of the structure. The figure shows the simple model of the GWK truss structure with two springs and two dashpots.

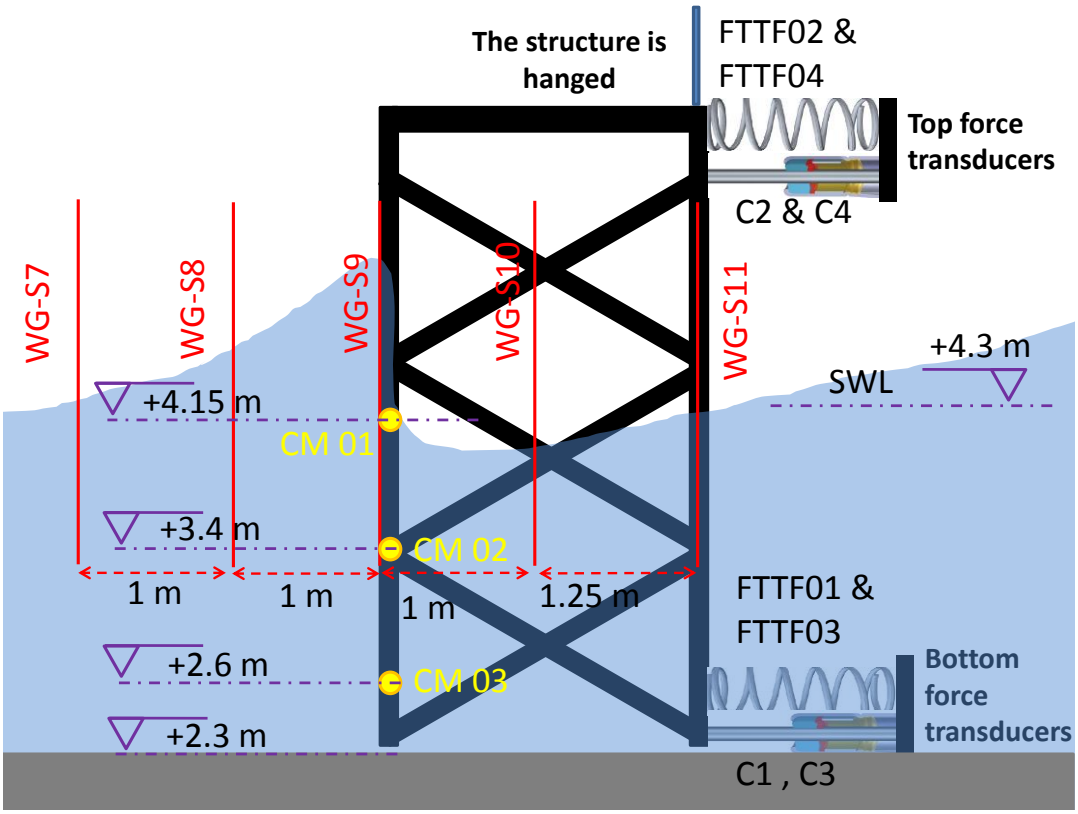

Figure 3-8. Simplified model of GWK truss structure under a breaking wave

In this section, the different types of wave breaking on the GWK structure and the resulting total force response of the truss structure are examined. In each case, the TFR of the structure is calculated by summing the force responses of all four force transducers (FTTF01-04 (Figure 3-8).

3.2.1 Types of incident waves on the GWK truss structure

In this section, different types of incident waves on the GWK truss structure are examined and classified by considering the distance of the incipient wave breaking location from the structure. In fact, the slamming forces on the front and rear face of the structure is significantly affected by the relative location of the incipient wave breaking and the structure. Table 3-3 shows different types of incident waves on the truss structure.

Table 3-3. Types of incident waves on the GWK truss structure

Type	***Incipient wave breaking location relative to the structure***	***Wave shape on the Front Face***	***Wave shape on the Rear Face***
1	Far in front of the structure	Breaking/Broken wave	Broken wave
2	In front of the structure	Breaking wave	Broken wave
3	At the front fact of the structure	Breaking wave	Breaking wave
4	In the middle of the structure	Near-breaking wave	Breaking wave
5	Behind the truss structure	Non-breaking wave	Near breaking wave

For each type of incident wave listed in Table 3-3, the *water surface elevation* and the *total force response* (TFR) of the truss structure is plotted and discussed below.

Water surface elevation

The highest wave crest occurs at incipient wave breaking and the wave crest height decreases then gradually (see Figure 3-26). Therefore, the records from the five wave gauges in Figure 3-26 are used to identify roughly the location of incipient wave breaking, resulting in the following five cases:

(i) *Wave breaks far in front of the structure (Type 1):* The incipient wave breaking locations forms far in front of the structure. Afterwards, the wave crest height decreases and the breaker tongue over-turns in front of the structure. (Figure 3-9a)

(ii) *Wave breaks in front of the structure (Type 2)*: The highest and steepest wave crest during the wave propagation is observed in front of the structure where the incipient wave has reached its critical steepness. Afterwards the wave crest height decreases gradually approaching the front face as shown in Figure 3-9b.

(iii) *Wave breaks at the front face (Type 3)*: The highest wave crest height is measured by the wave gauge located at the front face (WG-09). The incipient breaking wave strikes the front face of the structure with its highest wave crest meaning that the incipient wave breaking location is at the front face of the GWK truss structure (See ure 3-9c).

(iv) *Wave breaks in the middle of the structure (Type 4)*: The incipient wave crest height increases gradually until it breaks in the middle of the structure. The wave crest drops at S10 meaning that the wave is broken in the middle of the structure. (see ure 3-9d)

(v) *Wave breaks behind the structure (Type 5)*: As can be seen in Figure 3-9e the wave crest height increases consecutively representing the shoaling phenomenon for the in-

cident wave. The breaker tongue forms behind the rear face of and the wave drops after it passes the structure.

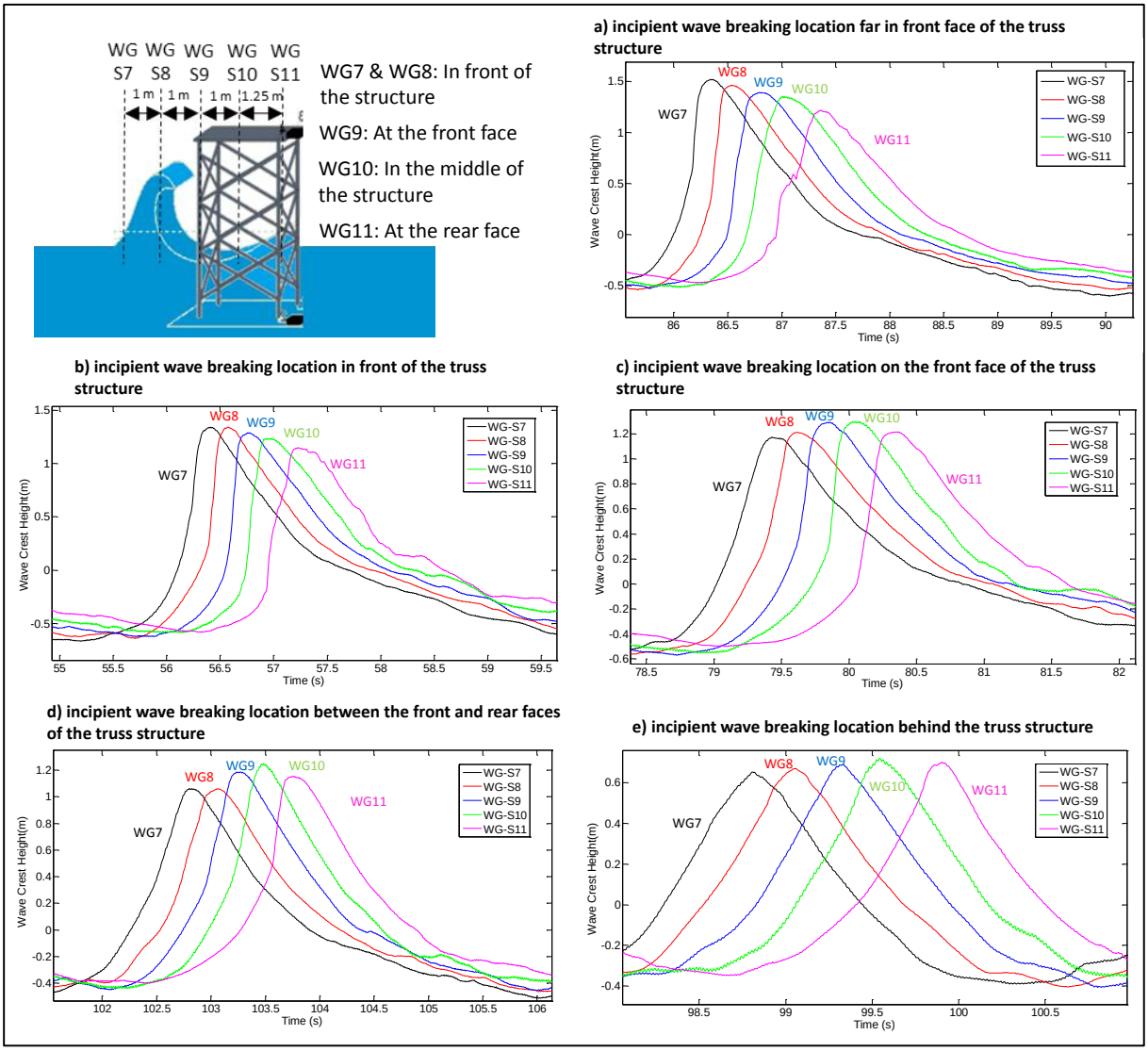

Figure 3-9. Water surface elevation for the incident wave close to the truss structure for: a) Test No. 2013061416 (H=1.8m; T=4.9s); b) Test No. 2013061421 (H=1.7m; T=5.2s); c) Test No. 2013061402 (H=1.5m; T=4.6s); d) Test No. 2013061707 (H=1.35m; T=4.6s); e) Test No. 2013061305 (H=1.1m; T=3s)

Total Force Response (TFR)

The following types of total force responses (TFR) of the truss structure to the incident waves (as classified above) were obtained from the records of the four transducers and are plotted respectively with the record of the corresponding wave gauge in Fig. 3.9:

(i) *Wave breaks far in front of the structure (Type 1)*: The wave is a broken wave with a foamy wave front due to the mixture of entrapped air and the mass of water. As the wave is over-curled, two impact forces by the wave breaker tongue and the wave

breaker tail will be applied on the front face of the truss structure and this may cause complex signals recorded by the force transducers. The wave loads by broken waves on the rear face of the truss structure are much less than those forces due to broken wave on the front face.

(ii) *Wave breaks in front of the structure (Type 2)*: The highest values of the total force response of the truss structure are measured to this type of breaking wave. The total force responses may change significantly, showing that breaking wave load on the truss structure is highly complex. As can be seen in Figure 3-10a, the breaking wave force is applied not only on the front face of the truss structure but also on the rear face. Two peaks are depicted in the TFR of the structure: the first peak is induced by the breaking wave on the front face and the second peak by the broken wave on the rear face. The analysis of the available data from the experiments shows that in this particular load case, the slamming force on the rear face of the truss structure is not as high as in the other load cases. The main reasons are: (a) the long distance between the incipient wave breaking location and the rear face of the structure and (b) the sheltering effect due to breaking wave impact on the front face of the truss structure.

(iii) *Wave breaks at the front face (Type 3)*: The total force response TFR due to breaking wave on the front face is lower than the case when the wave breaks far in front of the truss structure. However, the relative values of the impact force on the rear face to those on the front face of the truss structure are higher than in the other load cases. The analysis of the response of the GWK truss structure to this breaking wave type revealed that higher impact forces are applied on the rear face of the truss structure compared to the previous load cases. As can be seen in Figure 3-10b, two clean cut peaks are observed for this load case. The first and second peaks are related to breaking and broken wave impact on the front and rear face of the truss structure, respectively. The second peak is important and should be considered, when wave breaks directly at the front face of the truss structure.

(iv) *Wave breaks in the middle of the structure (Type 4)*: The results show that although the incident wave breaks within the structure, a considerable impact force is applied on the front face of the truss structure (see Figure 3-10c). The dynamic force response (DFR) of the structure changes according to the incipient wave breaking location within the structure. The higher the distance between the incipient wave breaking location and the front face, the higher is the dynamic force on the rear face and the lower it is on the front face of the truss structure.

(v) *Wave breaks behind the structure (Type 5)*: The applied force on the GWK truss structure may be considered as quasi-static force and is equal to the total force response TFR of the structure since no impact load is applied on the structure. A typical total force response TFR of the structure for this load case is shown in Figure 3-10d. In this case, Morison formula provides a good estimation of the total wave load on the structure.

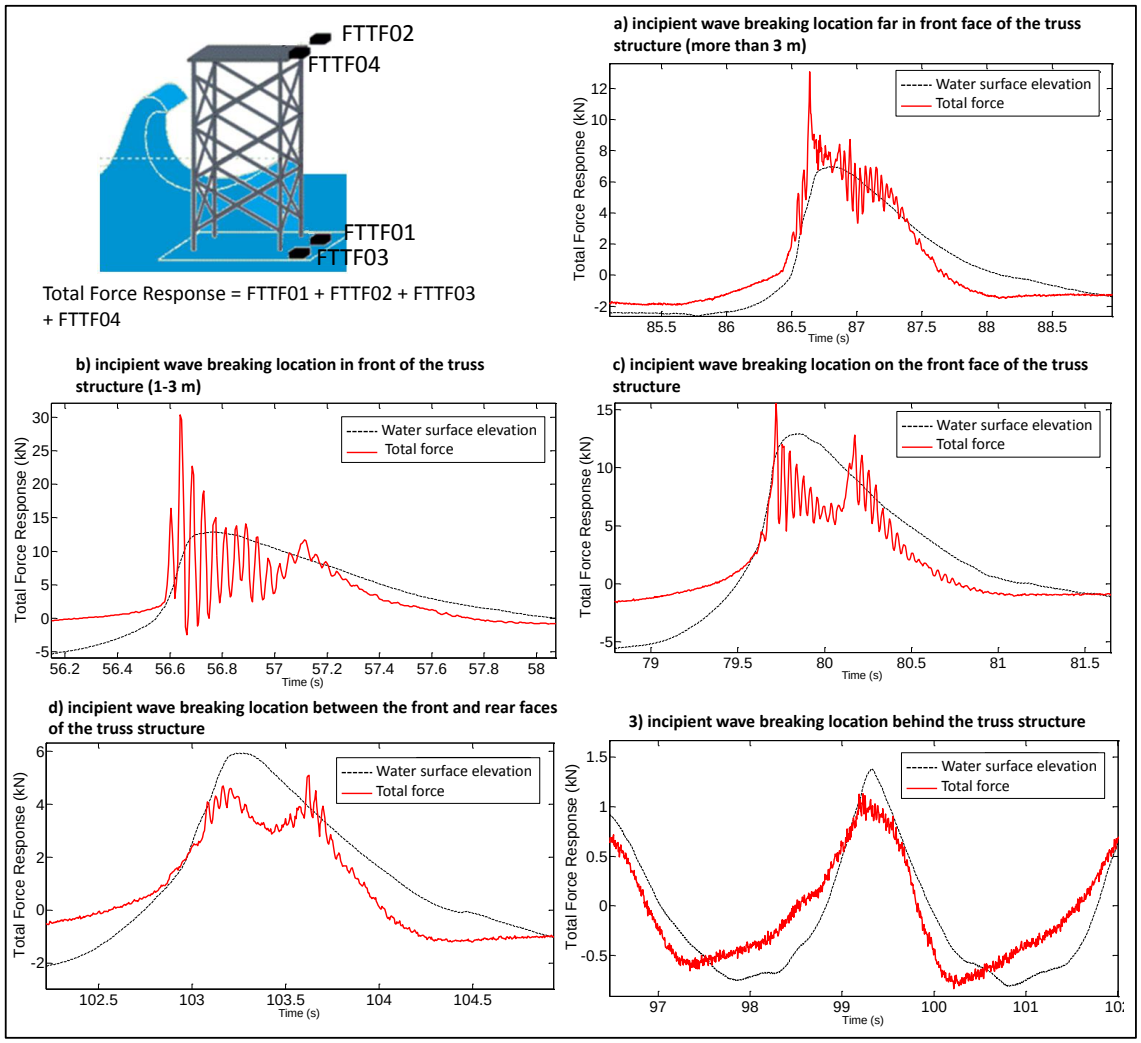

Figure 3-10. Total Force Response TFR of the GWK truss structure for: a) Test No. 2013061416 (H=1.8m; T=4.9s); b) Test No. 2013061421 (H=1.7m; T=5.2s); c) Test No. 2013061402 (H=1.5m; T=4.6s); d) Test No. 2013061707 (H=1.35m; T=4.6s); e) Test No. 2013061305 (H=1.1m; T=3s)

3.2.2 Classification of wave loads on jacket structures

The process involved in the interaction between breaking waves and truss structure is very complex. The investigation of the data from the GWK laboratory experiments revealed that the type of loading is significantly affected by the distance between incipient wave breaking location and the truss structure. Moreover, the ratio of the second impact on the rear face to the first impact on the front face changes according to the type of wave breaking on the front face of the truss structure. Therefore, five load cases (LC) are defined in order to investigate these highly complex interaction processes (see Figure 3-11). In general, the distance between the incipient wave breaking location and the rear face of the truss structure is decreased from load case 1 to load case 5. The classification is performed based on the observations of the waves (wave gauges WG7-11 near/inside the GWK truss structure and video records) and the analysis of the total force responses (TFR) caused by different breaking waves on the front and rear faces of the truss structure.

Loading Case	Definition Sketch	Experiments	Description	Schematic Signal
Load Case 1 Wave breaking far in front of the structure	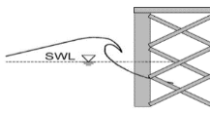		*Breaker tongue impinges the structure when reaching the trough →broken wave at the structure*	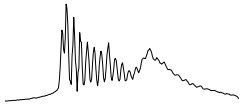
Load Case 2 Wave breaking in front of the structure	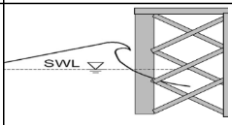	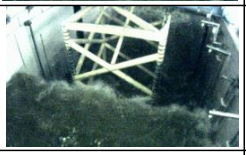	*Breaker tongue inclined →breaking wave at the structure*	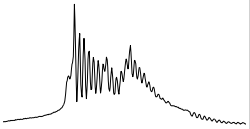
Load Case 3 Wave breaking just at the structure	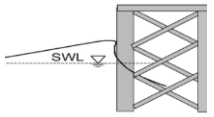		*Breaker tongue formed at the front face →partial breaking wave*	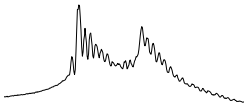
Load Case 4 Wave breaking within the structure	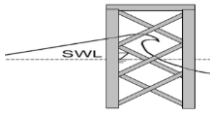		*Breaker tongue formed between the first and the second face of the truss structure →partial breaking wave*	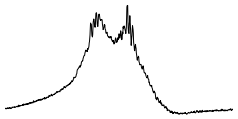
Load Case 5 Wave breaking behind the structure	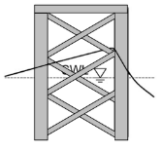		*Breaker tongue formed behind the structure →non-breaking wave*	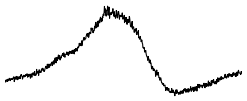

Figure 3-11. Classification of different loading cases on truss structures

The total force responses (TFR) of the truss structure recorded in the GWK tests are characterised by two peaks. The first peak is assigned to the breaking wave impact on the front face of the truss structure. The second peak is caused by the wave, which reaches the rear face as a broken wave.

The incipient wave breaking location is identified using the wave gauges installed near and inside the truss structure and the video records of each experiment. The classification of the breaking waves on the GWK truss structure is performed based on the incipient wave breaking location considering the force response (TFR & DFR) of the structure. Five load cases (LC) are identified:

(i) LC1: the wave breaks far (more than 3m) in front of the structure, so that the breaking wave force on the rear face of the structure is not significant;

(ii) LC2: the wave breaks (1-3m) in front of the structure and induces an extreme impact force on the front face of the jacket structure;

(iii) LC3: the wave breaks just at the front face. The total impact force on the front face is lower than in LC1 & LC2, but the relative values of the breaking wave force on the rear face to those on the front face of the truss structure are higher than for LC1 & LC2;

(iv) LC4: the wave breaks between the front and rear faces of the structure. Although the incident wave breaks within the structure, there is a significant impact force on the front face of the truss structure.

(v) LC5: the wave breaks behind the structure, so that only quasi-static forces are induced on the truss structure.

3.3 Wave slamming force formulae on the front face of jacket structures

While the processes and resulting slamming force magnitude and duration on the side braces and rear face of the jacket structure will be addressed respectively in sections 3.4 and 3.5, in this section, only the processes associated with breaking wave impact on the front face of the structure are addressed and formulae for the resulting parameterized slamming force time history are determined.

3.3.1 Convolution integral method for the GWK truss structure

A convolution integral method based code is developed in order to calculate the dynamic force response (DFR) of the structure to an impact load and to recover the impact load from the DFR. Figure 3-12 shows the process to identify the impact force from the DFR of the structure considering the structural properties. Based on (i) the dynamic force response DFR of the structure obtained by extraction of the signal from the measure total force response TFR, (ii) the truss structural properties as well as the natural frequency, total mass and structural damping, (iii) the total impact duration t_d and the slamming force load pattern as input information, the actual time series of the slamming force is recovered by applying the Duhamel's integral method considering the measured response in the experiment. Finally, the DFR of the truss structure is reproduced using the recovered slamming force.

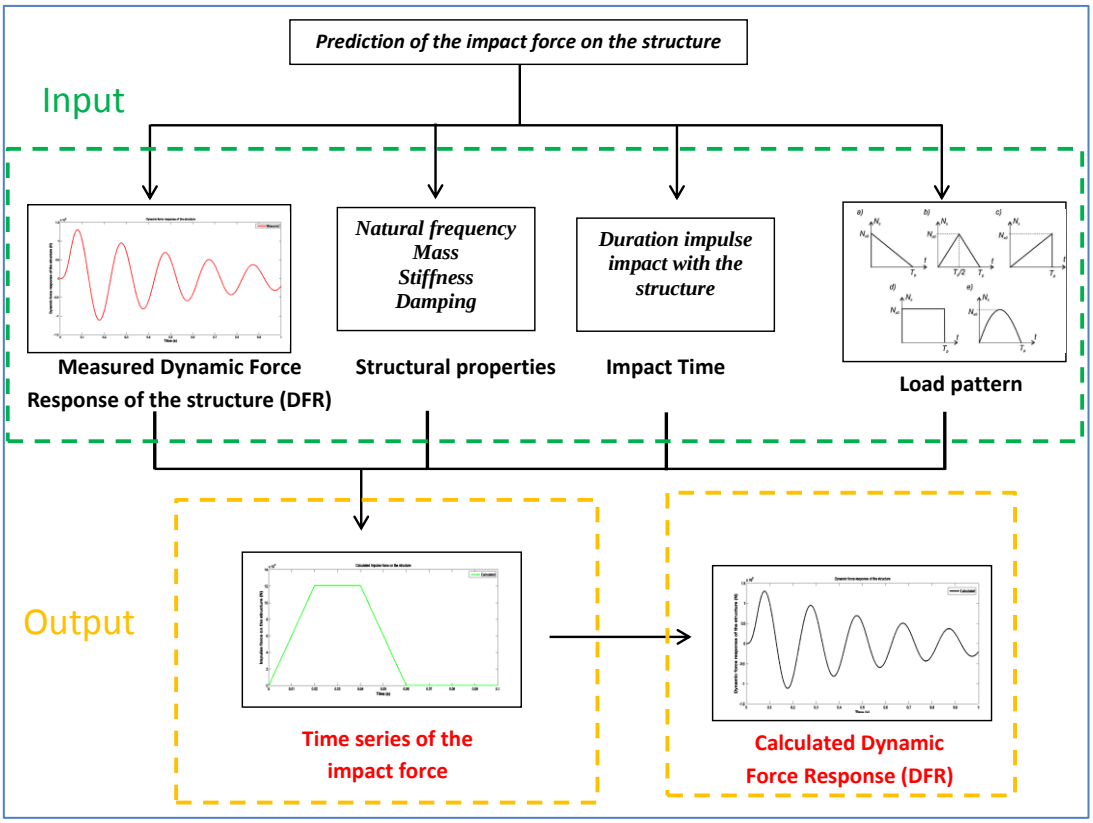

Figure 3-12. Procedure for the determination of the impact force from the measured dynamic force response (DFR) of the truss structure (shown exemplary for a the hammer tests)

In order to validate the developed code with the GWK experiments, the data from the hammer tests on the same truss structure are used. In fact, the total force response of the structure (TFR) to the hammer impulse consists only of a DFR without any quasi-static component. The natural frequency of the entire truss structure and its single members is determined by using two different hammers with 1.5 kg and 0.1 kg. Figure 3-13 shows the impact force of the 1.5kg hammer, which is measured directly at the hammer tip (Figure 3-13a) and the corresponding DFR of the GWK truss structure (Figure 3-13c). The TFR recorded by the top and bottom force transducers installed at the structure (Figure 3-13d) is characterised by damped oscillations, which are typical for the free vibrations caused by an impact force. The latter signal is fully different from the actually applied impact force in Figure 3-10a since it also includes the response effects of the loaded structure and the force transducer.

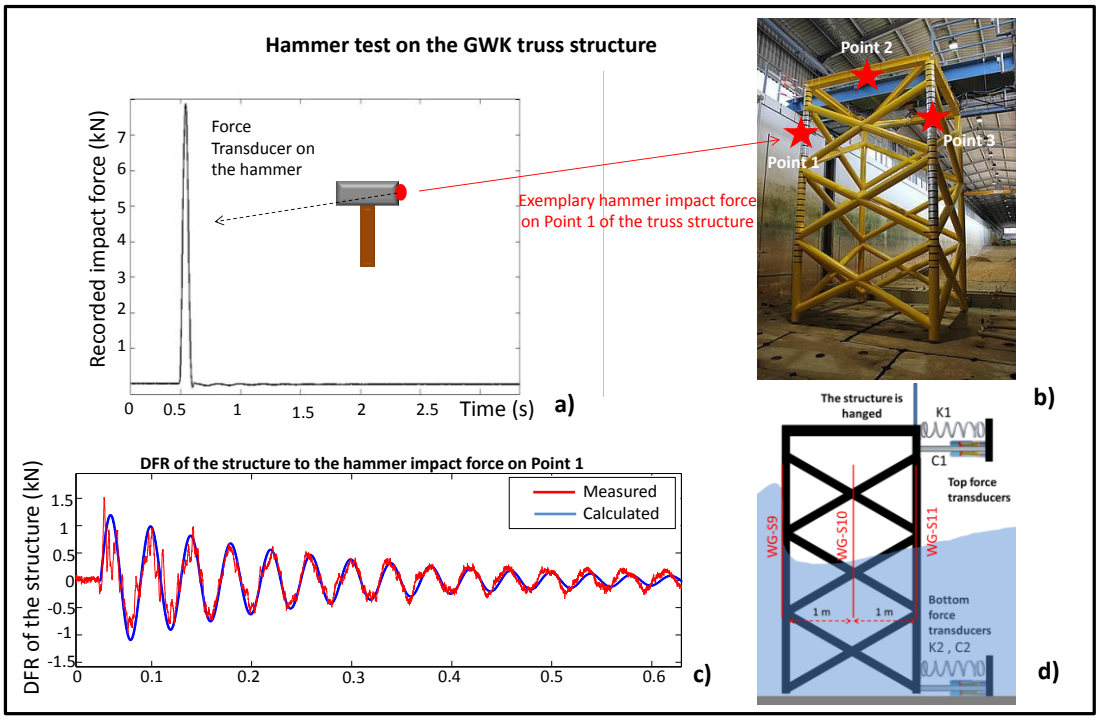

Figure 3-13. Impact hammer force at Point 1 (see) on the GWK truss structure a) measured hammer impact force b) hammer impact locations on the GWK truss structure, c) measured and calculated dynamic force response (DFR) of the truss structure to hammer impact at Point 1, d) top and bottom total force transducers installed at the structure.

The convolution integral based code is applied to reproduce the DFR of the GWK truss structure under the hammer impact force shown in Figure 3-13a. The latter, together with the structural properties of the GWK truss structure such as natural frequency (24.5 Hz) and total estimated mass (1700 kg), are the input to the code. As illustrated in Figure 3-13c, the calculated DFR reproduces the measured DFR very well.

3.3.2 Frequency Response Function method for the GWK truss structure

The total forces obtained from the sum of the signals recorded by the total force transducers FTTF01-04 (Figure 3-20c) on the truss structure subject to breaking/broken waves represent the total force response (TFR) of the structure and cannot be considered as the actually applied total impact force on the structure. Therefore, the actual slamming force is recovered from the measured TFR by applying the frequency response function (FRF) method. For this purpose, four steps are required (Fig. 3.14):

(i) the DFR is extracted from the TFR using low filter analysis.
(ii) the spectrum of the DFR, Sf(ω), is calculated using Fast Fourier Transformation (FFT);
(iii) the calculated spectrum is divided by the transfer function H(ω) obtained from the hammer test in GWK:

$$H(\omega) = \frac{S_{DRF,Hammer}(\omega)}{S_{Hammer}(\omega)} \quad (3\text{-}1)$$

where $S_{Hammer}(\omega)$ is the fast Fourier transform of the hammer impact force measured directly by a force transducer at the hammer tip (Figure 3-13a) and $S_{DRF,Hammer}(\omega)$ is the fast Fourier transform of the DFR of the structure to the actually hammer applied force (Figure 3-13c).

(iv) the slamming force actually induced on the structure by breaking/broken waves is calculated using the inverse Fourier Transform (IFFT) of (Sf(ω)/H(ω)).

The FRF method illustrated in Figure 3-14 is exemplarily applied for wave test number 2013061424 where the highest response of the structure to a breaking wave impact was recorded.

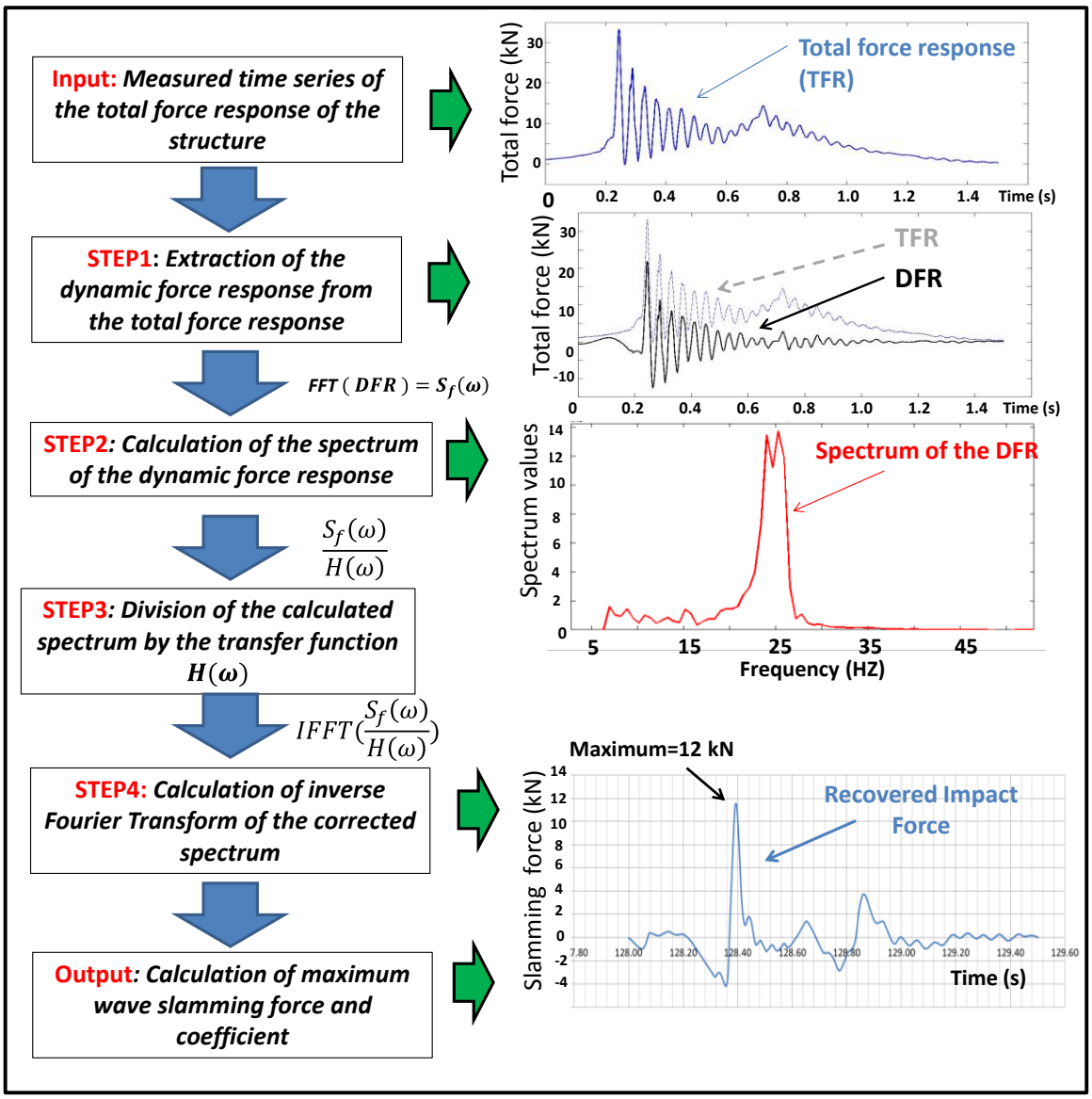

Figure 3-14. Frequency Response Function (*FRF*) method to extract the actual wave slamming force from measured total force response (TRF) (Test no. 2013061424, H=1.7m; T=5.55s)

3.3.3 Wave slamming force pattern on jacket-type structures

Currently, the available methods provided for mono-pile structures are adopted for the calculation of the maximum slamming force on the front face of jacket structures, in which the total maximum wave slamming force on the front face might be predicted by summation of slamming forces on each cylindrical member of the structure within the impact area. The application of the available formulae developed for single slender cylinders to truss structures (e.g. Wienke & Oumeraci, 2005), would result in a large overestimation of the peak of the slamming force as compared to that obtained by the FRF method. Table 3-4 shows the maximum slamming force on the front face of the GWK truss structure caused by a breaking wave with a height of 1.7 m and a period of 5.55 s in a water depth of 4.3m (Test no. 2013061424). The total slamming force on the front face is calculated using conventional models for single piles and results are compared with the measurements in the GWK. It is noteworthy that the impact duration is a crucial parameter, which must always be considered together with the force magnitude. Therefore, later, the Duhamel's integral method is employed to calculate the impact duration because the FRF method, which is used to calculate the magnitude of the impact force, fails to estimate accurately impact duration. While the processes and resulting slamming force and duration on the side braces and rear face of the truss structure will be addressed respectively in sections 3.4 and 3.5, in this section, only the processes associated with breaking wave impact and the resulting slamming force and duration on the front face of the structure are addressed.

Table 3-4. Total wave slamming force on the front face of the GWK truss structure using different slamming force models (Test no. 2013061424 with H=1.7 m, T=5.55s and h=4.3m)

Slamming force model	η_b***(m)***	$\lambda\eta_b$ ***(m)***	***Maximum slamming force on the front face (kN)***	***Maximum slamming coefficient on the front face***	***Impact duration on the front face (see Table 3-6)***
This study	1.44	0.66	12.0	1.63	0.0209
Goda (1966)		0.58	21.6	π	0.0135
Wienke & Oumeraci (2005)		0.66	49.7	2π	0.0055
Campbell-Weynberg (1980)		0.72	44.3	5.15	0.0050

This inconsistency is basically due to differences in the physical process involved in the interaction of breaking waves with the much more complex frame structure composed of different members as shown in Figure 3-15 and Figure 3-16. Therefore, the formulae by Wienke and Oumeraci (2005) and further formulae developed (Table 1) for the impact force and duration on single cylindrical piles cannot be readily applied for truss structures.

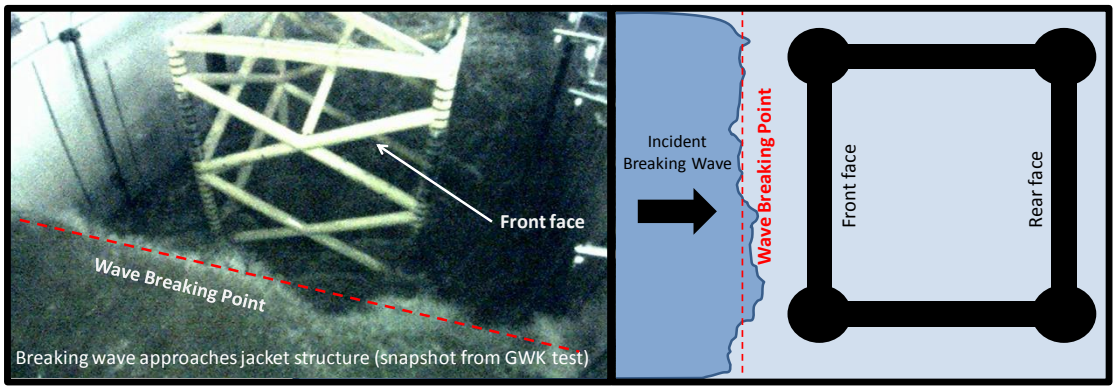

Figure 3-15. Breaking wave on the truss structure in GWK just before impact on the different structure members

As can be seen in Figure 3-15, the water particles in the broken wave crest do not reach the front face of the truss structure at the same time, which may result in several (successive) local impact forces on the legs and braces within the impact area at slightly different times. Figure 3-16 shows the successive impacts of a breaking wave on the front face of the truss structure. The total slamming force caused by the breaking wave on the front face of the truss structure can be calculated by linear superposition of the local impact forces, which might result in lower total slamming force and higher total impact duration compared to the case in which all local impacts are applied simultaneously. As will be shown in section 3.5, this process is even more critical for broken wave impact on the rear face of the truss structure as the broken wave crest asymmetry may be increased and the wave celerity might decrease after it hits the front face of the structure.

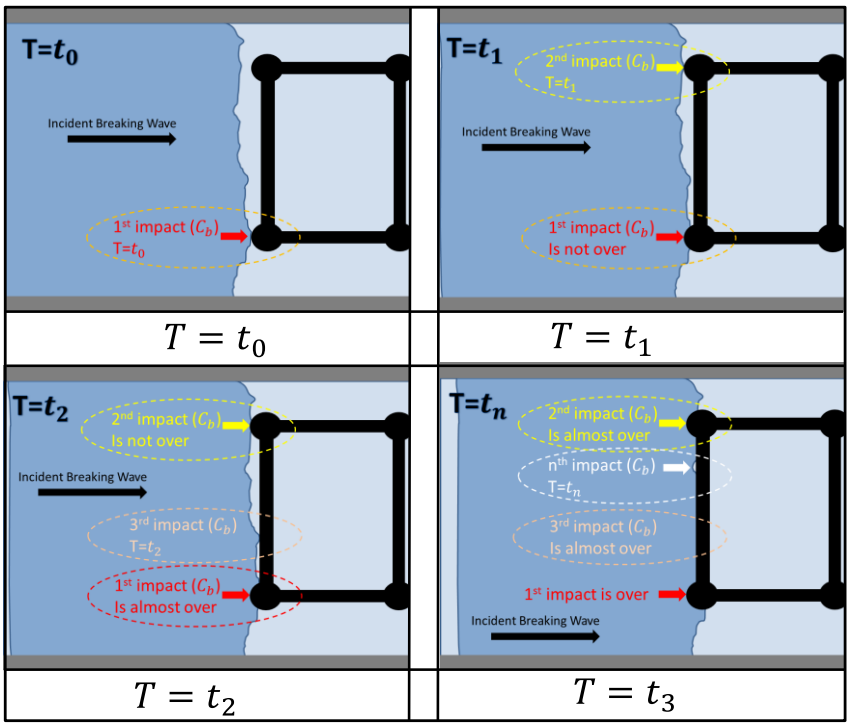

Figure 3-16. Successive local impacts induced by a breaking wave on the front face of the GWK truss structure

Considering the total impact force on the entire jacket structure, it is clear that its total impact duration t_d is much larger than the duration $(t_n - t_{n-1})$ of each local impact force. Therefore, the shape of the time history of the breaking wave impact force on a jacket structure is expected to basically different from that obtained for a single cylindrical pile.

For the front face of the structure, this total force-time function may be obtained by superposing the local impact forces on the exposed braces and legs of the front face with a total exposed length L_{tot} using the following six steps (Figure 3-17):

(i) The total exposed length l_{tot} of the jacket structure to a breaking wave is calculated using the following expression (Step 1 in Figure 3-17):

$$l_{tot} = 2\,\lambda\,\eta_B\left(\frac{1+\sin\theta}{\sin\theta}\right)$$

where λ is the curling factor which is considered 0.46 according to Wienke & Oumeraci (2005), η_B is water surface elevation at the front face of the jacket structure and θ is the angle between jacket's braces and the horizontal plane (roll angle of the member)

(ii) The total exposed length l_{tot} is discretized in a specific number of equal cells (N_L) where the length of each cell (δL) can be defined using the following expression (Step 2 in Figure 3-17):

$$\delta L = \frac{l_{tot}}{N_L}$$

(iii) The time series of the slamming force on each cell is obtained using Wienke & Oumeraci's model (Step 3 in Figure 3-17).

(iv) The induced impact forces on the mentioned cells are uniformly distributed over the total impact duration t_d (Step 4 in Figure 3-17).

(v) The actual total force history is calculated by superposing the distributed impact forces over the total impact duration (Step 5 in Figure 3-17).

(vi) The smoothed time history function of the total slamming force on the jacket structure is obtained (Step 6 in Figure 3-17).

The superposition of all these local forces in Figure 3-17 by considering the relatively short time lags results in a basically different shape (trapezoidal) of the total impact force history on the front face of the jacket structure characterised by a lower peak and a higher duration than those that would result for a single slender pile.

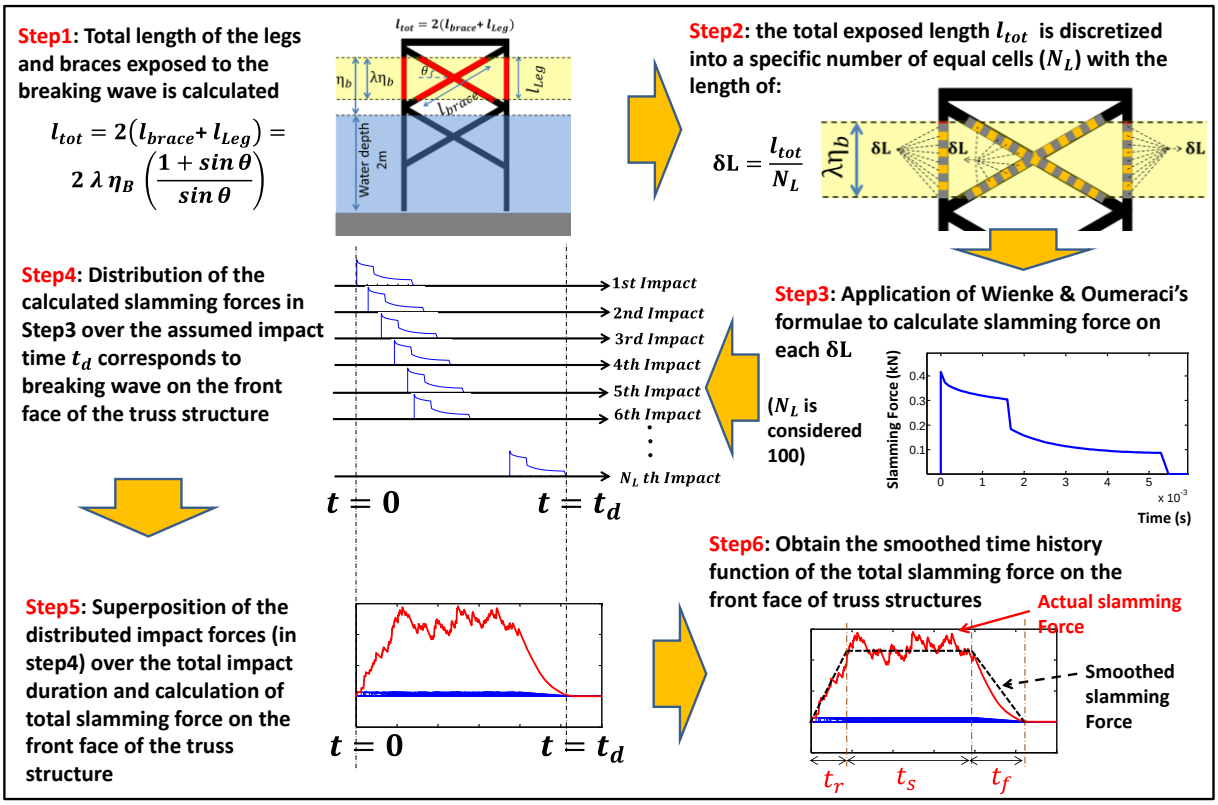

Figure 3-17. Superposition of successive local impacts induced by a breaking wave on the front face of the GWK truss structure ($N_L = 100$)

Considering Figure 3-17, the total slamming force duration can be expressed as:

$$t_d = t_r + t_s + t_f \tag{3-2}$$

where t_d is the total breaking wave impact force duration on the front face of the jacket structure; t_r is the "rise time" with $t_r = 0.15\ t_d$ considering the shape of the slamming force function obtained from the analysis illustrated in Figure 3-17; t_s is the time resulting from the successive local impacts with relatively short time lags on the front face of the jacket structure (Figure 3-17), and t_f is the "fall time", which is equal to the total impact duration of a breaking wave on a single pile as provided by Wienke & Oumeraci (2005): $t_f = \frac{13\ R}{32\ C_b}$ as a good agreement was observed between this relation and the measured impact time on local members of the front face (also adopted in the WiFi project by Burmester et al (2017) and in standards and guidelines such as ISO (2007), IEC (2009)).

Latter in section 3.3.4, the FRF and the convolution integral methods are applied in combination in order to calculate the total duration of the wave impact force on the truss structure (t_d).

3.3.4 Impact duration on the front face of jacket structures

The duration of the wave impact force on the front face of the truss structure is calculated by combining both FRF and Duhamel integral methods. First, the DFR of the GWK truss struc-

ture to the breaking wave on the front face is extracted using low filter analysis of the measured TFR. Then, the maximum wave slamming force is calculated using the FRF method and by considering the obtained transfer function from the hammer impact test on the GWK truss structure (Figure 3-14). The Duhamel's integral code developed for the GWK truss structure is applied to calculate the DFR of the structure to the input slamming force time history where the magnitude of the slamming force is obtained by the FRF approach and the impact force duration is determined iteratively. In this iteration process, the impact force duration is modified, so that the calculated DFR obtained from the Duhamel integral method fits to the DFR of the GWK truss structure extracted from the experiments. Finally, a formula for the calculation of the breaking wave impact force duration on the front face of truss structures is provided based on the assumption that the breaking wave impact duration is directly proportional to the ratio of the radius R of the leg and invers proportional to the breaking wave celerity C_b. Figure 3-18 shows the applied methodology for the calculation of the breaking wave impact force time on the front face of the structure.

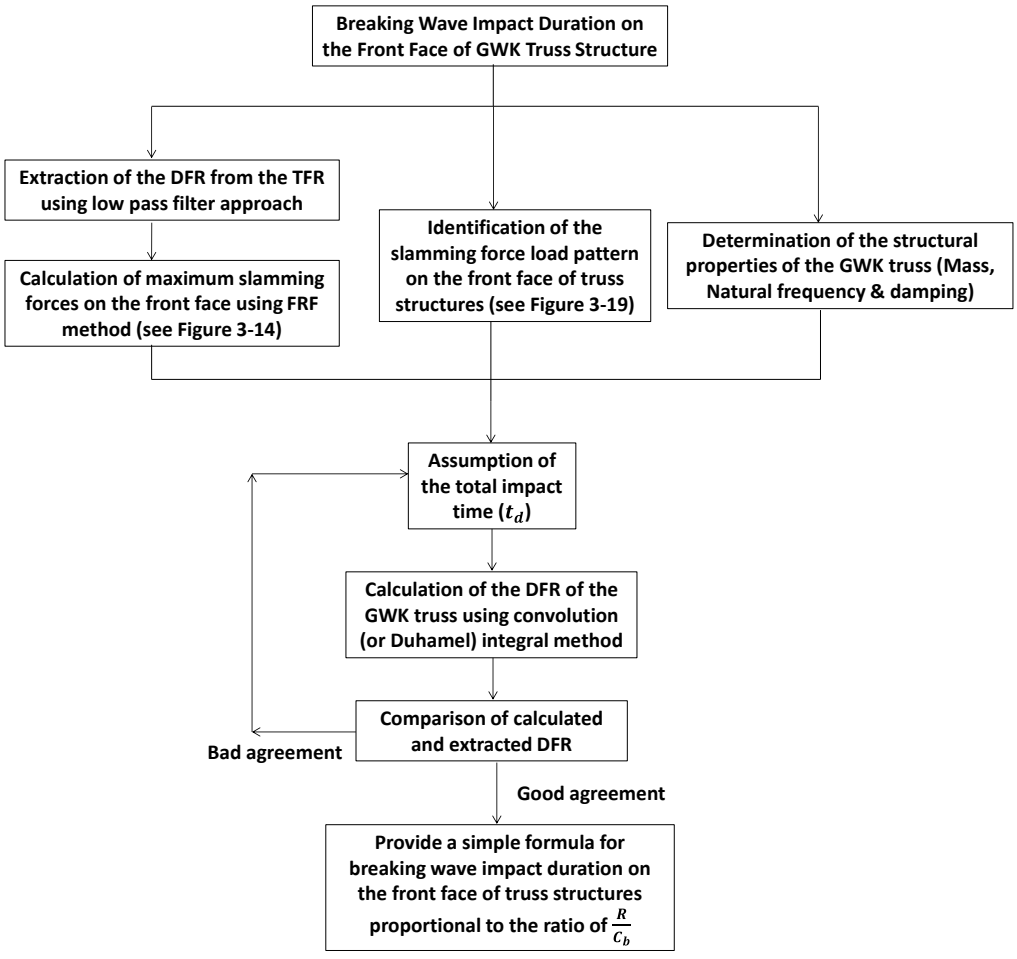

Figure 3-18. Methodology for the calculation of wave impact duration on a truss structure

An iterative approach is applied to analyse the wave test 2013061424 where the highest DFR of the GWK truss structure is recorded. The maximum slamming force is calculated using the FRF method (see Figure 3-19e). Afterwards the slamming force time history, and consequent-

ly the total impact duration t_d is calculated considering the measured DFR (Figure 3-19f), the incident wave crest celerity ($C_b = 5.2\ m/s$) and the water surface elevation ($\eta_b = 1.44\ m$). The DFR of the GWK truss structure is well-reproduced using the obtained slamming force time history and the Duhamel's integral method (Figure 3-19e).

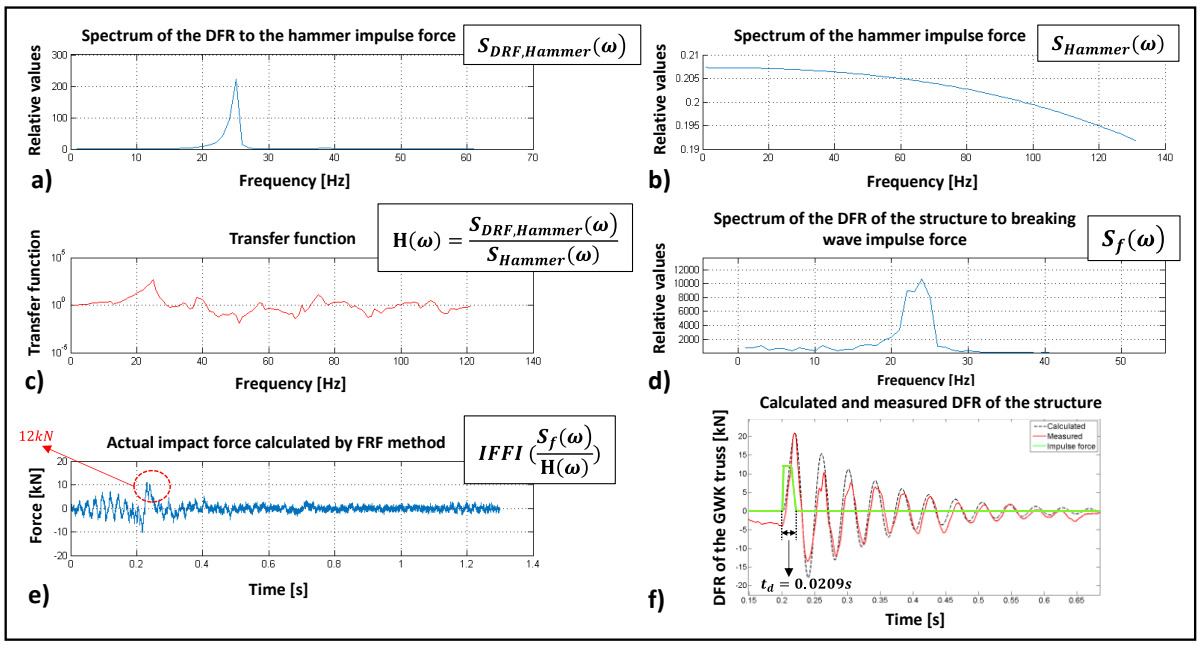

Figure 3-19. Calculation of the total impact duration of a breaking wave on the front face of the GWK truss structure: a) Spectrum of the dynamic force response of the GWK truss structure to the hammer impulse force, b) Spectrum of the hammer impulse force, c) Transfer function d) Spectrum of the dynamic force response of the GWK truss structure to the applied breaking wave force, e) Time series of the actual breaking wave impact forces on the structure, f) Measured and calculated dynamic force response (DFR) of the GWK truss structure using Duhamel's integral method

The total breaking wave slamming force duration on the front face of the GWK jacket structure can be expressed based on the fact that the impact time is directly proportional to $\frac{R}{C_b}$ (see Table 2-6). Therefore, the total duration of the impact force is given by the following equation:

$$t_d = 1.55\ \frac{R}{C_b} \tag{3-3}$$

where the correction factor 1.55 is obtained using the method described in Figure 3-18 by analysing the response of the GWK jacket to the extreme loads resulting from the laboratory tests.

3.3.5 Slamming force formulae for breaking waves on the front face of jacket structures

The slamming force time history function induced by a normal impact of a breaking wave on the front face of a truss structure is adopted for an oblique impact using three modifications (Figure 3-20):

(i) the immersion of an ellipse is considered instead of a circle;
(ii) the wave impact velocity normal to the structural member is obtained considering the angle γ between the direction of the impact velocity $\vec{V}$ and the normal to the member axis;
(iii) the impact area of the inclined members is considered.

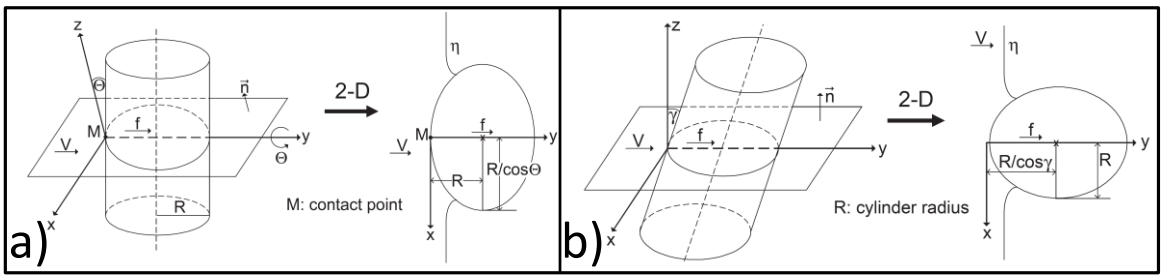

Figure 3-20. Breaking wave impact on a) vertical member (γ=0); b) inclined member (modified from Wienke & Oumeraci, 2005)

Therefore, the total wave slamming force normal to the structural members in the impact area in the front face of a truss structure can be expressed as follows according to the three zones as defined in Figure 3-21:

For zone 1:
$$\begin{cases} F_S = 2\,\lambda\,\eta_B \left(\frac{1+\sin\theta}{\sin\theta}\right) \rho\, R\, C_S\ {C_b}^2 \cos\gamma\,(4.292\ \frac{C_b\cos\gamma}{R}\ t) \\ 0 < t \le 0.233\,\frac{R}{C_b\cos\gamma} \end{cases} \quad (3\text{-}4)$$

For zone 2:
$$\begin{cases} F_S = 2\,\lambda\,\eta_B \left(\frac{1+\sin\theta}{\sin\theta}\right) \rho\, R\, C_S\, {C_b}^2 \cos\gamma \\ 0.233\,\frac{R}{C_b\cos\gamma} < t \le 1.144\,\frac{R}{C_b\cos\gamma} \end{cases} \quad (3\text{-}5)$$

For zone 3:
$$\begin{cases} F_S = 2\,\lambda\,\eta_B \left(\frac{1+\sin\theta}{\sin\theta}\right) \rho\, R\, C_S\, {C_b}^2 \cos\gamma\,(3.815\ -\frac{32}{13}\frac{C_b\cos\gamma}{R}\ t) \\ 1.144\,\frac{R}{C_b\cos\gamma} < t \le 1.55\,\frac{R}{C_b\cos\gamma} \end{cases} \quad (3\text{-}6)$$

The total impact duration corresponds to the duration calculated for an oblique impact caused by breaking wave on the inclined front face of the truss structure can be expressed as Eq.3-7.

$$t_d = 1.55\ \frac{R}{C_b\cos\gamma} \quad (3\text{-}7)$$

Where β is the angle between the braces and the horizontal plane, C_S is the maximum slamming coefficient which is provided in Table 3-5 based on the experiments performed on the GWK truss structure and C_b is the breaking wave celerity.

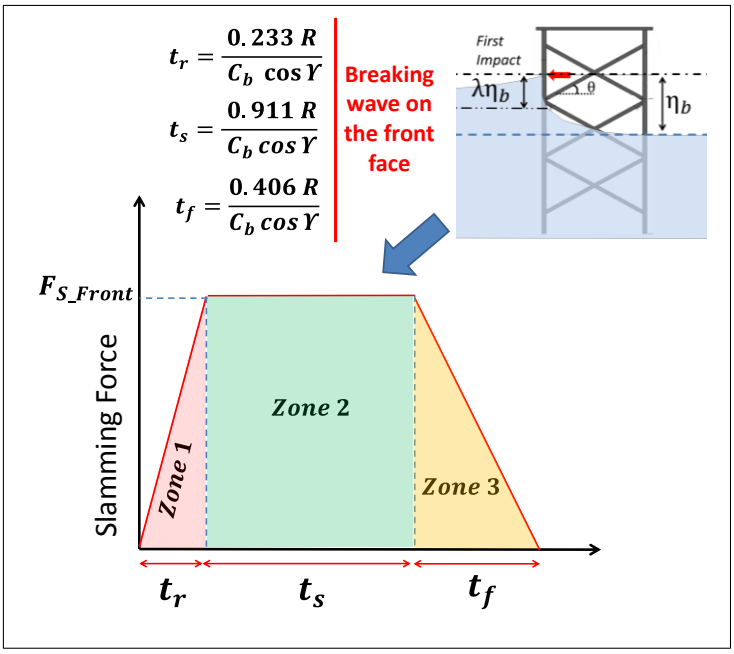

Figure 3-21. Generic time history of the slamming force induced by breaking wave force on the front face of truss structures

The total impact time on the front face of truss structures includes (i) impact rise time t_r (zone 1); (ii) successive impact forces t_s (zone 2); (iii) impact fall time t_f (zone 3). The detailed description of each of these three identified zones is provided in Table 3-5.

Table 3-5. Breaking wave impact on the front face of truss structures for zones 1-3 shown in Figure 3-21

Zone	***Wave Load Description***	***Water Particle Velocities (C_b)***	***Impact Duration***	***Slamming coefficient (Cs) for different load cases (LC)***
1	Time required for the impact force to rise from zero to max value	Use dispersion relation in shallow water depth, for instance according to linear wave theory: $C_b = \sqrt{g\,(d+\eta_b)}$ or CFD Modelling	$0.233\,\frac{R}{C_b \cos\gamma}$	LC1: Wave breaking point far in front of the structure **Cs=1.30 ;** LC2:Wave breaking point in front of the structure **Cs=1.63 ;** LC3:Wave breaking point just at the structure **Cs=0.75** LC4:Wave breaking point in the middle of the structure **Cs=0.35**
2	Successive impacts caused by *local impact forces* on the *front face* of the jacket structure		$0.911\,\frac{R}{C_b \cos\gamma}$	
3	Time taken for the impact force to decrease (fall) from max value to zero		$\frac{13R}{32\,C_b \cos\gamma}$	

The slamming coefficient (Cs) proposed for each load case in Table 3-5, is the highest slamming coefficient obtained for each load case corresponding to the highest recorded DFR for the entire structure.

The proposed formulae in this study are applied to predict slamming force and duration caused by load cases 1-3 on the front face of GWK truss structure and the dynamic force response DFR of the structure is reproduced by Duhamel's integral method based on the calculated slamming force time history function (Figure 3-22). The slamming force and its duration on the front face of the truss structure are also obtained using the models of Wienke & Oumeraci (2005) and Goda (1966) which were developed for breaking wave impact forces on single slender piles as can be seen in Table 3-6. The results show that the force time history on the front face of the truss structure significantly differs with the force time history obtained using single-pile based models. This is due to the successive impacts of the incident breaking wave on the legs and braces of the front face which results in an increase of the breaking wave impact duration (3-4 times larger than Wienke's model) and consequently in a decrease of the slamming coefficient (4 times lower than Wienke's model).

Table 3-6. Wave slamming force Fs and duration t_d on the front face of GWK truss structure induced by breaking waves (load cases LC1-LC3 as defined in Figure 3-22)

Test number	***LC***	***H (m)***	***h(m)***	***T (m)***	η_b***(m)***	***Measured DFR (kN)***	***Calculated Fs (kN)***			***Calculated t_d (s)***		
							F_{S_1}	F_{S_2}	F_{S_3}	T_{d_1}	T_{d_2}	T_{d_3}
2013061709	1	1.7	2.0	5.2	1.32	15.13	11.27	43.39	23.58	0.0211	0.0055	0.013609
2013061424	2	1.7	2.0	5.55	1.44	20.91	11.27	49.68	27.00	0.0209	0.0055	0.013457
2013061704	2	1.7	2.0	5.55	1.58	20.93	12.68	55.86	30.36	0.0206	0.0054	0.013294
2013061423	3	1.6	2.0	5.55	1.37	9.00	4.87	46.62	25.34	0.0210	0.0055	0.013544

F_{S_1}=Slamming force by the model in this study; F_{S_2}=Slamming force by Wienke & Oumeraci (2005); F_{S_3}=Slamming force by Goda (1986); T_{d_1}= Impact duration by the model in this study; T_{d_2}=impact duration by Wienke & Oumeraci (2005); T_{d_3}=Impact duration by Goda (1986);

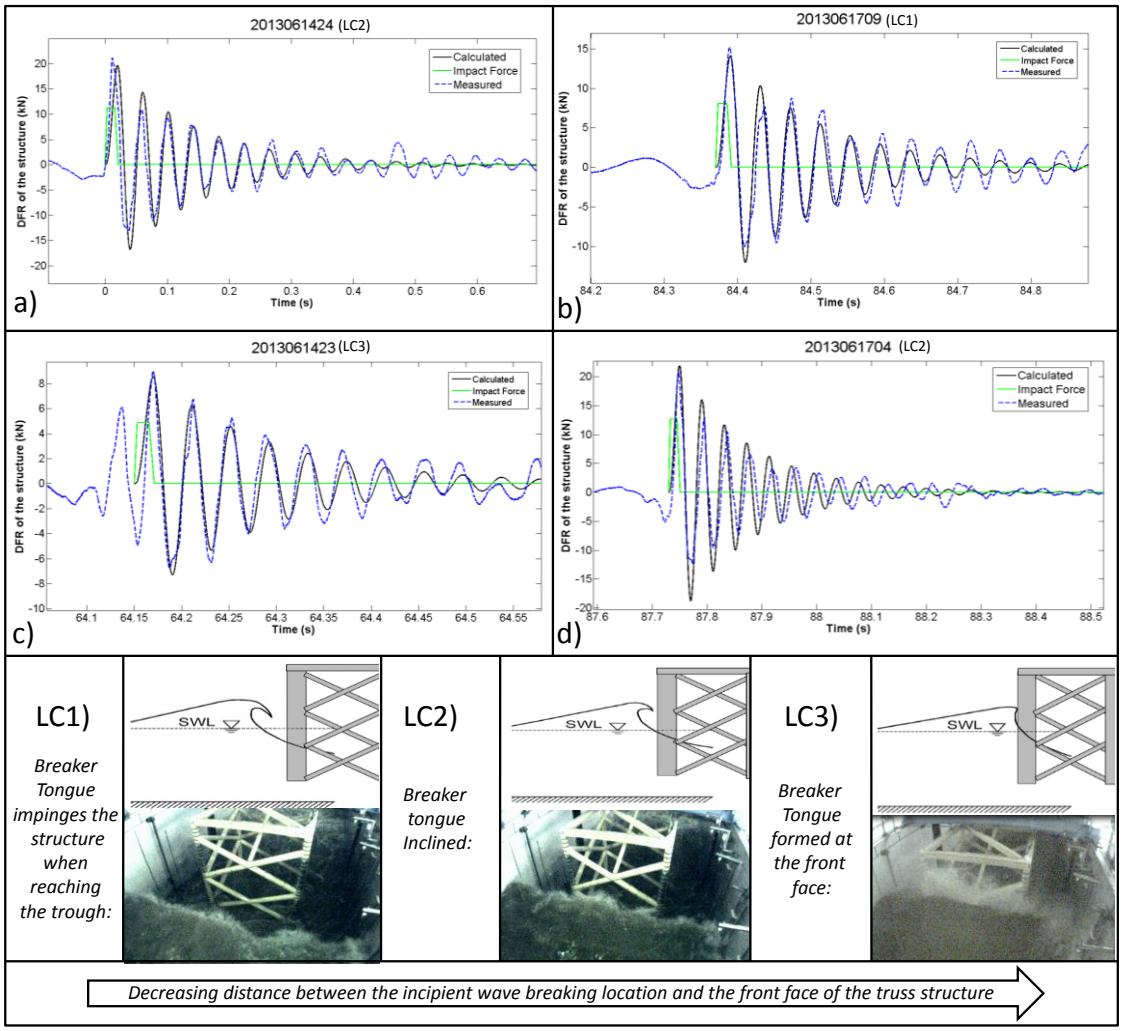

Figure 3-22. Measured and calculated dynamic force response DFR of the GWK truss structure induced by breaking waves on the front face using the proposed formulae in this study

Two Matlab codes are developed to recover the actual slamming forces on the front face of the GWK truss from the measured TFR using: (i) Duhamel's integral method (ii) Frequency Response Function FRF method. Both codes are validated against the experimental data (sections 3.3.1 & 3.3.2).

The wave slamming force pattern for breaking waves on truss-type structures is determined considering the physical process involved in the interaction of breaking waves with different members of the jacket structure (section 3.3.3).

FRF code is applied to calculate the peak of the actual slamming force on the front face. Duhamel code is then combined with the FRF code to obtain the breaking wave impact time on the front face (section 3.3.4). Finally, the formulae for the prediction of slamming force on the front face of jacket structures are provided considering: (i) slamming force pattern; (ii) Maximum slamming forces on the front face; (iii) impact time of the breaking wave on the front face.

3.4 Wave slamming force on the side braces of jacket structures

The wave slamming force on the inclined side braces of the jacket structure is examined for wave direction parallel to the side faces. To provide prediction formulae for the wave slamming force time history on an entire jacket structure, it is also crucial, in addition to the slamming force on the front and the rear faces of the jacket structure, to analyse the breaking wave force on the inclined braces of the side faces of the structures. As this study is strongly based on the large wave flume tests as described in Section 3.1, it is important to stress that the results and conclusions are valid only for wave directions normal to the front/rear faces and parallel to the side faces of the jacket structures. The instrumented members on the side and front braces of the structure are shown in Figure 3-3. Since the length of the instrumented structure members and the structural properties are the same for both side and front braces, the relevant magnitude of the slamming forces can be compared directly.

In order to compare the impact forces by breaking waves on the front face of the jacket structure to those on the side braces, the summation of the DFR on two braces and legs of the front face within the impact area ($DFR_{FB} + DFR_{FL}$) is compared with the summation of the DFR on eight side braces (four braces on each side) of the jacket structure (DFR_{SB}). For this purpose, the following assumptions are made:

- The incident wave acts normal to the front face (and consequently parallel to side braces) and therefore, the slamming forces on both side faces are symmetric. In the other words, the recorded slamming force on both side faces (y=+ 1125mm & y=-1125mm) are approximately equal.
- The recorded slamming force on the front braces (FTBF01-04) can be used to estimate the slamming force on the front legs considering the corresponding length of the front legs in the impact area.

The dimensionless index of 'α_{SF}' is introduced to compare the slamming forces on both side braces and those on the front face in terms of the magnitude of the measured force peaks as follows for load cases LC1-LC4 (Figure 3-23):

$$\alpha_{SF} = \frac{DFR_{SB}}{DFR_{FB}+DFR_{FL}} = \frac{2 * (\sum_{j=5}^{12} FTBFj)}{\sum_{i=1}^{4} FTBFi + \sin\beta \sum_{i=1}^{4} FTBFi}$$

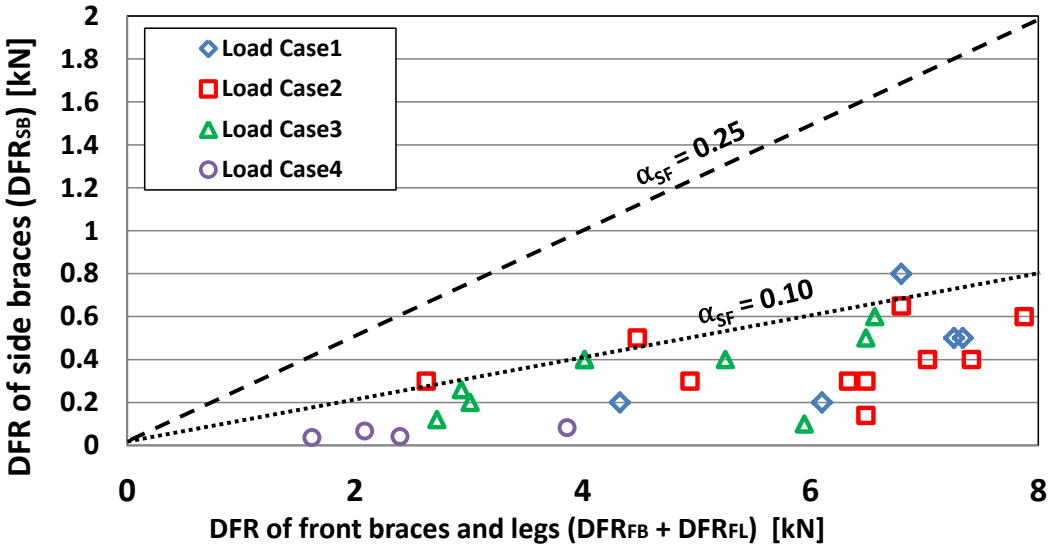

Figure 3-23. Slamming force on both side braces vs, slamming force on the front face of the GWK jacket for load cases LC1-LC4

The GWK experiments and the obtained α_{SF} (< 10%) for several tests showed that the wave slamming forces on both side braces of jacket structure are very small compared to the slamming force on the front face of the structure. The most important reasons are:

(i) The area of impact for the breaking wave on the side braces of the jacket structure is much smaller compared to the area of impact for the front and the rear faces; i.e. when the breaking wave hits the front face of the structure, a larger part of the structure contributes in blocking the incident breaking wave. However, when the - breaking wave is within the structure, there are just two inclined side braces, which are blocking the breaking wave (Figure 3-24)

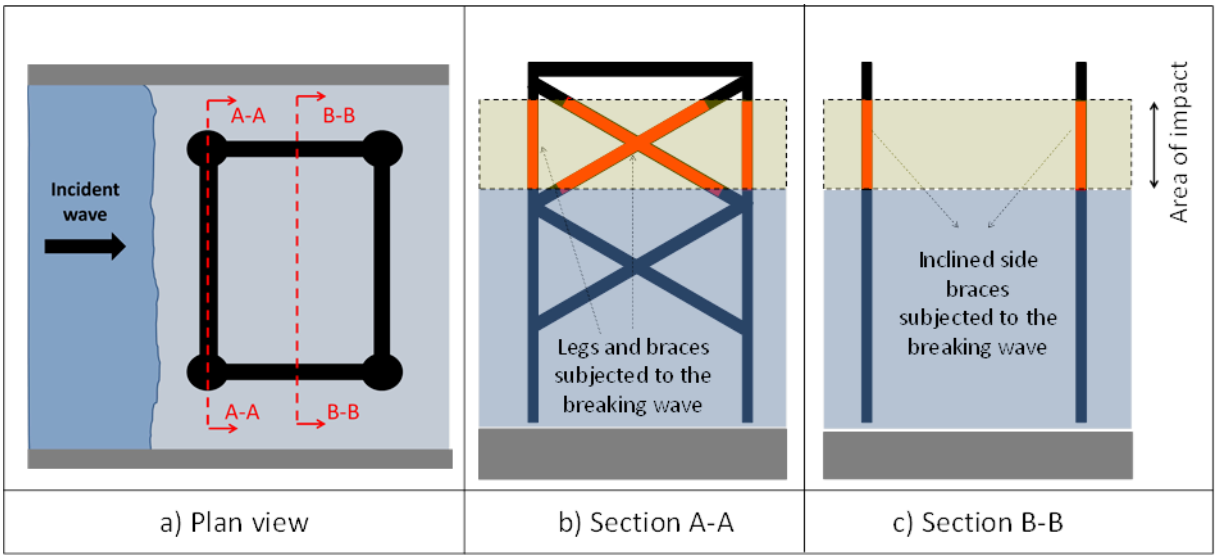

Figure 3-24. Area of impact for the front face and the side braces of the jacket structure exposed to a breaking wave

(ii) The inclination of the side braces of the jacket structure reduces the severity of the breaking wave impact with the structure for positive angles ($\alpha > 0$) (Wienke & Oumeraci, 2005). The mass of water hits the cylinder not normally but oblique by an angle $\alpha \neq 0$. In this case, the shape of the cylinder has to be represented by an elliptic instead of a circular shape. The over curling breaker tongue hits the inclined cylinder obliquely which significantly reduces the magnitude of the slamming force (Figure 2-6).

(iii) The side braces of the jacket structures are located just after the front legs of the structure. Therefore, the breaking wave impact on the side braces is affected by the breaking wave impact on the front legs of the structure so that the magnitude of the slamming force decreases significantly due to the "sheltering effect". Sheltering effect in pile group occurs on the single piles behind the front pile thus affecting the incident breaking wave which impact on the latter as a broken wave. The side braces of the jacket structure are affected by the sheltering effect caused by breaking wave impact on the front legs that may significantly reduce impact force on the side braces.

Given the very small magnitude of the impact forces on the side braces of the truss structure as compared to those on the front face (<10%) and in order to come up with simpler formulae for slamming force on truss-type structures, the impact force on the side braces are neglected. Therefore, the prediction formulae for wave slamming force on the entire truss structure will be developed ignoring the wave loads on the side braces.

3.5 Wave slamming force on the rear face of jacket structures

The analysis of the available experimental data and video records revealed that the wave impact load on the rear face of a truss structure is characterised by two main processes called hereafter "sheltering effect" and "wave dropping effect". In this section, both sheltering and dropping effects are examined separately and a new approach is provided to consider both effects in the calculations of the impact force on the rear face. It should be stressed that no specific approach for the calculation of the impact force on the rear face of a jacket-type structure is yet available. The approaches developed for single piles are inappropriate for the prediction of impact forces on the rear face, because

(i) the impact duration related to breaking/broken waves on jacket structures is different from that on a single pile. In fact, for jacket structures, the breaking/broken wave crest reaches different members on the rear face at different time, which results in several local impact forces with short time lags as reported in section 3.3.

(ii) The truss structure members have a significant effect on the propagation of the wave inside the structure as well as on the wave sheltering caused by wave impact on the front face of the truss structure.

(iii) The wave characteristics (e,g. wave celerity, crest shape and height) may noticeably change when approaching the rear face of the jacket structure. In addition, the wave crest height may "drop" when reaching the rear face.

The aforementioned reasons underline the necessity of providing new slamming formulae to calculate breaking/broken wave impact force on the rear face of truss-type structures. In order to fill the knowledge gaps in the processes involved in wave-rear face interaction, a methodology including four work main steps is defined in Figure 3-25. While the first and second work steps are addressed more precisely in this section, the 3rd and 4th work steps were already described in section 3.3 and are implemented for broken waves on the rear face of the truss structure.

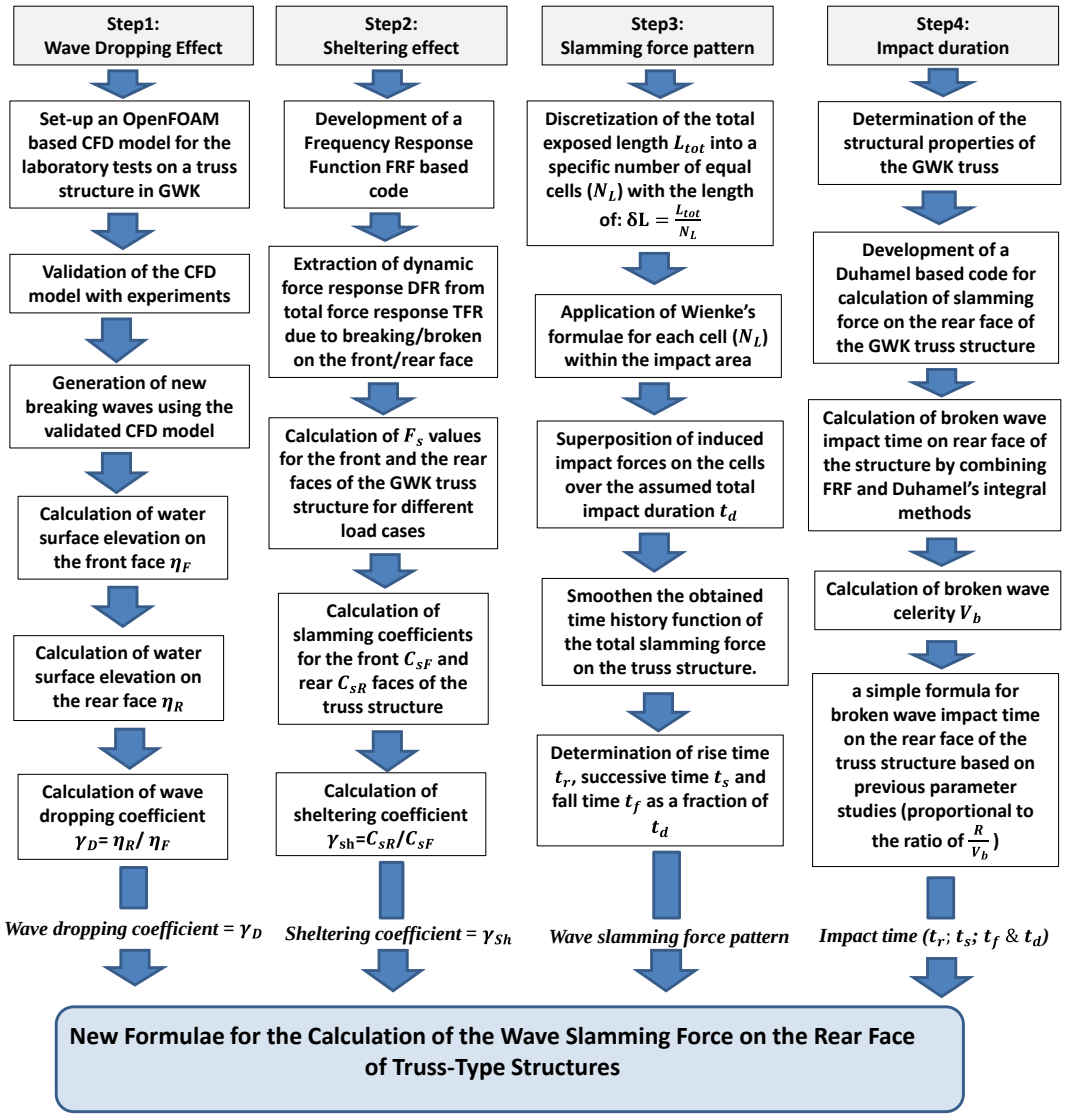

Figure 3-25. Proposed methodology for the development of new slamming formulae for broken wave on the rear face of truss structures

3.5.1 Dropping effect

Several numerical, experimental and field studies have investigated the wave propagation on sloping sea beds. The results revealed that, among the mechanisms governing the characteristics of wave propagation on a sloped bottom, wave shoaling and wave breaking are the most crucial. The former generally results in an increasing wave height and decreasing wavelength

causing the wave to increasingly steepen until it becomes unstable and breaks (Figure 3-26). Breaking wave occurs not only in shallow water but also in deep water. One of the main reasons for wave breaking in deeper water is wave-wave interaction. The wave and sea-bed characteristics largely define the way they break (breaker types). The largest wave crest during wave propagation is at the breaking point. Afterwards, the wave crest height decreases gradually as shown in Figure 3-26.

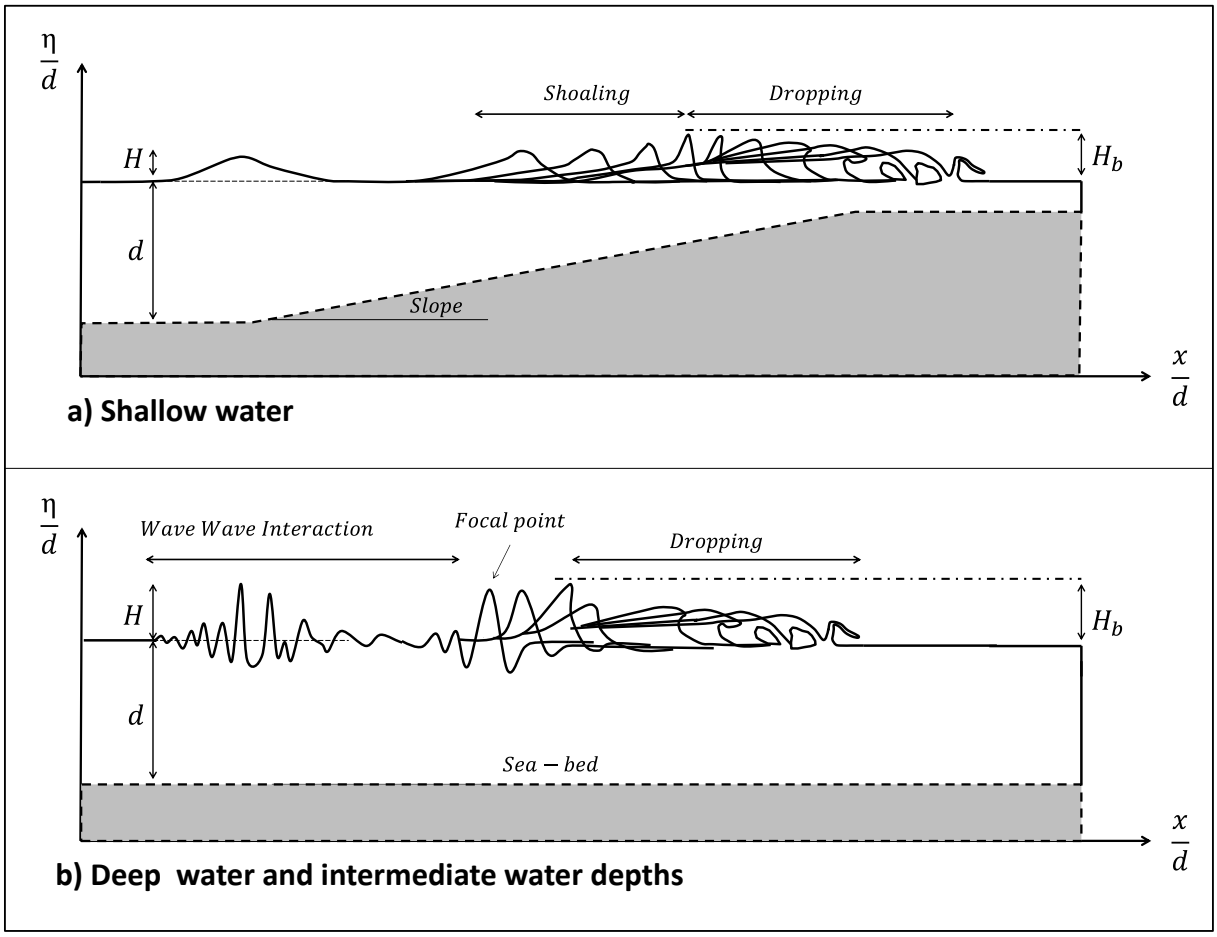

Figure 3-26. Wave breaking process in (a) shallow water; (b) deep water and intermediate water depths

For wave-jacket interaction, modelling the real impact time history at all legs and braces is very complicated due to the phase lags of the wave hitting the different structure members, particularly those on the front face and on the rear face. When the breaking wave crest hits the front legs, the same wave may reach the rear legs as a broken wave, so that no impact force is simultaneously induced on the rear legs. Depending on the geometry of the structure and the wave celerity, the broken wave crest approaches the rear legs and braces of the jacket structure in a relatively short duration (Figure 3-27), but the elevation at which the wave crest hits the rear face of the jacket structure is not the same as that of the first impact on the front face due to the possible deformation/decrease of the broken wave crest while propagating inside the structure. Therefore, the breaking/broken wave impacts on the front and the rear face of the jacket structure respectively are not easy to predict. In addition, the breaking/broken wave

characteristics are very complex and affected by several parameters such as wave steepness, slope steepness, water depth and structure geometry/configuration/dimensions.

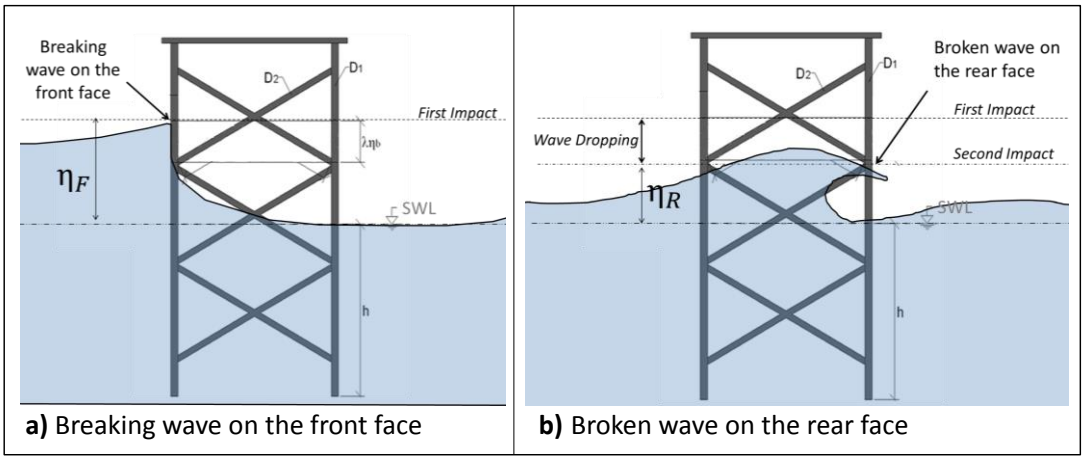

Figure 3-27. Definition sketch showing the wave dropping through the jacket structure

Therefore, it is crucial to predict the broken wave characteristics at the rear face (e,g. bore shape, height and velocity) as well as the crest height and celerity of the breaking wave at the front face of the structure. Therefore, the dropping coefficient γ_D is applied to predict the wave crest height at the rear face of the truss structure as a function of the wave crest height at the rear face:

$$\gamma_D = \frac{\eta_R}{\eta_F} \tag{3-8}$$

, where η_R and η_F are the breaking and broken wave crest heights at the front and the rear faces of the truss structure, respectively.

In order to analyse the wave dropping effect, a CFD model based on OpenFOAM is applied to reproduce the GWK experiments performed by Irschik (2004) on a single pile under breaking waves. The numerical model is validated in order to generate more data covering different types of breaking waves on the slope. Figure 3-28 shows the developed CFD model and the large number of virtual wave gauges (70) applied to reproduce the aforementioned laboratory tests for a single pile located just after the slope 1:10. Figure 3-28 shows snapshots from the CFD model simulating a breaking wave propagating over the slope approaching the single pile. In both numerical model and the laboratory test the incipient wave breaking location forms far in front of the structure (load case 1).

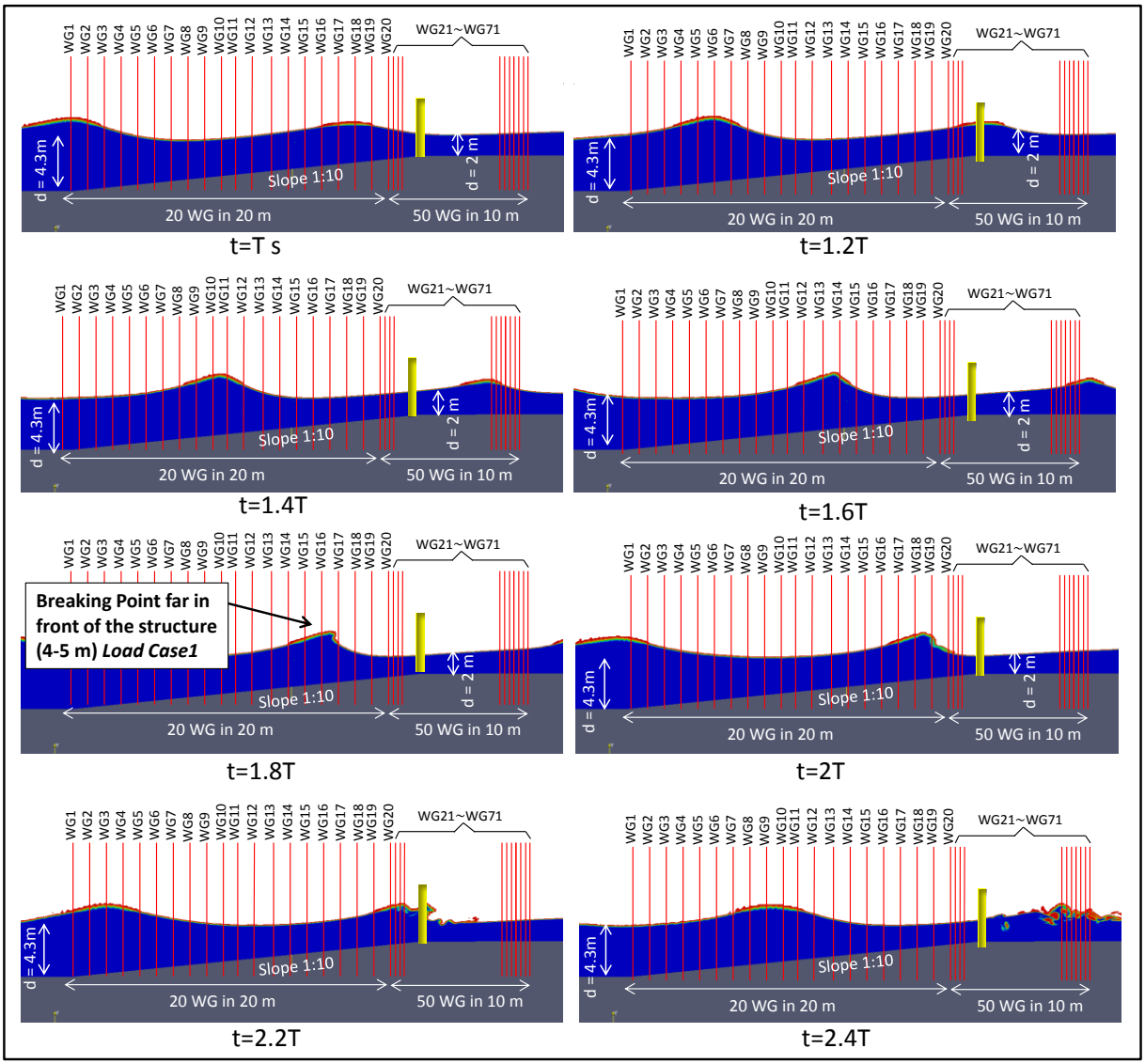

Figure 3-28. CFD model of a wave approaching a single pile tested in the large wave flume GWK (H=1m; T=5s, d=4.3 to 2m)

Figure 3-29 shows the water surface elevation of the incident wave recorded by 70 virtual wave gauges (WG) considered along the numerical wave flume (20 WGs over the slope & 50 WGs in the area close to the single pile). As can be seen, the water surface elevation increases gradually until the inception of breaking wave. Afterwards, the wave crest drops relatively fast. The incipient wave breaking location is identified in the numerical results of the wave evolution over the computational domain considering the visual investigation of the shape of the breaker type in ParaView which is an open source, multi-platform data analysis and visualization application and can be used to build visualizations to analyse data using qualitative and quantitative techniques. The wave dropping after the breaking point is investigated using the records from the 70 virtual wave gauges considered in the numerical wave flume in order to ensure a high resolution of the water surface elevation

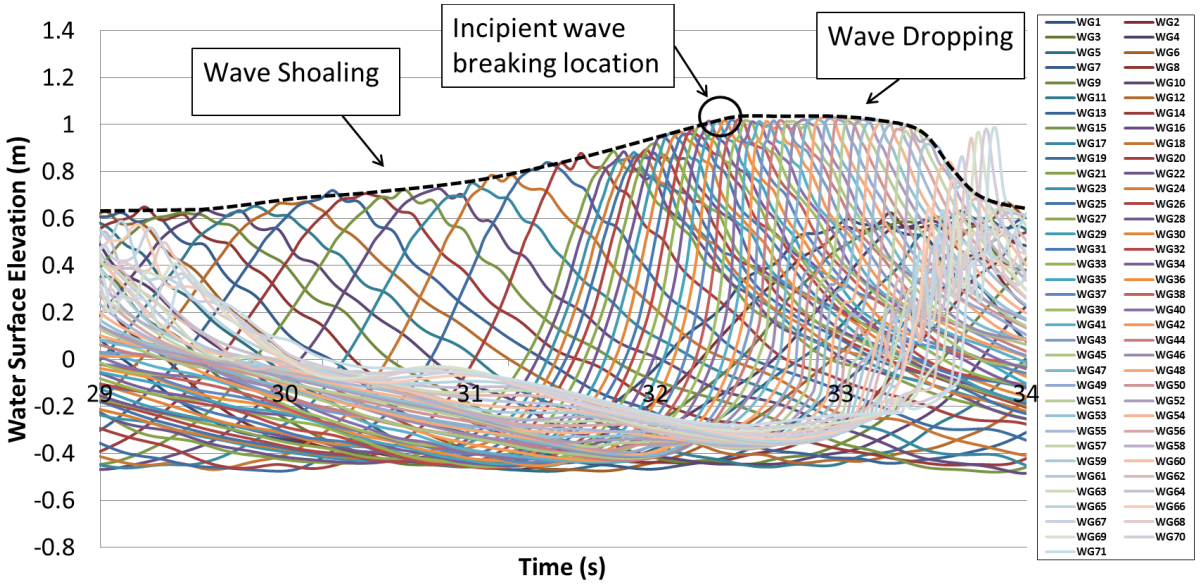

Figure 3-29. Calculation of the wave dropping using the CFD model (H=1m; T=5s)

The numerical model set-up in OpenFOAM is adopted for the experiments performed on the GWK truss structure under breaking waves to compute the wave crest height at any location of the wave flume. Figure 3-30 shows the calculated water surface elevation using the CFD model against the measured data by the eleven wave gauges along the wave flume (WG-S1 to WG-S11)

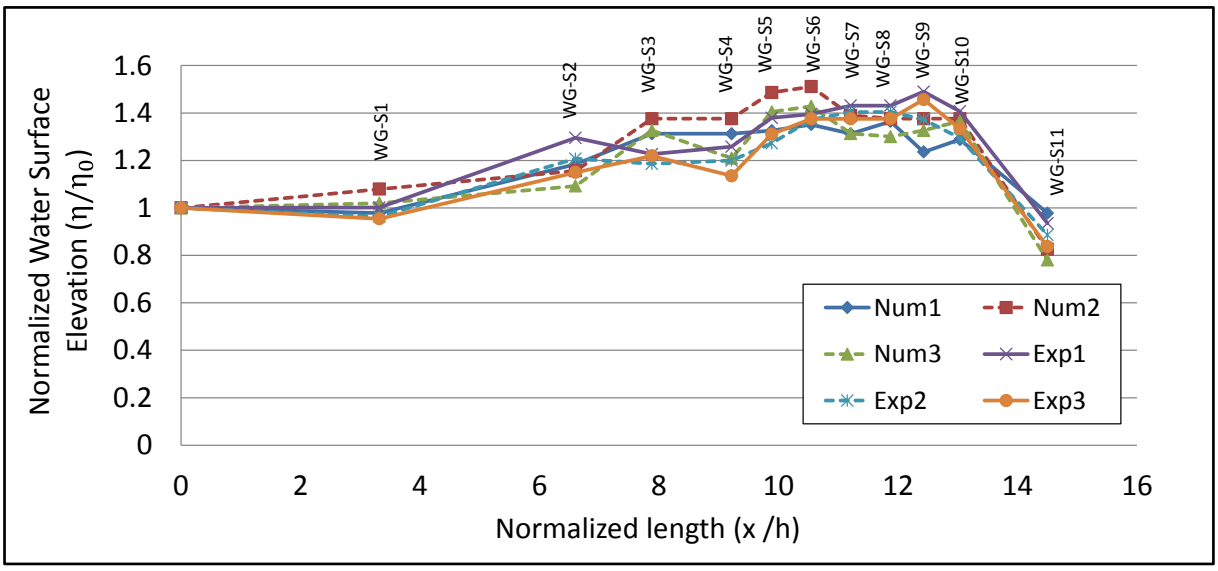

Figure 3-30. Comparison of the simulated and measured water surface elevation for GWK tests, H=1.2m; T=4s; d=4.3m (see Figure 3-2 for the location of wave gauges)

Figure 3-31 shows exemplarily for load case LC3 the results of the numerical model describing a breaking wave approaching the GWK truss structure. The main objective of this simulation is to investigate the “dropping effect” which starts just after wave breaking inception. The

wave crest height continues to decrease significantly thus affecting the wave impact on the rear face of the truss structure. For plunging breakers, the wave drops rapidly over a short distance after incipient breaking.

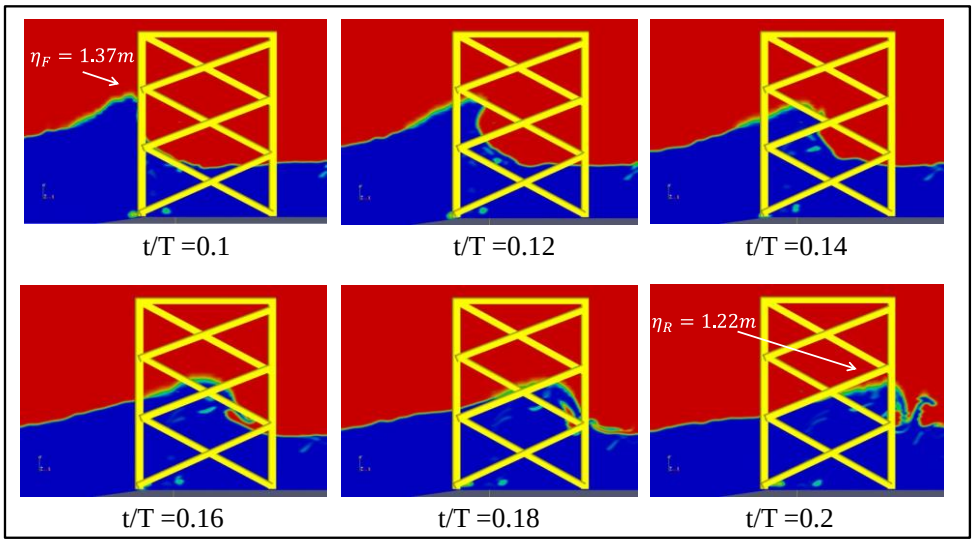

Figure 3-31. Breaking/Broken wave crest at the front and the rear legs of the truss structure, Test No. 203061423, H=1.6m; T=5.55s, h=2m (for the model set-up in the flume see Figure 3-2)

As can be seen in Figure 3-31, the breaker tongue forms at the front face of the truss structure representing LC3 according to Figure 3-11. There is a significant change in the wave crest shape as it reaches the rear legs. Therefore, it is crucial to consider the wave dropping effect when calculating the wave slamming force on the rear face of the jacket structure. Based on the water surface elevation on the front face (η_F=1.37m) and rear face (η_R=1.22m) of the structure (Figure 3-31), a wave dropping coefficient $\gamma_D = 0.89$ is obtained according to Eq 3.8.

3.5.2 Sheltering effect

Sheltering effect for jacket structures occurs on the structure members behind the front face of the structure (downstream face) thus affecting the breaking wave, which might reach the sheltered members as a broken wave. When the breaking wave strikes members of the jacket structure on the front face, the water splashes. The breaking wave reaches the rear face of the structure as a broken wave causing a second impact. In general, for jacket structures, the second impact is significantly affected by the first impact. Therefore, slamming wave force and consequently the slamming coefficient may be decreased, when broken wave reaches to downstream members of the jacket structure as well as legs and braces (Figure 3-32).

Figure 3-32. Water splash due to breaking wave impact on first face of the jacket structure (Arnsten, 2013)

So far, there is no approach to consider the sheltering effect for pile groups and truss-type structures. This effect is neglected, when calculating the broken wave load on downstream members of offshore structures. Several studies have experimentally investigated the sheltering effect for tandem arrangement of slender piles (e.g. Chakrabarti, 1980; Apelt & Piorewicz,1986; Mindao et al., 1987; Bonakdar, 2014), and a few of them have resulted in reliable and process-based models to predict the sheltering effect induced by non-breaking waves on slender piles including the study performed by Bonakdar et al, (2015) in which wave load formulae for prediction of non-breaking wave induced forces on a slender pile within a group of piles were proposed. Unlike for non-breaking waves on slender piles, where a large number of diverse studies are available, less attention has been paid to consider the sheltering effects due to breaking waves on a group of piles. Moreover, the sheltering effect has not yet been investigated for truss-type structures. Figure 3-33 shows the snapshots of a laboratory test performed by Bonakdar (2014) on pile groups with tandem configuration subject to breaking waves. As shown, the second impact is significantly affected by the first impact, so that the slamming force and consequently the slamming coefficient are decreased up to 25% when broken wave reaches to the downstream pile.

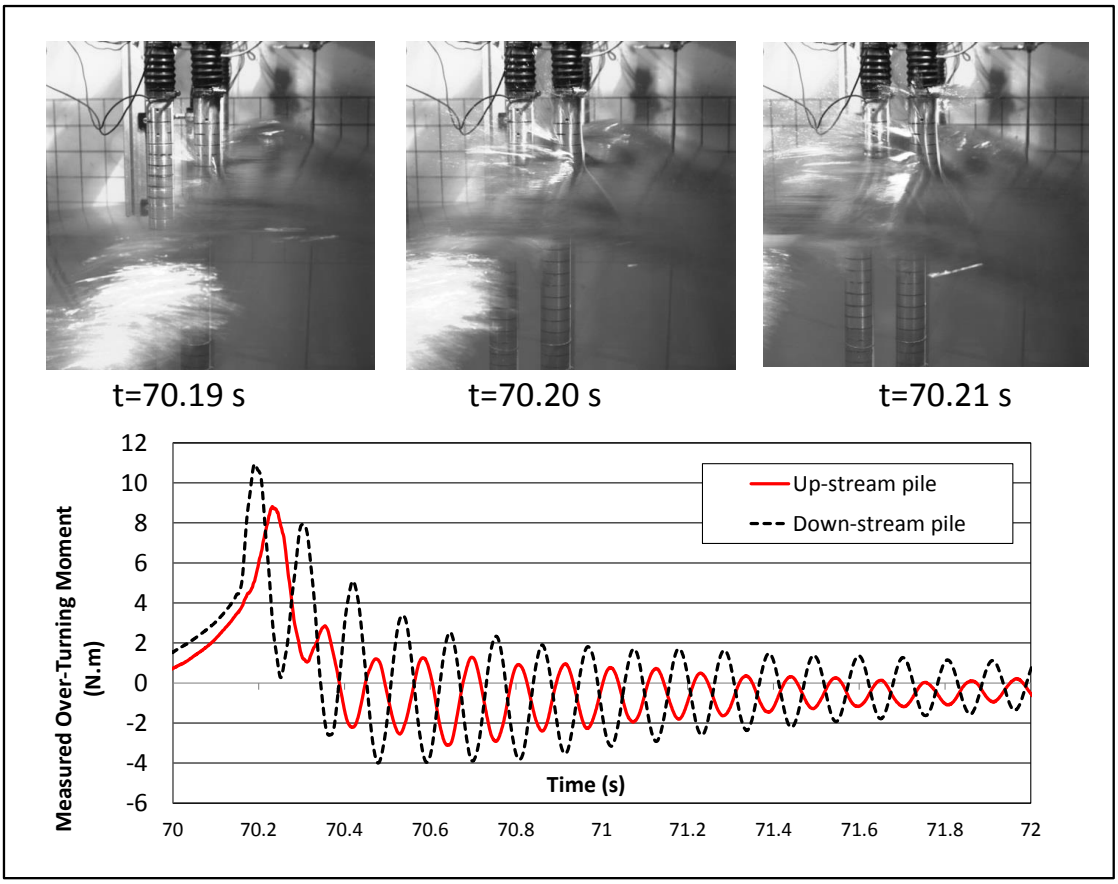

Figure 3-33. Sheltering effect for two single piles exposed to a breaking wave H_b=0.31m; T=2.13s; h=0.65m (Experiments performed by Bonakdar in 2014)

In this study, slamming forces and consequently slamming coefficients for the impact force on the front and rear face of the GWK truss structure are calculated using the Duhamel's integral approach considering the structural properties of the GWK truss structure (e.g. stiffness and mass) which are summarised in the natural frequency of the structure. The sheltering coefficient in this study is defined as follows:

$$\gamma_{sh} = \frac{C_{sR}}{C_{sF}} \tag{3-9}$$

Where C_{sR} and C_{sF} are maximum slamming force coefficient on the rear and the front faces of the truss structure, respectively. This effect is investigated, based on the improved understanding of the processes gained from the analysis of the data and video records. The sheltering coefficients are calculated according to the following five steps which are exemplarily illustrated in Figure 3-33 for Test no.2013061709 (H=1.7m; T=5.2s, d=4.3m) of the GWK truss structure:

(i) The Total Force Response (TFR) of the GWK truss to breaking and broken waves is calculated.

(ii) The Dynamic Force Response (DFR) is extracted from the TFR.

(iii) The Frequency Response Function (FRF) and Duhamel's integral methods are applied to calculate the maximum slamming force F_s on the front and rear faces of the jacket structure.

(iv) The maximum slamming coefficient C_s is calculated for the front and rear faces using the following expression:

$$C_s = F_s/(\rho_w\ R\ \ {C_b}^2\ l_{tot}) \tag{3-10}$$

(v) The sheltering coefficient is calculated using: $\gamma_{sh} = \frac{C_{sR}}{C_{sF}}$

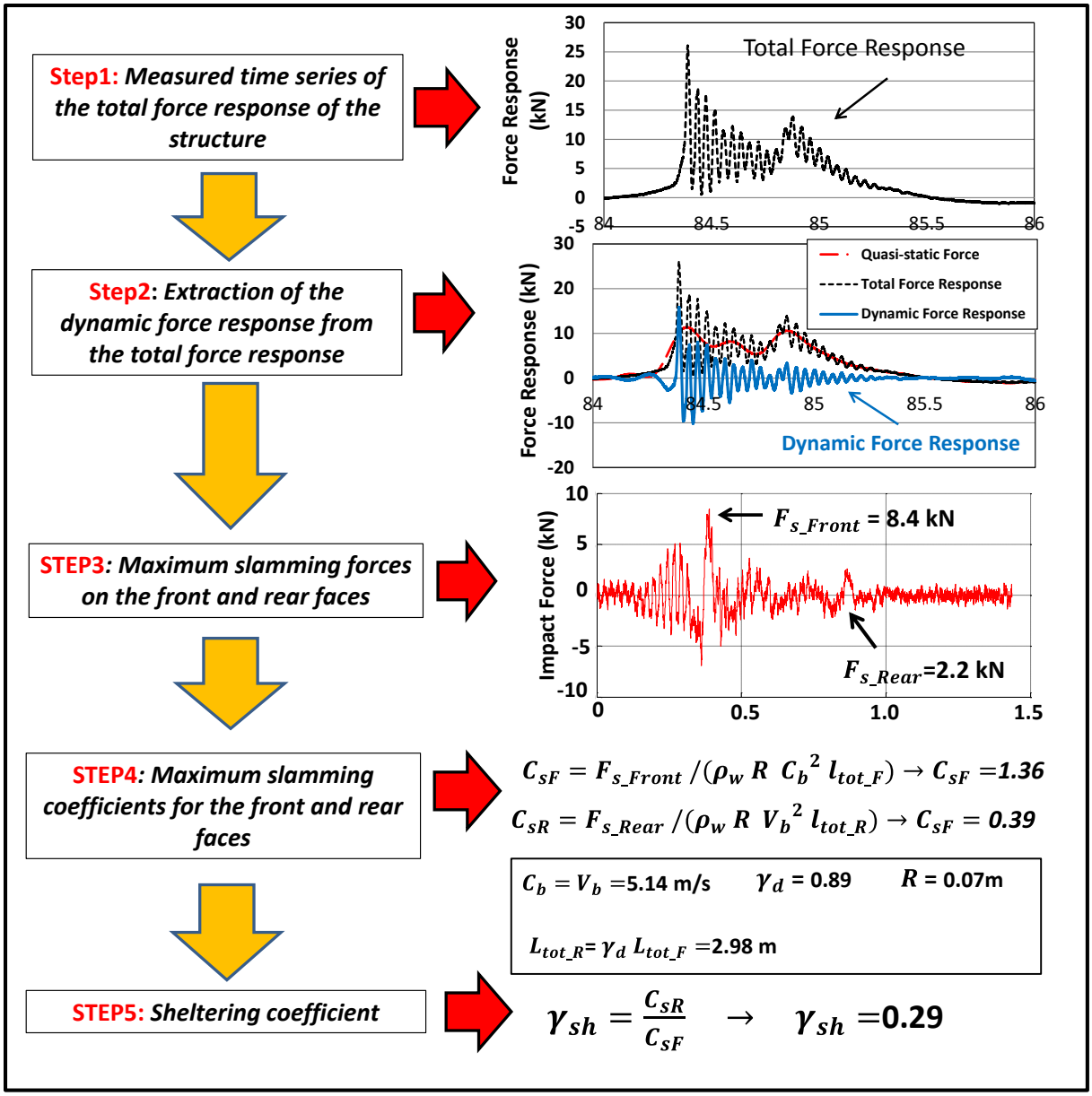

Figure 3-34. Methodology for the calculation of sheltering coefficient γ_{sh} for GWT-truss structure with example application for Test no.2013061709 (H=1.7m; T=5.2s, h=4.3m)

The breaking wave tests performed on the GWK truss are classified in five load cases considering the distance of the incipient wave breaking location from the structure (LC1, LC2, LC3 & LC4). For each load case, a range of sheltering coefficient is determined by calculation of the slamming coefficients on the front and rear faces of the truss structure using the approach depicted in Figure 3-34 for each wave test (see Table 3-7).

Table 3-7. Slamming and sheltering coefficients for breaking wave impact on truss structures

Load cases	***Maximum Slamming coefficient on the Front Face (C_{sF})***	***Sheltering coefficient (γ_{sh})***
Load case 1	1.3	0.1-0.25
Load Case 2	1.63	0.25-0.4
Load Case 3	0.75	0.4-0.7
Load Case 4	0.35	0.7-4.0

3.5.3 Impact duration on the rear face of jacket structures

The breaking wave impact is a highly dynamic force. Therefore, time is an integral characteristic of the impact load, which necessarily needs to be considered in the analysis of the response of the structure.

The total impact duration by breaking and broken waves on the GWK truss structure can be expressed using $\frac{R}{C_b}$ since the impact time is directly proportional to this ratio. As the radius of the legs and braces (R) is a constant parameter, the impact duration is inverse proportional to breaking (C_b) or broken (V_b) wave celerity. The breaking wave celerity can be calculated using CFD modelling or the dispersion relation for shallow water depth using Eq.3-11 considering the wave crest height. In fact, comparison of the calculated wave celerity using the CFD model set-up for GWK tests with the dispersion relation for shallow water depth showed that Eq. 3-11 is valid to predict the breaking wave celerity. However, application of the dispersion relation for intermediate water depth will underestimate the wave celerity.

$$C_b = \sqrt{g\,(d + \eta_b)} \tag{3-11}$$

For the broken wave celerity however, the numerical model set-up in this study cannot be used as the truss structure is not modelled directly in the wave flume and the flow fields are simulated based on the assumption that the diffraction effects are negligible due to the small diameter of the legs and braces. Moreover, the dispersion equation might not predict accurate-

ly wave celerity as the effect of upstream members in blocking the incident breaking wave cannot be considered in the formula. Therefore, the laboratory tests are used to estimate the broken wave celerity using the signal of the dynamic force response (DFR) of the GWK truss structure measured for each wave test. The signal of the DFR shows two peaks: one is related to the breaking wave on the front face and the other one is related to the broken wave on the rear face. The duration t_{span} between these two peaks corresponds to the time interval that the broken wave travels from the front face to the rear face of the structure (Figure 3-35).

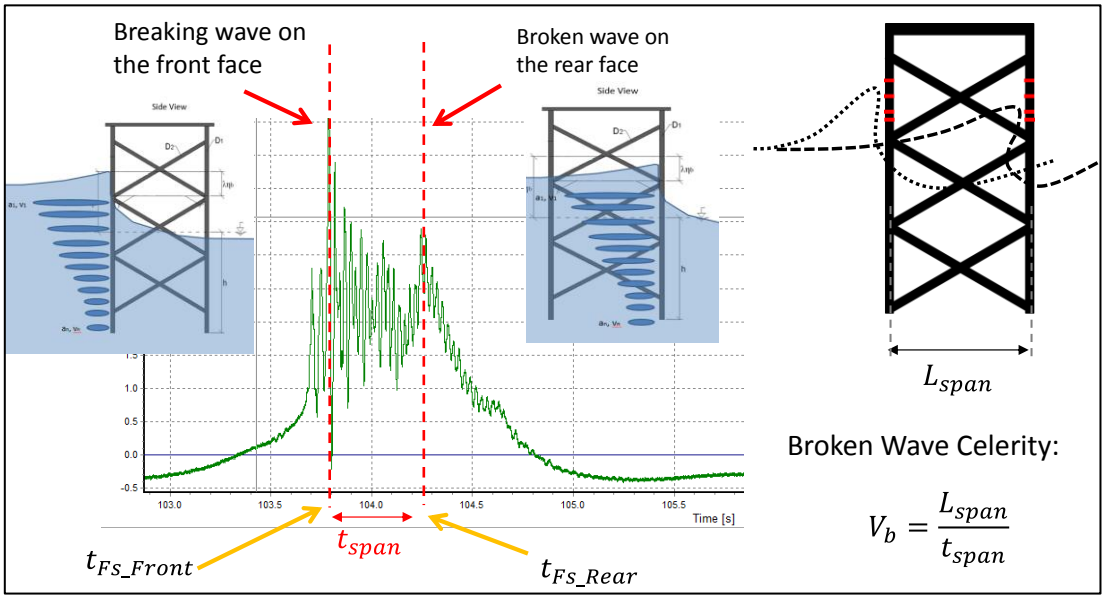

Figure 3-35. The estimation of the broken wave celerity

Therefore, the broken wave celerity V_b can also be calculated considering the following equation:

$$L_{Span} = V_b \,.\, t_{Span} \tag{3-12}$$

Where L_{Span} is the distance between the front and the rear face of the jacket structure (2.25m for the GWK truss structure), t_{Span} is the required time for the broken wave to travel the distance between the front face to the rear face of the jacket structure. Moreover, t_{Span} is considered as the time interval between two peaks of the total dynamic force response of the truss structure.

The comparison of the breaking wave celerity C_b obtained from the CFD model and the broken wave celerity V_b calculated by the aforementioned approach resulted $\frac{V_b}{C_b}$ = 0.9 -1.0 showing that the incident wave celerity reduces moderately after it hits the front face of the structure (Figure 3-36).

Breaker type in GWK tests	*Breaking wave crest (η_b) [m]*	*Breaking wave celerity (C_b) [m/s]*	*Broken wave celerity (V_b) [m/s]*	*Ratio (V_b/C_b)*
LC1	1.40	5.78	5.36	0.93
LC2	1.43	5.80	5.23	0.90
LC3	1.24	5.63	5.63	0.91
LC4	1.17	5.58	5.48	0.98

LC1: Incipient wave breaking location far in front of the front face
LC2: Incipient wave breaking location in front of the front face
LC3: Incipient wave breaking location at the front face
LC4: Incipient wave breaking location between the front and rear faces

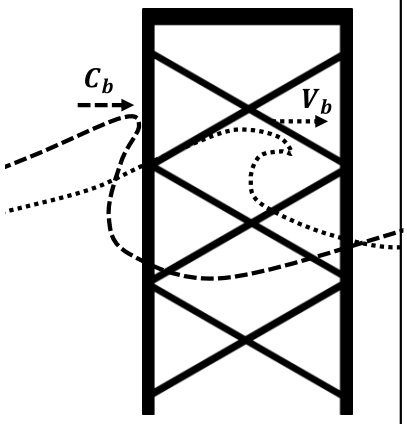

C_b: Breaking wave celerity
V_b: Broken wave celerity

Figure 3-36. Propagation of the waves through the structure and its effect on the wave celerity

Considering the same slamming load pattern as the one considered for breaking waves on the front face (Figure 3-17), the duration of the impact force on the rear face of the structure can be expressed as follows:

$$t_d = 1.55 \frac{R}{V_b \cos\gamma} \tag{3-13}$$

Overall, the impact duration of the broken wave on the rear face of the structure is significantly affected by the propagation of the breaking wave through the structure and its effect on the broken wave celerity V_b. Nevertheless, more investigation of the broken wave characteristics on the rear face of the truss structure (e.g. celerity, shape and evolution of the bore) is recommended using powerful CFD models.

3.5.4 Slamming force formulae for broken waves on the rear face of jacket structures

As discussed in section 3.2.1, the slamming force not only applies on the front face of the structure, but also on the rear face. The detailed analysis of the GWK tests revealed that the wave slamming load on the rear face of the jacket structure is affected by two phenomena: sheltering effect and wave "dropping" effect. The latter is caused by the breaking wave which reaches the rear face as a broken wave. In sections 3.5.13.5.2, both sheltering and dropping effects were investigated separately and new approaches are provided in order to consider both effects in the calculations. For any prospective formulae to predict wave slamming forces on the entire truss structure, it should be stressed that both magnitude and duration of the impact force are strongly linked and that the duration is also crucial for the dynamic response of the structure. Therefore, a new approach by combining the frequency response function (FRF) and the Duhamel integral was applied for the impact duration. Afterwards, the impact duration formula caused by the broken wave on the rear face of truss structure was determined in section 3.5.3 by modifying of the wave celerity in the basic impact duration formula (Eq.3-3).

Taking both wave impact loads on the front and the rear faces of the jacket into consideration, a generic slamming force time series is schematically illustrated in Figure 3-37. The total force history is divided in seven zones and the process involved in the generation of the slamming force induced by breaking/broken wave on the structure is discussed specifically for zones 4-7 in Table 3-8. In general, there are two significant differences between the slamming forces on the front and rear faces:

(i) Due to the so called 'sheltering' and 'dropping' effects, the peak of the slamming force on the rear face is smaller than the slamming force on the front face ($F_{S\_Rear} = \gamma_D \gamma_{sh} F_{S\_Front}$) except load case 4 where the wave breaks within the jacket structure;

(ii) Since the broken wave celerity is moderately smaller than the breaking wave celerity ($V_b < C_b$), the broken wave impact duration on the rear face is larger than the breaking wave impact duration on the front face.

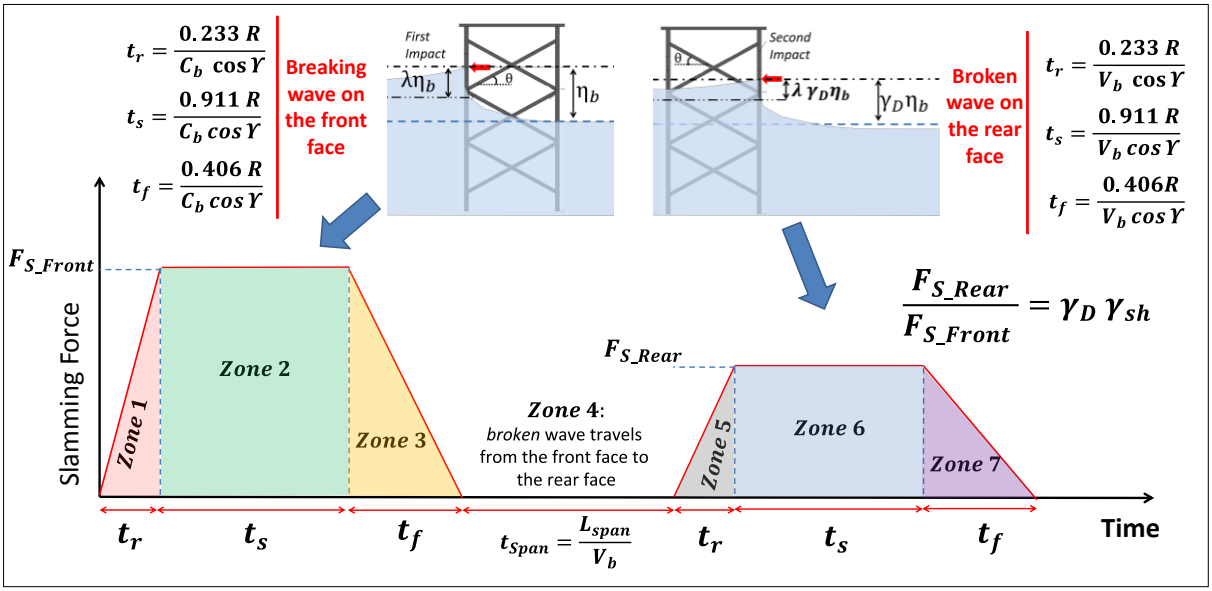

Figure 3-37. Slamming force time series on a truss structure (Principle sketch)

As shown in Table 3-8 and Figure 3-37, the duration of the total impact force on the truss structure consists of the following components:

(i) The duration corresponds to the breaking wave on the front face (zones 1, 2 & 3);

(ii) Time t_{span} required for the broken wave to travel from the front face to the rear face of the jacket structure (zone 4);

(iii) The duration corresponds to the broken wave on the rear face of the jacket structure (zones 5, 6 & 7).

While the processes and resulting forces by breaking wave on the front face is addressed more precisely in section 3.3.5 (zones 1, 2 & 3), in this section, only the processes associated with broken wave impact and the resulting force on the rear face of the structure are addressed as described in Table 3-8 (zones 4, 5, 6 & 7).

Table 3-8. Broken wave impact time series on the rear face of truss structures

Zone	***Wave Load Description***	***Water Particle Velocities***	***Duration***	***Considered/ Modified Parameters***
4	Time required for the *broken* wave to travel from the front face to the rear face	$V_b = (0.9 \sim 1)\, C_b$	$\frac{L_{Span}}{V_b}$	Geometry of the Structure
5	Time required for the impact force to rise from zero to its max value	And C_b from dispersion relation in shallow water depth, for instance according to linear wave theory: $C_b = \sqrt{g\,(h+\eta_b)}$ or by using CFD Models	$0.233\,\frac{R}{V_b \cos\gamma}$	Impact Duration Wave Celerity Load History function Dropping Effect Sheltering Effect
6	Successive impacts caused by local impact forces on the rear face of the jacket structure		$0.911\,\frac{R}{V_b \cos\gamma}$	
7	Time required for the impact force to decrease (fall) from its max value to zero		$\frac{13\,R}{32\,V_b \cos\gamma}$	

The formulae for the prediction of slamming force caused by broken wave on the rear face of jacket structures are as follows (zones 5, 6 &7 in Figure 3-37):

For zone 5:
$$\begin{cases} F_S = 2\,\gamma_{Sh}\,\gamma_D\,\lambda\,\eta_B\left(\frac{1+\sin\theta}{\sin\theta}\right)\rho\,R\,C_S\;{C_b}^2\cos\gamma\,(4.292\;\frac{C_b\cos\gamma}{R}\;t'\;) \\ 0 < t' \le 0.233\,\frac{R}{C_b\cos\gamma} \end{cases} \quad (3\text{-}14)$$

For zone 6:
$$\begin{cases} F_S = 2\,\gamma_{Sh}\,\gamma_D\,\lambda\,\eta_B\left(\frac{1+\sin\theta}{\sin\theta}\right)\rho\,R\,C_S\,{C_b}^2\cos\gamma \\ 0.233\,\frac{R}{C_b\cos\gamma} < t' \le 1.144\,\frac{R}{C_b\cos\gamma} \end{cases} \quad (3\text{-}15)$$

For zone 7:
$$\begin{cases} F_S = 2\,\gamma_{Sh}\,\gamma_D\,\lambda\,\eta_B\left(\frac{1+\sin\theta}{\sin\theta}\right)\rho\,R\,C_S\,{C_b}^2\cos\gamma\,(3.815\;-\frac{32}{13}\,\frac{C_b\cos\gamma}{R}\;t'\;) \\ 1.144\,\frac{R}{C_b\cos\gamma} < t' \le 1.55\,\frac{R}{C_b\cos\gamma} \end{cases} \quad (3\text{-}16)$$

and $t' = t - (1.55\,\frac{R}{C_b\cos\gamma} + \frac{L_{Span}}{V_b})$

where V_b is the broken wave crest velocity, γ_D is the dropping coefficient which might be calculated using a CFD model or theoretical/experimental based models, γ_{sh} is the sheltering

coefficient given in Table 3-7 for load cases LC1-LC4. It should be stressed that $\lambda\,\eta_B\,\left(\frac{1+\sin\theta}{\sin\theta}\right)$ in the above formulae corresponds to the total length (l_{tot}) of legs and braces in the front face which are exposed to slamming.

Wave slamming force on the rear face of a truss structure is affected by two main processes, called "*sheltering effect*" and "*wave dropping effect*". The *wave dropping effect is* introduced and a validated CFD model is used to take this effect into account, considering the water surface elevation at the front and rear faces of the GWK truss structure. The *sheltering effect* is considered by means of the frequency response function (FRF) method considering the maximum slamming coefficients on the front and rear faces of the GWK truss for different load cases.

The prediction formulae for broken wave slamming force on the rear face of the truss structure is provided considering: (i) wave slamming load pattern on truss structures (obtained in section 3.3.3); (ii) sheltering effect (section 3.5.1); (iii) dropping effect (section 3.5.2); (iv) broken wave impact time on the rear face (section 3.5.3)

3.6 Application of the developed total slamming force formulae for the GWK truss structure

The formulae developed in this study for the calculation of the wave slamming force on the front face and rear face of the jacket structure are applied to reproduce the dynamic force response of the truss structure tested in the GWK. The calculated dynamic force response using the Duhamel's integral method is compared with the measurements from the laboratory tests shown in Table 3-9 in order to evaluate the performance of the proposed slamming formulae for different wave breaker types.

Table 3-9. Selected tests for the evaluation of the provided formulae in this study

Test number	*LC*	*H (m)*	*h (m)*	*T (m)*	η_F*(m)*	η_R*(m)*	γ_D	C_{sR}	γ_{sh}
2013061709	1	1.70	4.3	5.2	1.32	1.18	0.89	1.3	0.3
2013061424	2	1.70	4.3	5.55	1.44	1.28	0.88	1.63	0.35
2013061704	2	1.75	4.3	5.55	1.58	1.4	0.88	1.63	0.2
2013061423	3	1.60	4.3	5.55	1.37	1.22	0.89	0.75	0.7

LC= Load case; H=Wave Height behind the slope; d=Water depth behind the slope; T= Wave Period behind the slope; η_F= Wave Crest Height at the Front Face; η_R= Wave Crest height at the Rear Face; γ_D= Dropping Coefficient; C_s= Slamming Coefficient at the front face;

In each experiment, the truss structure is subject to more than 20 regular breaking waves and the time series of the total force response (TFR) of the GWK truss structure is measured. The force responses may change significantly from one wave to another. For each test, the highest

measured DFR is taken into account (Figure 3-38). The DFR of the structure is extracted from the TFR using low pass filter analysis (Figure 3-38) by subtraction of the quasi-static force from the TFR of the truss structure.

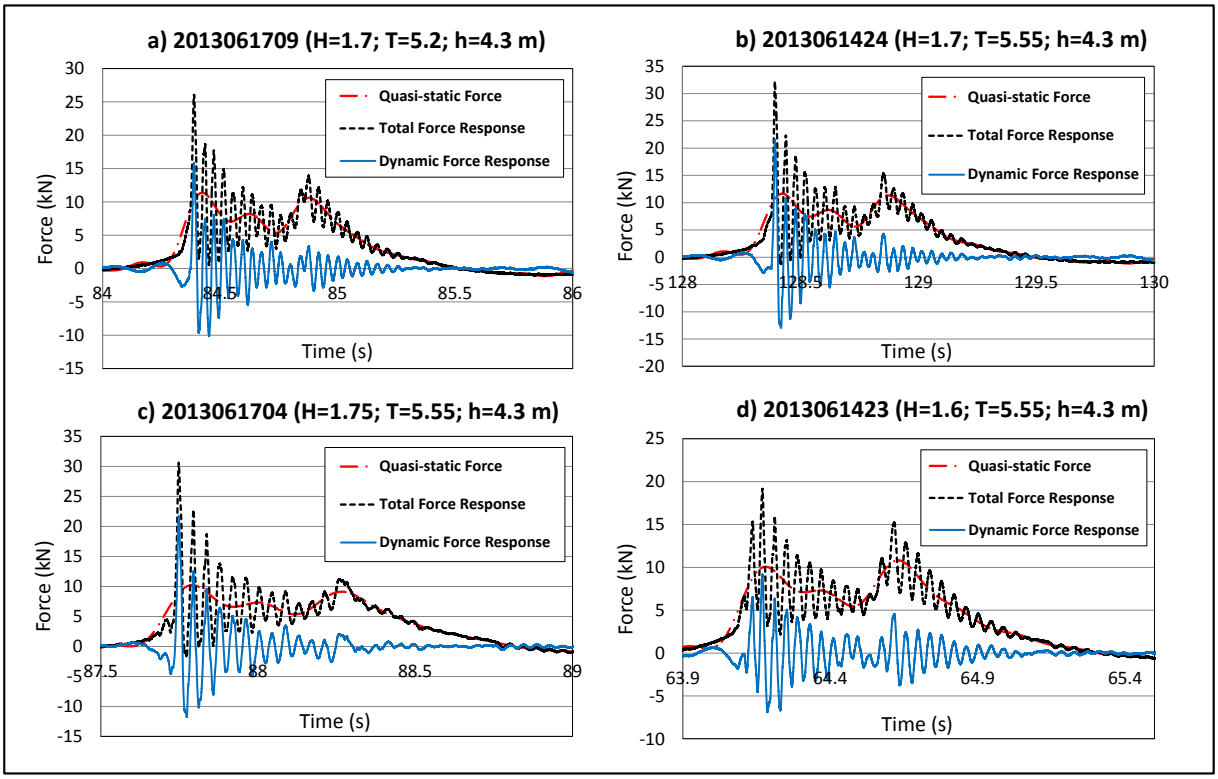

Figure 3-38. Extraction of the dynamic force response DFR from the total force response TFR for the wave tests: a)2013061709, LC1 ; b)2013061424, LC2; c)2013061704, LC2; d)2013061423, LC3

The accuracy of the provided slamming force in this study is examined using the following steps:

(i) The slamming force and duration caused by the incident wave on the front and the rear faces of the GWK truss structure is predicted using the new slamming force formulae (Eq.(3-4) to Eq.(3-6) & Eq.(14) to Eq.(16)) proposed in this study. (see Figure 3-37, Table 3-4 & Table 3-8)

(ii) The dynamic force response (DFR) of the GWK truss structure to the impact force by the slamming model in this study is reproduced using Duhamel's integral approach and is plotted against the measured DFR. (see Figure 3-39)

(iii) The time series of the impact forces on the GWK truss structure are recovered using frequency response function (FRF) method. The obtained impact forces on the front and rear faces are compared with the slamming forces predicted by other slamming models originally proposed for single piles (i.e. Wienke & Oumeraci (2005) and Goda (1966)). (see Figure 3-40)

As shown in Figure 3-39, two distinct peaks can be observed in the DFR of the structure. The first peak is related to the breaking wave impact on the front face of the truss structure and the second peak is for the broken wave load on the rear face. For some simulations, the second impact on the GWK truss structure is simulated with a very small shift (less than 0.02s) compared to the measurements (e.g. Figure 3-39a,c). This might be due to the fact that it is not possible to predict entirely the highly complicated shape of the wave front and motions of the water particles associated with breaking and broken waves at and inside such complex structures even with powerful CFD models such as OpenFOAM used in this study.

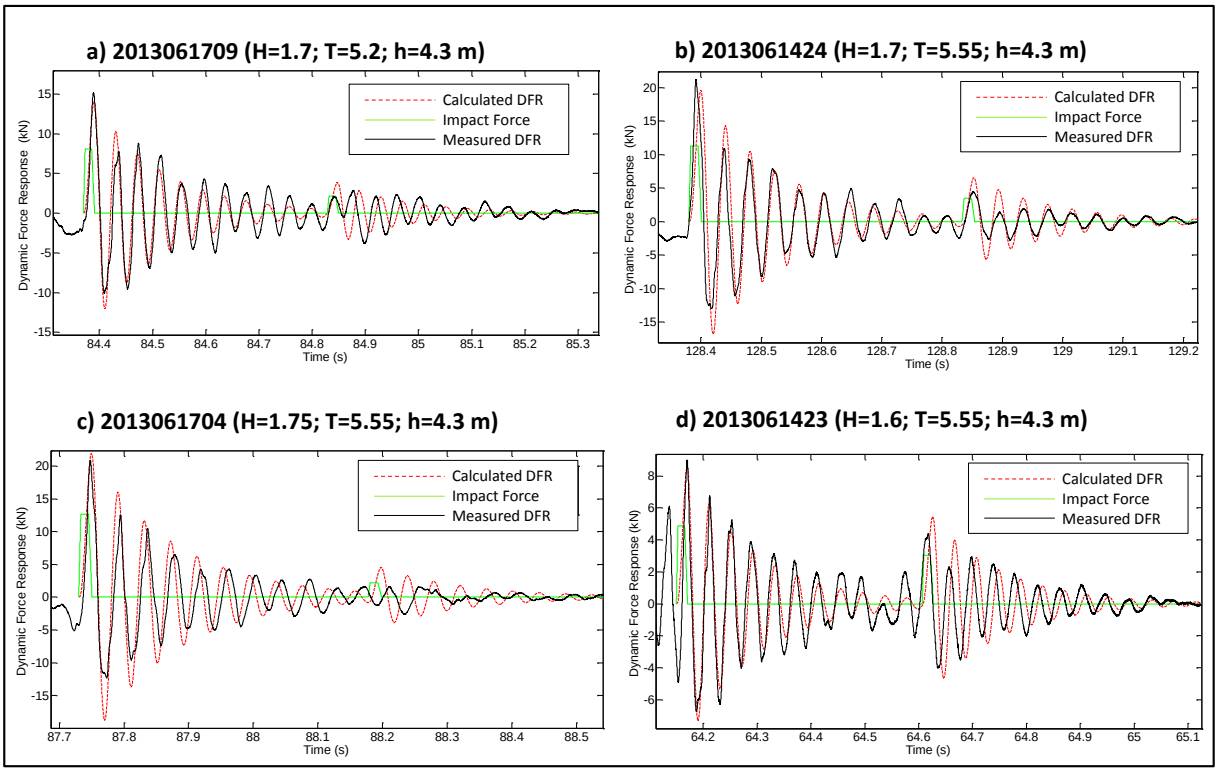

Figure 3-39. Calculated and measured DFR for the wave tests: a)2013061709, LC1 ; b)2013061424, LC2; c)2013061704, LC2; d)2013061423, LC3

In previous analysis performed on GWK tests, the Duhamel's integral approach is implemented to recover just the slamming forces on the local force transducers on the front face of the structure considering only the peak of the measured and calculated signals. In fact, no statistical index is implemented to evaluate the similarities of the calculated and measured signals (e.g. Navaratnam, 2013; Navartnam et al, 2013). In this study, the following analyses are conducted to assess the similarities between measured and calculated force responses shown in Figure 3-39 (results are provided in Table 3-10)

(i) *Peak-to-peak comparison*: The peaks of the measured and calculated signals due to the maximum slamming force on the truss structure are compared.

(ii) *Signal-Correlation*: The correlation coefficient between two time series related to measured and calculated dynamic force response of the structure is obtained.

(iii) *Spectrum-Correlation*: The power spectrum of the measured and calculated time series is calculated. Afterwards, the correlation coefficient between two spectrums is calculated.

Table 3-10. Statistical assessment of the similarities between the measured and calculated DFR

Test No	***2013061709***	***2013061424***	***2013061704***	***2013061423***
Peak-to-peak	0.9610	0.9409	0.8131	0.9932
Signal_Correlation	0.8758	0.8217	0.8572	0.7535
Spectrum_Correlation	0.8478	0.9214	0.8104	0.8025

As can be seen in Table 3-10, there is a good agreement between the measured and calculated (DFR) of the GWK truss structure. Figure 3-40 shows the recovered time-series of the slamming force on the GWK truss structure considering the measured dynamic force response (DFR) of the structure shown in Figure 3-38 and the transfer function obtained by the approach depicted in Figure 3-14. As expected, two distinct peaks related to breaking /broken wave on the front/rear are also obtained using the FRF approach.

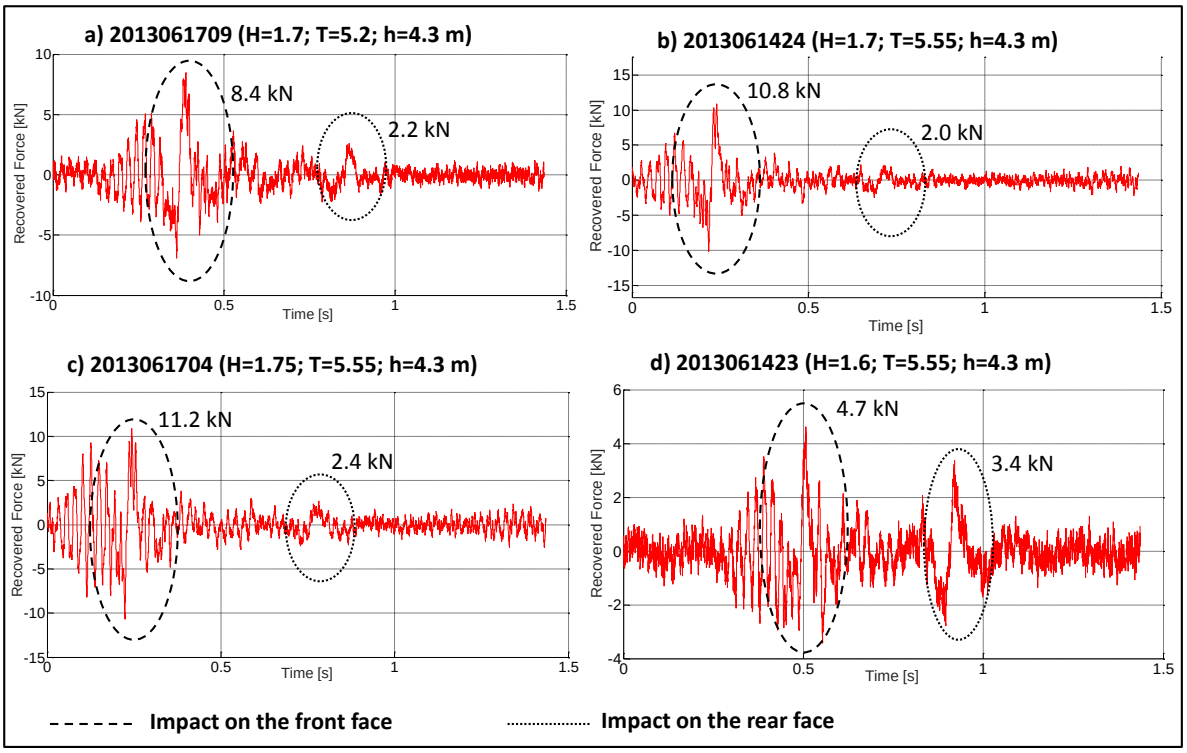

Figure 3-40. Recovered impact forces on the front and rear faces of the GWK truss structure using the FRF method

The slamming formulae proposed in this study are applied to predict the impact forces by one of the wave tests of the GWK experiments (test no. 20131413) and the result is compared with the impact force time history obtained by applying other available slamming models (see Figure 3-41). Although the model developed in this study is also applicable to predict the impact forces on the rear face of the jacket structure, for this comparison only the formulae for the front face are used. The reason is that, the other slamming models cannot be conceptually applied to predict the loads by breaking wave on the rear face and thus on the entire structure. It should be stressed that, all slamming models plotted in Figure 3-41 are originally developed for breaking waves on mono-piles except the model proposed in this study for the prediction of breaking wave induced loads on the front face of jacket structures.

The results in Figure 3-41 show that the force time history entirely differs in the case of jacket structures and mono-piles. This is due to the consecutive impacts of the incident breaking wave on the different members of the jacket structure which may decrease the slamming coefficient and increase the breaking wave impact duration.

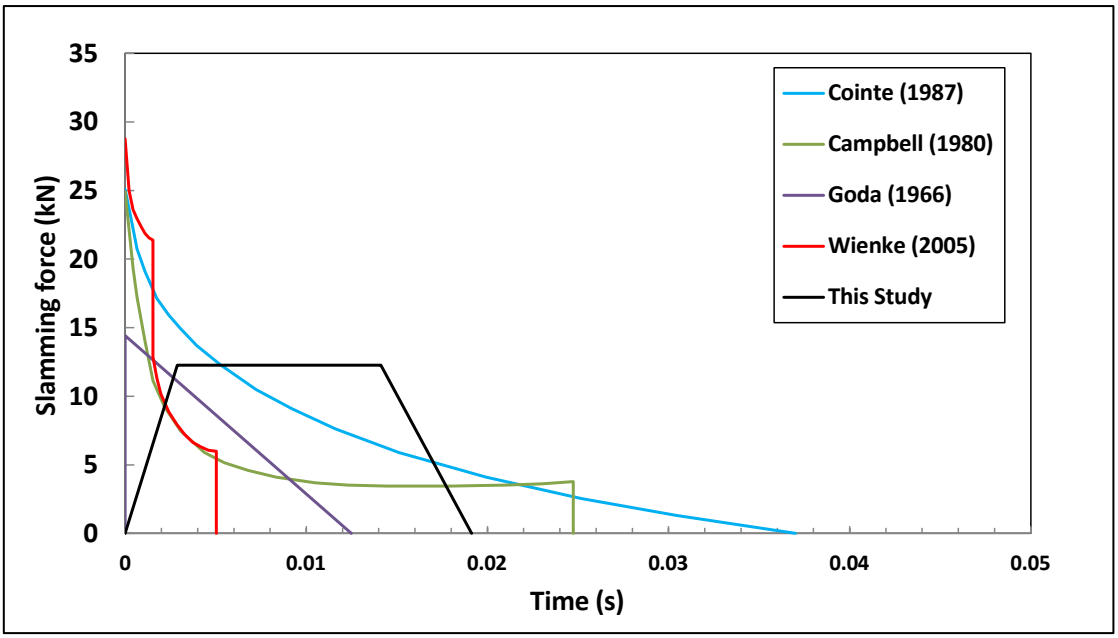

Figure 3-41. Comparison of the available slamming models with the new model proposed for breaking waves on jacket structures (here only on the front face: H_b=1.82 m; η_b=1.27 m; T=4.9 s; h_{str}=2.0 m)

The area beneath the force-time graph shown in Figure 3-41 represents the so-called 'impulse' which is the overall effect of the force acting over time. According to impulse-momentum theory, this area must be equal to the momentum change of the breaking wave which is transferred to the structure during its impact on the front face.

The prediction formulae for wave slamming force on the entire jacket structure (Eqs.3-4 to 3.6 & Eqs.3-14 to 3-16) is applied to predict slamming forces induced by breaking waves on the GWK truss for selected tests performed in the large wave flume. The DFR of the GWK truss to the slamming model in this study is reproduced by Duhamel's integral method and com-

pared with the measured DFR. The magnitude of the slamming forces on the front and rear faces is also obtained using FRF approach. A comparison of the slamming force on the GWK truss structure for the slamming model developed in this study and the models conceptually developed for breaking wave on single slender piles is performed.

The new slamming formulae will be applied to predict slamming forces induced by breaking waves on the front and rear faces of a full-scale jacket structure called 'OC4 jacket'.

3.7 Summary of key results

Unlike the case of single slender piles, where a large number of diverse studies are available, including the aforementioned well-known equations (e.g. Goda, 1966; Tanimoto et al., 1986; Wienke & Oumeraci, 2005) which are widely applied for the calculation of breaking wave force on mono-piles, less attention has been paid to the total forces induced by breaking waves on jacket structures. In fact, no reliable wave load formula is yet available for the prediction of wave slamming force on a truss-type structure. Therefore, the formulae developed for the calculation of the wave slamming force on mono-piles are still applied for jacket structures. This might result in uncertainties of breaking wave-induced forces on this type of structures. In fact, the total dynamic response of the structure is affected by the characteristics of the wave load (e.g. slamming force pattern, slamming coefficient, impact load duration, impact area, breaking wave celerity for the different members of the structure), which might be significantly different from those applied on a single pile due to the interactions of the different processes and their time lags at the different structures members (Figure 3-16).

Given the aforementioned knowledge gaps, the data from a total of 94 laboratory (regular) wave tests performed in the large wave flume GWK within the frame of the WaveSlam project are analysed to improve the understanding of the process involved in wave-jacket structure interactions. The implementation of the developed codes based on the Duhamel's integral and Frequency Response Function methods on the GWK experiments by considering the physical processes involved in the interaction of breaking waves with different members of the jacket structure resulted in a new set of formulae for the prediction of slamming forces induced by breaking waves on the front face and rear face of jacket structures. The concluding remarks drawn from the new slamming formulae are summarized as follows:

(i) Considering the very small magnitude of the slamming forces on the side braces of the truss structure as compared to those on the front face (<10%) and in order to come up with simpler prediction formulae for slamming force on truss-type structures, the impact force on the side braces are neglected. Therefore, the wave slamming formulae for breaking waves on the entire truss structure were developed by considering only the wave impact forces on the front and rear faces.

(ii) The new slamming model and formulae for breaking waves on the front and rear faces of jacket structures are physically-based and based on a relatively simple shaped (trapezoidal) force history; they allows us to systematically predict the wave slamming forces

depending on the distance between the incipient wave breaking location and the structure front, the characteristics of the incident wave and the geometry of the structure.

(iii) The high accuracy of the new formulae in predicting the wave slamming force and duration has been proven by comparing the amplitude, signal-correlation and spectrum correlation of the measured dynamic force responses (DFR) with those DFR induced by the slamming force history obtained from the proposed formulae.

The new slamming model is valid for jacket structures subject to depth-induced wave breaking on a sloped bottom (i.e. plunging breaker) for the hydrodynamic conditions tested in the large wave flume GWK as described in Section 3.1, but may also be applied for similar types of wave breaking in larger water depths induced for instance by wave-wave interaction (i.e. focused waves). It should also be stressed that only regular wave tests were considered for the development of the new formulae, so that verification for irregular waves might be required. Moreover, the formulae are developed with the assumption that the structure is rigid. Consideration of the moveable slender piles due to the “rocking motions” of the entire structure might affect the process involved in the interaction of breaking wave and slender piles (e.g. pile-up process) and may consequently change both magnitude and duration of the impact forces on the structure.

The magnitude of the forces on the braces of the side faces of the jacket, which are omitted in the new formulae for the sake of simplicity, might be considered conservatively by an additional force with a magnitude of 10% of the slamming force on the front face and an impact duration proposed in this study. However, more investigation is required to obtain a more realistic impact time for breaking waves on side braces.

4 Wave loads by breaking and non-breaking waves on jacket structures

Jacket structures are commonly fixed in intermediate to deep water depth; they are frequently subject to breaking and near-breaking waves. Breaking waves may apply very high forces on jacket structures possibly affecting their stability (Figure 4-1). Although a breaking wave induced force might create the worst loading case scenario on a jacket structure, so far, no method for the prediction of this extreme load on truss-type structures is provided. The design procedure of a jacket structure in practice is commonly performed using the significant non-breaking wave height with a return period of 100 years.

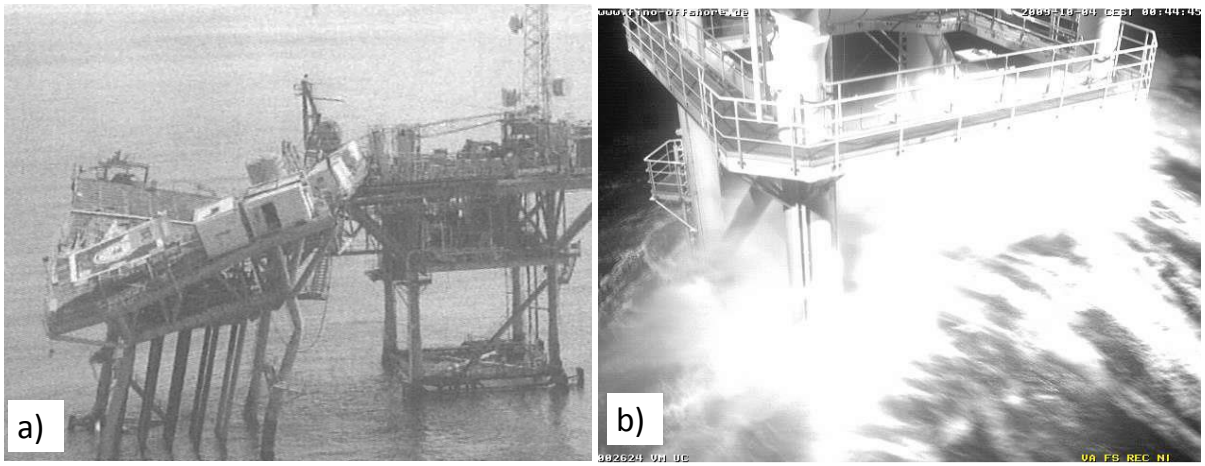

Figure 4-1. a) Damaged jacket platform EUGENE ISLAND 322 in the Gulf of Mexico in 2002 due to extreme waves on the structure (Nickerson, 1993); b) Snapshot of an approximately 15m breaking wave with a crest to crest period of 9s captured at FINO I on the 4th of October 2009. (Germanischer Lloyd, 2009)

With this background, the main objective of this chapter is to improve the understanding of the process associated with the interaction of breaking and near-breaking waves with jacket structures and to improve the methods and techniques to calculate total breaking, near-breaking and non-breaking wave loads on these structures. For this purpose, the CSD model set-up for the GWK truss structure and the model discretization are first briefly described in section 4.1. Second, a CFD model set-up for the GWK tests is introduced and the numerical model is validated against the measurements in the laboratory tests (section 4.2). Afterwards, the Morison equation is implemented to calculate the wave forces by non-breaking to near-breaking waves on the GWK truss structure and the validity range of the Morison Formula is investigated based on the data from the GWK tests (section 4.3). In section 4.4, an approach is proposed to calculate total breaking wave loads and the corresponding DFR & TFR of truss-type structures by combining the Morison formula and the new wave load formulae proposed in Chapter3 of the present study. Finally, the key results are summarized and concluding remarks are drawn in section 4.5.

4.1 CSD model of the GWK truss structure

The CSD model of the GWK truss structure is set-up in the ANSYS software using the BEAM 188 element. BEAM188 is an element for the analysis of slender to moderately stubby/thick beam structures. The element characteristics are based on the Timoshenko beam theory considering shear deformation effects, which is a first order shear deformation theory that considers a constant transverse shear strain through the cross-section. This means that the cross-sections remain plane and undistorted after deformation.

The element used for braces and legs of the truss structure is a linear (2-node) or a quadratic beam element in 3-D. This element has six transitional and rotational degrees of freedom at each node and includes stress stiffness terms. The provided stress stiffness terms enable the elements to analyse flexural, lateral, and torsional stability problems (using eigenvalue buckling or collapse studies with arc length methods). Elasticity, creeping, and plasticity models can be supported (irrespective of cross-section subtype) by the element which has been used to develop the model. A cross-section associated with this element type can be a built-up section referencing more than one material. In general, this element is suitable to model slender or stout beams. Due to the limitations of the first order shear deformation theory, only moderately "thick" beams may be modelled and analysed using this element.

When the material associated with the elements has an inelastic behaviour or when the temperature varies across the section, constitutive calculations are performed at the section integration points. For more common elastic applications, the element uses pre-calculated properties of the section at the element integration points. However, the stresses and strains are calculated in the output pass at the section integration points.

BEAM188 allows for the analysis of built-up beams (i.e., those fabricated of two or more pieces of material joined together to form a single, solid beam). The pieces are assumed to be perfectly bonded, so that the beam is assumed to behave as a single member. In general, the limitations and restrictions of the element can be summarised as follows: (i) the beam must not have zero length; (ii) the effect of warping restraint is assumed to be negligible; (iii) cross-section failure or folding is not accounted for; (iv) rotational degrees of freedom are not included in the lumped mass matrix if offsets are present; (v) it is recommended not to use this element for problems dominated by large rotations since this element works best with the full Newton-Raphson solution scheme (that is, the default choice in solution control); (vi) As mentioned before, only moderately "thick" beams may be analysed using this element.

The structural elements support linear as well as nonlinear analyses, includes plasticity, large deformation and nonlinear collapse. Figure 4-2 shows the discretized model (FE) of the GWK truss structure in ANSYS.

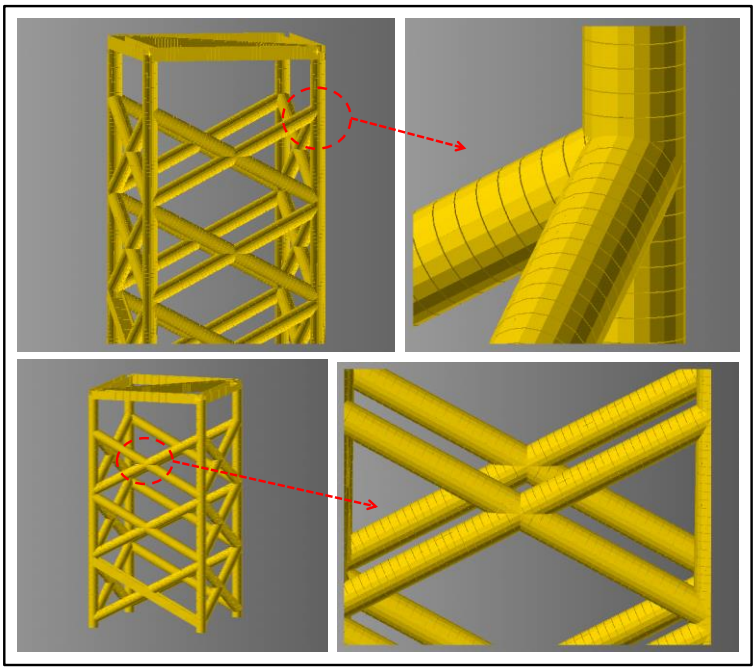

Figure 4-2. Discretization of the GWK truss structure in the CSD model ANSYS

The structure is discretised into 2184 nodes with the distance of approximately 5 cm in order to achieve a high accuracy and computational efficiency. The location of each node in Cartesian coordinate is obtained in order to define similar nodes in the set-up CFD model of the GWK wave flume.

The model of the GWK truss structure is set-up in ANSYS. The model is discretised into a large number of nodes representing the legs and braces of the structure. The information of the node coordinates is obtained from the FE model and will be imported latter in the CFD model which is set-up for the large wave flume GWK.

4.2 CFD model of the large wave flume GWK

The open-source CFD library OpenFOAM contains a method for solving free surface Newtonian flows using the Reynolds Averaged Navier Stokes equations coupled with a Volume of Fluid method (RANS-VOF). In this section, a brief description of the set-up model is provided. The wave generation and absorption method termed ‘wave relaxation zones’ implemented in the model is described, and the model set-up is applied to reproduce the GWK tests.

4.2.1 Governing equation

The governing equations for the two phase flow (air and water) are the following Reynolds Averaged Navier–Stokes equations (Jacobsen et al, 2012):

$$\frac{\partial \rho \boldsymbol{u}}{\partial t} + \nabla.[\rho \boldsymbol{u}\boldsymbol{u}^T] = -\nabla p^* - \boldsymbol{g}.\boldsymbol{x}\nabla\rho + \nabla.[\mu\,\nabla \mathbf{u} + \rho\boldsymbol{\tau}] + \sigma_T\,\boldsymbol{k}_\gamma\,\nabla\gamma \quad (4\text{-}1)$$

Coupled with the continuity equation for incompressible flow:

$$\nabla.u = 0$$

Where $\boldsymbol{u} = (u, v, w)$ is the velocity field in Cartesian coordinates, p^* is the pressure in excess of the hydrostatic pressure, ρ is the fluid density, $\boldsymbol{g}$ is the acceleration due to gravity and μ is the dynamic viscosity of the fluid. $\rho = \rho(x)$ varies with the air/water content in the computational cells. $\boldsymbol{\tau}$ is the specific Reynolds stress tensor which can be expressed as follows:

$$\boldsymbol{\tau} = \frac{2}{\rho}\mu_t\,\boldsymbol{S} - \frac{2}{3}k\,\boldsymbol{I} \quad (4\text{-}2)$$

where μ_t is the dynamic eddy viscosity, **S** is the strain rate tensor ($\frac{1}{2\,(\nabla \mathrm{u} + (\nabla \mathrm{u})^T)}$) and $\boldsymbol{k}$ is the turbulent kinetic energy per unit mass. ∇ is $(\frac{\partial}{\partial x}, \frac{\partial}{\partial y}, \frac{\partial}{\partial z})$, where $\boldsymbol{x} = (x, y, z)$ are the Cartesian coordinates. The last term in Eq (3-2) is the effect of surface tension, where σ_T is the surface tension coefficient and k_γ is the surface curvature. The surface tension coefficient between air and water at 20 C is 0.074 kg/s^2; however, its presence will only have minor effects in civil engineering applications.

The equations are solved for the two immiscible fluids simultaneously where the fluids are tracked using a scalar field γ. γ is 0 for air and 1 for water, and any intermediate value is a mixture of the two fluids. Using γ, one can express the spatial variation in any fluid property, such as μ and ρ, through the weighting:

$$\phi = \gamma\,\phi_{water} + (1-\gamma)\;\phi_{air} \quad (4\text{-}3)$$

4.2.2 Mesh definition

The mesh is generated from a dictionary file named blockMeshDict located in the constant/polyMesh directory of a case. blockMesh reads this dictionary, generates the mesh and writes out the mesh data to points and faces, cells and boundary files in the same directory.

The principle behind blockMesh is to decompose the domain geometry into a set of 1 or more three dimensional, hexahedral blocks. Edges of the blocks can be straight lines, arcs or splines. The mesh is ostensibly specified as a number of cells in each direction of the block, sufficient information for blockMesh to generate the mesh data. (OpenCFD, 2012)

Each block of the geometry is defined by 8 vertices, one at each corner of a hexahedron. The vertices are written in a list so that each vertex can be accessed using its label, remembering that OpenFOAM always uses the C++ convention that the first element of the list has label '0'.

Figure 4-3 shows the generated Mesh for the large wave flume GWK using blockMesh. As can be seen, the mesh is chosen fine enough in order to achieve a good accuracy. For the area

beside the SWL, the mesh is denser since in one way the water particle kinematics has a complex behaviour beside SWL, and in the other way the model should be capable to consider the breaking wave – air interactions. In the higher part of the flume, which is not reached by the waves, the selected mesh is coarser to ensure higher computational efficiency.

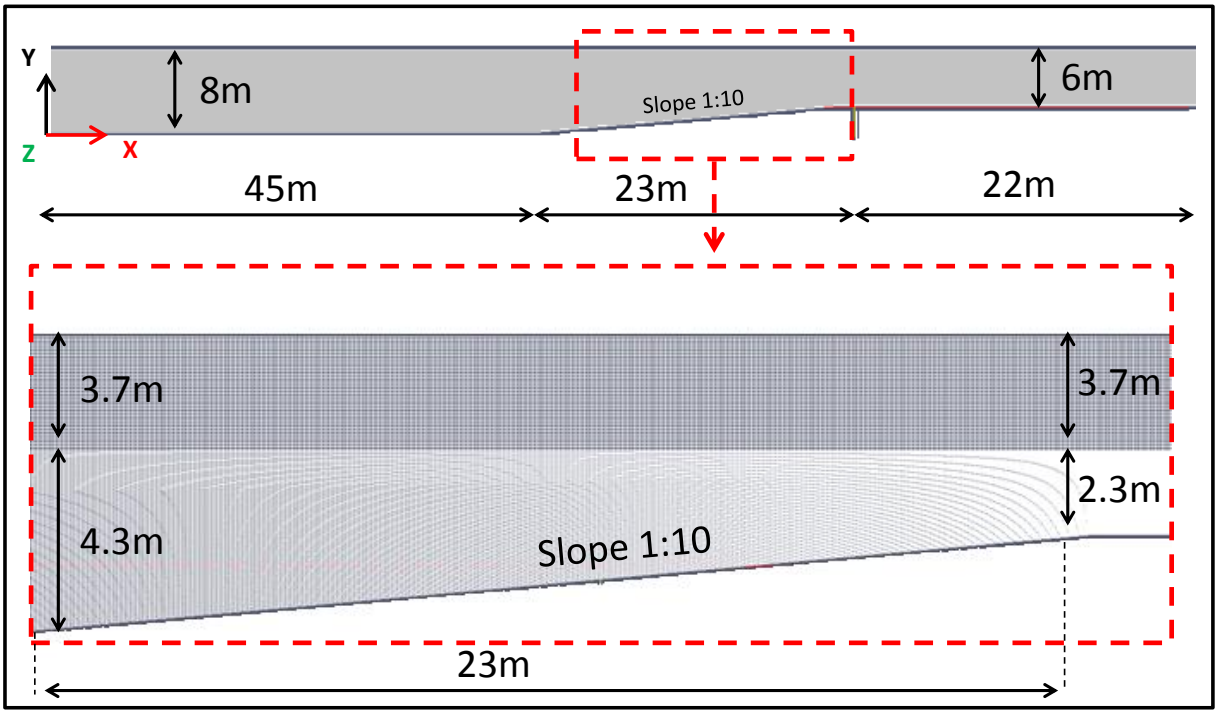

Figure 4-3. Generated mesh for the GWK large scale wave flume using blockMesh

The total length of the large wave flume GWK is 347 meter, which is too long to be entirely modelled by OpenFOAM. Therefore, only a selected part of the flume is considered. It means that the wave propagation in some parts of the far field is ignored. The considerable changes in water particle kinematics and water surface elevation mainly occur when the incident non-breaking/breaking wave approaches the foreshore slope which is located in front of the structure in the GWK wave flume and before the slope, between the wave maker and the foreshore slope the wave characteristics may not change significantly since the cross section of the flume is constant along the aforementioned zone. Therefore, this length is shortened from 150 meter in GWK to 45 meter in the numerical model set-up (Figure 4-3). In addition, the hydrodynamic properties of the post breaking wave for the region far behind the GWK truss structure are also excluded. Therefore, the flume length behind the GWK truss structure considered in the numerical model set up is 22 meter instead of 174 meter in reality. Using the aforementioned simplifications the run time of the CFD model is decreased significantly.

4.2.3 Wave absorption

Relaxation zones are added to the model in order to avoid wave reflection from outlet boundaries and in addition to avoid internal wave reflection in the simulation domain to interfere

with the wave maker boundaries. The former effect obviously affects the results and leads to miscalculation of the water particle kinematics and surface elevation. This might lead to discontinuities in the water surface elevation at the boundary of wave maker, which may result in divergent solutions. The implemented relaxation technique is an extension to the Mayer et al. (1998) approach. The following relaxation function is applied in the relaxation zone (Jacobsen et al, 2012):

$$\alpha_R(x_R) = 1 - \frac{\exp(x_R^{3.5}) - 1}{\exp(1) - 1} \qquad \text{for} \qquad x_R \in [0;\ 1] \tag{4-4}$$

This function is implemented in the relaxation zone using the following formula:

$$\phi = \alpha_R\, \phi_{computed} + (1 - \alpha_R)\, \phi_{Target} \tag{4-5}$$

where ϕ is either u or γ. The variation of α_R is the same as in Fuhrman et al. (2006). The definition of x_R is such that α_R is always 1 at the interface between the non-relaxed part of the computational domain and the relaxation zone, as illustrated in Figure 4-4.

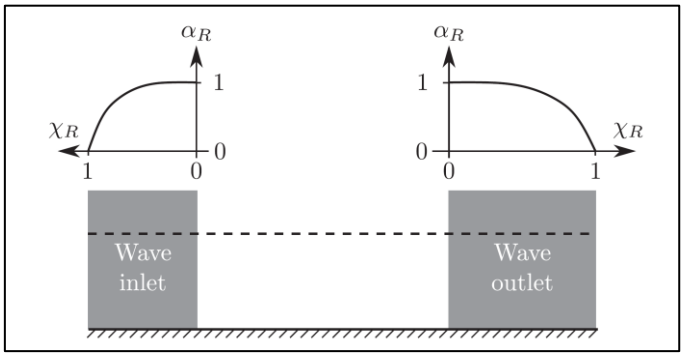

Figure 4-4. A sketch of the variation of $\boldsymbol{\alpha_R(x_R)}$ for both inlet and outlet relaxation zones (Jacobsen et al, 2011)

The length of the relaxation zones is optimized to fulfil the accuracy of the simulation on one hand and increase the computational efficiency on the other hand. Generally, one should try to find the shortest length of the relaxation zone (and consequently the domain) that would not result in wave reflection.

The waves2Foam toolbox (Jacobsen et al, 2011) is implemented to the hydrodynamic solver to allow for generation and dissipation of the water waves inside the domain. For this purpose, the library uses two combined approaches: (i) for inlet of waves, a boundary condition is introduced according to different wave theories, which distinguishes three types of cell faces: dry, wet and interface cell faces; (ii) at interface cells, the VOF value is calculated rather than simply considering all boundary cells just wet or dry.

4.2.4 Validation of the CFD model

In order to validate the CFD model, the records from the measuring instruments shown in Figure 4-5 are used. Three velocity meters are installed close to the front face of the truss

structure in different water elevations. Since the main purpose for the set-up of the numerical model is to reproduce the water particle kinematics for different wave tests performed in GWK, the measurements by the three velocity meters CM01, CM02 & CM03 indicated in Fig, 4.5 are in the main focus.

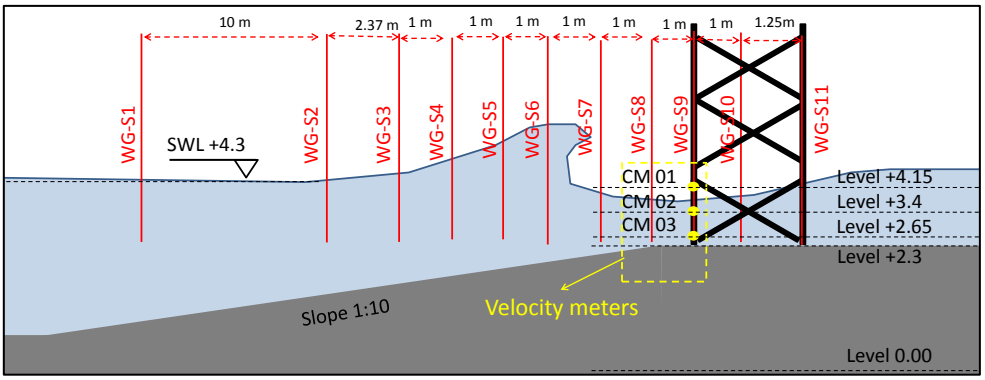

Figure 4-5. Instruments deployed in the GWK tests of the truss structure

Figure 4-6 shows the results of the CFD model for a breaking wave propagating over the slope and approaching the GWK truss structure located just after the slope for load case 2. Incipient wave breaking in the CFD model occurs at time 21.8s and just in front of the structure, which indeed represents loading case 2 according to Figure 3-11. The test diary of the same wave test in the GWK wave flume shows the same load case for the breaking wave on the truss structure.

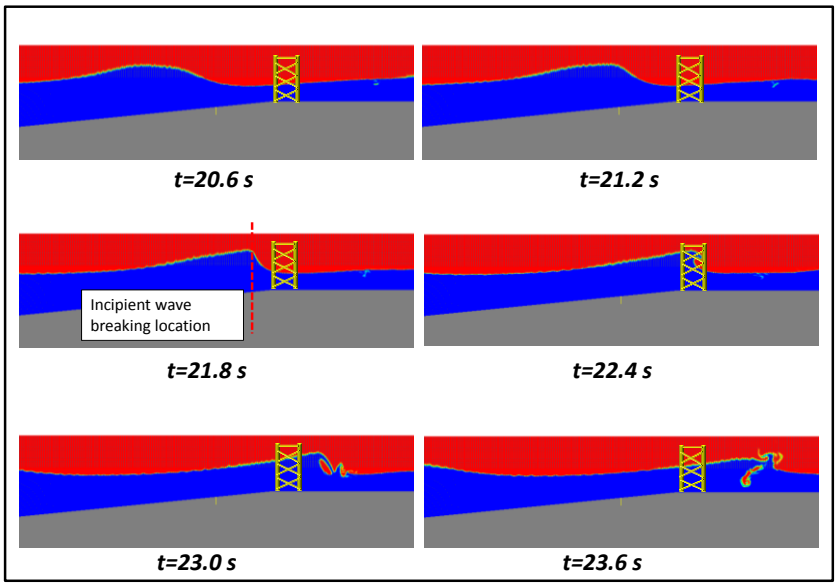

Figure 4-6. Numerical simulation of breaking/broken wave propagation in the large wave flume GWK (Test no. 2013061424; H=1.7m, T=5.55 s, d=4.3m)

Figure 4-7 shows the experimental and numerical results of the water particle velocities for the velocity meters shown in Figure 4-5 for a non-breaking wave on the truss structure. There

is a relatively good agreement between the results of the numerical simulation and the measurements in GWK. It should be stressed, that Figure 4-7a is processed using high frequency filtering considering the fact that velocity meter CM01 is not always submerged.

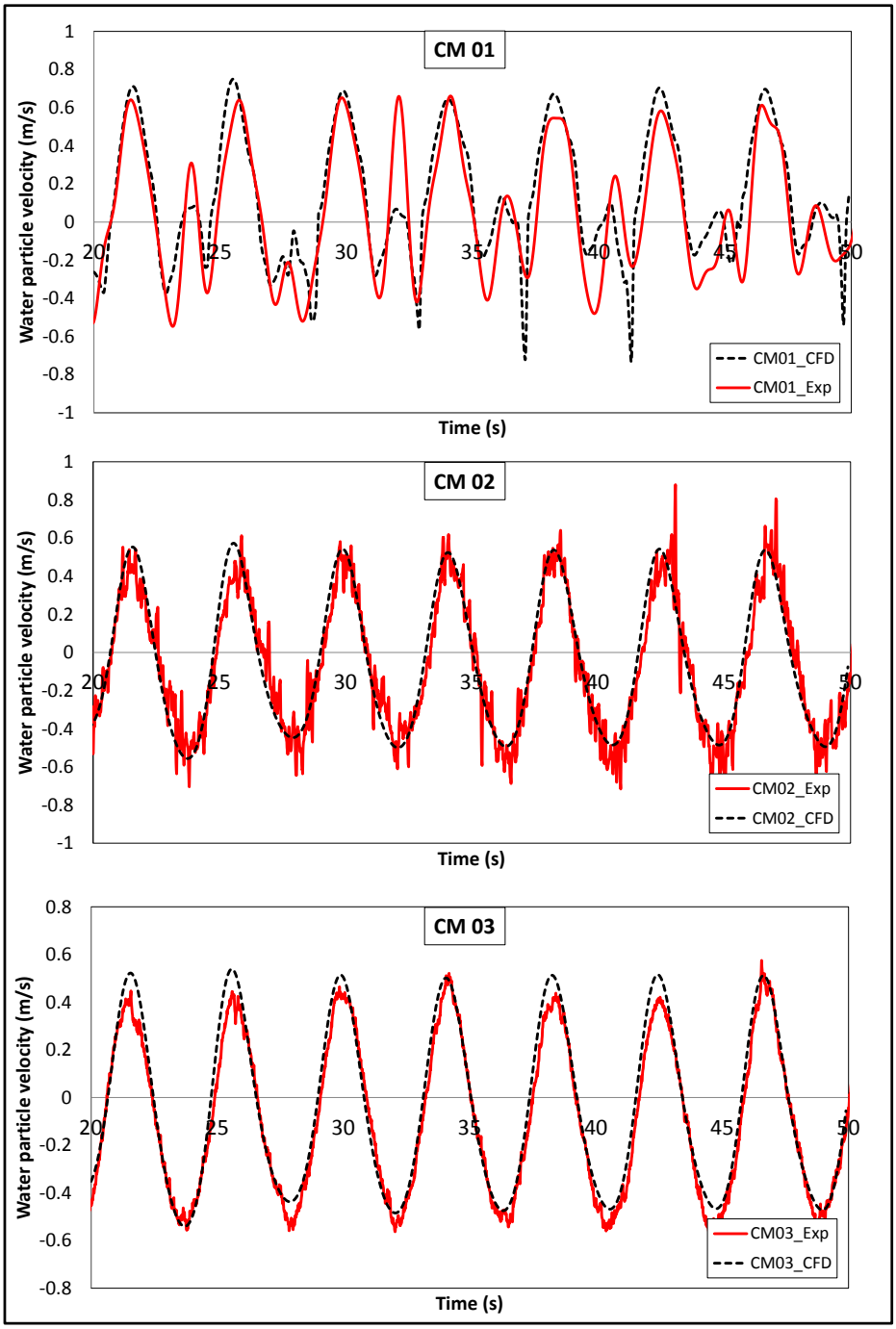

Figure 4-7. Numerical results vs. experimental results of water particle velocities at different elevations for a) CM01; b) CM02 & c) CM03 (Test No. 2013062002; H=0.5m, T=4.2s, d=2m) (see Figure 4-5 for locations of current meters 01-03)

4.2.5 Definition of the nodes representing the truss structure in the CFD model

The model set-up of the GWK truss structure in ANSYS is discretised into 2184 nodes uniformly distributed over the braces and legs of the structure (Figure 4-8a). The selected nodes on the members are defined so that they represent the geometry of the truss structure (Figure 4-8b). The validated CFD model is used to generate more data for water particle velocities in the defined nodes of the truss structure (Figure 4-8c). Numerical computations in the selected nodes provide the required hydrodynamic information to calculate the quasi-static component of the incident breaking/non-breaking wave force on the GWK truss structure. Figure 4-8 shows schematically the defined nodes in the numerical wave flume.

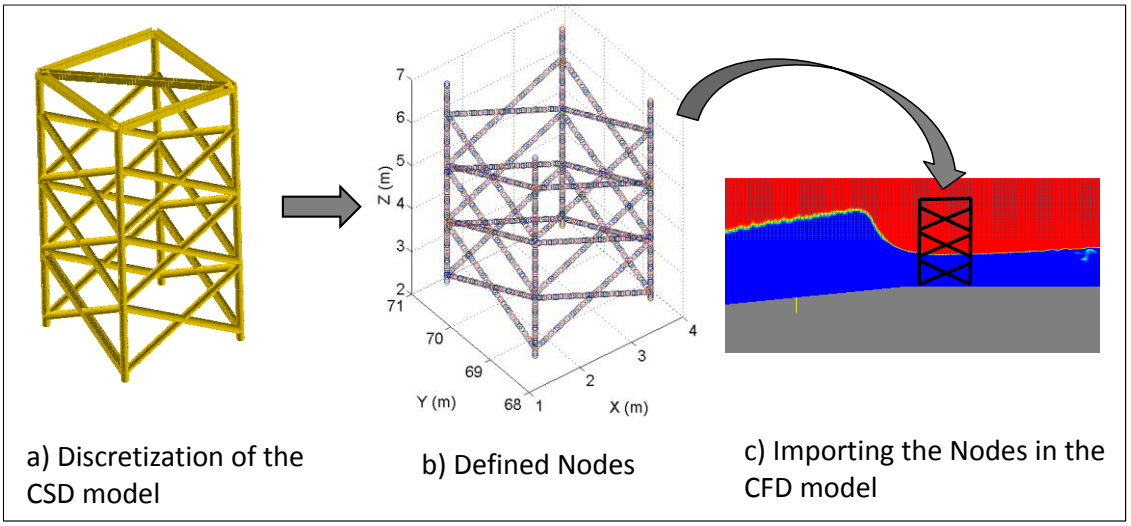

Figure 4-8. Importing the nodes defined in the discretized GWK truss structure into the CFD model

Considering the time series of the flow field obtained in each defined node, *for the quasi-static* component of the force, the Morison equation can be applied by considering the relative values for drag and inertia coefficients. *For the slamming* component, the wave crest celerity obtained from the CFD model can be used as input parameter in the new proposed slamming formulae for truss structures (Eqs.3-4 to 3-6 & Eqs.3-14 to 3-16). Application of the aforementioned approach has the following advantages:

(i) The effect of the water surface elevation phase shifts is considered as the information in each node is obtained according to the geometry of the structure;
(ii) The time series of the water particle velocities are computed with a high accuracy/resolution in space and time;
(iii) Wave-air interaction which might affect the wave propagation, and consequently the wave characteristics, is considered ;
(iv) This approach provides relatively good accuracy for the calculation of the wave forces on the truss structures with relatively lower computational efforts.

It should be stressed that the diffraction effects are not considered as the structural members are slender (D/L=0.002-0.007); and they do not significantly affect the flow considering the

slender members of the structure. Moreover, as the GWK truss structure is fixed, the hydro-elasticity effects are neglected.

A CFD model is set-up for the large wave flume GWK in OpenFOAM which is able to generate non-breaking, near-breaking and breaking waves in the wave flume. The CFD model is applied to reproduce the wave propagation in the GWK and the results for the orbital flow field are validated against the measured. The discretised model of the GWK truss structure is imported in the wave flume just after the slope as in the GWK experiments. The validated CFD model will be used to reproduce the flow parameters (e.g. velocity, acceleration, water surface elevation) at the defined nodes on the legs and braces of the GWK truss structure, which are required to calculate the loads induced by non-breaking and breaking waves on the truss structure.

4.3 Total non-breaking and near-breaking wave loads on jacket structures

The quasi-static wave force on each structural member is calculated by means of the Morison equation using the flow velocity and acceleration obtained from the CFD model. The total quasi-static force is then obtained by superposition of the wave forces on each member of the truss structure. Figure 4-9 shows the methodology used for the calculation of quasi-static forces on the GWK truss structure.

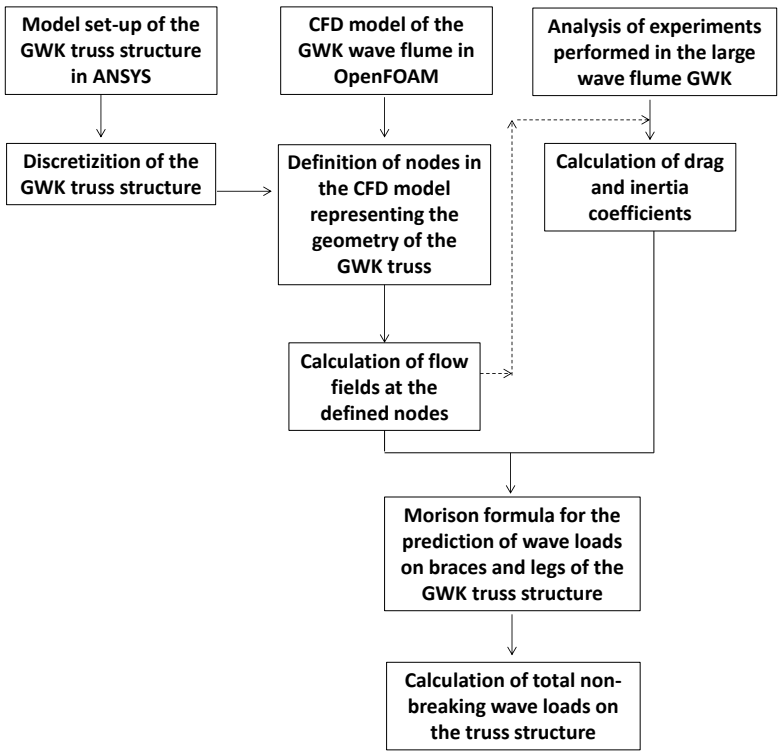

Figure 4-9. Methodology for the calculation of non-breaking wave loads on jacket structures

This section is followed by a description of the approach for the calculation of the time series of wave forces using the Morison equation on legs, side braces and front/rear braces of jacket structures. The aforementioned approach is implemented to reproduce several non-breaking wave tests performed in the GWK and the results are compared with measurements (section 4.3.1). Finally, the validity range and applicability of the Morison equation is discussed in section 4.3.2, considering the wave tests performed for non-breaking and near-breaking waves on the truss structure.

4.3.1 Application of the Morison formula on jacket structures

Morison Formula for each member of the jacket structure

The Morison equation is a semi-empirical equation for the calculation of quasi-static loads on a slender body which consist of a linear superposition of the drag force and inertia force on the body. The results are highly dependent on empirical coefficients C_D and C_M representing drag and inertia, respectively. The Morison equation is applied to estimate the quasi-static component of the wave force on the different members of the jacket structure according to the following seven steps, considering Figure 4-10:

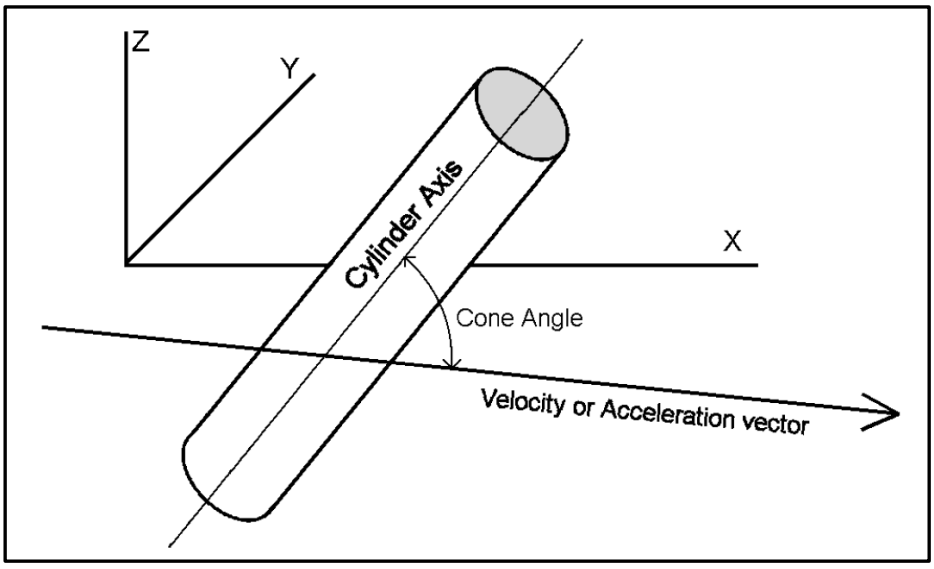

Figure 4-10. A slender member in a fixed x,y,z coordinate system (Definition sketch)

(i) Calculation of the flow velocity and acceleration at the structure member
(ii) Determination of drag and inertia coefficients C_D and C_M
(iii) Determination of the instantaneous wave-induced flow velocity v and acceleration dv/dt. The magnitude and direction of the wave-induced flow velocity ($\vec{v}$) and ($d\vec{v}/dt$) acceleration are determined in a fixed x,y,z coordinate system and their phase should be related to that of the water surface elevation.

(iv) The orientation of the axes of the structural members. The cone angle between the wave-induced flow direction ($\vec{v}$ & $d\vec{v}/dt$) and the structural member is obtained considering the orientation and the geometry of the member.
(v) Based on the results of steps (iii) & (iv), the instantaneous components of velocity and acceleration normal to structural member are determined. These two vectors are both in the plane perpendicular to the member axis but will generally not have to be co-linear.
(vi) Evaluation of the inertia and drag force components at each time step, their direction being defined by that of velocity v and acceleration dv/dt, respectively.
(vii) Integration of the separate forces component over the length of the member in order to calculate the total wave-induced force on the entire member. The calculated loads to be applied at the structure nodes can be found by assuming each member as a simple beam.

In order to apply the Morison Equation to the GWK truss structure, the structure members are classified in three groups: (a) Vertical members or legs (see Figure 4-11a); (b) Front and rear braces (see Figure 4-11b); (c) Side braces of the truss structure (see Figure 4-11c&d). The Morison equation is implemented for each member group as follows:

a) *Vertical members*: The leg is discretized into small cells with the size of 5 cm. The time series of velocity and acceleration are calculated at each cell using the CFD model. The Morison formula is applied for each node considering the obtained velocity and acceleration and the relative drag and inertia coefficient. The total quasi-static force on the entire leg is calculated by superposition of the wave forces on the defined cells.
b) *Front and rear braces:* The water particles at these members induce inline and uplift forces to the structure. In this study, the lateral uplift forces on the structure are ignored since the focus of the study is to calculate the response of the structure to the applied inline forces. It should be stressed, that the lateral uplift force on the structure is much smaller than the inline force and usually not considered for the ultimate limit state analysis of jacket structures. Furthermore, no measurement is performed for the vertical component of the total force on the GWK truss as the total force transducers in the large wave flume (FTTF01-04 in Figure 3-1) have only measured the force response of the structure to inline induced forces.
c) *Side braces:* For side braces parallel to the incident wave, not only the horizontal components (v_h & dv_h/dt), but also the vertical components (v_v & dv_v/dt) of the water particle velocity and acceleration, contributes to the inline force on the structure (see Figure 4-11d). In order to account for both components, they are projected on an axis v_N , (see Figure 4-11d) which is vertical to the inclined member. The resultant force is then calculated by considering both force components projected on axis v_N. The Morison formula is applied for the resultant velocity and acceleration and the two components of the wave force is calculated on each cell (dL) of the braces. The vertical component induces an uplift force on the structure and the horizontal component induces the inline force. In this study, the inline component of the total force is con-

sidered. In general, the total inline forces on side braces of the jacket structures are much smaller than those on the front/rear braces or legs of the structure.

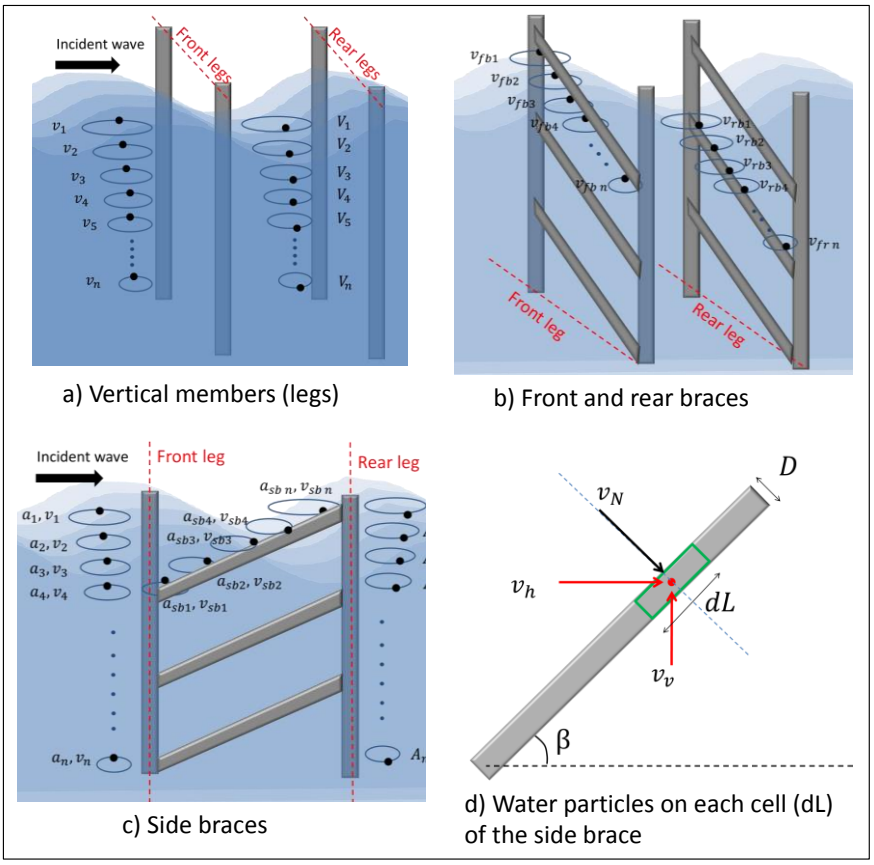

Figure 4-11. Water particle kinematics at different members of jacket structures

Drag and Inertia coefficients

The Morison equation consists of two terms. The inertia term having the phase of the water particle acceleration and the drag term that is proportional to the square of the water particle velocity with a phase shift of 90^o to the inertia term. In addition, this equation contains two empirical hydrodynamic coefficients: drag coefficients C_D and inertia coefficient C_M. Once the necessary data time series are obtained, one is still faced with the problem of determining the appropriate C_D and C_M, coefficients. For this purpose, several approaches are available, depending on the complexity of the structure and the loading, and also on the available computational and laboratory facilities (Chakrabarti, 1980). In this study, the approach proposed by Morison et al (1950) is used in order to obtain drag coefficient C_D. Morison provided a convenient method to determine the coefficients based on the theoretical principles of the oscillating motion. In this method, it is assumed that for an orbital flow under sine or cosine waves, the water particle acceleration is zero when the velocity is maximum.

Based on this simple approach, when the flow water particle velocities are maximum the total wave-induced force on the cylinder is equal to the drag term of the Morsion equation. Therefore, the drag and inertia coefficients can be calculated by the following expressions:

$$C_D = \frac{2\, f_D}{\rho\, D\, u\, |u|} \tag{4-6}$$

$$C_M = \frac{4\, f_M}{\rho\, \pi\, D^2\, \frac{du}{dt}} \tag{4-7}$$

Where f_D and f_M are the drag and inertia forces per unit member length (N/m). The calculation of drag and inertial coefficients is more complicated for the GWK experiments, due to the configuration of the instruments installed in the wave flume. Figure 4-12 shows the configuration of the velocity-meters at the front face of the truss structure. The force measurements are performed for the semi-submerged local force transducer FLTF10 at elevation +4.55 m. This is the lowest local force transducers installed on the GWK structure. However, the measured time series of the water particle velocities for CM01 to CM03 are obtained at lower elevations. It means that, there is no direct measurement of the water particle velocity at the same elevation as that of the force transducer FLTF10.

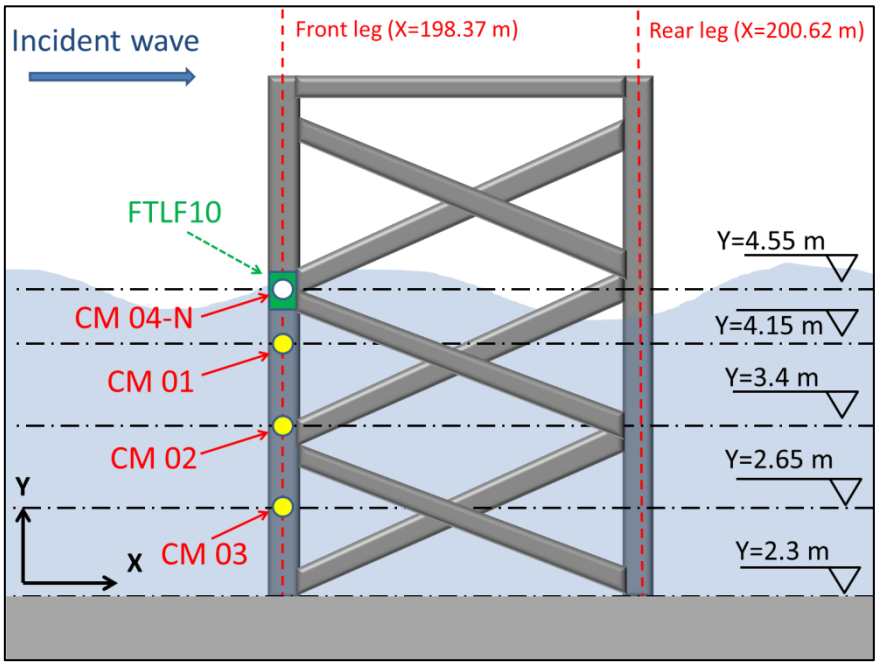

Figure 4-12. GWK truss structure, local force transducer FTLF10 and velocity-meters CM01-CM03

In order to fill this gap, the required data at the same elevation (+4.55 m) as that of FLTF10 are generated using the validated CFD model. For this purpose, the virtual velocity meter "CM04-N" is introduced in the CFD model at elevation +4.55 m as indicated in Figure 4-12. The CFD model is firstly calibrated against the measured data in CM01 to CM03 as was shown in Figure 4-7. The CFD model is then applied to the generated time series of the water particle kinematics at the force transducer FTLF10. Figure 4-13 shows the velocities obtained from the velocity meters CM01, CM02, CM03 and the virtual current meter CM04-N as well as the corresponding time series of the total force on the force transducer FTLF10 (test no. 2013062002). Using Eqs. 4.6 & 4.7, the drag and inertia coefficients are determined by combining the measured local wave-induced force at FTLF10 and the numerically calculated horizontal velocity component at the virtual current meter CM04-N.

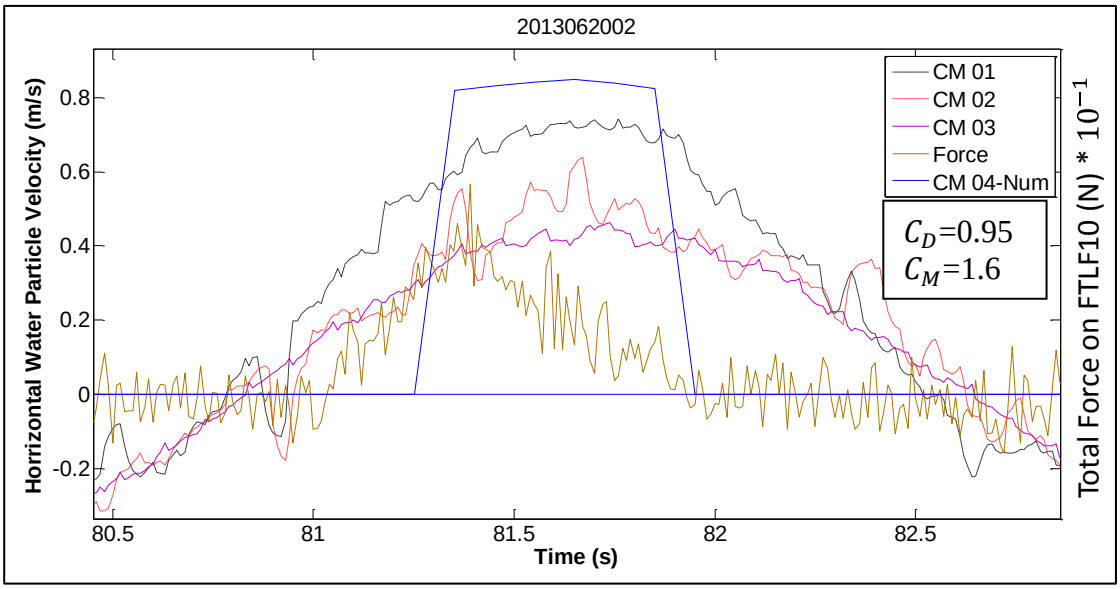

Figure 4-13. Time series of water particle velocity and associated local force on the front leg of the GWK truss structure for test no. 2013062002 (H=0.5 m, T=4.2 s, d=2m)

The time series of the horizontal water particle velocity obtained from CM01, CM02, CM03 and CM04-N as well as those of the local force recorded at FLTF10, together with the calculated drag coefficient, are shown in Figure 4-14 for GWK tests 2013061905. The simulated time series of the total wave forces on the GWK truss structure using the calculated drag coefficients for the mentioned wave tests can be seen in Figure 4-16 and Figure 4-17, respectively.

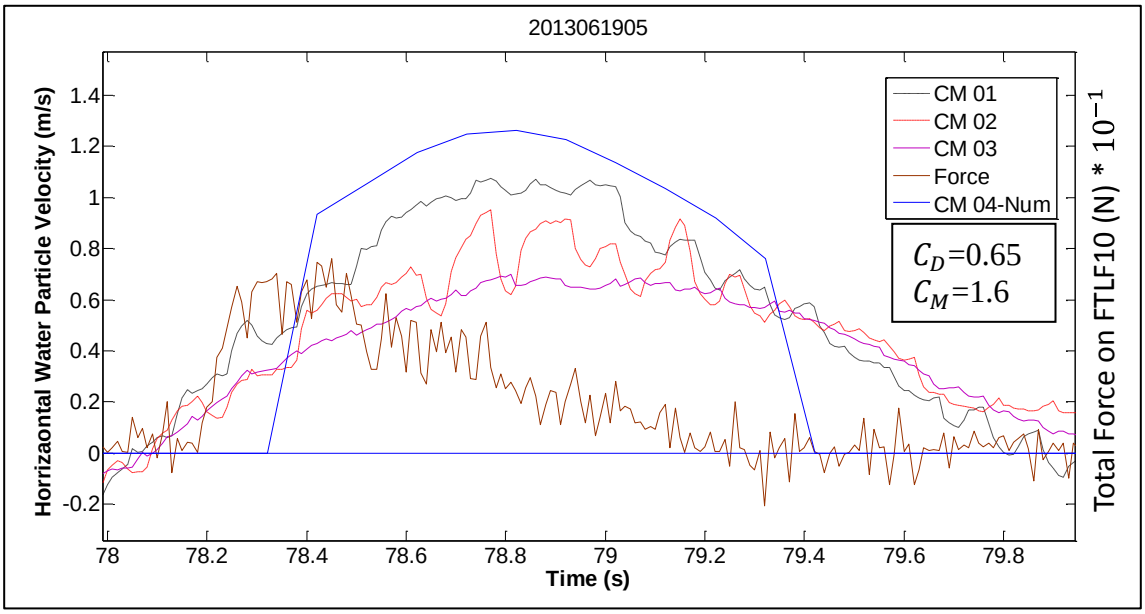

Figure 4-14. Time series of the water particle velocity and associated local force on force at the front leg of the GWK truss structure for test no. 2013061905 (H=0.75 m, T=4.9 s, d=2m)

It has to be stressed, that most of the physical tests in the GWK were performed under hydrodynamic conditions in the range of KC values (KC=25-200) where drag and inertia coeffi-

cients do not vary significantly (Figure 4-13). Figure 4-15 shows the test conditions in the large scale wave flume for non-breaking, near-breaking and breaking waves. As the focus of these experiments are placed on breaking waves on the truss structure, the KC value ($\frac{u\,T}{D}$) for most of the wave tests (87 out of 94 tests) is higher than 40, where the inertia coefficient is approximately constant and the drag coefficient varies in the small range of 0.55 to 0.65, considering the frequency parameter $\boldsymbol{\beta}$ ($\frac{Re}{K} = \frac{D^2}{\vartheta\,T}$) shown in Figure 4-15, (k is surface roughness and ϑ is the viscous kinematic) which varies in the range of 3500 to 6600 for the GWK tests.

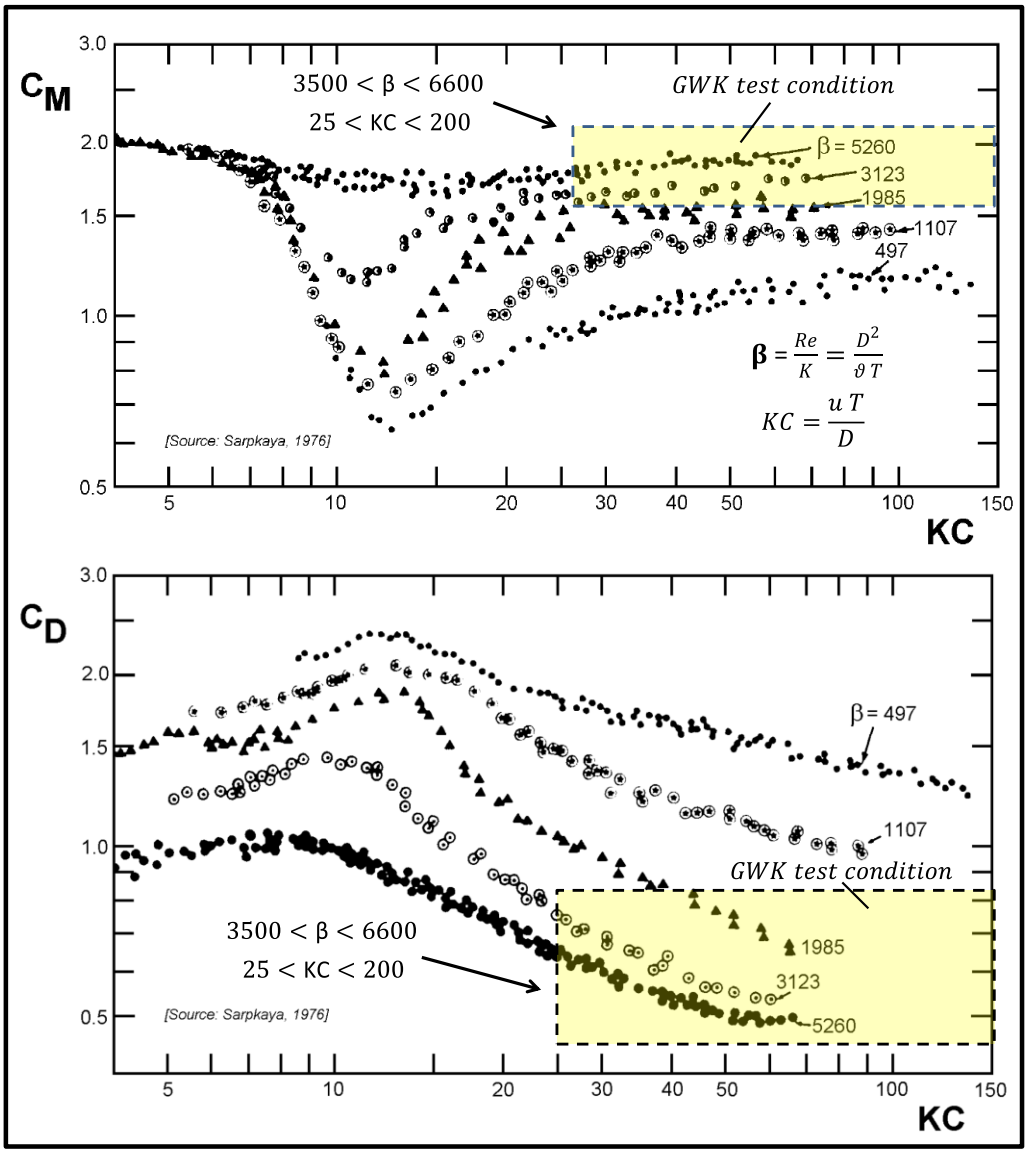

Figure 4-15. Range of Keulegan-Carpenter number KC and frequency parameter $\boldsymbol{\beta}$ for the laboratory tests performed in the large scale wave flume GWK (Modified from Sarpkaya, 1976)

Total non-breaking and near-breaking wave loads

The non-breaking and near-breaking wave force on a member of the truss structure consists of only a quasi-static component and this force is directly measured by strain gauges installed on the structure members. The total non-breaking and near-breaking wave force on the entire GWK truss structure however, is measured by 4 force transducers connected to the structure (see FTTF01-04 in Figure 3-1).

In this section, the quasi-static loads induced by non-breaking and near-breaking waves on each member of the GWK truss structure is computed by means of the Morison equation using the flow velocity and acceleration obtained from the validated CFD model, as well as the C_D and C_M coefficients obtained from the aforementioned approach based on Eqs.4-6 & 4-7. Finally, the total wave force is calculated by superposition of the quasi-static forces on each member of the truss structure and plotted versus the measured force in the GWK flume as well as the surface elevation recorded by WG 9-11 (see locations in Figure 3-8). The results in Figure 4-16 to Figure 4-18 show the total non-breaking and near-breaking wave loads on the entire GWK truss structure reproduced for selected tests (H=0.5 to 1m; T=4.2 to 4.9s; h=4.3m, H_{str}/L_{str}=0.032 to 0.07 & H_{str}/h=0.285 to 0.60).

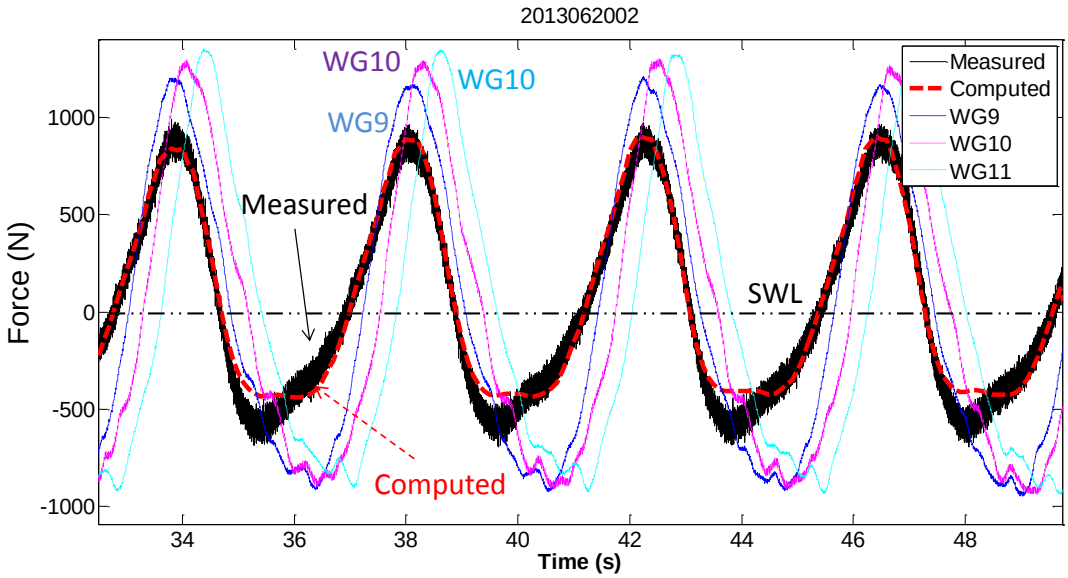

Figure 4-16. Computed and measured total non-breaking wave force on the entire GWK truss structure for wave test 2013062002 (H=0.5 m, T=4.2 s, d=4.3m; H_{str}/L_{str}=0.032 & H_{str}/h=0.285)

As can be seen from Figure 4-16 & Figure 4-17 the total force induced by each non-breaking wave on the truss structure, has only a single peak. Once the height of the incident non-breaking wave increases and the wave becomes steeper, the total force peak becomes narrower. It is probably due to the increasing non-linearity of the wave and the associated increase of the wave celerity. When the wave celerity increases, the wave pass through the structure faster. This implies that the duration of the force transferred from the wave to the structure decreases, thus leading to narrower peaks and wider troughs.

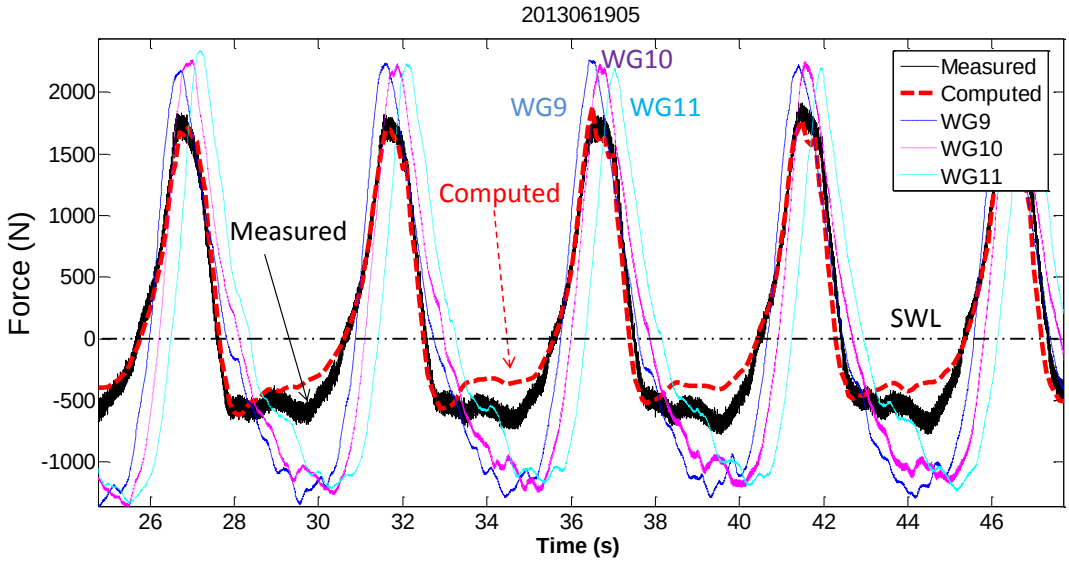

Figure 4-17. Computed and measured total non-breaking wave force on the GWK truss structure for wave test 2013061905 (H=0.75 m, T=4.9 s, d=2m; H_{str}/L_{str}=0.038 & H_{str}/h =0.405)

Figure 4-18 shows a near-breaking wave force on the GWK truss structure. Comparison of the measurements and numerical results for wave test 2013061818 reveals that the difference is less than 5% for the total force magnitude (from crest to trough) and less than 10% for the force amplitude (positive or negative). However, the numerical time series depict two very distinct peaks for each wave event which are much less distinct in the measured time series. The main reason of this difference is that the wave height 1m represents in this test the threshold for incipient wave breaking, called "near-breaking" wave in this report. As can be seen in the measurements and especially at t=37 s, the second peak for the non-breaking wave force is slightly emerging. However, in the numerical simulations, this phenomenon is taking place earlier in time or in space, because the point of incipient wave breaking is one of the issues which are very difficult to predict accurately by any numerical model.

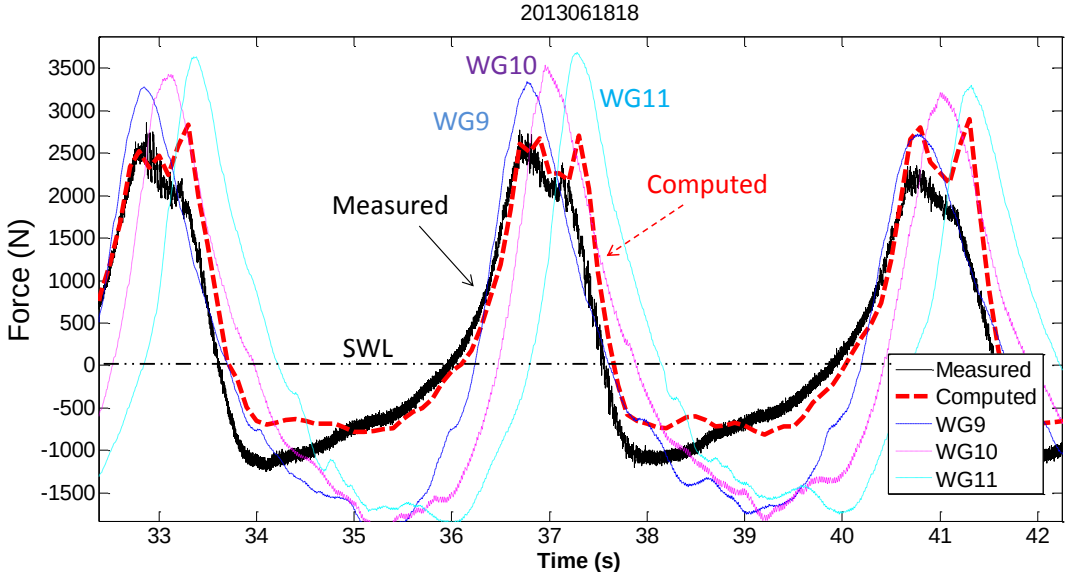

Figure 4-18. Computed and measured total near-breaking wave force on the GWK truss structure- for wave test 2013061818 (H=1 m, T=4 s, d=2m; H_{str}/L_{str}=0.07 & H_{str}/h =0.6)

Overall, the comparison of the measured and calculated forces induced by non-breaking and near-breaking waves (Figure 4-16 to 4-18) on the GWK truss structure shows that, the Morison formula can precisely predict the quasi-static force component on truss structures. The most challenging issue in calculating the wave forces using the Morison Formula is the determination of inertia and drag coefficients. This issue is even more complex for multi-member structures (e.g jackets) as they consist of different vertical, horizontal and inclined members. For *non-breaking* waves (Figure 4-16 and Figure 4-17) on the GWK truss structure the peak and trough of the force were predicted accurately. For *near-breaking* waves (Figure 4-18) however, although the maximum difference for peak to peak amplitudes was less than 10%, the wave non-linearity in the numerical models was higher than that of the actual incident wave in the large wave flume (Actual H_{str}/L_{str}=0.070; Numerical H_{str}/L_{str}=0.076). In general, the applicability of the Morison formula becomes questionable for the prediction of forces induced by steep waves. In the following section, the validity range of the Morison formula for the prediction of forces induced by non-breaking and near-breaking waves in GWK tests is examined.

4.3.2 Applicability and validity range of Morison formula

Currently, wave forces caused by non-breaking and near-breaking waves on jacket structures are estimated using Morison's equation considering the average values of drag and inertia coefficients recommended by different guidelines. Several studies have shown that the Morison equation with drag and inertia terms underestimate the highly nonlinear and breaking wave force on such members and the applicability of this approach is highly questionable with increasing the wave non-linearity (e.g. Wienke and Oumeraci, 2005; Goda, 1966) . However, the validity range and applicability of Morison's equation is not fully clarified yet.

Based on the aforementioned gaps in knowledge and practice, it is crucial for the design and safety assessments to develop an improved understanding of the process involved in the interaction of non-breaking and near-breaking waves with jacket structures and to evaluate the current approaches for the calculation of extreme wave loads on jacket structures. For this purpose, the available laboratory tests on the GWK truss structure under non-breaking and near-breaking waves are used in this section.

In order to discriminate non-breaking and near-breaking waves, a definition of near-breaking wave is tentatively provided as follows: 'Near-breaking waves are those steep waves which apply dynamic force on the structure though their breaker tongue is not fully developed' while non-breaking waves induce only quasi-static loads on the structure. As the Morison Formula cannot predict the dynamic force induced by near-breaking waves on the structure, the threshold between near-breaking and non-breaking waves using a threshold parameter $(H/L)_{crit}$ will determine the validity range of this formula.

The laboratory tests for the GWK truss structure under non-breaking and near-breaking waves are listed in Table 4-1, including the corresponding parameters of the incident waves and other non-dimensional parameters describing the non-linearity (H/L & H/h) and dispersion (h/L) of the waves.

Table 4-1. Non-breaking and near-breaking wave tests performed on the GWK truss structure

Test No.	*H (m)*	*T (s)*	L_{str} *(m)*	H_{str} *(m)*	h_{str} *(m)*	*Wave steepness* (H_{str}/L_{str})	*Wave dispersion* (h_{str}/L_{str})	*Water depth-parameter* (H_{str}/h_{str})	*Description*
2013062002	0.5	4.2	18.00	0.57	2	0.032	0.111	0.285	Non-breaking
2013062101	0.5	5.2	22.70	0.61	2	0.027	0.088	0.305	Non-breaking
2013061903	0.75	4	17.03	0.81	2	0.048	0.117	0.405	Non-breaking
2013061904	0.75	4.6	19.91	0.86	2	0.043	0.100	0.430	Non-breaking
2013061905	0.75	4.9	21.31	0.81	2	0.038	0.094	0.405	Non-breaking
2013061906	0.75	5.2	22.70	0.86	2	0.038	0.088	0.430	Non-breaking
2013061907	0.75	5.55	24.31	0.99	2	0.041	0.082	0.495	Non-breaking
2013061305	1.1	3	11.87	1.14	2	0.096	0.168	0.570	Near breaking
2013061306	1.2	3	11.87	1.16	2	0.098	0.168	0.580	Near breaking
2013061307	1.3	3	11.87	1.16	2	0.098	0.168	0.580	Near breaking
2013061308	1.35	3	11.87	1.2	2	0.101	0.168	0.600	Near breaking
2013061309	1.35	4	17.03	1.43	2	0.084	0.117	0.715	Near breaking
2013061310	1.45	4	17.03	1.6	2	0.094	0.117	0.800	Breaking
2013061410	1.3	4.9	21.31	1.62	2	0.076	0.094	0.810	Breaking
2016061418	1.3	5.2	22.70	1.61	2	0.071	0.088	0.805	Breaking
2013061427	1.4	5.55	24.31	1.71	2	0.070	0.082	0.855	Breaking
2013061818	1	4	17.03	1.2	2	0.070	0.117	0.600	Near breaking

H_0=Wave height far from the structure; T=Wave period; h_{str}=water depth at the structure; H_{str}= Wave height at the structure; L_{str}= Wave length at the structure

Figure 4-19 shows the selected non-breaking waves applied on the GWK truss structure. The total quasi-static force and the corresponding TFR and DFR of the structure are plotted for each wave test. Once the wave becomes steeper, the peak of the TFR becomes narrower. It is probably due to the shape of the non-linear waves with narrower crests and wider troughs. The measurement for these waves show equal signals of the quasi-static forces and TFR meaning that no dynamic force has been applied on the structure. Therefore, these waves are classified in non-breaking waves.

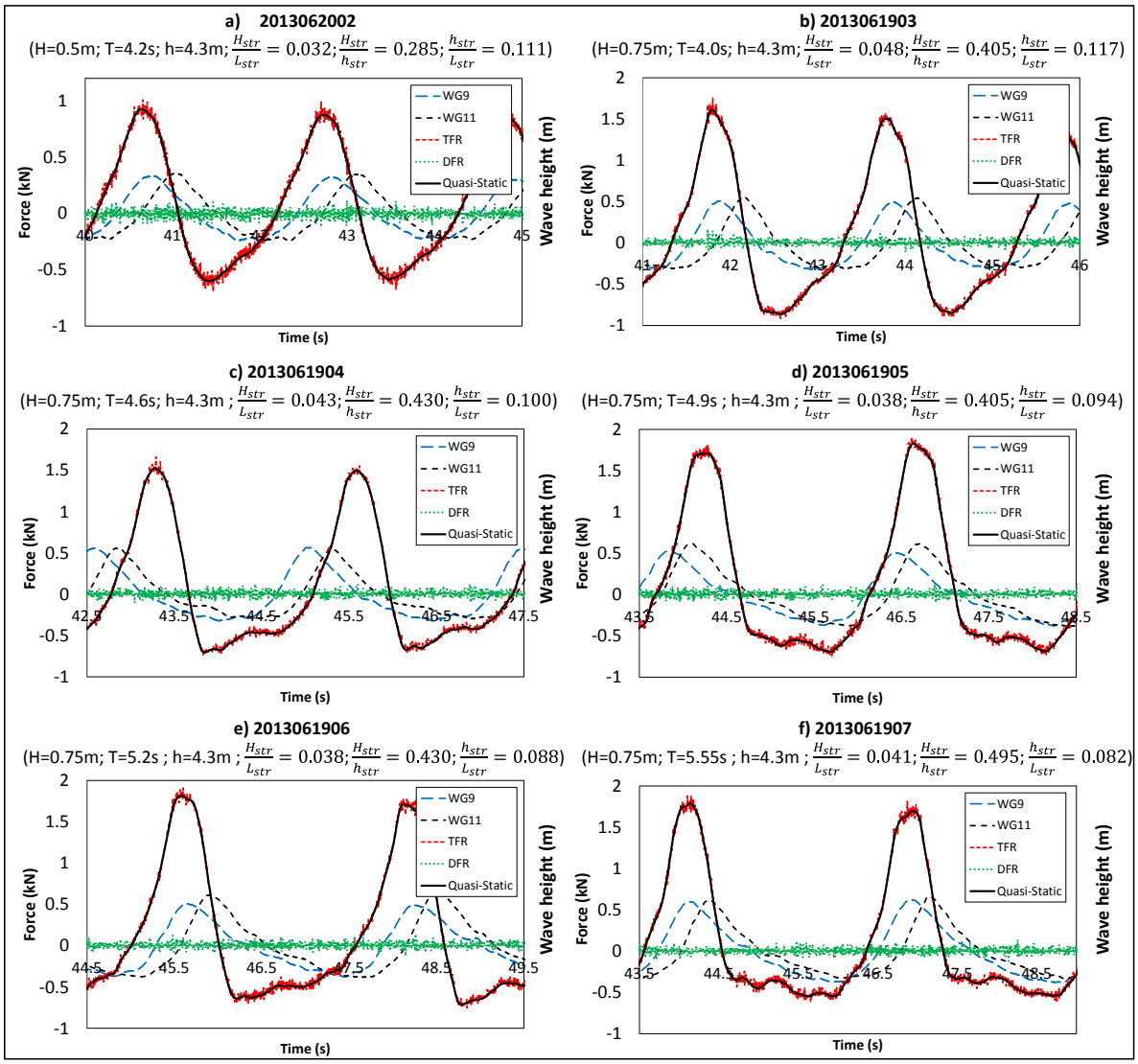

Figure 4-19. Non-breaking waves on the GWK truss structure with total quasi-static force and corresponding TFR and DFR of the structure

Figure 4-20 shows the selected tests for near-breaking waves on the GWK truss and the associated TFR and DFR of the structure. As can be seen, these waves have not only applied a quasi-static force on the structure, but also a slight slamming force on the rear or front face which has been identified by extracting the DFR from TFR using low-pass filter analysis (Frequency=5 Hz). In each wave test shown in Figure 4-20, the magnitude of the slamming force Fs on the GWK truss is obtained in order to quantify the wave loads underestimation neglecting the induced impact force on the structure. The results show that the application of Morison formula for the prediction of forces induced by such waves (see Figure 4-20) might underestimate the actual force considerably (up to 35%).

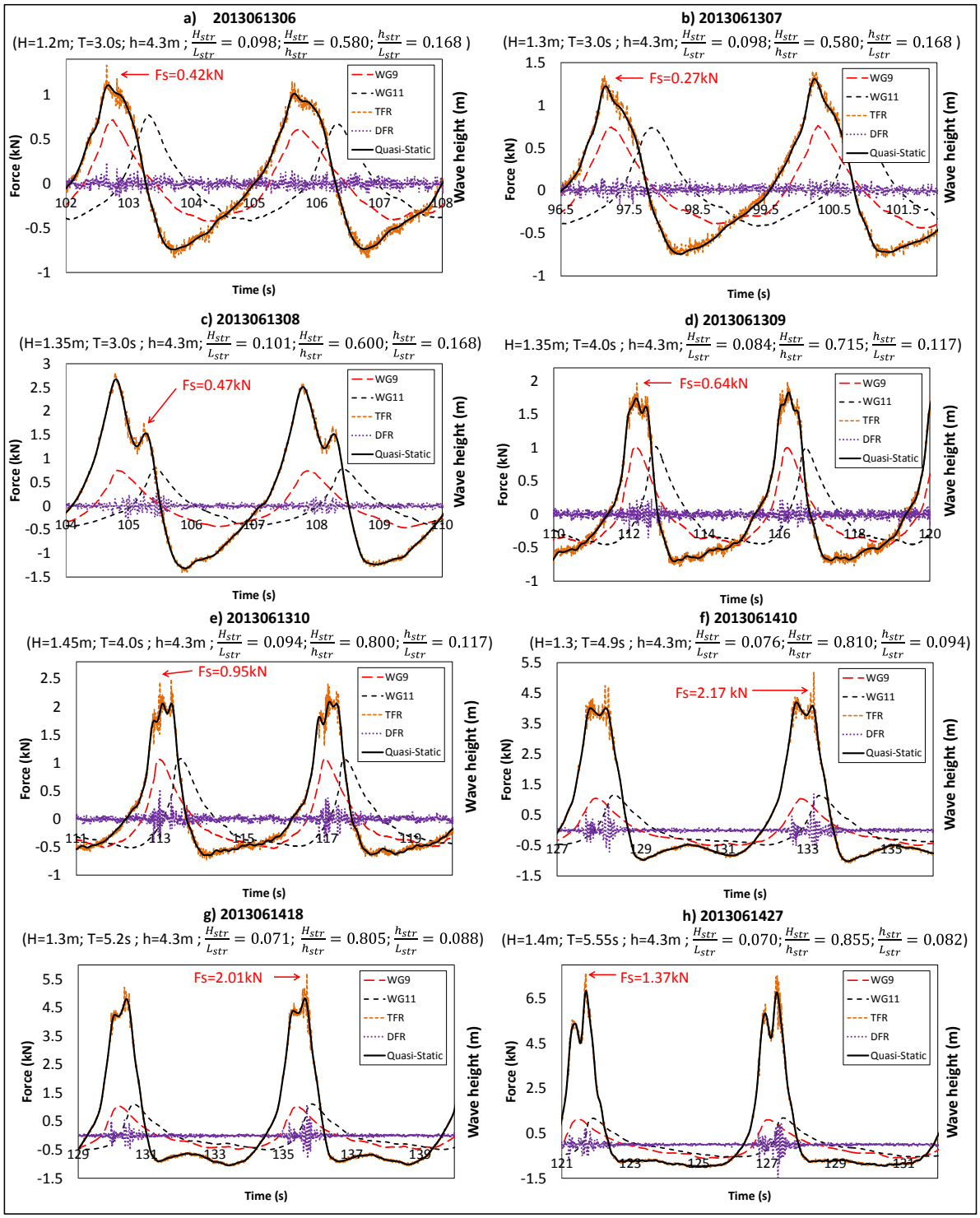

Figure 4-20. Near-breaking and breaking waves on the GWK truss structure with total quasi-static force and corresponding TFR and DFR of the structure

In Figure 4-21, the threshold between near-breaking and non-breaking waves has been identified using the following non-linearity parameters H/L (wave steepness) and H/h (water depth ratio) by analysing the laboratory tests listed in Table 4-1. The investigations re-

vealed that the Morison formulae might underestimate the loads induced by the waves having the following characteristics on truss-type structures:

$$\begin{cases} \frac{H_{str}}{L_{str}} \geq 0.059 \\ \frac{H_{str}}{h_{str}} \geq 0.53 \end{cases} \quad (4\text{-}9)$$

Moreover, the threshold between near-breaking and breaking waves can be determined by Eq.4-10 using the non-linearity parameter $\frac{H_{str}}{h_{str}}$ beyond which the breaker tongue will be formed and the wave induces significant impact forces on the structure:

$$\frac{H_{str}}{h_{str}} = 0.76 \quad (4\text{-}10)$$

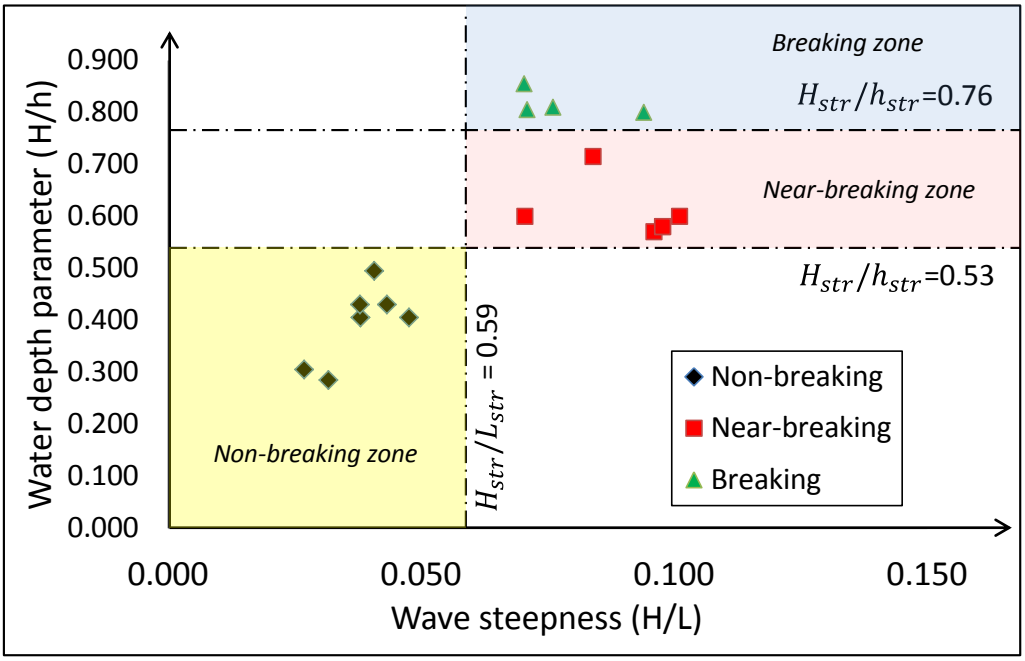

Figure 4-21. The threshold between non-breaking and near-breaking waves

Near-breaking and *non-breaking* wave induced forces on the GWK truss structure are calculated using the Morison equation considering the relative values of drag and inertia coefficients and the flow parameters obtained from the CFD model.

For *non-breaking waves*, the Morison equation can appropriately predict the wave induced forces on the structure.

For *near-breaking waves* however, application of Morison formula might underestimate the wave loads.

As a result of an analysis of the available GWK tests, the threshold values of local wave steepness H/L=0.06 and breaker index H/h=0.53 at the structure tentatively proposed, beyond which the application of Morison formula may result in an underestimation of the force in-

duced by highly non-linear breaking waves by more than 30%. Moreover, the non-linearity parameter of water depth ratio is determined H/h=0.76 for the threshold between near-breaking and breaking waves.

4.4 Total breaking wave forces on jacket structures

In this chapter, total wave induced loads by breaking waves on the entire truss structure are calculated by linear superposition of the *quasi-static* and *slamming* force components according to the methodology proposed in Figure 4-22. The *quasi-static* force component is the part of the force which excludes the effect of wave breaking; i.e. it is similar to the force induced by a non-breaking wave and is calculated using the method described in section 4.3 for the calculation of non-breaking waves on jacket structures. The *slamming* force component is obtained using the new slamming formulae proposed in Chapter 3 for the prediction of impact loads induced by breaking waves on jacket structures. The force response of the GWK truss to quasi-static and slamming loads is then calculated for the selected wave tests. Finally, the total force response (TFR) of the GWK truss structure to selected breaking waves in GWK tests is reproduced and the results are compared against measurements.

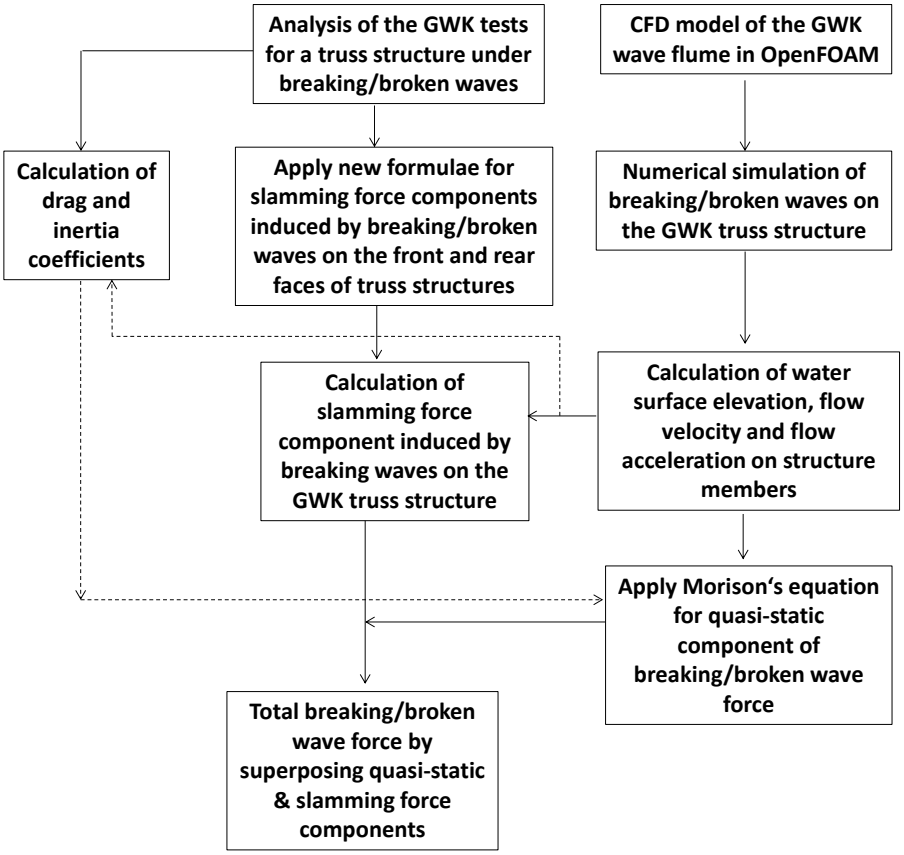

Figure 4-22. Proposed methodology for the calculation of the total force induced by a breaking wave on the GWK truss structure

The total quasi-static component of the force is calculated in section 4.4.1. The total slamming component of the force which applies on the impact area on the front and rear faces and the associated DFR of the structure are calculated in section 4.4.2. Finally, the total force response (TFR) of the truss structure is computed in section 4.4.3.

4.4.1 Quasi-static component of the total breaking wave force

As described in sections 4.2 and 4.3, water particle kinematics and water surface elevation associated with the breaking and non-breaking waves tested in GWK are extracted from the validated CFD model. The surface elevations as well as the time series of water particle velocities and accelerations obtained from the CFD simulation, together with drag and inertia coefficients C_D and C_M, are used in the Morison equation to calculate the time series of the individual quasi-static forces on each leg and on each brace of the truss structure. Through superposition of these individual time series (with due consideration of the related time shifts), the time series of the total quasi-static force on the GWK truss structure are finally obtained. These computations are performed for several wave tests and the calculated results are compared with the pre-processed quasi-static force signals obtained from the measurements in the GWK tests by applying a low-pass filter with a frequency of 5Hz (Figure 4-23)

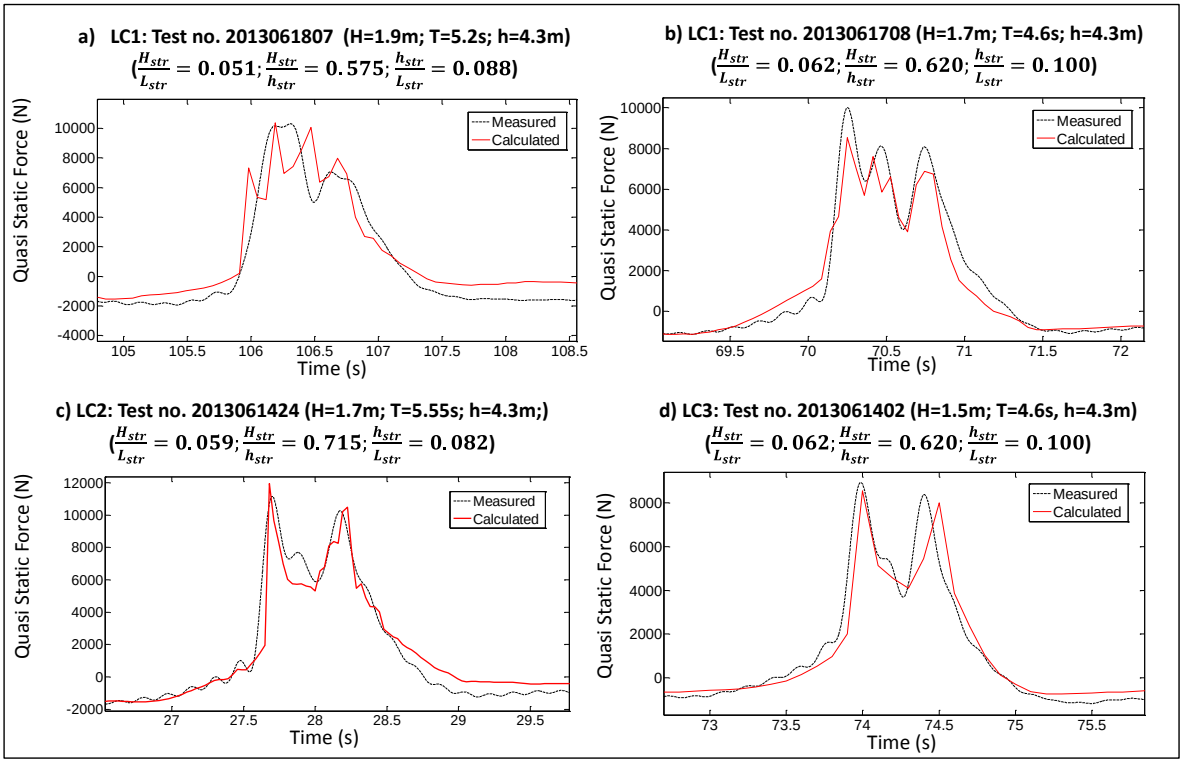

Figure 4-23.Quasi-static component of the total breaking wave force on the GWK truss structure for selected GWK tests and loading cases LC1-LC3

In Figure 4-23 the black curve shows the pre-processed measured signals of the quasi-static component of the response of the structure as extracted from the TFR using a low-pass filter

in comparison with its calculated counterpart (in red) for breaking wave in the selected tests. It should be stressed that breaking wave impact load on truss-type structures is a very stochastic process and thus difficult to predict exactly. This statement is confirmed by the significant variations from wave to wave in the GWK tests, so that the discrepancies between computed and measured forces in Figure 4-23 are still in an adequate range.

4.4.2 Impact component of the total breaking/broken wave force

For any prospective formulae for wave impact forces on structures, it should be stressed that both magnitude and duration of the impact force are not only strongly linked, but also equally important for the dynamic response of the structure. Therefore, a new approach by combining the frequency response function (FRF) and the Duhamel integral was proposed to calculate both magnitude and duration of breaking wave impact forces on truss structures using the insight of underlying processes (see section 3.3), which were gained from the GWK tests. This approach was implemented as follows to calculate magnitude and duration of the impact force on the different faces of the truss structure:

(i) *Front face of the truss structure:* The breaking wave impact force and duration on the front face of the GWK truss structure is calculated by combining the Frequency Response Function (FRF) approach and the Duhamel's integral method (see Eqs. 3-4 to 3-6 in section 3.3)

(ii) *Side braces of the truss structure*: The laboratory tests revealed that the wave impact force on the side braces of the structure are not high compared to the impact force on the front and the rear faces (less than 10%).

(iii) *Rear face of the truss structure*: The analysis of the available experimental data showed that the wave slamming force on the rear face of a truss structure is affected by two main processes called *"sheltering effect"* and *"wave dropping effect"*. Both sheltering and dropping effects are examined separately and a new approach is provided to consider both effects in the calculations of the total impact force on the rear face (see Eqs. 3-14 to 3-16 in section 3.5)

Considering the wave impact load on the front face and that on the rear face of the structure, the time series of the slamming forces on the entire GWK truss structure are determined using the developed slamming formulae (see Figure 3-37) for selected wave tests related to load cases LC1-LC3. The slamming forces on the front and rear faces of the structure are obtained by considering the wave kinematics calculated in the CFD model set-up for waves in the large wave flume GWK. The calculated total slamming forces are then distributed uniformly on the impact area for a curling factor of $\lambda = 0.46$ as recommended by Wienke and Oumeraci (2005). The Duhamel's integral based approach is then implemented to compute the DFR of the GWK truss to these slamming forces considering the truss structure properties (mass=1700kg, natural frequency=24.5s). The computed DFR are compared with the DFR measured in the GWK experiments (Figure 4-24).

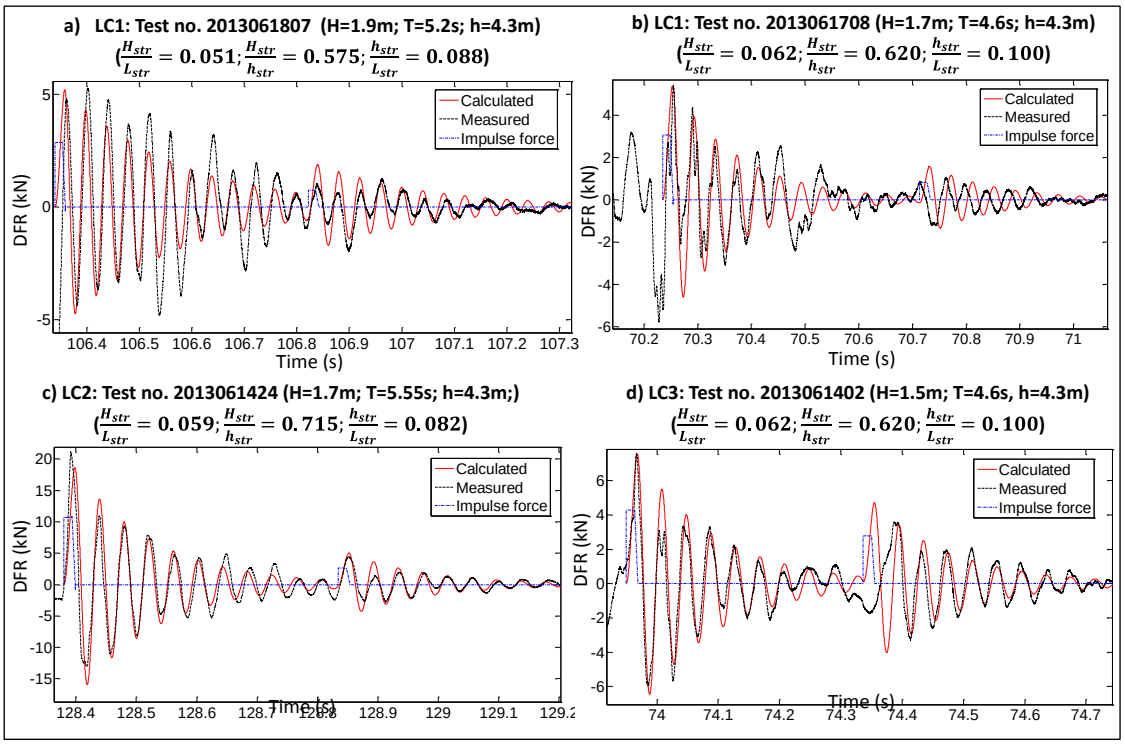

Figure 4-24. Application of the proposed slamming formulae (see section 3.3) on the GWK truss and comparison of the calculated and measured DFR for selected GWK tests and loading cases LC1-LC3

4.4.3 Total Force Response of jacket structures to breaking waves

The total force response (TFR) of the structure is obtained by superposing the quasi-static force response (QSFR) and the dynamic force response (DFR) of the structure as shown in Figure 4-25.

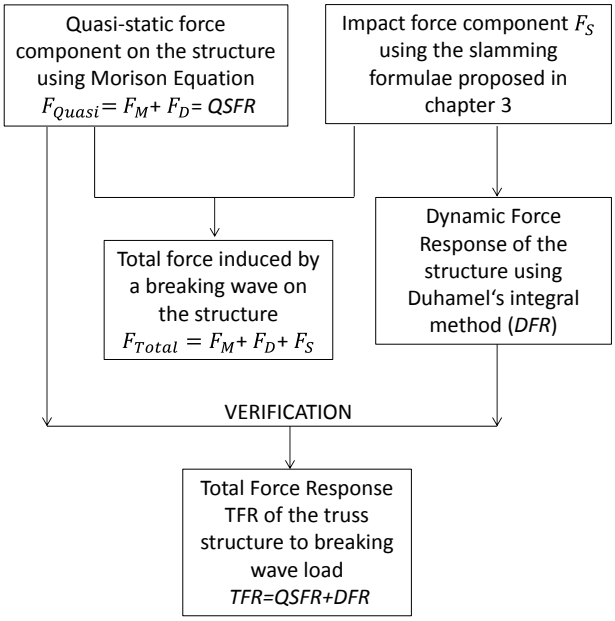

Figure 4-25. Calculation of the total breaking wave force and the associated total force response of the structure (TFR)

Quasi-Static Force Response (QSFR): The force response of the structure to quasi-static forces component is equal to the actual quasi-static force on the structure.

Dynamic Force Response (DFR): As the actual slamming force is not equal to the measured DFR of the structure, a Duhamel's Integral based code is implemented to calculate the DFR. For this purpose, (i) the truss structural properties as well as natural frequency, total mass and structural damping and (ii) the time series of the impulse force as well as total impact time t_d, magnitude F_s and the slamming force load pattern are considered as input parameters. Finally, the total force response (TFR) of the structure for each of the selected wave tests is obtained by superposing the QSFR and DFR of the structure to breaking waves and compared to the TFR measured in the GWK experiments.

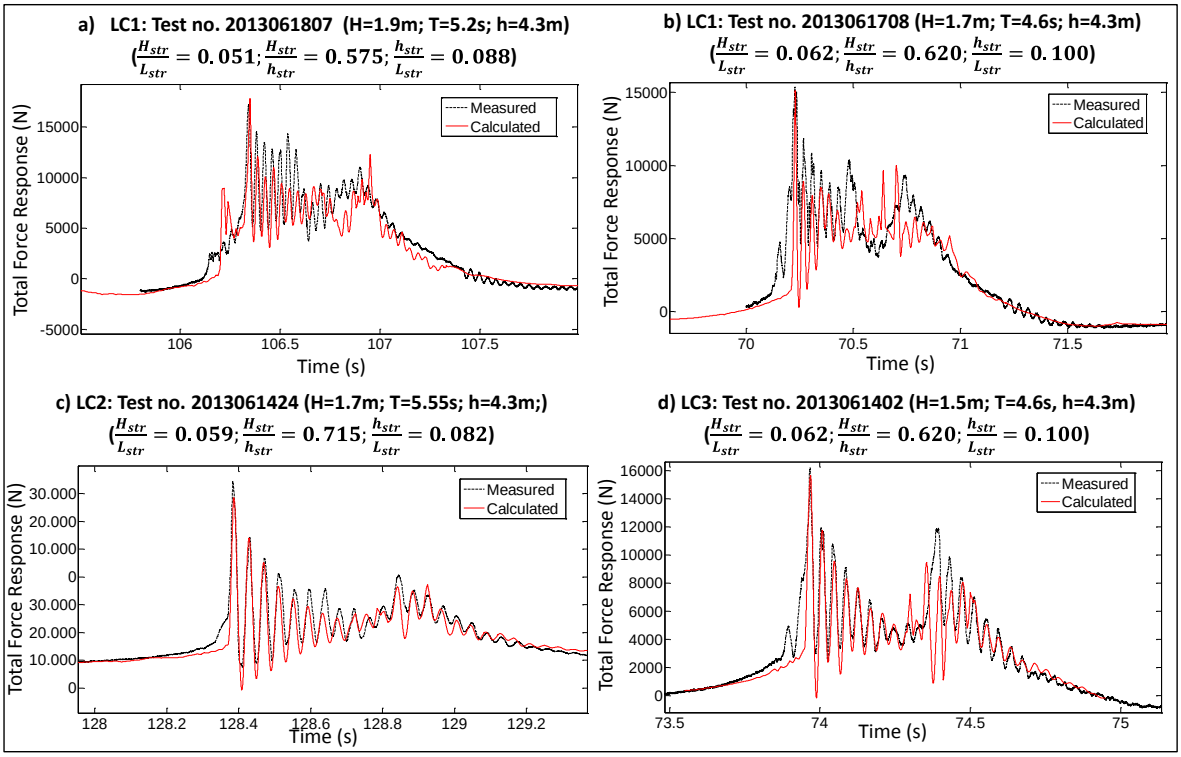

Figure 4-26. Calculated and measured Total Force Response TFR of the GWK truss to breaking waves for selected GWK tests and loading cases LC1-LC3

The computed broken wave impact on the rear face of the GWK truss structure is in some cases is slightly shifted as compared to the measurements (e.g. Figure 4-26a). This might be due to the fact that the advanced CFD model used in this study (OpenFOAM version 2.3.0) is not capable to predict entirely the highly complicated shape of the wave front and kinematics of the water particles associated with breaking and broken waves at and inside such highly complex structures. For this particular wave test and load case in Figure 4-26a (test number 2013061807, LC1), the crest of the broken wave overturns just before approaching the rear face of the truss structure thus releasing a large amount of energy and leading to the complex behaviour of water particles (see Figure 4-27). This process is highly complex to be numerically simulated, so that deviations of the calculated wave forces on the rear face and the asso-

ciated force response of the structure from their measured counterparts can hardly be excluded.

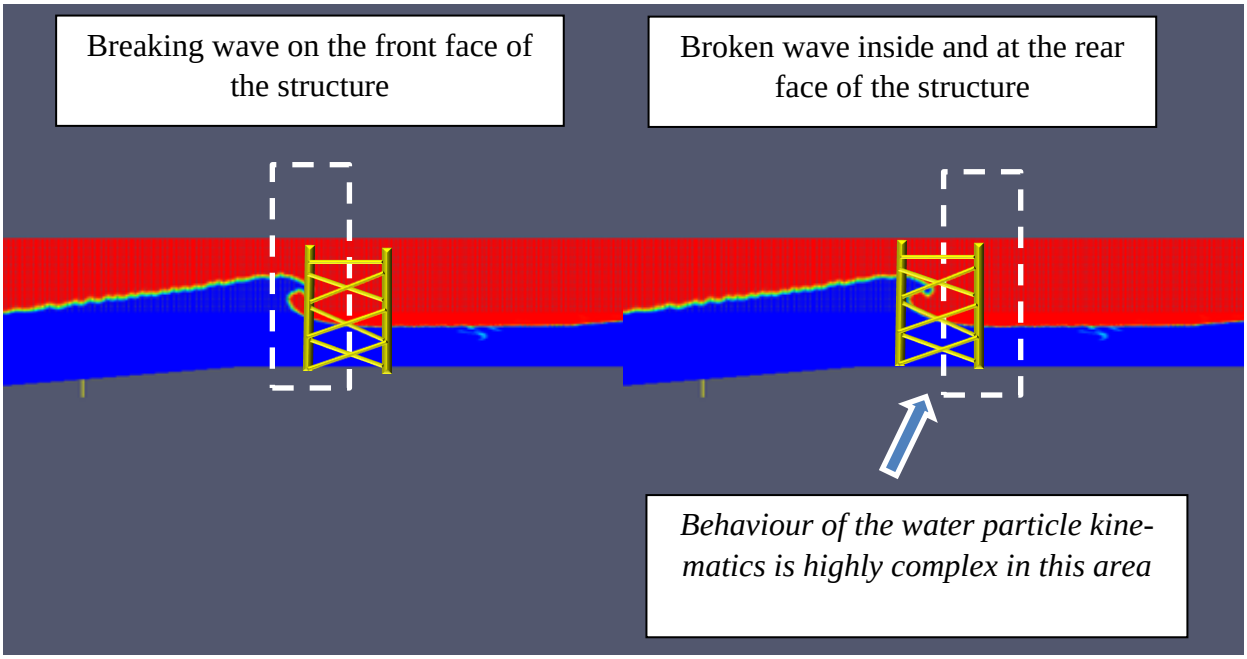

Figure 4-27. Breaking and broken wave on the front and rear face of the truss structure, respectively (Numerical results for Test no. 2013061807; H=1.9 m & T=5.2 s, d=4.3m)

Among all wave tests performed in GWK, the most extreme force response of the tested truss structure to breaking waves is shown in Figure 4-26c. As can be seen in Figure 4-26d, although the calculated peak of the TFR to the broken wave on the rear face is underestimated by ca. 25%, the period of the oscillations and the maximum TFR of the structure are relatively well-simulated.

Breaking wave induced forces on the entire GWK truss structure are calculated through superposition of: (i) the quasi-static force component obtained by means of the Morison equation using the flow parameters calculated by the CFD model and (ii) the slamming force component calculated using the new prediction formulae proposed in chapter 3.

The total force response (TFR) of the GWK truss to the loads induced by slamming and quasi-static force components is calculated using the Duhamel's integral code developed for the GWK truss structure. The validity of this approach is evaluated by comparing the results with the measured TFR in the large wave flume. Despite the inaccuracies in the prediction of broken wave impact loads on the rear face of the truss structure (up to 25% underestimation) due to difficulties in the simulation of broken wave kinematics associated with the high complexity of the flow, the discrepancies between computed and measured forces on the front face of the structure is adequate (less than 10% difference). The aforementioned approach will be applied in chapter 5 to calculate breaking and broken wave induced loads on a full-scale jacket structure.

4.5 Summary of key results

The main objective of this chapter was to calculate the total forces induced by non-breaking, near-breaking and breaking waves on jacket structures. One of the challenges of this study was the correct reproduction of the GWK tests using a reliable numerical model as this is necessary for conducting a parameter study for the dynamic response of jacket structures to breaking waves. For this purpose, a CFD model (in OpenFOAM) of the waves in the large wave flume (GWK) together with a CSD model (in ANSYS) of the GWK truss structure were used to predict forces induced by non-breaking and breaking waves on the structure as follows:

(i) The incident *non-breaking wave force* on each member of the GWK truss structure is calculated by means of the Morison equation using the flow velocity and acceleration obtained from the validated CFD model set up for the laboratory tests. The total non-breaking force is obtained by superposition of the wave forces on each member of the truss structure.

(ii) The incident *breaking wave force* on the truss structure is calculated by linear superposition of the quasi-static and impact force components. The quasi-static component is calculated using the aforementioned approach applied for non-breaking waves. The impact component is calculated using the formulae for slamming force on truss structures developed in Phase 2 of the PhD study.

The results of the parameter study using the numerical CFD and CSD models and the analysis of the laboratory tests in large wave flume GWK leads to the following conclusions:

(i) Application of the Morison formula for the prediction of the forces induced by non-breaking waves on the different members of a jacket structure and their proper superposition to obtain the force on the entire structure might provide reliable results as the total force consists of only quasi-static components.

(ii) Applying the Morison equation for near-breaking waves might result in an underestimation up to 35 % of the wave forces on jacket structures. A tentative analysis of the GWK tests revealed that the Morison formula cannot be applied for near-breaking waves with the following non-linearity parameters: H_{str}/L_{str} >0.059 & $H_{str}/h_{str} > 0.53$.

(iii) The proposed approach in this study for the calculation of non-breaking and breaking wave forces on an entire jacket structures and the associated total force response TFR of the structure might be used for the preliminary design of truss-type structures.

The limitations of the proposed methodology may be summarised as follows:

(i) Similar limitations for the application of the Morison equation

(ii) Since no formulae are yet available to predict the shape and kinematics of breaking, broken and post-breaking waves, computationally expensive CFD modelling needs to be used.

(iii) The effect of the motion/deformation of the structure on the wave load is neglected. This assumption is valid when the lateral displacement of structure is not large. More investigations are required to consider the effect of hydro-elasticity on wave loading of jacket structures.

Prior to the implementation of the proposed methodology developed in the present study for the prediction of non-breaking and breaking wave loads on a full scale jacket structure in Chapter 5, and to calculate consequently the associated dynamic response of the structure, the accuracy of the method were evaluated, including the prediction formulae for the calculation of wave slamming force on the truss structure and the CFD model for the prediction of wave parameters (e.g. water surface elevation,) considering water-air interaction. Overall, a relatively good agreement was observed between the computed forces induced by breaking and non-breaking waves on the truss structure and those measured in the GWK tests.

5 Dynamic response of a full-scale jacket structure to breaking and non-breaking induced wave forces

The dynamic response of jacket structures to non-breaking waves has been addressed in a large number of diverse studies. However, less attention has yet been paid to the calculation of the dynamic response of these structures to breaking waves. Currently in practice, jacket structures are designed under the most extreme non-breaking wave, which may occur once in 100-years. The application of the current approach might result in considerable uncertainties in the obtained extreme wave loads and consequently also in the dynamic response of the structure since the significant impact force caused by breaking waves on the structure is not considered. Moreover, the implications of such extreme wave load events and the associated uncertainties for the dynamic response of the entire jacket structure, particularly including the response of the pile foundation, are still not fully satisfactorily addressed. This latter issue is even more crucial as the foundation piles of jacket structures for wind turbines are significantly shorter (i.e. with a basically different behaviour) than those commonly found in jacket structures supporting oil and gas offshore platforms for which a large experience is available.

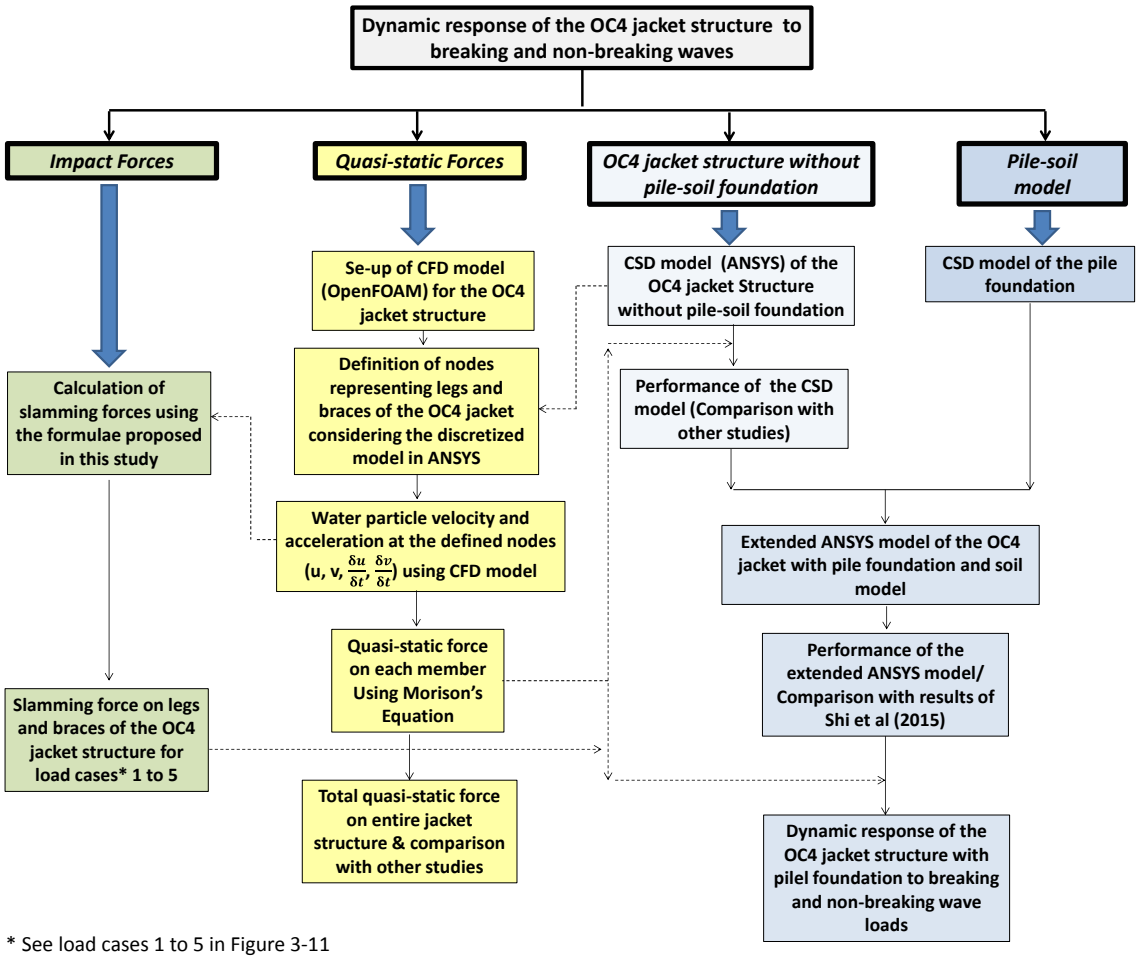

Figure 5-1. Methodology applied for the calculation of dynamic response of a full-scale jacket structure to breaking and non-breaking waves

Given the aforementioned knowledge gaps, an attempt is performed in this chapter to investigate the dynamic response of a full-scale jacket structure, the so called 'OC4 jacket', with pile foundation to breaking waves using the methodology shown in Figure 5-1.

The model of the full-scale OC4 jacket is introduced in section 5.1. A CSD model (in ANSYS) of the clamped jacket structure without pile foundation and a CFD model (in OpenFOAM) of the incident waves, set-up for the OC4 jacket are described in section 5.2. The basic CSD model of the OC4 jacket structure is modified in section 5.3 by introducing a pile foundation and soil models. The performance of the extended model is examined by comparison of the results with the other numerical models developed for the OC4 jacket. In section 5.4, the method proposed for the prediction of breaking wave loads on jacket structures, including the slamming formulae developed in this study, is applied to calculate total breaking wave induced loads on the OC4 jacket structure. Finally, a systematic parameter study is performed to identify the most relevant parameters affecting the dynamic response of the jacket structure to breaking waves.

5.1 Introduction of the full-scale OC4 jacket structure

5.1.1 Structural model

In this section, the model of the OC4 jacket structure is introduced. This jacket was designed by Rambøll A/ S (Vemula, 2010) in the UpWind project, which was the largest R&D wind energy project Europe. UpWind was a five year project (2006 to 2011) that aimed to develop and verify substantially improved models of substructures and wind turbine components, which are needed by the industry for the design and manufacture of offshore wind turbines for very large-scale future applications. In this PhD study, the well-known NREL 5-MW baseline turbine is considered on the top of the jacket structure (Jonkman et al., 2009). The wind turbine components such as rotors and nacelle are modelled as a lumped mass on the top of the wind tower.

The four legged OC4 jacket structure has four levels of X-braces and is founded on four piles with a penetration depth of 45 m into the soil. The piles are grouted to the jacket legs (see Figure 5-5c). The transition piece (TP) between the jacket and the tower is a block of concrete that is penetrated by the upper parts of the four jacket legs (see Figure 5-5b). The total height of the jacket from the mudline to the transition piece (TP) is 70.15 m. The water depth is 50 m. The conical tower has a total length of 68m leading to a realistic hub height over the mean sea level (MSL) of 90.55 m.

The dimensions of the tubular members are illustrated in Figure 5-2. Each dimension set is illustrated with a specific colour describing the geometry of the members as well as outer diameter and wall thickness.

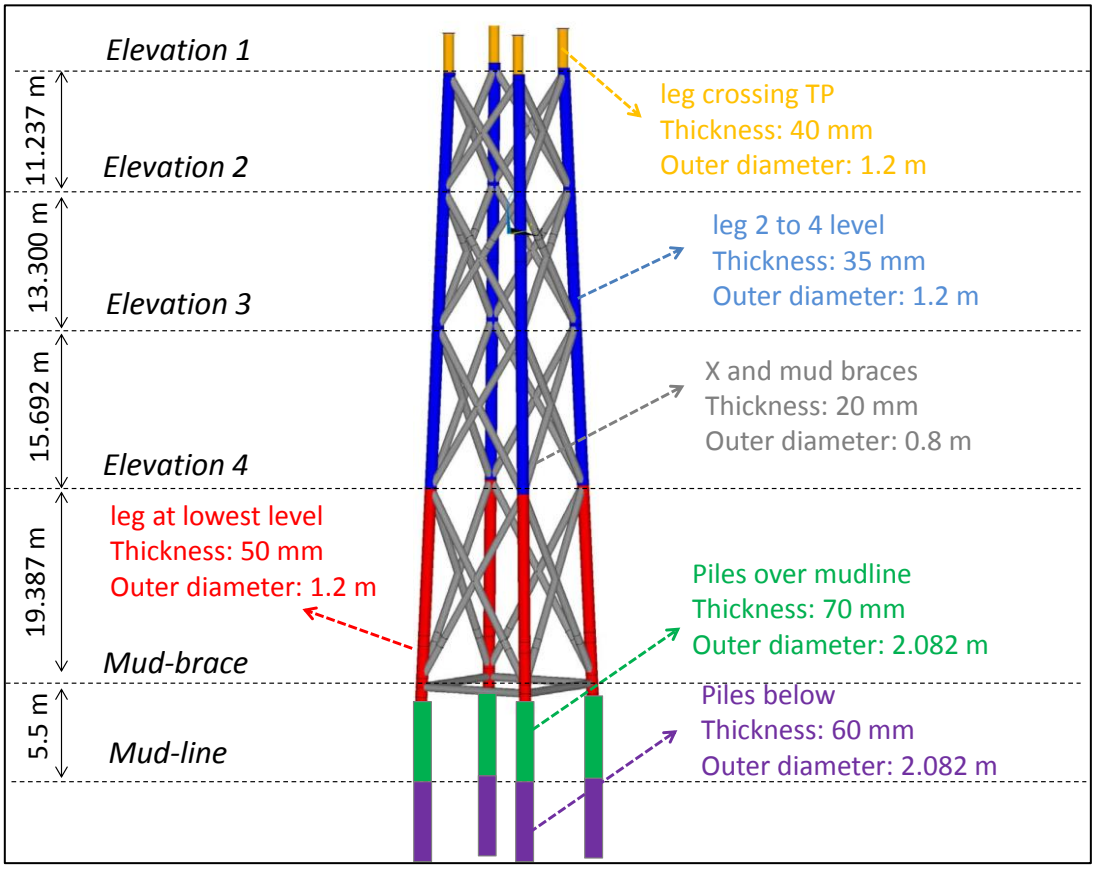

Figure 5-2. Dimensions of the OC4 jacket structure members

In the basic model of the OC4 jacket structure called hereafter ‘‘clamped structure’’, which has mainly been modelled by the available tools in previous research studies, the structure is cantilevered at the mudline, which means that all six degrees of freedom (DOF) are set to zero at the mudline. Therefore, only a short length of the piles over the mudline is considered in the model (4.5 meter). In this PhD study, after completion of the evaluation of the performance of the modelled clamped structure, a particular focus is paid to the interactions between pile and soil and as a result, the basic model is extended with the pile foundation and a soil model (see section 5.3).

5.1.2 Load cases

In this section, the load cases applied on the OC4 jacket structure are defined. Loads of increasing complexity are applied on the structure to allow for a stepwise comparison of results and to enable to trackback possible errors. Since the focus of this PhD study is the dynamic response of the jacket structure to extreme wave load events, and since the turbine is switched off under storm conditions, the wind is ignored in all load cases. The load cases are defined and classified in three groups: (i) the static self-weight of the jacket structure and wind turbine neglecting wind, wave and water effects (LC-W); (ii) non-breaking waves consisting of linear to steep waves (LC-N); (iii) breaking waves for different distances of the incipient wave breaking location to the structure (LC-B). For LC-N and LC-B, regular waves are generated

and the simulation time using the CSD model is respectively 60s and 30s. For breaking waves (LC-B), the incipient wave breaking location is varied in order to simulate load cases 1-5.

Table 5-1. Definition of wave load cases on the OC4 jacket structure in a water depth h=50m (regular waves)

Load Cases	***Wave Conditions***	***Type of Analysis***	***Description***
LC-W1	No wave	Self-weight Modal analysis	Absence of water
LC-N1	Non-breaking Regular airy wave H=6m , T=10 s.	Time-series simulation	Analysis Includes: -Marine growth -Added mass -Flooded members
LC-N2	Non-breaking Regular stream function H=8m , T=10 s	Time-series simulation	
LC-N3	Near- breaking Regular stream function H=10m , T=10 s	Time-series simulation	Steep wave on the structure
LC-B1	Breaking wave Load case 1 H_b=10 m , T=10 s	Time-series simulation	Incipient wave breaking location far in front of the front face
LC-B2	Breaking wave Load case 2 H_b=10 m , T=10 s	Time-series simulation	Incipient wave breaking location in front of the front face
LC-B3	Breaking wave Load case 3 H_b=10 m , T=10 s	Time-series simulation	Incipient wave breaking location on the front face
LC-B4	Breaking wave Load case 4 H_b=10 m , T=10 s	Time-series simulation	Incipient wave breaking location on the rear face of the jacket
LC-B5	Near- breaking Load case 5 H_b=10 m , T=10 s	Time-series simulation	The wave becomes unstable after passing the structure

Marine growth is applied in all the simulations according to Table 5-2. Marine growth is considered within the range of -40 m to -2 m based on the description provided by Vorpahl & Popko (2013) for the basic model of the UpWind reference jacket in the OC4 project.

Table 5-2. Marine growth in the OC4 jacket model (Vorpahl et al, 2013)

Depth range (z_{MG})	$-40\ m \leq z_{MG} \leq\ -2\ m$
Thickness (t_{MG})	100 (mm)
Density (ρ_{MG})	1100 (kg/m3)

5.1.3 Type of analysis outputs for dynamic response

The outputs of hydrodynamic forces and corresponding dynamic responses are obtained in terms of time series as the numerical analysis simulates the regular waves for total duration of 30 to 60 seconds. The time history of the dynamic response of the structure is calculated numerically using a staggered time stepping procedure. This means that the induced wave force is discretized in 1000 time steps and the corresponding force in each time step is applied on the FE model structure. The dynamic response of the structure in terms of velocity, acceleration and displacement at each node of the structure is computed for each time step, which is considered as initial conditions for the next time step. The analysis settings for non-breaking wave loads (LC-N) and breaking wave loads (LC-B) are provided in Table 5-3. The drag and inertia coefficients in the Morison equation are selected according to the recommended values in Vorpahl & Popko (2013) as a function of the KC-number and by considering that the drag coefficient CD < 0.7 when the effect of marine growth is taken into account.

Table 5-3. Simulation setting for the calculation of the dynamic response for non-breaking wave loads (LC-N) and breaking wave loads (LC-B)

Symbol	***Value***		***Description***
	LC- N	**L-C B**	
C_D	1	0.7	Drag Coefficient
C_M	2	2	Inertia Coefficient
g	9.806 m/s^2	9.806 m/s^2	Gravity acceleration
Δt_{CFD}	0.05 s	0.001 s	Time step for data output in the CFD model
Δt_{in}	0.1 s	0.001 s	time step for wave data generation (input of the CSD model)
Δt_{out}	0.1 s	0.001 s	Time step for data output in the CSD model
T_{FE}	60 s	30 s	Simulation time for deterministic load cases

For each simulation, the analysis outputs of the dynamic response are calculated and recorded at a number of nodal points called ‘Sensors’. Generally, these virtual sensors are placed at the top of the wind tower (WT), on the transition piece (TP), on the jacket support structure (e.g. LF3, X4S2, LR2 & etc.), on the pile foundation (PH, PH, PL1-9) and the springs representing the soil stiffness (SPR) as shown in Figure 5-3.

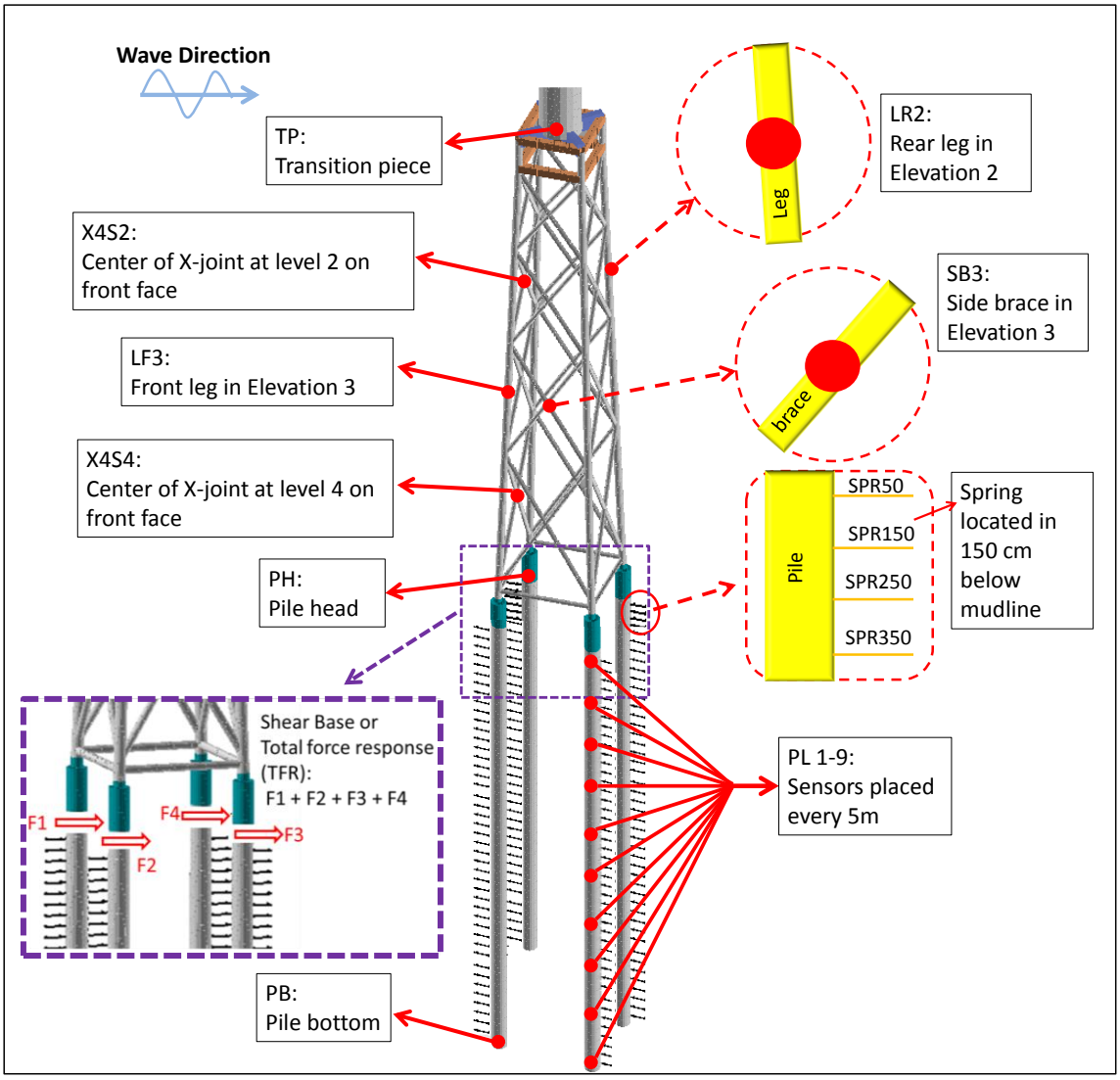

Figure 5-3. Placed virtual sensors on the OC4 jacket structure -

The sensors are defined so that they calculate: (i) the global dynamic response of the entire jacket structure which is dominated by the tower head and top side mass (i.e. WT, TP, PB and etc.) and (ii) the local dynamic response of the structural members caused by the local vibration of members (i.e. X4S2, SB4 and etc.). Figure 5-4 shows the top view of the OC4 jacket structure modelled in this study.

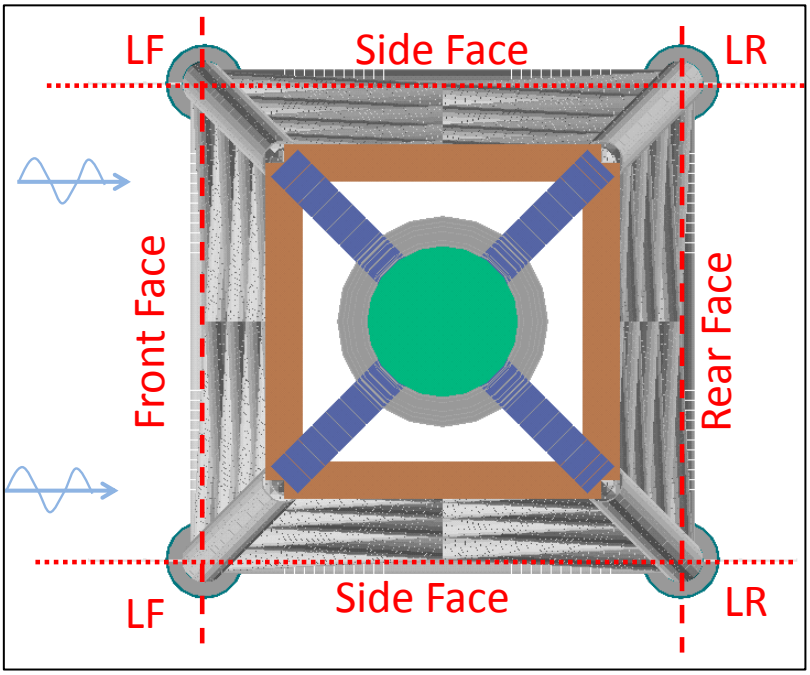

Figure 5-4. Top view of the OC4 jacket structure modelled in ANSYS

A full-scale jacket structure called 'OC4 jacket' is introduced, which will be considered later to perform a numerical parameter study. The non-breaking and breaking wave load cases, the type of analysis and the virtual sensors on the structure are defined to compute local and global dynamic response of the jacket structure with pile foundation to non-breaking and breaking wave loads.

5.2 OC4 jacket structure without pile foundation model

5.2.1 Numerical model for the clamped OC4 jacket under non-breaking waves

In this section, the method described in chapter 4 is applied to calculate non-breaking wave forces on the OC4 jacket structure and the corresponding dynamic response. The computation is performed using a CFD model (in OpenFOAM) and a CSD model (in ANSYS). The models are set-up according to the following steps:

Step1: A CSD model of the clamped OC4 jacket structure without pile foundation and 5MW NREL wind turbine is set-up in ANSYS. The actual model of a jacket structures is very complicated and without proper idealization and simplifications, an effective modelling would be hardly possible. Figure 5-5 indicates the simplifications considered in this study to model the jacket structure and the wind turbine. These can be briefly summarized as follows:
a) The wind turbine components such as rotors, nacelle and assembly (RNA) are modelled as a lumped mass on the top of the wind tower (Figure 5-5a);

b) The rigid concrete block as a transition piece, which connects the wind turbine to the jacket substructure, is modelled by four horizontal stiff beams. The density of the beams surrounding the replaced concrete block is set so that they represent the equivalent mass of the concrete block (Figure 5-5b);
c) The piles and the legs are overlapped in their connection region and the gap between them is filled with grout material. This piece is replaced with an equivalent tubular member representing the same mass and stiffness (Figure 5-5c).

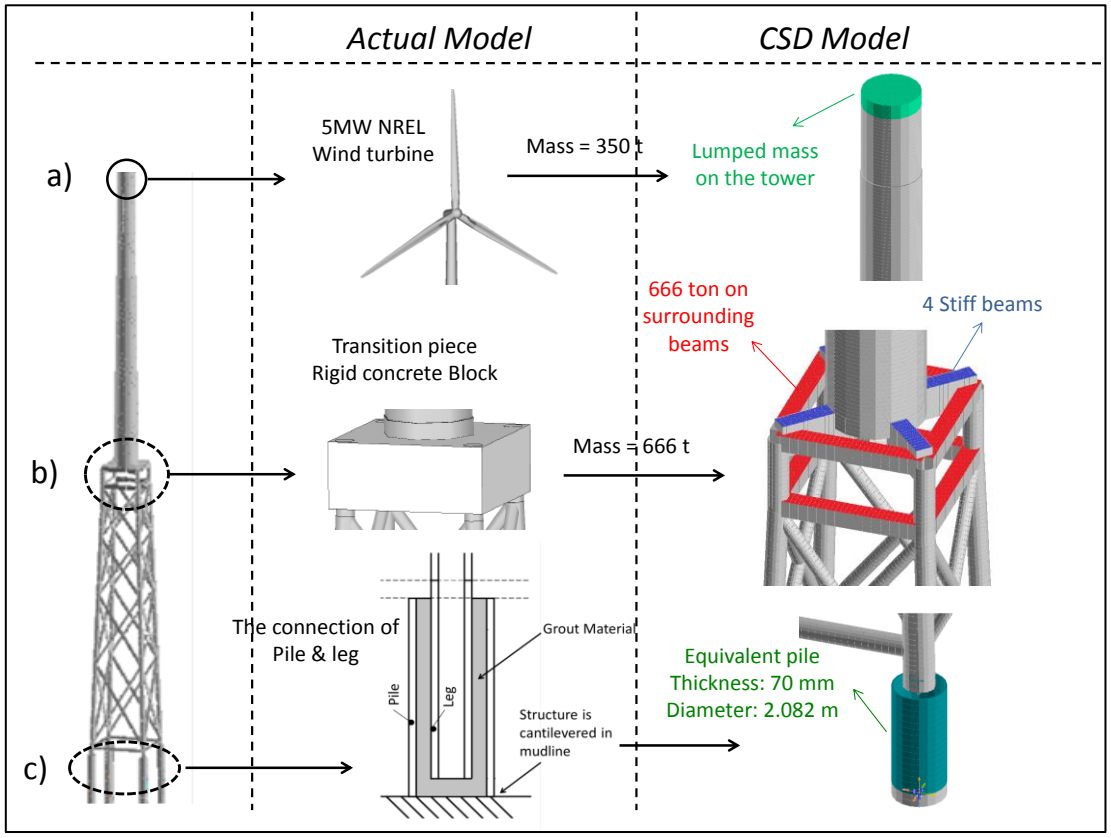

Figure 5-5. Simplified model of the OC4 jacket structure and NREL wind turbine: a) wind turbine (rotors, nacelle and assembly; b) transition piece; and c) pile and leg connection;

Step2: The CFD model set-up in OpenFOAM for the GWK truss structure in Chapter 3 is upscaled to prototype conditions in order to generate full-scale waves approaching the legs and braces of the OC4 jacket structure (see example for non-breaking waves in Figure 5-6). Water surface elevation, flow velocity and acceleration induced by incident waves on the structure members are determined by the CFD model.

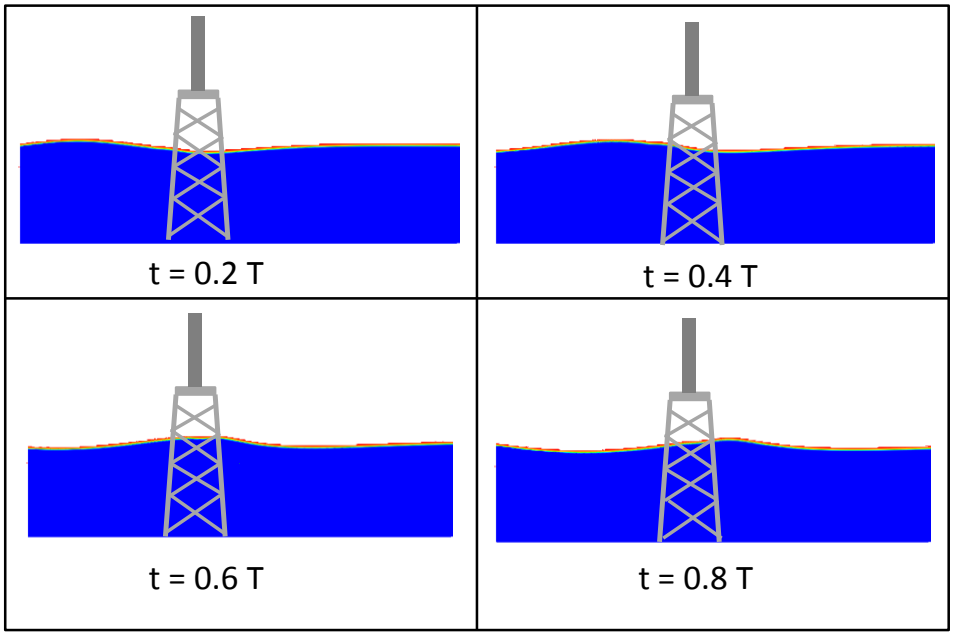

Figure 5-6. Example of numerical simulation of a non-breaking wave approaching the OC4 jacket structure in OpenFOAM (LC-N1; H=6m , T=10 s, h=50m)

Step3: The quasi-static force induced by non-breaking wave on each member of the OC4 jacket structure is calculated using Morison equation. For this purpose, the flow velocity and acceleration obtained from the validated CFD model are considered, together with the drag and inertia coefficients from Table 5-3, as implemented also in section 4.3 for the calculation of wave forces on the GWK truss structure. The total wave force is obtained by superposition of the quasi-static forces on each member of the jacket structure. (see examples in Figure 5-8c & d)

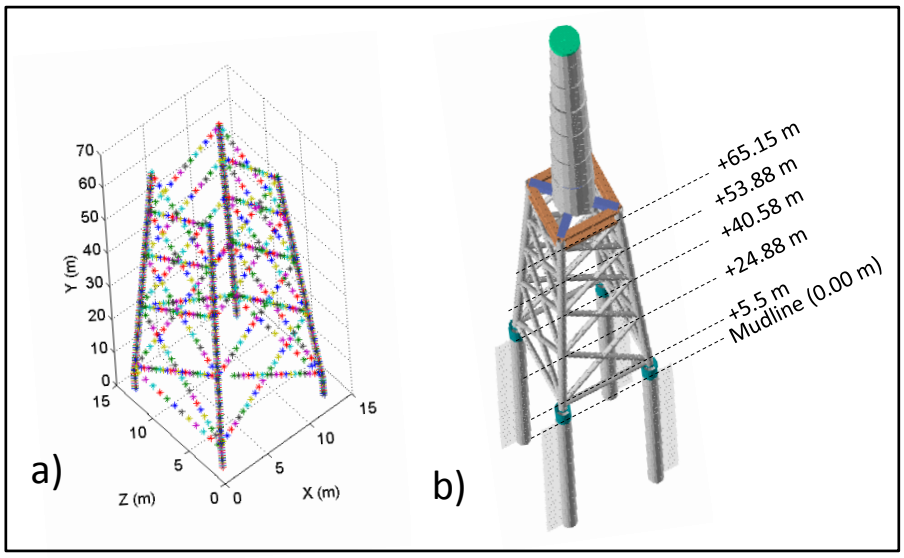

Figure 5-7. OC4 jacket structure: a) defined nodes in OpenFOAM representing the legs and braces; b) FE model in ANSYS

5.2.2 Performance of the numerical model for clamped OC4 jacket structure without pile foundation

The performance of the numerical model in this study is evaluated by comparing the results with those of other numerical models developed for the clamped OC4 jacket structure under non-breaking wave loads (Figure 5-8). The following steps are performed to validate the numerical model:

(i) A *verification of the structural masses* of the OC4 jacket structure including the body of the jacket structure, the transition piece, the tower and the Rotor Nacelle Assembly (Figure 5-8a) is conducted through comparison of different studies.

(ii) A *modal analysis* is performed of the *clamped OC4 structur*e in the absence of water and soil (Figure 5-8b) in order to compare the results obtained in this study with other studies.

(iii) The *total wave loads* induced by non-breaking waves calculated by superposing of quasi-static wave forces on members of the structure, is obtained (for LC-N1 & LC-N2). The total force response (TFR) at the base of the structure on the direction of the incident wave (fore-aft force) is computed and plotted together with the results from the other studies in Figure 5-8c & d.

(iv) *The displacement of the clamped OC4 structur*e (without pile foundation) under non-breaking waves is calculated and compared with other numerical models developed for the same structure. (Figure 5-8e & f).

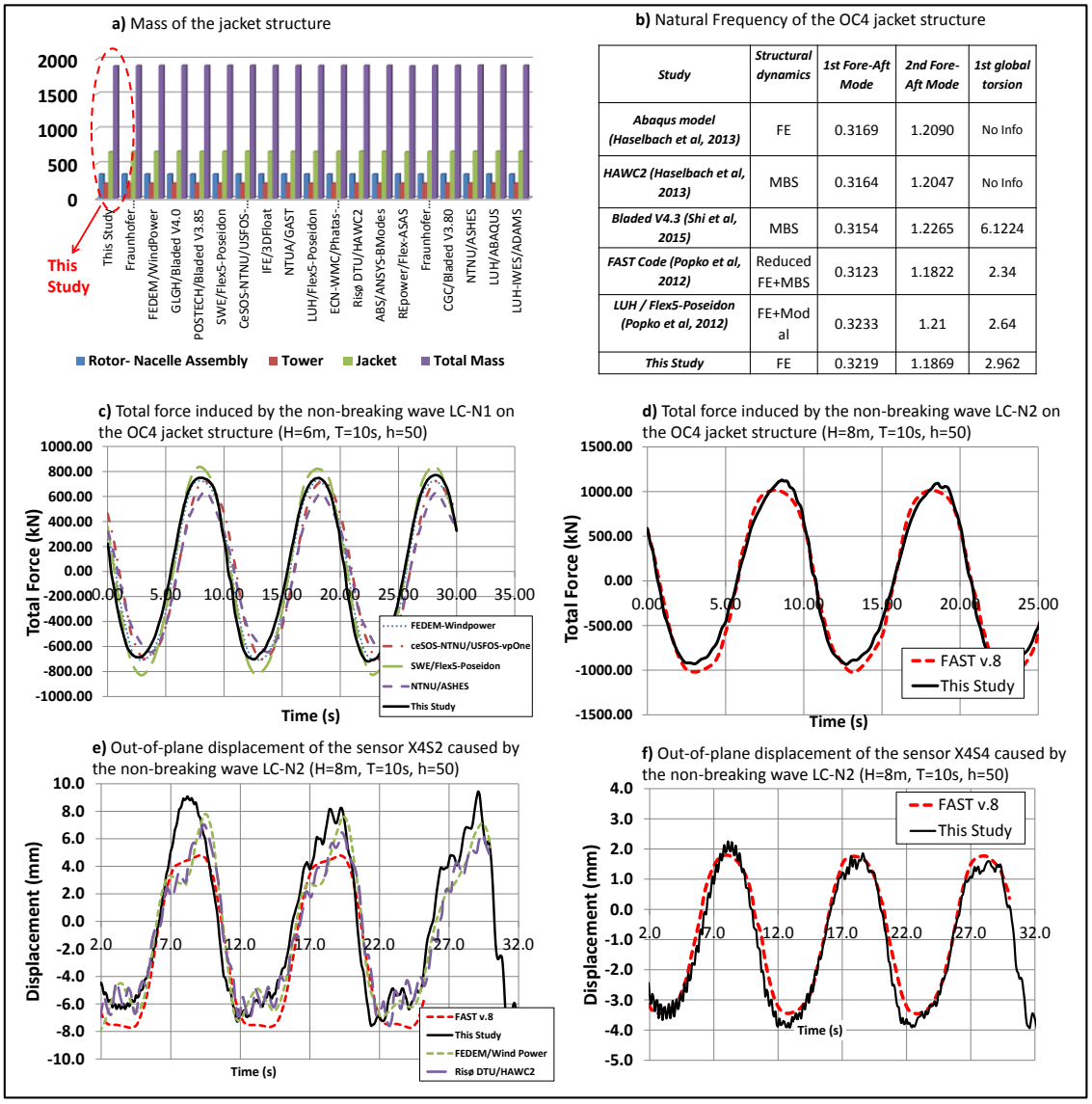

Study	*Structural dynamics*	*1st Fore-Aft Mode*	*2nd Fore-Aft Mode*	*1st global torsion*
Abaqus model (Haselbach et al, 2013)	FE	0.3169	1.2090	No Info
HAWC2 (Haselbach et al, 2013)	MBS	0.3164	1.2047	No Info
Bladed V4.3 (Shi et al, 2015)	MBS	0.3154	1.2265	6.1224
FAST Code (Popko et al, 2012)	Reduced FE+MBS	0.3123	1.1822	2.34
LUH / Flex5-Poseidon (Popko et al, 2012)	FE+Modal	0.3233	1.21	2.64
This Study	FE	0.3219	1.1869	2.962

Figure 5-8. Validation of the numerical model for the clamped OC4 jacket structure

For the *structural masses*, a very good agreement between different models is observed. Only a very slight difference in the total mass of the structure exists (less than 1%) which might be mainly due to: (i) discrepancies in the tower mass resulting from the different sections of the members (cylindrical or variable section) used for modelling; (ii) discrepancies in the jacket mass caused by slightly different modelling techniques.

For the *modal analysis* of the structure, slight discrepancies between the natural frequencies in different studies was observed (less than 4%) because

(i) The RNA model in different studies is implemented using different approaches (e.g. lumped mass, fully flexible blades, rigid blades, etc.);

(ii) The numerical models in different studies incorporate different degrees of freedom (DOF). For example, some codes such as FAST code use a method to reduce the de-

grees of freedom (DOF) for solving the equation of motion, while FE based models such as ANSYS or Abaqus incorporating several DOFs are also able to calculate the local response of the members;

(iii) Different models are developed using dissimilar structural dynamic approaches as well as Finite Element (FE), Multi-Body System (MBS) or Modal representative (Modal) methods. In general modal based models predict slightly higher natural frequencies compared to FE or MBS based models. The reason is in the modal representative (Modal) approach, where the structure indicates a stiffer behaviour as the number of DOFs is lower. However, FE and MBS based models accommodate more DOFs, which allow the structure for more vibrational modes and result in a reduced stiffness of the structure. This can be well observed in the natural frequencies obtained from the model developed by Flex5-Poseidon, which are slightly higher (less than 4%) than the natural frequencies calculated in other studies (Figure 5-8b).

For *the total wave loads* on the structure, some differences (less than 20%) in time series of the total wave force calculated in different studies using different tools were observed (Figure 5-8c). The differences are mainly due to dissimilarities in the application of wave kinematics and Morison equation on the structure. The code Flex5-Poseidon provides the highest force amplitude, which is due to neglecting of the overlapping effect. Therefore, the calculated force is slightly overestimated. The discrepancies in the other models may arise from the discretization of the threshold regions for marine growth modelling, which may change the drag and inertia force. In general, an acceptable agreement is observed for the results from the different codes and the maximum difference for peak to peak amplitudes is less than 20% (The difference is less for the majority of the codes). A very slight discrepancy is observed between the simulations performed in this study with the result of the FAST code where the simulated wave force in this study is slightly shifted upward (Figure 5-8d). This difference might be due to:

(i) the slight inconsistency on the simulated flow field in the CFD model in this study compared to the stream function wave theory employed in FAST,

(ii) dissimilarities in the application of wave kinematics on the structure, especially the area above mean water level where the approach applied in this PhD study (CFD & Morison equation) is more reliable as it considers wave-air interactions. To sum up, a peak to peak amplitude comparison shows a discrepancy of less than 2%, which is very low.

For the *displacement of the clamped OC4 structure*, the comparison of the calculated out of place displacement of the structure in this study and the other studies showed relatively good agreements and discrepancy for peak to peak amplitude is about 10% (Figure 5-8e & f). As the model developed in FAST employs less DOFs, the structure shows a stiffer behaviour compared to the models developed using a large number of DOFs such as the model applied in this study. The computation of the dynamic response of a jacket structure to wave loads is very complex as the response significantly depends on diverse uncertain issues such as:

(i) Simulation of the flow field (e.g. CFD models, wave theories),

(ii) Wave loads on the members (e.g. water added mass, overlapping effect, flooded members, application of marine growth),
(iii) Structural dynamics of the model (e.g. FE, dynamics system reduction, MBS and Modal methods),
(iv) Structural element characteristics (e.g. 2D or 3D members, linear or non-linear elements, mesh discretization),
(v) Analysis procedure (e.g. run time, time interval between the time steps,
(vi) Effect of joint flexibility, etc.

Therefore, such discrepancies in the simulated dynamic response of complicated multi-member structures are common as can be seen in Figure 5-8e for the out-of-plane displacement of X2S2 calculated by FEDEM and FAST, which both apply a dynamic system reduction method, but resulted in slightly different responses.

The approach proposed in Chapter 4 is applied on a full-scale jacket structure (OC4 jacket structure) to calculate non-breaking wave forces on the clamped jacket structure and to compute the corresponding dynamic response. The simulation is performed by using a CFD model in OpenFOAM for the water waves and a CSD model in ANSYS for the OC4 jacket structure. The performance of the model is evaluated by comparing the results with those of other numerical models developed for the OC4 jacket.

The numerical model will be extended later to consider: (i) pile foundation with an appropriate soil model; (ii) the slamming force by using the formulae proposed in Chapter 3 for the calculation of total wave loads induced by breaking waves on the OC4 jacket structure.

5.3 OC4 jacket structure with pile foundation

In this chapter, the CSD model of the clamped OC4 jacket structure is modified by introducing a pile foundation with an appropriate soil model. The performance of the extended model is examined by comparison of the natural frequencies with the model developed by Shi et al (2015), which represents the only study performed so far on the pile and soil foundation of the OC4 jacket structure.

5.3.1 Extension of the CSD model to consider pile foundation with an appropriate soil model

The pile foundation of an offshore jacket structure should be capable enough to endure all types of static, cyclic and transient loads over its lifetime. Cyclic shear loading of piles induces cyclic shear stresses in the soil that result in a gradual increase of pore pressure. Higher pore pressure may lead to increase the permanent shear strains and thus to reduce the shear strength of the soil. Moreover, the natural frequency of the structure is significantly affected by the pile-soil interaction. As a result, the dynamic response of a jacket structure to environmental loads is strongly influenced by the soil behaviour and shall be based on an integrated analysis of the jacket structure, the foundation piles and soil. The analysis should be per-

formed by considering realistic assumptions for the stiffness and the damping of both soil and structure. Diverse models may be utilized to determine pile-soil interaction for a jacket structure. However, only very few can account for the nonlinear response behaviour of the soil. Among the available models, those using nonlinear springs connected to the pile foundation in different soil layers, are recommended in several guidelines such as API (2005) and DNV (2013). Such a modelling approach, called p-y method, has indeed provided relatively good results for offshore platforms (see Section 2.3 in Chapter 2). Figure 5-9 shows a schematic configuration of these springs in different soil layers. These springs work independently; i.e. the deformation of each spring doesn't affect the other springs behaviour. Springs introduced along a pile are classified in three groups (Figure 5-9): (i) springs resisting against lateral loads to describe the lateral pile-soil interaction (p-y); (ii) springs considering axial pile resistance due to internal and external pile skin friction (t-z); (iii) springs considering the tip resistance (Q-z).

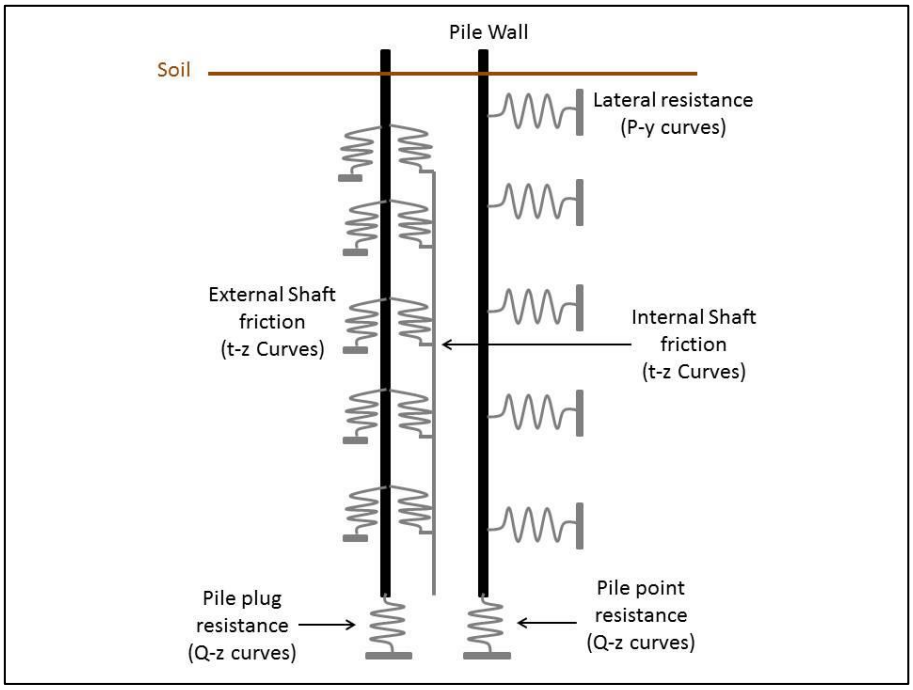

Figure 5-9. Pile-soil interaction modelling by different types of springs uniformly distributed along the pile

In multi-member substructures of wind turbines, the lateral pile-soil interaction modelling (lateral springs) governs the horizontal displacement of the pile head and significantly influence the structural response. Therefore, in this study, only the lateral soil stiffness is considered (Shi et al, 2015) meaning that no vertical springs are included, i.e. no t-z springs for the shaft friction and no Q-z curves for the pile tip resistance are considered.
In this study, the implemented pile-soil model for the foundation of the OC4 jacket structure is based on p-y curves developed in a research study (sponsored by a group of five oil companies) on laterally loaded piles for offshore structures including laboratory model testing and field tests with an instrument pile (Matlock, 1970; O'Neill & Murchinson, 1983).

The method for the calculation of non-linear p-y curves for both clay and sandy soils is more precisely described in Section 2.3.
The FE model (ANSYS) of the OC4 jacket structure is extended by introducing four foundation piles with a penetration depth of 45 m into the soil. The soil is modelled using several lateral springs connected each meter along the piles by considering the aforementioned non-linear p-y approach (Figure 5-10). The CSD model of the clamped OC4 jacket structure is modified to consider the effect of pile foundation and soil parameters by performing the following steps:

*Step1***:** The CSD model of the OC4 jacket structure is extended by adding four piles with the diameter of 2.086m, the thickness of 7mm and the length of 45m.

Step2: The pile-soil interaction is modelled by implementing linear springs along the piles (soil plasticity and non-linearity not considered). The plausibility of the extended model is examined by comparing the natural frequencies of the model with the study by Shi et al (2015).

Step3: The pile foundation model is improved by implementing a non-linear soil model to the foundation using a p-y approach in order to consider the non-linear behaviour of the soil for higher displacements of the pile foundation.

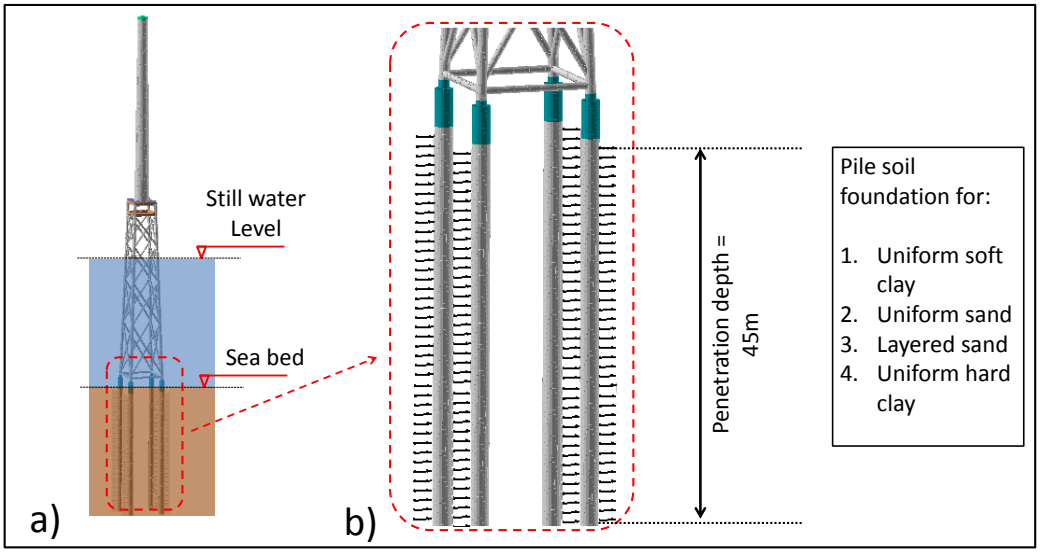

Figure 5-10. Side view of the a) OC4 jacket structure with pile foundation; b) lateral springs along the pile foundation representing the soil

Four types of soils are considered for the foundation of the OC4 jacket structure:

(i) uniform soft clay (Type 1 in Figure 5-11a);
(ii) uniform sandy soil (Type 2 in Figure 5-11b);
(iii) layered sandy soil like in the Shi et al. (2015) study (Type 3 in Figure 5-11c);
(iv) uniform hard clay (Type 4 in Figure 5-11d).

The soil parameters are given in terms of the effective unit weight (γ_s) and the angle of internal friction (ϕ) for the two sandy soils, and in terms of effective unit weight (γ_s), undrained shear strength (c), dimensionless empirical constant (J) and soil strain (ε_c) for the two clayly soils.

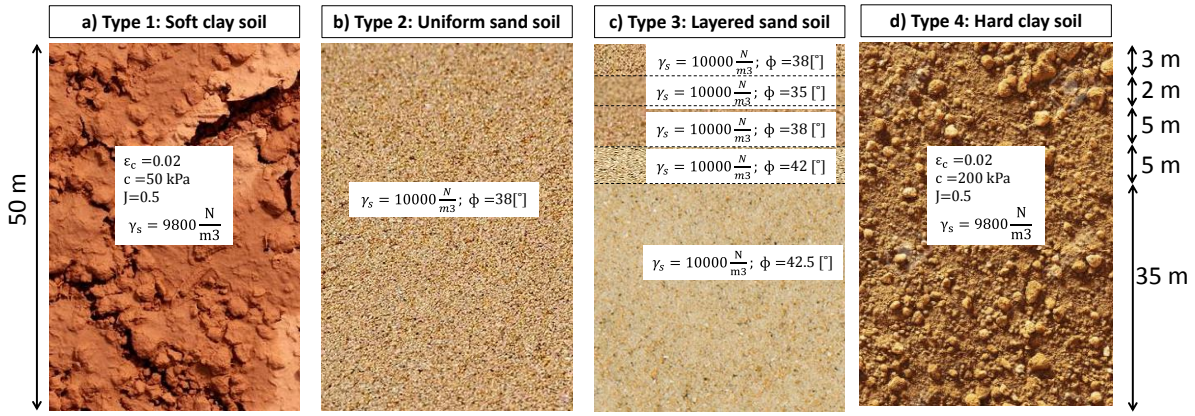

Figure 5-11. Considered soil types 1-4 for modelling pile-foundation interaction a) uniform soft clay; b) uniform sand soil, c) layered sand soil, d) uniform hard clay

5.3.2 Performance of the OC4 jacket structure with pile foundation

The pile foundation model of the OC4 jacket is set-up for different soil types described in Figure 5-11. In order to evaluate the performance of the extended CSD model for the structure with pile foundation, the natural frequencies obtained for the clamped structure (without pile foundation) and for the structure with pile foundation in soil types 1-4 are tentatively compared with the results of Shi et al. (2015) for soil type 3. In the latter, the effect of the soil-structure interaction is considered with a particular focus on pile group effect on the response of a jacket support structure to non-breaking waves. The modal analysis is performed for the fully flexible jacket substructure and tower with a lumped mass atop, which represents a rigid RNA at the top of the structure, and the results are summarized in Table 5-4. As can be seen, the fore-aft natural frequency of the structure with piles in clay (Type 1) is 6% lower than that of the structure with piles in sand (Type 2), showing a more flexible behaviour of the structure with piles founded in clay. Given the same jacket substructure and piles, the natural frequency of the entire structure increases with higher soil stiffness.

Table 5-4. Natural frequencies (Hz) of the OC4 jacket structure only clamped and with pile foundation in soil types 1 to 4 as obtained in this study and by Shi et al, 2015 for soil type 3 (see Fig. 3.7)

Model	***1st fore-aft***	***2st fore-aft***
Structure only clamped, i.e. without pile foundation	0.3219	1.1869
Structure with pile foundation in soft clay (soil type1)	0.2607	0.6510
Structure with pile foundation in uniform sand (soil type2)	0.2748	0.8499
Structure with pile foundation in layered sand (soil type3)	0.2749	0.8512
Structure with pile foundation in soil type3 (Shi et al, 2015)	0.2771	0.8931
Structure with pile foundation in hard clay (soil type4)	0.2684	0.7541

It should be stressed that the OC4 jacket structure modelled in this study is symmetric as the turbine's blades, rotor, nacelle and assembly are modelled as a lumped mass, and springs representing soil are connected from both fore-aft and side-side directions. As a result, the fore-aft natural frequencies are equal to side-to-side. Therefore, the comparison of natural frequencies is performed only in fore-aft direction, showing a difference of less than 5% between this study and Shi et al (2015) for soil type 3.

Comparison of the natural frequencies obtained from the modal analysis of the OC4 jacket structure with and without pile foundation (Table 5-4) indicates higher values of the natural frequency for the former case up to 20% and 45% for 1st and 2nd mode shapes, respectively. Therefore, the consideration of the pile foundation with a proper soil model is crucial as it may significantly affect the dynamic response.

The numerical model is extended by adding pile foundation with soil models using linear and non-linear p-y springs. The plausibility of the extended model is tentatively examined by comparing the results with the study performed by Shi et al (2015). The model of the pile foundation is set-up for four different soil types including: (i) uniform soft clay; (ii) uniform sand soil; (iii) layered sand soil; (iv) uniform hard clay.

The model of the OC4 jacket structure with pile foundation will be used to apply a parameter study for the dynamic response of jacket structures to different breaking waves.

5.4 Parameter study of the dynamic response to breaking waves

In this chapter, the CSD model (ANSYS) of the OC4 jacket structure with pile foundation together with the CFD model (OpenFOAM) are applied to perform a systematic parameter study and comparative analyses in order to identify the most relevant parameters influencing the dynamic response of the jacket structure under breaking waves. The parameters are classi-

fied in three groups as shown in Figure 5-12. Results and discussions are provided in sections 5.4.1- 5.4.3.

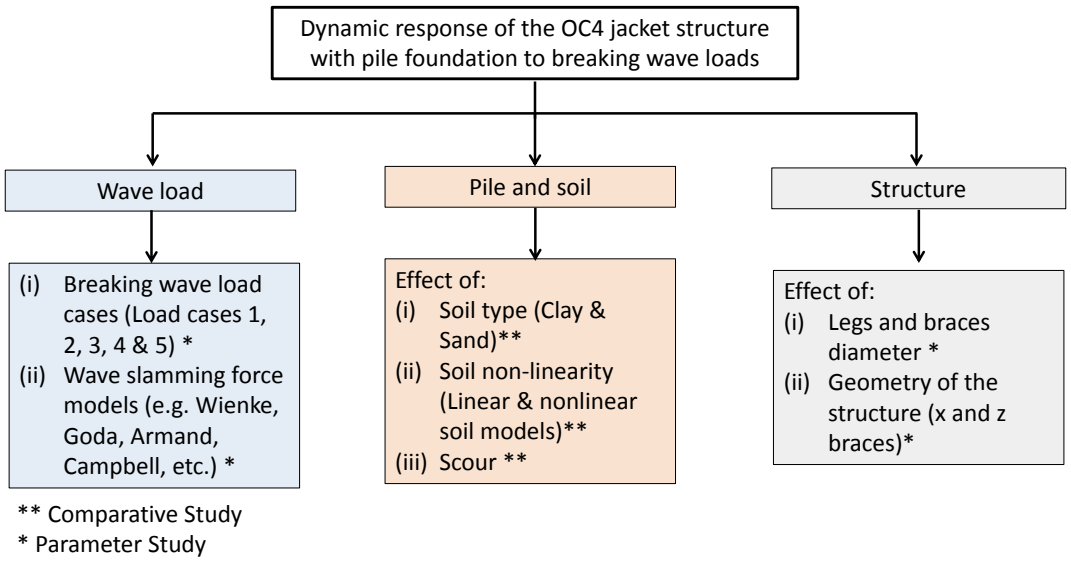

Figure 5-12. Numerical parameter study and comparative analyses for the OC4 jacket structure with pile foundation (see Figure 5-11 for soil types and Figure 3-11 for load cases)

5.4.1 Effect of load cases induced by breaking waves on the OC4 jacket structure

Breaking wave Load Cases (LC)

In this section, the OC4 jacket structure is subject to different wave loads caused by breaking waves (Five load cases: LC1 to LC5 as also defined in Figure 3-11) as shown in Figure 5-13. In each simulation, the characteristics of the incident breaking wave are kept constant, and only the distance between the incipient wave breaking location and the jacket structure is varied to generate different types of breaking waves on the jacket structure as follows (Figure 5-13):

(i) *Load case 1 (LC-B1)*: the wave breaks far in front of the structure (10-20m) and the breaking wave force on the rear face of the structure is much less than the force on the front face.

(ii) *Load case 2 (LC-B2)*: the wave breaks in front of the structure (3-10m) and induces an extreme impact force on the front face of the jacket structure;

(iii) *Load case 3 (LC-B3)*: the waves breaks directly at the front face and the relative values of the breaking wave force on the rear face to those on the front face of the truss structure are higher than previous load cases (LC-B1 & LC-B2);

(iv) *Load case 4 (LC-B4)*: the wave breaks between the front and rear faces of the structure. Although the incident wave breaks within the structure, there is a significant dynamic force on the front face of the truss structure;

(v) *Load case 5 (LC-B5)*: the wave breaks behind the structure and only quasi-static forces are induced on the jacket structure.

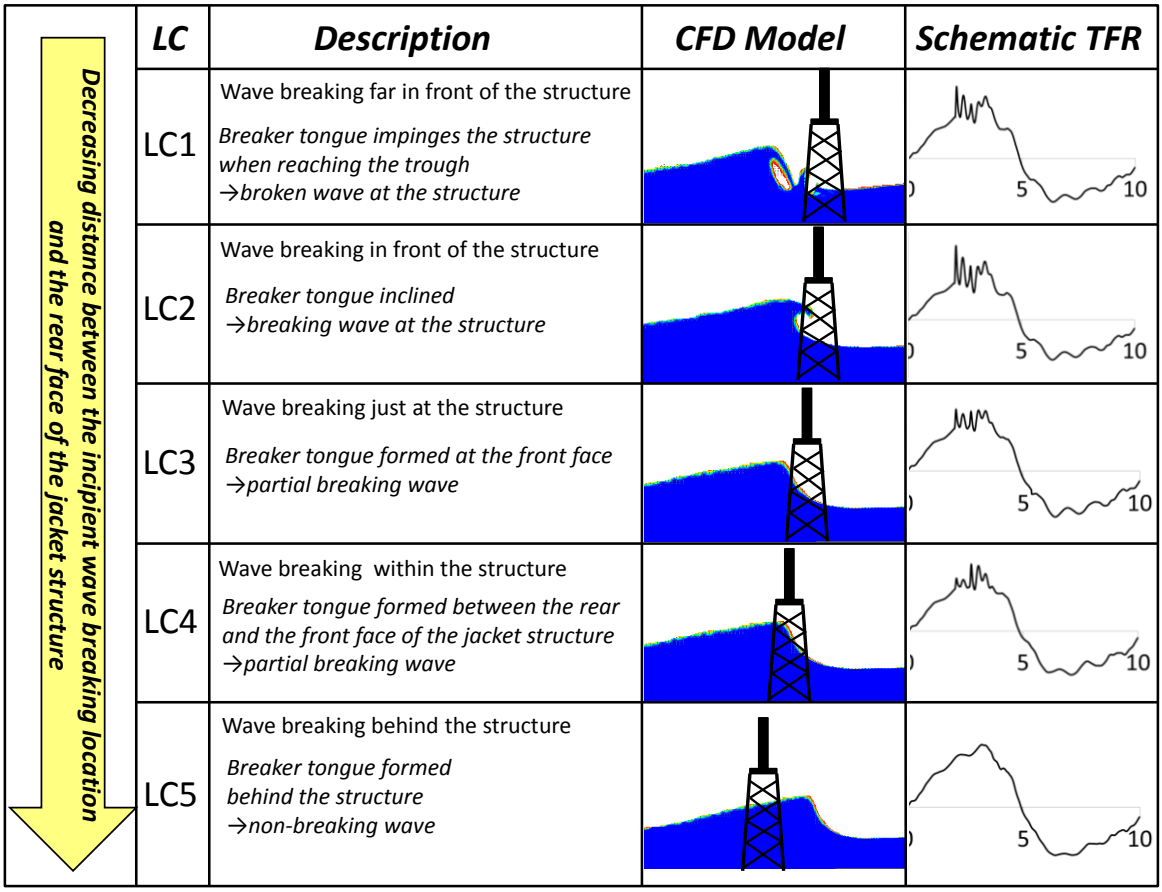

Figure 5-13. Load cases induced by breaking waves on the OC4 jacket structure

For each load case, the quasi-static component of the force on each member of the OC4 jacket structure is calculated by means of the Morison equation using the water surface elevation, flow velocity and acceleration obtained from the CFD model. The time series of the calculated forces are then applied on respective members of the jacket structure in the CSD model. The total quasi-static force on the structure might be obtained by superposition of the wave forces on each member of the jacket structure (Figure 5-14(1)). The impact forces caused by the breaking wave on the front and rear faces of the jacket structure is predicted using the formulae proposed for slamming force on truss structures developed in Chapter 3 (Eqs.3-4 to 3-6 & Eqs.3-14 to 3-16) of this thesis (Figure 5-14(2)). The calculated impact forces are then introduced in the CSD model by considering the impact area on the front and rear faces of the OC4 jacket structure. The total wave force caused by the breaking wave on the jacket structure is calculated by linear superposition of the quasi-static and impact force components (Figure 5-14(3)).

The total force response TFR of the OC4 jacket structure with pile foundation to breaking waves LC1-LC4 is calculated by ANSYS (Figure 5-14(4)) which consists of quasi-static and dynamic force components. In order to extract the dynamic force response DFR, the total force response TFR (Figure 5-14(4)) is subtracted from the quasi-static force response QSFR (Figure 5-14(5)). Therefore, the QSFR is obtained by calculating the response of the jacket

structure to the quasi-static force (LC5) calculated by the Morison equation as shown in Figure 5-14(1). Finally, the dynamic force response DFR of the jacket structure to LC1-LC4 is calculated (Figure 5-14(6)).

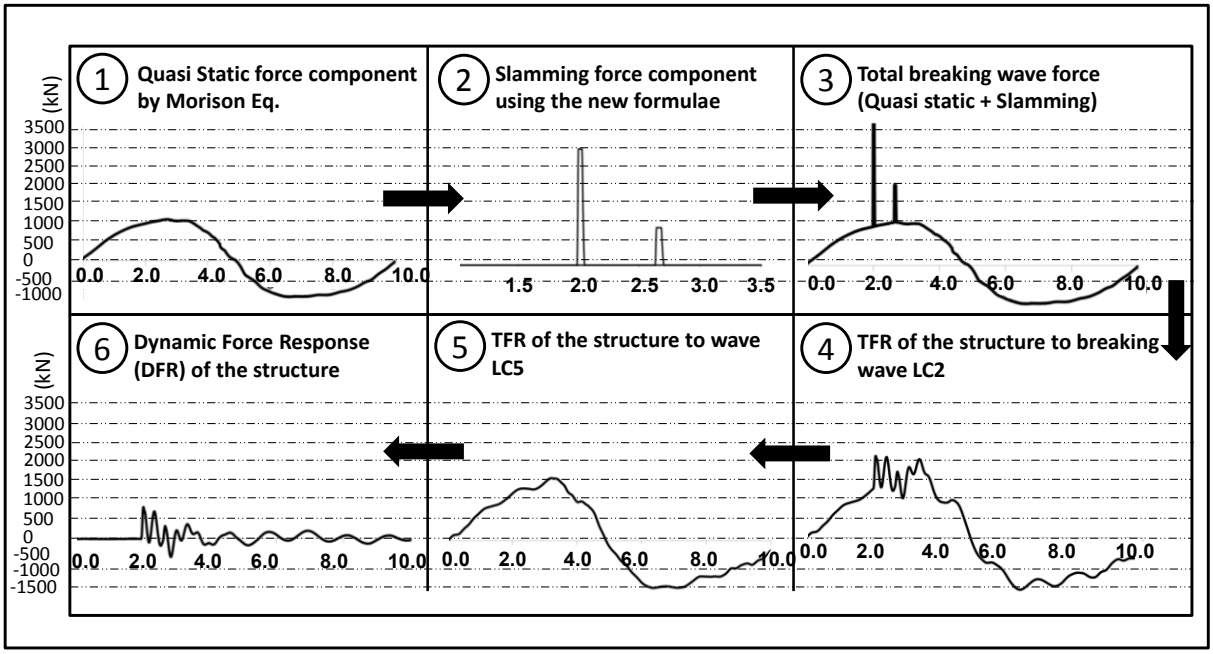

Figure 5-14. Approach for the extraction of the DFR time history from the TFR of the OC4 jacket (Exemplarily for Load Case LC-B2)

It should be stressed that the calculated quasi-static force response QSFR of the jacket structure to LC5 (Figure 5-14(5)) is moderately different (20% higher peak value) from the quasi-static force calculated by Morison equation (Figure 5-14(1)). This might be explained by the P-Delta effect, which may significantly affect the response of the jacket structure. In structural engineering, the P-Δ effect refers to the abrupt changes in ground shear, overturning moment, and/or the axial force distribution at the base of a sufficiently tall structure subject to a lateral displacement. The P-Δ effect is a destabilizing moment equal to the force of gravity multiplied by the horizontal displacement of the structure when loaded laterally. In a perfectly rigid body subject only to small displacements, the effect of a gravitational or concentrated vertical load at the top of the structure is usually neglected in the computation of the force response. However, the mass of the wind turbine on the top of a tower on jacket structures can exhibit relatively large lateral displacements under extreme waves/wind loads. When the structure is subject to such lateral displacements, the vertical mass of the RNA or transition piece (TP) might adversely perturb the overturning moment/shear base of the structure which causes higher forces and deformation in the legs and braces of the structure. In fact, 'base shear' or called hereafter 'total force response (TFR)' is the maximum expected lateral force that might occur at the base of the structure just over the sea bed due to dynamic or quasi-static forces (see Figure 5-3).

The slamming forces due to breaking waves (LC-B1 to B5) on the front and rear faces of the OC4 jacket structure are calculated using the proposed formulae in this study and plotted in Figure 5-15a. The first and second impacts on the front and rear faces of the jacket structure are applied at t=2s and t=2.66s, respectively, considering the relative breaking/broken wave celerity.

The total force response (TFR) of the OC4 jacket structure to the slamming forces in Figure 5-15a with the quasi-static forces is calculated and plotted in Figure 5-15b over a wave period (T=10s). As can be seen, the highest TFR is obtained for load case 2 (LC-B2) meaning that the highest lateral force on the pile foundation of jacket structures might be applied when the wave breaks 3-10m in front of the structure and the breaker tongue hits inclined the front face of the structure. As shown in Figure 5-15a, for the design procedure of jacket structures, it is crucial to consider breaking waves as those inducing the most extreme wave loads on the structure. Considering only non-breaking waves may indeed underestimate the total force response of the structure as shown in Figure 5-15 for the OC4 jacket, where underestimation of the extreme forces up to 35% might result. Moreover, the impact force components on the braces and legs of the structure are ignored when considering a design based only on the quasi-static forces on the structure.

Figure 5-15c shows the dynamic force response DFR of the structure calculated using the approach illustrated in Figure 5-14. Comparing the DFR of the jacket structure in Figure 5-15c to the slamming forces in Figure 5-15a shows lower magnitudes of the DFR than the corresponding values of the slamming forces meaning that the dynamic amplification factor (DAF) of the OC4 jacket structure is lower than 1. DAF is a dimensionless parameter (see Figure 5-15d) which describes the ratio of deflections X (or forces DFR) induced by dynamic loads to those caused by static loads ($DAF = \frac{X_{Dynamic}}{X_{Static}}$ or $DAF = \frac{DFR_{Dynamic}}{DFR_{Static}}$).

Considering the calculated slamming forces and obtained DFR of the structure (Figure 5-15a & c), the dynamic amplification factor of the OC4 jacket structure is much less than 1 (DAF= 0.36 to 0.39). This might be explained by the duration of the impact force, which is much lower than the natural period of the structure ($\Omega = \frac{T_n}{T_d} = 4 \sim 6$). For such a system (Figure 5-15d), the structure causes a reduction of the "effective" impact forces so that a dynamic force response DFR lower than the applied slamming loads is obtained (Chopra, 1981).

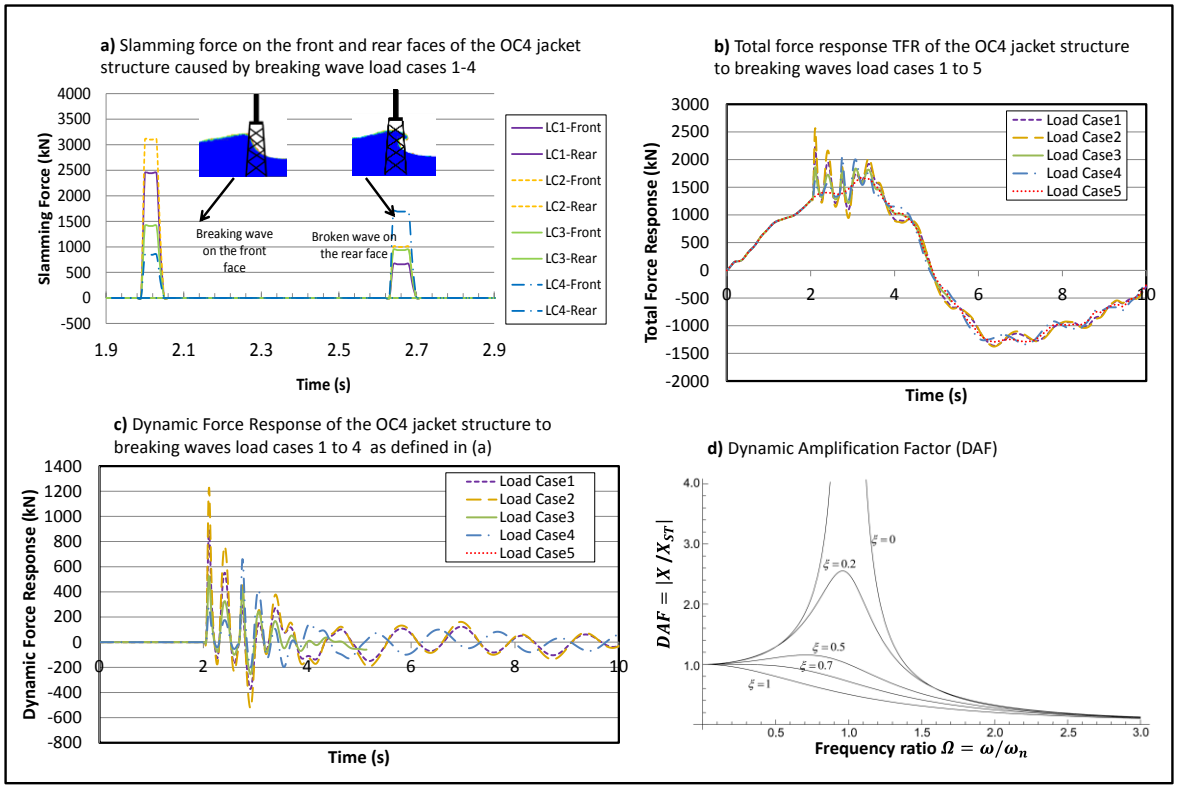

Figure 5-15. Dynamic response of the OC4 jacket structures to breaking wave load cases 1-5 as defined in Figure 5-13 (H=10m; T=10s, h=50m)

Prediction of slamming forces using different formulae

Jacket structures should withstand diverse environmental loads over their lifetime. Among the diverse types of loads acting on a jacket structures, breaking waves induce the largest loads on the structure and therefore, should be considered as an important threat for the stability of jacket structures. Currently, wave slamming forces on jacket structures are predicted using conventional models initially developed for breaking waves on single slender cylinders. However, the laboratory tests in large wave flume GWK and the preliminary analysis of the GWK tests in Chapter 3 showed that the application of the available formulae developed for single slender cylinders to truss structures (e.g. Wienke & Oumeraci, 2005; Goda, 1966) would result in a different time series of the slamming force as compared to the measured slamming forces caused by breaking wave on jacket structures. In particular, the impact duration for jacket structures is significantly higher than those estimated by slamming models for single piles, which is mainly due to the successive impacts of the incident breaking wave on the legs and braces of jacket structures (see Table 3-3).

In this section, a comparative analysis of the dynamic response of the OC4 jacket structure to impact loads according to different slamming formulae is performed as follows:

(i) the slamming force caused by breaking waves on the front face of OC4 jacket structure is calculated by applying the available models initially developed for slamming force on single piles (Table 3-4a & b)

(ii) the formulae proposed in Chapter 3 of this PhD study for slamming force on truss-type structures is implemented to predict the slamming force on the front face of the OC4 jacket structure. The calculated slamming forces are compared in ble 3-4a & b.

(iii) the dynamic force response DFR of the OC4 jacket structure to different slamming forces shown in Table 3-4b is obtained.

It should be stressed that, the slamming models initially developed for breaking waves on mono-pile structures are not applicable on the rear face of a jacket structure. Therefore, the slamming model proposed in this PhD study is only considered for the front face so that a better assessment of the performance of different slamming models can be achieved through direct comparison of the DFR and TFR of the jacket structure to slamming forces depicted in Table 3-4 a & b.

Figure 5-16a shows the peak and duration of the slamming force on the front face of the OC4 jacket structure caused by a breaking wave with crest $\eta_b = 6.67$m and period T=10s (LC-B2). The total slamming force on the front face is calculated using the available slamming formulae for single piles, and the results are compared with the slamming force calculated by the formulae developed in chapter 3 for jacket structures. It is important to stress that the impact duration is crucial parameter which is inherently linked to the associated peak of the impact force, and has thus been considered for each slamming model.

In addition to the comparison in Figure 5-16a, the time series (obtained from the different slamming formulae) of the impact forces on the front face of the OC4 jacket structure are shown in Figure 5-16b. Significant differences are observed between the slamming force time history obtained in this study and the results from other slamming formulae for a single pile. This inconsistency is basically due to differences in the physical process involved in the interaction of breaking waves with the much more complex frame structure composed of different members, which cause the magnitude and the impact duration of the slamming force to decrease and increase, respectively.

Figure 5-16c shows the dynamic force response (DFR) of the OC4 jacket structure to the slamming forces on the front face shown in Figure 5-16b calculated using the Duhamel's integral method (proposed in chapter 4) by considering the natural frequency of the OC4 jacket structure obtained from a modal analysis in ANSYS. Although the magnitude of the slamming force calculated by the model proposed in this study is considerably lower than those obtained by the models for a single pile (Figure 5-16a), the DFR of the structure to the slamming model in this study is higher (Figure 5-16c). This result highlights the significant effect of the impact duration on the dynamic response of a structure. It is noteworthy that the lowest DFR of the structure is obtained by using Wienke's model (2005) which, among all available slamming models, results in the highest slamming coefficient (2π) and shortest impact duration. In fact, besides the maximum peak of the slamming force, the associated duration is a crucial parameter for the design as it may significantly affect the response of the structure and its foundation. Therefore, considering a slamming force function with a maximum peak of 2π does not certainly induce a higher response of the structure due to the effect of the impact duration on

the dynamic response a should be accurately considered as an integral part of the impact force history. With this background and considering Figure 5-16, the formulae by Wienke (2005) and further formulae developed for the impact force and duration on single cylindrical piles cannot be readily applied for jacket structures as they might underestimate the dynamic force response (DFR) of the structure.

The total force response (TFR) of the OC4 jacket structure to breaking wave LC-B2 is computed by superposing the quasi-static and dynamic force response of the OC4 jacket structure (Figure 5-16d). For the quasi-static force response (QSFR), ANSYS is applied to calculate the response of the structure to the quasi-static forces on the legs and braces of the structure (Figure 5-16d). For the dynamic force response (DFR), the Duhamel's integral method is applied to calculate the response of the structure to slamming forces obtained in Figure 5-16b.

a) Slamming force and duration on the front face of the OC4 truss structure obtained from different slamming force models

Slamming force model	*Wave crest height η_b (m)*	*Total length in the impact area L_{tot} (m)*	*Maximum slamming force (kN)*	*Impact duration (t)*	*Maximum slamming coefficient*
This study	6.67	16.54	3062	0.0607	1.63
Goda (1966)		18.39	6415	0.0391	π
Wienke & Oumeraci (2005)		16.54	11804	0.0159	2π
Campbell-Weynberg (1980)		18.39	13350	0.0148	5.15

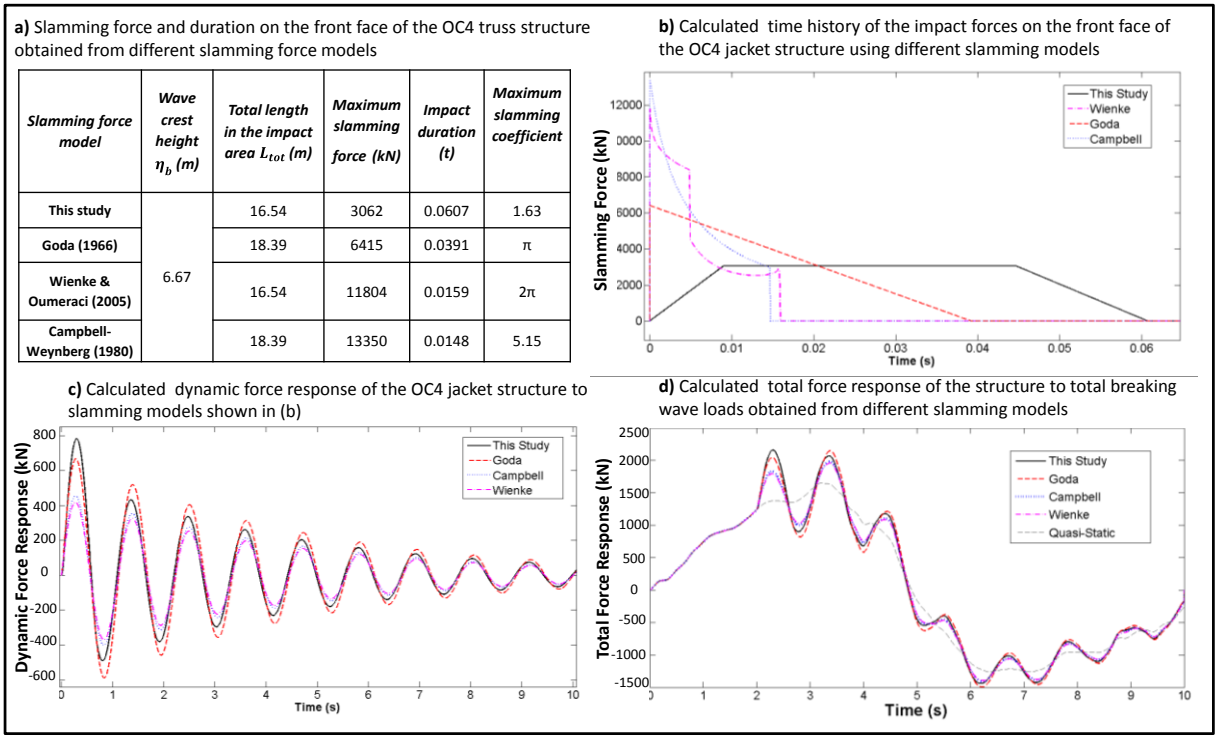

Figure 5-16. Dynamic response of the OC4 jacket structure to impact forces induced by different slamming models (LC-B2)

The results revealed a significant underestimation of the dynamic force response DFR to impact forces predicted by the models initially developed for breaking wave on single piles such as Goda (15%), Campbell (42%) and Wienke (47%).

5.4.2 Effect of the foundation piles and soil properties

Effect of soil type and soil properties

In this section, a comparative study of the dynamic response of the OC4 jacket structure to breaking waves for soil types 1-4 in Figure 5-11 and the same foundation piles (with diameter

of 2.086m, thickness of 0.06m and length of 45m) is performed to identify the effect of the soil properties on the response of the structure. The FE model of the pile foundation is modified based on the soil characteristics defined in Figure 5-11 for uniform soft clay (Soil Type 1 in Figure 5-11a), uniform sand (Soil Type 2 in Figure 5-11b), layered sand (Soil Type 3 in Figure 5-11c) and uniform hard clay (Soil Type 4 in Figure 5-11d). The analysis of the natural frequencies of the jacket structure considering different soil types revealed the high sensitivity of the FE model to the soil stiffness (Table 5-4). The difference for clay and sandy soils (soil types 1 & 2) reaches up to 25% for the 2nd fore-aft frequency.

Figure 5-17 shows the dynamic response of the structure considering different soil types. As the characteristics of soil types 2 and 3 are very similar, no significant difference is observed in the response of the structure considering these two soils. As shown in Figure 5-17a, b & c , the lateral displacement of the structure with clay (Soil-Type1 & Soil-Type 4) is significantly higher than the structure with sand (Soil-Type2 & Soil-Type3). This might be explained by the stiffness of the springs connected to the pile foundation which is higher for sand than for clay since these springs represent the soil stiffness. Figure 5-17d describes the total force response TFR of the structure, which consists of the quasi-static force response QSFR and the dynamic force response DFR. As expected, the dynamic force response DFR of the structure for sand is much higher than for clay. This might be explained by the smaller value of the dynamic amplification factor DAF for the model with clay as compared to the model with sand, which is due to the more flexible behaviour of the foundation with clay. The latter results in larger natural period of the structure with clay type 1 (T_n=3.85s) than with sand (T_n=3.64s) implying respectively DAF=0.36 and 0.39 and for clay and sand foundation. Figure 5-17e shows the axial force in the side brace of the jacket structure at Elevation 4 (SB4). The maximum axial force in SB4 is 1020, 940 and 990 kN considering soil types 1, 2 and 4, respectively, which shows a differences up to 8.5%. This comparison reveals that the axial forces in side braces of the jacket structure with pile foundation in clay increase since the structure behaves more flexible and the lateral displacements and consequently the deformation in members is higher. Figure 5-17f shows the axial force in the spring connected to the pile 10.5m below the seabed (SPR1050). Tension forces occurs in the spring representing clay (soil types 1 and 4) in the time interval from t=0s and t=5s, while compression forces are observed in the spring representing sand (soil types 2 & 3) at the same location. The reason is the different deformation shape of the pile in sand or clay as shown in Figure 5-18.

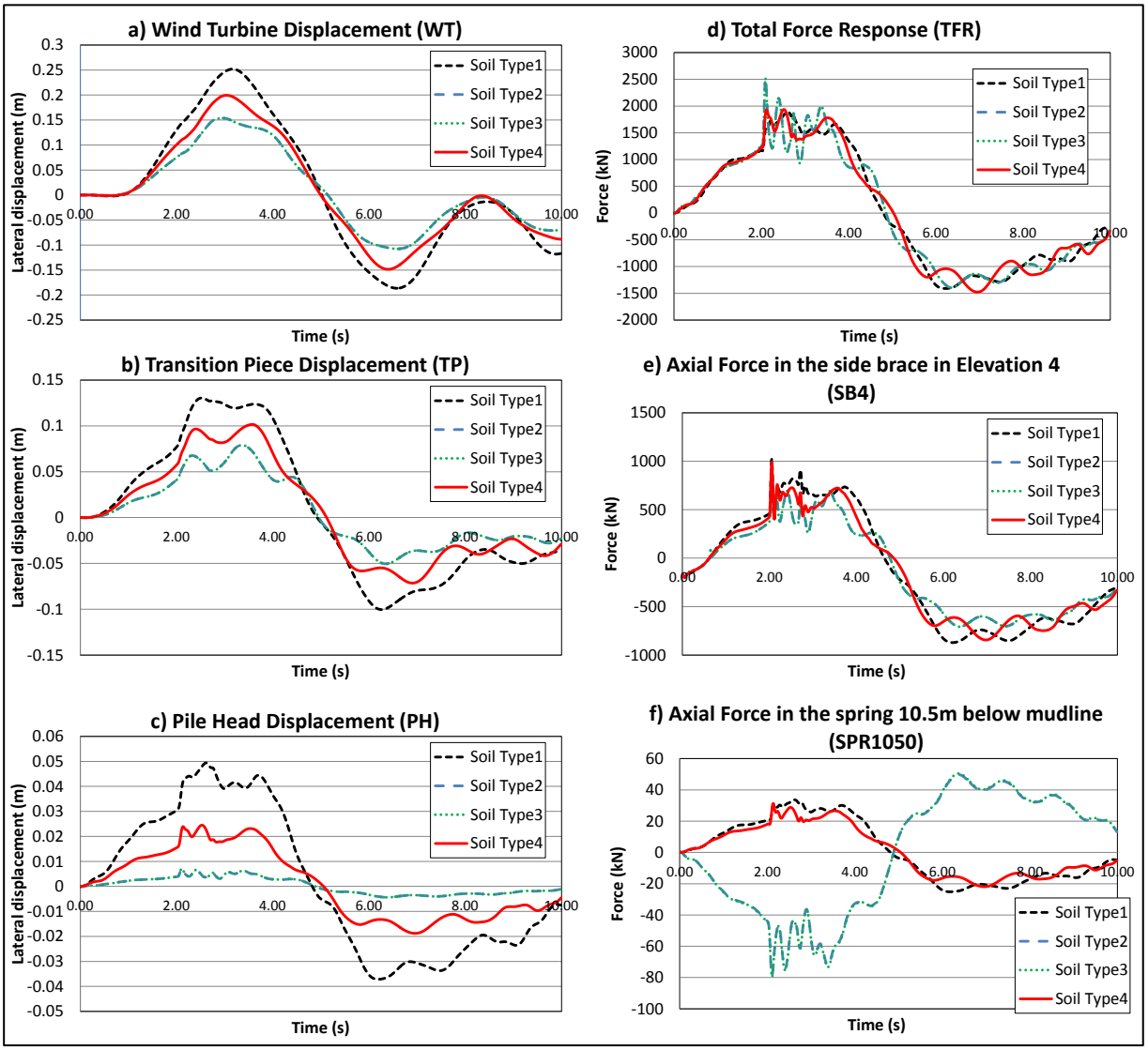

Figure 5-17. Dynamic response of the OC4 jacket structure to wave with different soil types for the pile foundations (P-S.type1 to 4) to breaking wave LC-B2 (see Figure 5-11)

The deformation shape of the pile foundation embedded in soil types 1-4 is calculated and plotted versus the soil depth in Figure 5-18a considering the virtual sensors placed along the pile foundation (PL1-9). For the soft clay (Soil-Type1), the deformations are much larger than other soil types. Moreover, as the stiffness of the soft clay soil is relatively small, the pile slides in the bottom. For sand (Soil-Types 2 & 3), which is relatively stiff, the displacement of the pile is highly restricted by the soil surrounding the pile except in the top layer close to the mudline where the soil stiffness is much less than the stiffness in deeper layers.

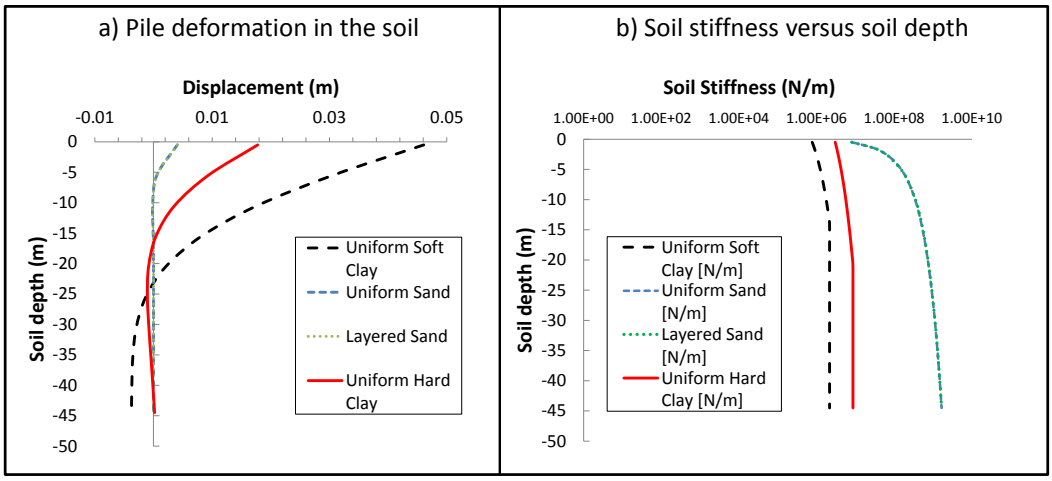

Figure 5-18. Deformation of the pile foundation in different soil depths at t=2.7s under breaking wave LC-B2

Effect of non-linearity of soil behaviour

In this section, the effect of non-linearity of soil behaviour on the dynamic response of jacket structures is examined. In fixed-bottom support structure of wind turbines, the lateral pile displacement and rotation might significantly affect the movements of the entire structure. Therefore, the pile-soil interaction model (p-y) should be accurate enough to appropriately distribute the lateral forces among different soil layers according to the soil stiffness. Among the approaches available, p-y models that are based on nonlinear modelling of springs in different soil layers connected to the pile foundation, are recommended in several guidelines such as API (2005) and DNV (2013) (as explained in section 2.3.2). However, the application of non-linear models is much more complex and more computationally demanding than linear models. Furthermore, in some cases, especially for lower loads and smaller soil deformations, the soil exhibits a linear behaviour and using non-linear approaches might increase computational cost and complexity without providing any extra accuracy. This can be seen in Figure 5-19 where the soil behaviour becomes non-linear only when the displacements exceed a certain value (y_2). In such areas (between y_0 to y_2) application of linear and non-linear approaches might lead to similar results. Therefore, it is important to optimize the numerical simulation by employing a proper soil model to achieve both accuracy and computational efficiency.

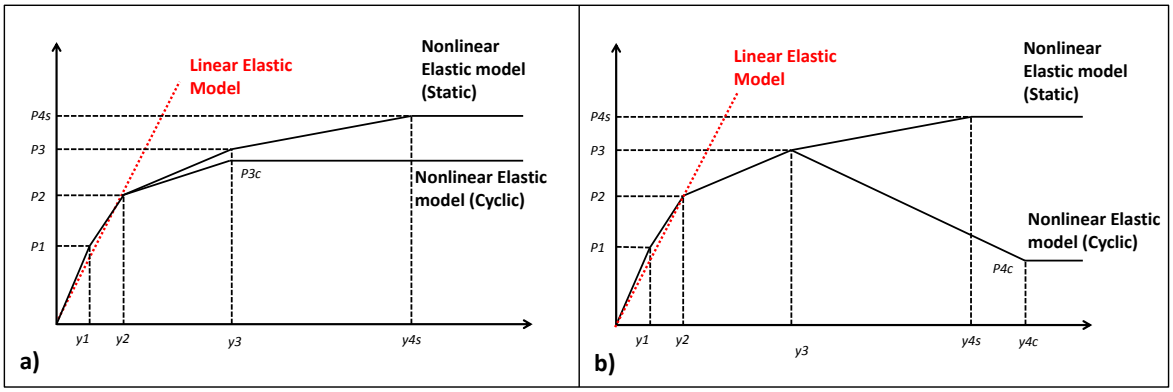

Figure 5-19. Linear and non-linear p-y curves for a) clay; and b) sand under cyclic and static loading

Based on the aforementioned background, the p-y method described in Chapter 2 is implemented to investigate the applicability of linear p-y springs for the pile foundation of jacket structures.

Linear and non-linear dynamic analyses are conducted comparatively to study the dynamic response to breaking waves for both linear and non-linear soils with a particular focus on pile-soil behaviour. Figure 5-20 shows the comparison of the displacements and forces in the pile foundation of the OC4 jacket structure for linear and non-linear soil models.

The results show that the non-linear behaviour of the soil beside pile foundation of a jacket structure is not severe because the pile foundation is significantly restrained from pile-head displacement. In general, except the very top soil layer (First 2 meters) of the foundation (Figure 5-20d), the pile-soil behaviour of the OC4 jacket structure exhibits a linear behaviour (Figure 5-20a, b, c & d). The main reasons are:

(i) The brace system of the jacket structure provides a high stability and resistance to lateral loads and causes small lateral displacements of the pile-head that keeps the soil in the linear range;

(ii) The hydrodynamic force on the slim members of jacket structures (leg=1.2m; brace=0.8m for OC4) is significantly lower as compared to the thicker member of other fixed-bottom offshore structures such as monopile (D>8m for water depth larger than 30m);

(iii) In jacket structures, at least four individual piles must withstand the base shear and overturning moment caused by the extreme wave load, and as a result the force applied on each foundation pile is significantly lower than the force on the foundation of a mono-pile structure where one individual pile must withstand the total overturning and base shear forces.

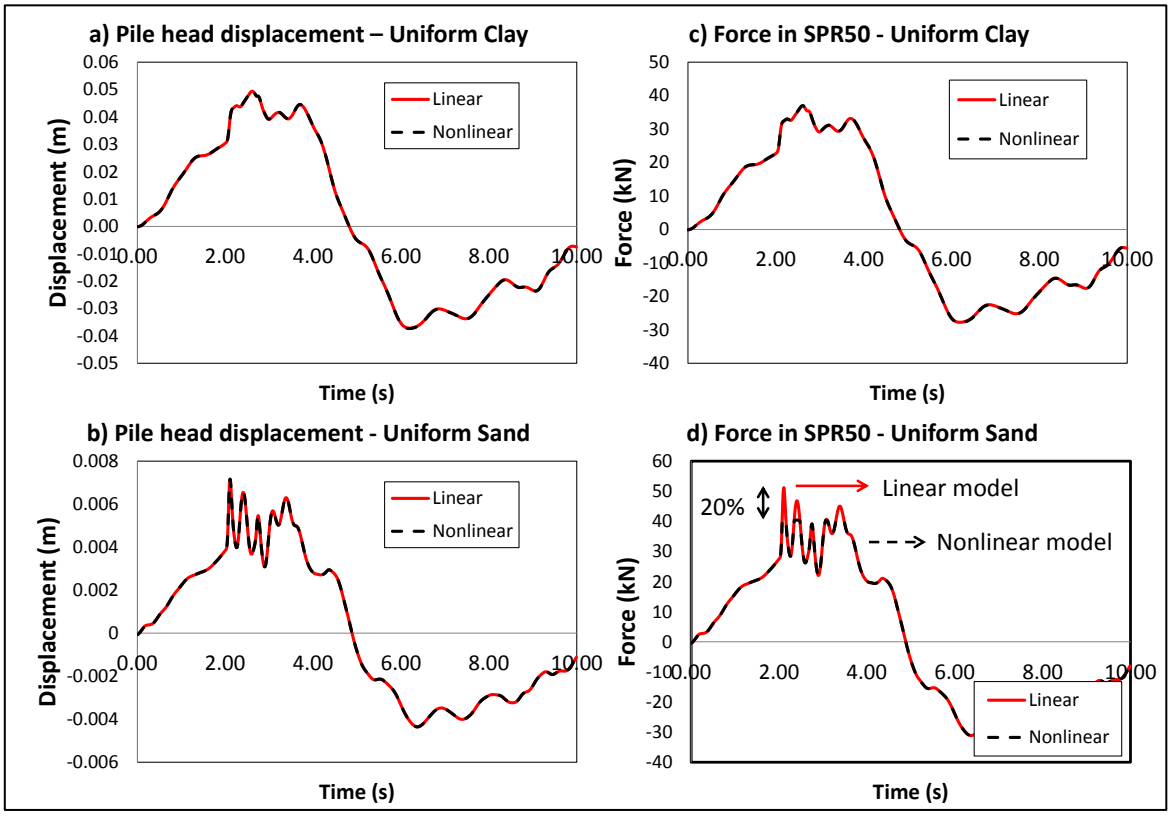

Figure 5-20. Dynamic behaviour of the pile foundation of the OC4 jacket structure considering linear and non-linear soil models under breaking wave LC-B2

Effect of sea-bed scour

Seabed scour is the removal of soil material by near bed flow in the vicinity of coastal and offshore structures. Although the occurrence of scour around piles of a jacket structure is a well-known phenomenon (Figure 5-21a), to the author knowledge no study has yet addressed the effect of scour on the dynamic response of jacket structures. Scour might mainly have two important effects on the dynamic response:

(i) As the soil in the area close to the mudline is removed, the soil resistance may be reduced. Moreover, the geodynamic mass contribution to inertia is also decreased, These changes in the stiffness and mass matrixes, might change the natural frequency of the structure;

(ii) The hydrodynamic forces on the entire structure will be increased as the soil beside the pile foundation will be eroded due to scour effects.

Therefore, the effect of scour on the dynamic response of the OC4 jacket structure to breaking wave induced forces is examined below. For this purpose, the maximum scour depth around piles of the OC4 jacket structure, which is considered as the lowest probable bottom level over 30 years structure life time (H=10m; T=10m, h=50m) , is calculated as follows (Figure 5-21):

(i) The global scour depth S_G (Figure 5-21b) is defined by $S_G = 0.37\, D_{calc}$ (Sumer & Fredsøe, 2002) where D_{calc} is the pile diameter including marine growth. Consid-

ering the value of $D_{calc} = 2.082m$ the maximum global scour depth is equal to 0.77m.

(ii) The local scour depth S_L (Figure 5-21a) around piles of the structure might be defined by the expected value $S_L = 1.3\, D_{calc}$ (DNV, 2013) for sand soil which means $S_L = 2.71m$.

Therefore, the total scour depth is obtained from the following equation $S_T = S_L + S_G$ which is 3.48m.

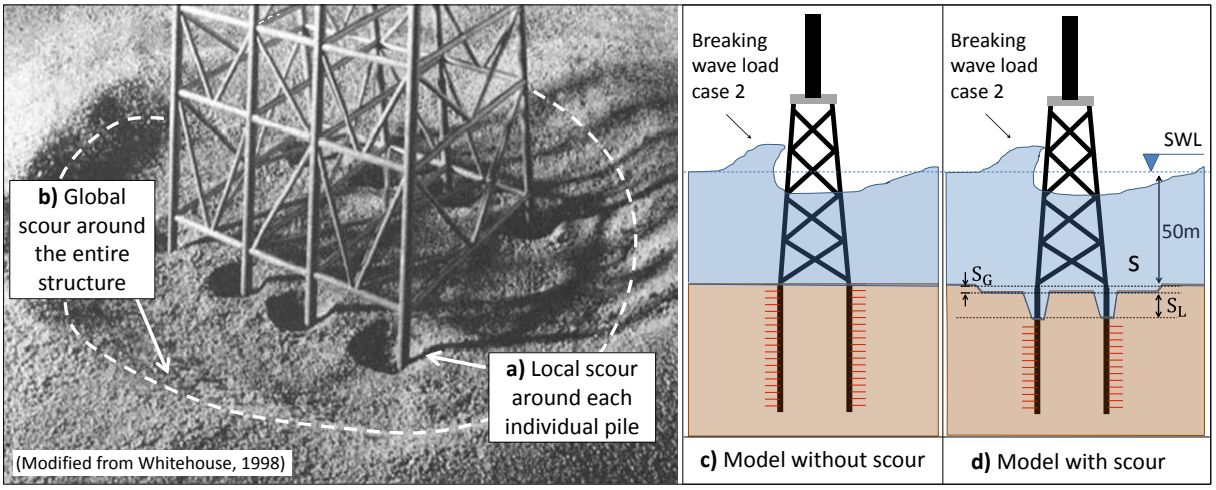

Figure 5-21. Representation of global and local scour development around jacket structures

The set-up of the FE model of the OC4 jacket structure with pile foundation is modified based on the obtained global and local scour depths (Figure 5-21d) in order to perform a comparative study of the dynamic response of the structure to breaking wave loads with and without scour effect. For the global scour, which is characterised by general erosion and removal of soil over a large area (Figure 5-21a & d), all p-y curves are regenerated on the basis of a modified seabed level which is taken as the initial seabed level lowered by a height equal to the depth S_G of the global scour. For the local scour, which is characterised by erosion and removal of soil only locally around each pile (Figure 5-21 a & d), the p-y curves are generated with due account for the depth S_T of the total scour hole. Moreover, the mass of the soil oscillating with piles of the structure is removed according to the total scour depth.

Figure 5-22 shows time series of the dynamic response of the OC4 jacket structure with pile foundation in clay (soil type 1) to the breaking wave LC-B2 by considering the effect of scour (Figure 5-21d) and without scour effect (Figure 5-21c) . The slamming forces are applied at time t=2s & t=2.66s on the front and rear faces of the jacket structure, respectively. The time series of the lateral displacement of the structure (using the virtual sensors WT, TP, PH shown in Figure 5-3) is shown in Figure 5-22a ,b & c. As can be seen, neglecting the scour effect results in an underestimation of the lateral displacement of the structure by up to 25%. The main reasons are the significant reduction of the soil mass and stiffness considering scour effects.

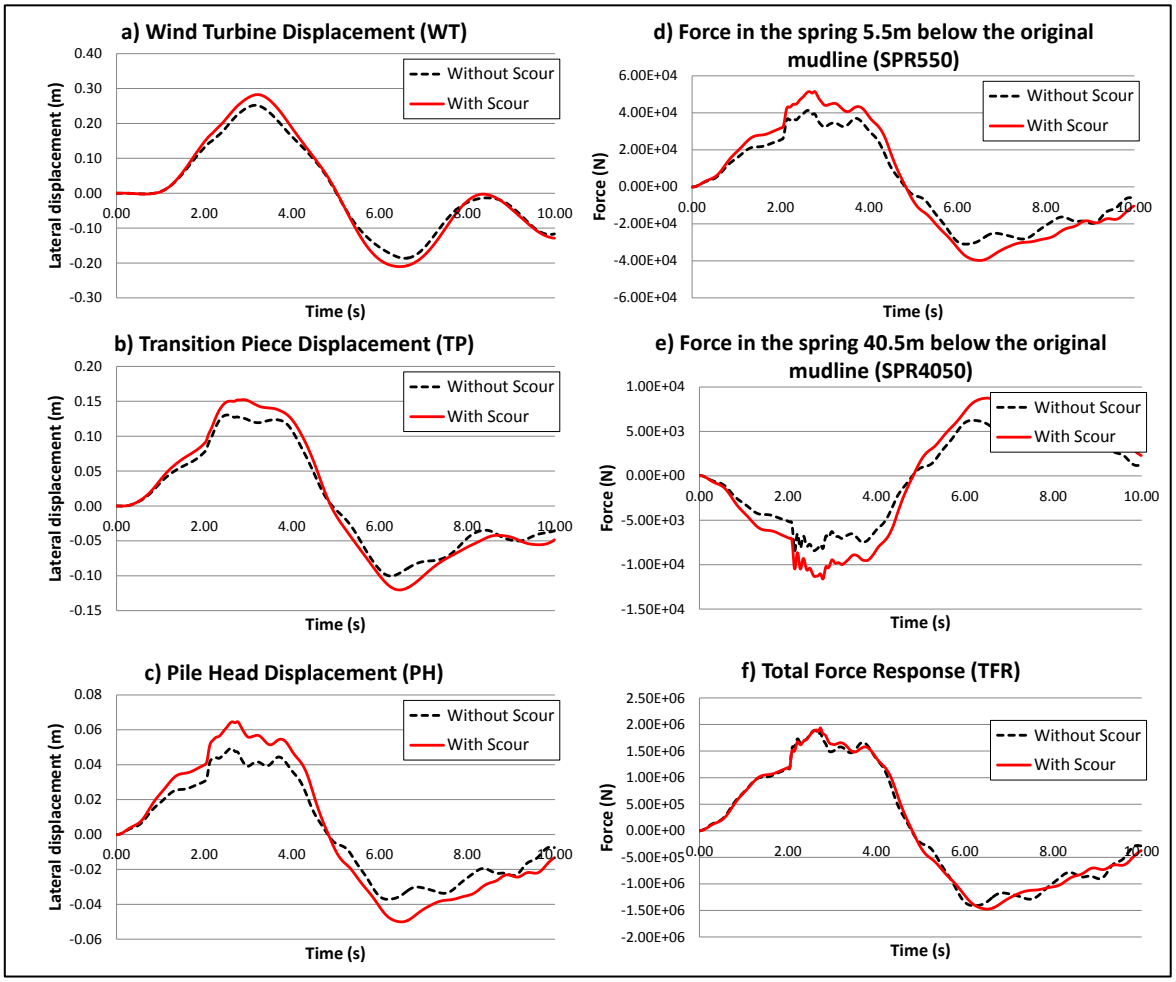

Figure 5-22. Dynamic response of the jacket structure with pile foundation in clay (type1) with and without scour consideration seabed scour (H=10m; T=10m, h=50m), (see Figure 5-3 for location of virtual sensors)

Basically, the stability of the jacket structure to lateral applied loads is mainly provided by the following structural members (see Figure 5-23):

(i) Within the braced zone (L_{Br}), the side braces of the structure parallel to the incident wave withstand the lateral forces considering their axial stiffness (EA/l_{br}). In this zone, the jacket structure behaves very stiff (Figure 5-23).

(ii) Within the unbraced zone (L_{UB}), the piles and legs of the jacket structure withstand the lateral forces considering their bending stiffness (EI/L_{UB}) (Figure 5-23).

Since the length of the unbraced zone of the jacket structures is relatively short (6m for the OC4 jacket), the bending stiffness of the member in this zone is very high (EI/L) thus ensuring the stability to the structure. However, the scour around the piles may increase the height of the unbraced zone of the structure significantly (from 6m to 9.5m for OC4 jacket) which might reduce the bending stiffness considerably (Figure 5-23). Therefore, as shown in Fig-

ure 5-22a, b & c, the displacement of the structure considering scour is moderately higher than the model set-up without scour.

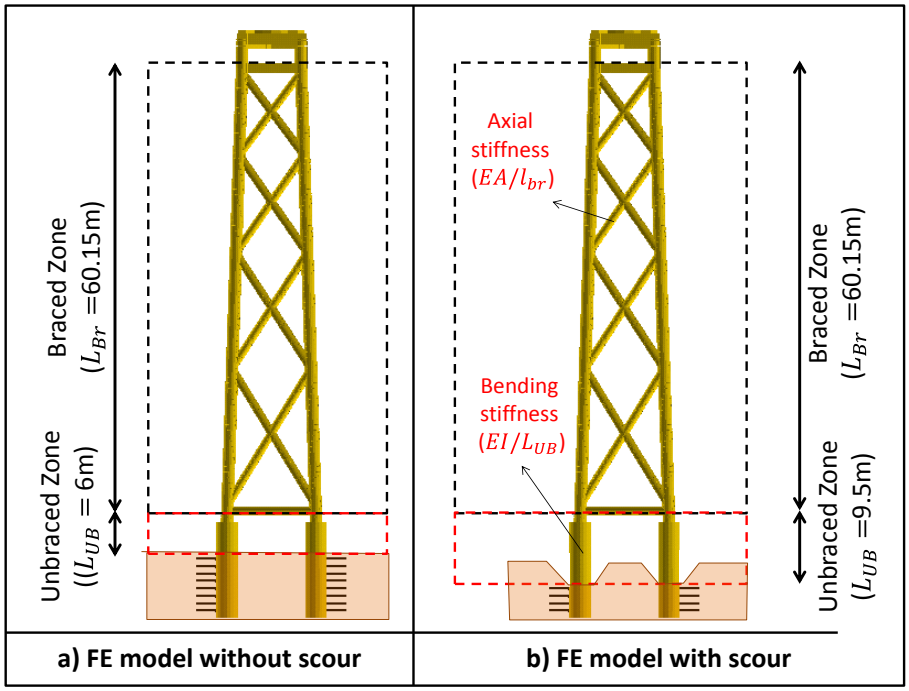

Figure 5-23. Braced and unbraced zone of the OC4 jacket structure a) without scour; b) with scour effects

In summary, scour (i) reduces the foundation bearing capacity and consequently, might increase the failure probability in terms of both serviceability and ultimate limit state; (ii) reduces the natural frequency of the structure embedded in the soil and therefore, might significantly affect the dynamic response of the structure (Figure 5-22 d & e). Therefore, the results of this preliminary analysis indicate that the scour effect should be considered in the design process of jacket support structures.

5.4.3 Effect of structural parameters

Legs and braces diameter

Offshore wind energy represents one of the most promising sources of renewable energy. However, the costs of this form of energy are still high. A reduction in cost can be achieved by an optimized design of the support structure, since it constitutes a significant part of the capital costs. For offshore wind energy projects, the supply and installation of the substructure represent around 20% of the capital costs (Azau & Casey, 2011). For multi-member support structures such as jackets, the optimization process becomes a challenging task due to the large number of parameters, the complexity of numerical models and the time-consuming time-domain analyses (Muskulus & Schafhirt, 2014). This might be even more complex when the jacket structure is subject to breaking waves. In particular, the legs and braces should be designed properly, in order to achieve a safe dynamic response and reasonable manufacturing

costs. The higher the dimension of legs and braces of the jacket structure, the higher the stiffness and mass of the structure and consequently, the higher the manufacturing costs. The quasi-static and impact forces might also significantly increase by increasing the dimension of the legs and braces. Moreover, increasing the diameter of the legs and braces might not necessarily enhance the dynamic response but even degrade the structural performance due to the higher hydrodynamic forces.

This section is dedicated to the effect of the legs and braces diameter on the dynamic response of the OC4 jacket structure to breaking waves for load case LC-B2. Diverse parameters such as structural mass, tentative manufacturing costs, natural frequency, deformation and stress in members of the jacket structure are preliminary examined in order to tentatively optimize the model of the structure considering the structural behaviour of 5 types of jacket structures shown in Figure 5-24.

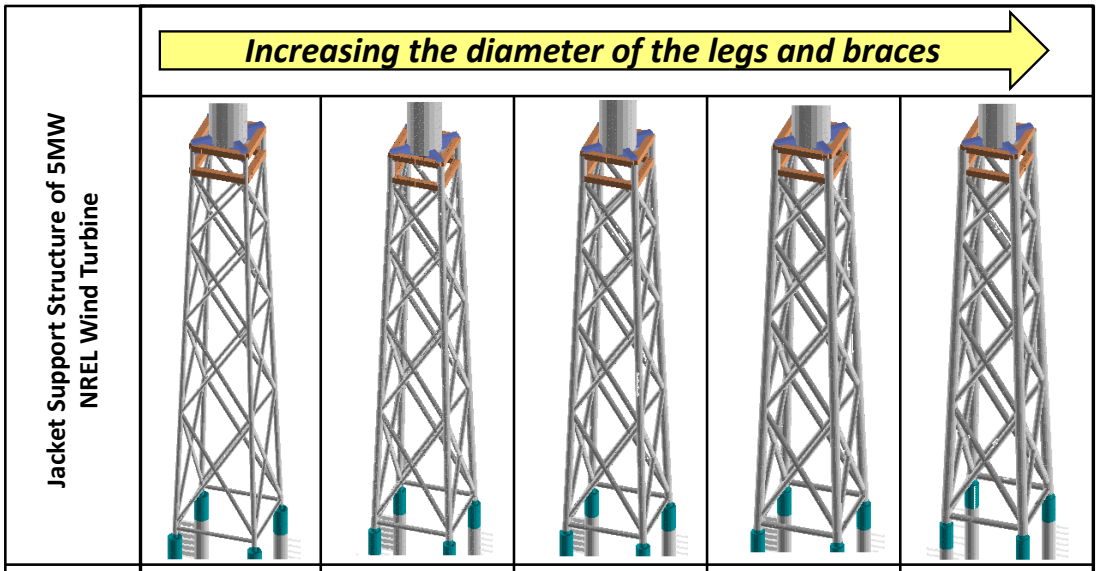

Jacket	J1		J2		J3		J4		J5	
	D (m)	t_{str} (m)	D (m)	t_{str} (m)	D (m)	t_{str} (m)	D (m)	t_{str} (m)	D (m)	t_{str} (m)
leg crossing TP	0.8	0.040	1.0	0.040	1.2	0.040	1.4	0.040	1.6	0.040
leg 2 to 4 level	0.8	0.035	1.0	0.035	1.2	0.035	1.4	0.035	1.6	0.035
leg at lowest level	0.8	0.050	1.0	0.050	1.2	0.050	1.4	0.050	1.6	0.050
x- and mud braces	0.4	0.020	0.5	0.020	0.6	0.020	0.7	0.020	0.8	0.020

Figure 5-24. Different jacket structures modelled to support 5MW NREL wind turbine (for dimensions see also Figure 5-2)

Using the set-up models for jacket structures J1-J5 shown in Figure 5-24, the following tentative analyses are performed:

(i) *Modal analysis using ANSYS*. The simplifications described in section 5.2.1 have been adopted for the modal analysis in order to decrease the complexity of the

modelling (Figure 5-25a). The larger the dimension of the legs and braces, the higher the natural frequency of the structure since the structural stiffness increases by enlarging the diameter of the members. Moreover, the total mass and tentatively estimated fabrication costs of the jacket structures J1-5 are calculated. It should be stressed that the total manufacturing costs are directly proportional to the mass of the structure and are currently considered 1200 Euro/ton and 400 Euro/ton for fabrication and installation, respectively (Verhaegh, 2014). As can be seen optimizing the model of the jacket structure may significantly reduce the manufacturing costs. For example, the total costs of the J1 jacket structure is 16% lower than the J5 jacket structure.

(ii) *Quasi-static wave load using Morison equation*. Since the Keulegan Carpenter number of the incident breaking waves (KC) varies in the range of 35 to 60, the drag and inertia coefficients are almost constant and therefore these coefficients have not been varied while changing the diameter of the structure (Figure 5-25b). According to the Morison equation, the drag and inertia force on a slender member is directly proportional to member diameter D. Therefore, as can be seen in ure 5-25b, the total quasi-static force on the structure significantly depends on the legs and braces diameter. The total calculated quasi-static force on the J1 structure is almost twice larger than the quasi-static force on the J5 structure.

(iii) *Slamming forces using the new developed formulae*. The impact forcers on the front and rear faces of the jacket structures J1-5 are calculated (see Figure 5-25c). According to the proposed slamming formulae for breaking/broken waves on truss structures (Eqs. 4-4 to 4-6 & Eqs. 4-14 to 4-16), the magnitude of the impact force and the impact duration vary proportionally with the diameter of legs and braces. Therefore, the estimated impact caused by the breaking wave on the J5 jacket is dramatically higher than the impact on the J1 jacket structure.

(iv) *Total Force Response TFR of the structures J1-J5,* The TFR of structures J1-J5 to the breaking waves for load case LC-B2 is calculated and plotted in Figure 5-25d. As can be seen, the TFR of the J1 structure is considerably lower than J5. The main reasons are: (a) The quasi-static force on the J1 structure is lower than J5 structure (Figure 5-25b); (b) The impact force on the J1 structure is lower than the impact force on the J5 structure (Figure 5-25c); (c) As the natural frequency of the J1 structure is lower (Figure 5-25a), the dynamic amplification factor DAF is lower and therefore, the dynamic force response DFR of the J1 structure to the applied impact force is smaller. This has significant implications for the optimization of the pile-foundation of the jacket structure because the lateral forces on the pile-head of the jacket structure (TFR) might be decreased considerably when decreasing the diameter of the legs and braces.

(v) *Lateral displacement of the transition piece*. It is calculated for breaking wave load case LC-B2 (Figure 5-25e). Although enlarging the diameter of the legs and braces of the jacket structure might increase the lateral stiffness of the structure, it also increases the quasi-static and impact forces significantly. Therefore, it is highly questionable whether the performance of the structure will be improved, when increasing the diameter of the member. As shown in Figure 5-25e, the maximum displacement of the jacket structure with slimmer legs and braces (J1 & J2) is de-

creased and shifted slightly to the right. Since the natural frequencies of the jacket structures with slimmer members (J1 & J2) are lower than those with thicker members (J4 & J5), they behave more flexible.

(vi) *Axial stresses in leg of the jacket structures J1-J5,* They are computed for breaking wave load case LC-B2 (Figure 5-25f). Although decreasing the diameter of the legs and braces of the OC4 jacket structure leads to a significant improvement of the global response of the jacket structure to lateral loads, this might have negative effects on the structural performance under static loads (e.g. body weight, mass of the transition piece and turbine). The results show that enlarging the diameter of the leg will increase the axial and bending resistance of the members and consequently decreases the available stress in the members.

a) Natural Frequency , Mass and estimated costs of the structures J1-J5

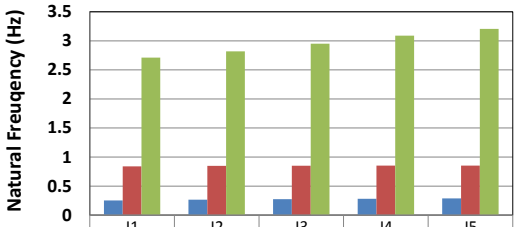

	J1	J2	J3	J4	J5
1st Fore-aft	0.25352	0.26587	0.27493	0.28185	0.28729
2nd Fore-aft	0.83865	0.84723	0.85124	0.85255	0.85204
Global Torsion	2.7105	2.8181	2.9497	3.0894	3.2046

Mass (ton)	1733	1816	1897	1979	2061
Total Cost (Euro)	3466000	3632000	3794000	3958000	4122000

b) Quasi-static component of the total force induced by the breaking wave LC-B2 on jacket structures J1-J5

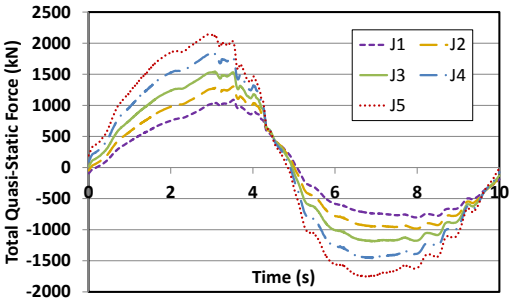

C) Slamming component of the total force induced by the breaking wave LC-B2 on jacket structures J1-J5

Jacket	*Wave crest height on the front face [m]*	*Maximum slamming force on the front face [N]*	*Maximum slamming force on the rear face [N]*	*Impact duration [s]*
J1	6.67	2179131	701680	0.0404
J2	6.67	2620619	843859	0.0506
J3	6.67	3099800	998136	0.0607
J4	6.67	3503774	1128215	0.0708
J5	6.67	3945322	1270394	0.0809

d) Total Force Response of jacket structures J1-J5 to the breaking wave LC-B2

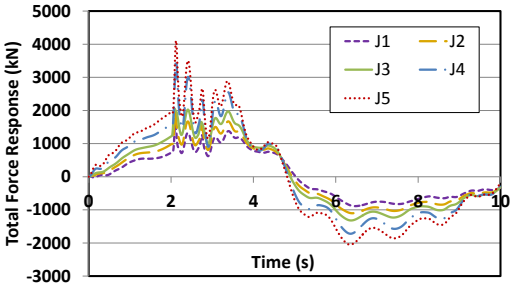

e) Lateral displacement of the transition piece (sensor TP) of jacket structures J1-J5 under the breaking wave LC-B2

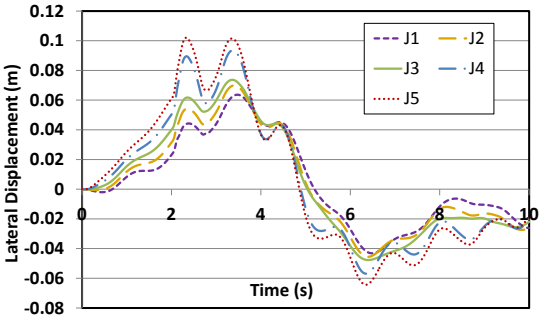

f) Axial stress in the leg of jacket structures J1-J5 (sensor LF2) at Elevation2 under the breaking wave LC-B2

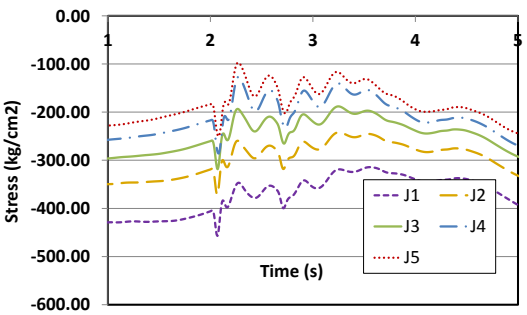

Figure 5-25. Dynamic response of jacket structures J1-J5 to breaking wave load LC-B2 (H=10m, T=10s, h=50m)

The results of the parameter study for different legs and braces diameters show that the local response of the structure might be significantly affected by reducing the diameter of the legs and braces (Figure 5-26). The buckling phenomenon, which is characterized by a sudden sideways failure of a structural member subject to high compressive stress, has been frequently observed in the legs and especially braces of the jacket structures J1 & J2. This might be explained by the compressive stress at the point of failure, which is less than the ultimate compressive stress the material is capable to withstand. Indeed, reducing the diameter of the members increases the slenderness ratio (λ_r) according to $\lambda_r = \frac{l_e}{i}$, where i is the appropriate radius of gyration of the member ($i = \sqrt{\frac{I}{A}}$), l_e is the effective length of the member and is calculated by multiplying the unsupported length of the compression member (L_{us}) to the column effective length factor (K_f).

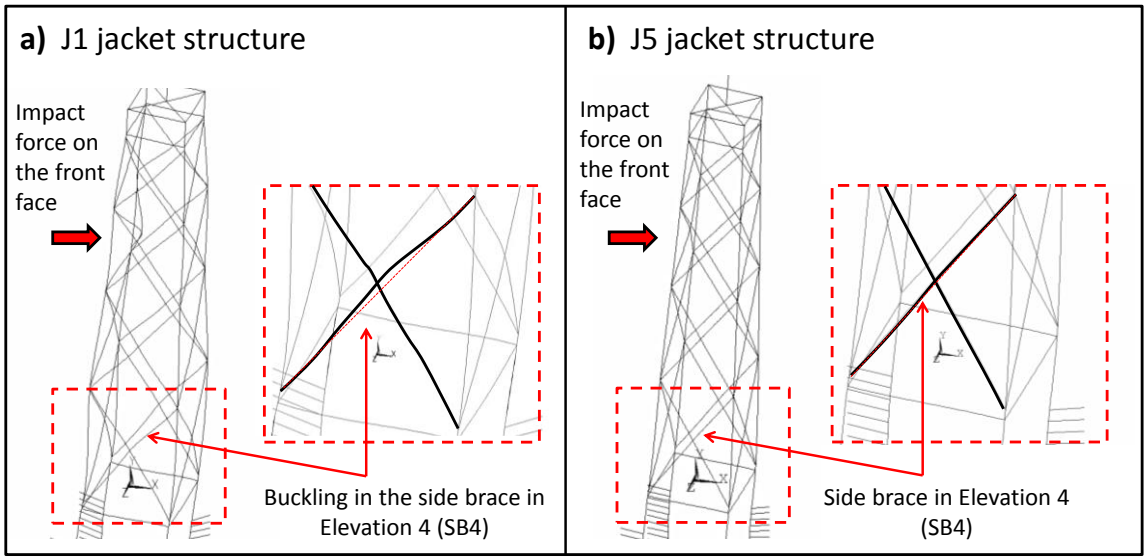

Figure 5-26. Deformed shape of the jacket structures a) J1 and b) J5, immediately after the breaking wave impact on the front face

In general, decreasing the diameter of the legs and braces of the jacket structure might improve the structural performance to hydrodynamic forces as the quasi-static and impact components of the wave force will be significantly reduced. However, this might also increase the axial stresses in the legs of the structure due to the available static forces such as structural masses. Moreover, the resistance of the members to buckling has to be checked as decreasing the member radius of gyration will increase the probability of buckling occurrence.

Geometry of the structure

Jacket structures are commonly manufactured with different types of braces such as X, Z, V. Among different types of braces, X and Z braces are the mostly used. In this section, a comparative analysis of the dynamic response of two types of jacket structures (with X & Z Braces) to breaking waves is performed using two FE models of the jacket support structure set-up in ANSYS as follows:

(i) *Jacket structure with X braces:* The original model of the OC4 jacket structure as shown in Figure 5-27a. (Figure 5-2 & Figure 5-4)

(ii) *Jacket structure with Z braces:* The braces of the original model are replaces with Z braces with dimension of D=0.8m & t=0.02m. The horizontal braces are added to the FE model in order to stabilize the truss model in each face of the structure as shown in Figure 5-27b.

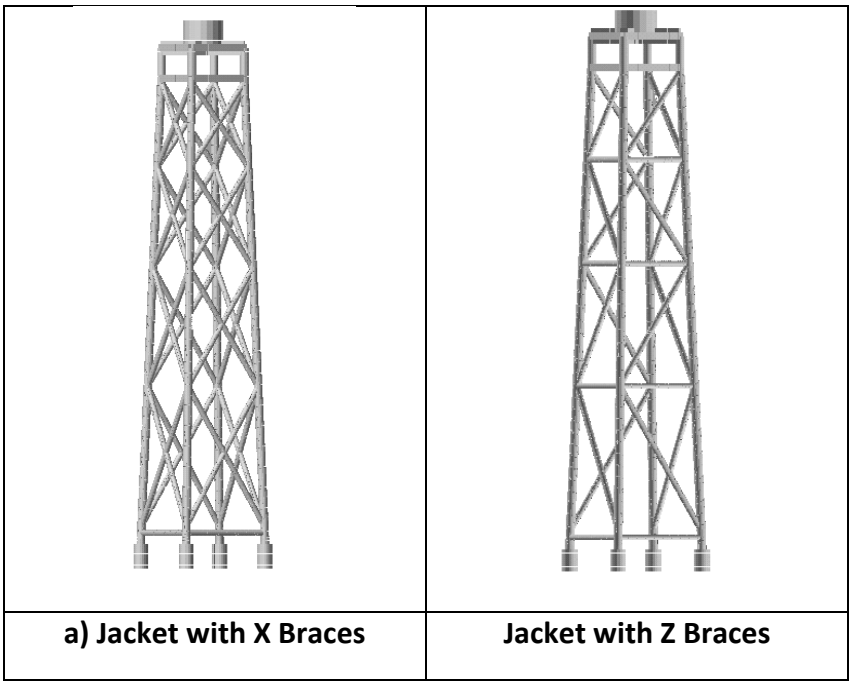

Figure 5-27. Set-up finite element model of the jacket structure: a) with X braces; b) with Z braces (see Figure 5-2 for dimensions)

The self-weight analysis, modal analysis and dynamic time-domain analysis are performed to evaluate the performance of each model under static, quasi-static and dynamic loads. Figure 5-28 shows results of the self-weight and modal analysis.

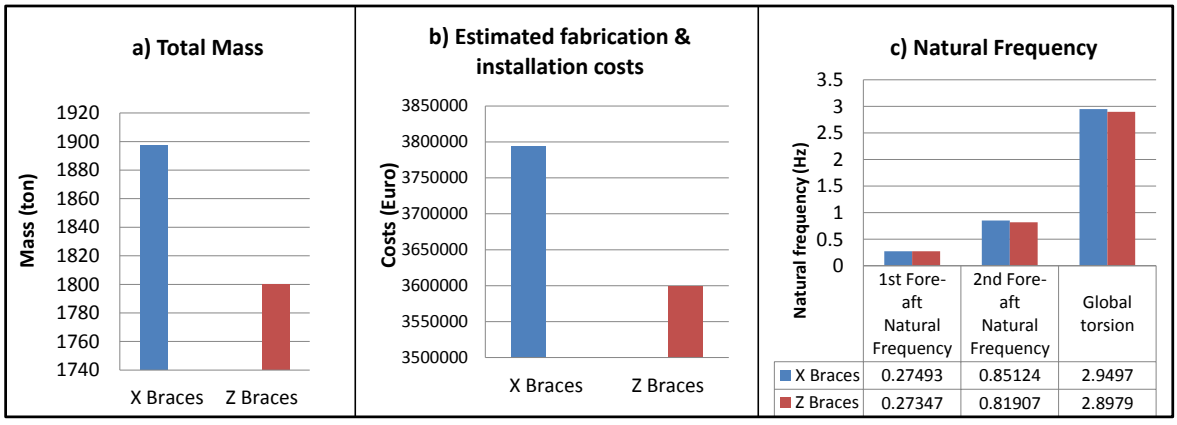

Figure 5-28. Performance of the jacket structure with X and Z braces t: a & b) self-weight analysis; c) modal analysis

As shown in Figure 5-28a & b, the total mass and consequently the total manufacturing costs of the structure with z braces is 10% smaller than the jacket with x braces. As can be seen in Figure 5-28c, the natural frequency of the structure with z braces is slightly lower than that of the structure with x braces. The reasons are: the mass of the structure with Z braces is lower than the structure with X braces (Figure 5-28a) and the diagonal X braces provide higher lateral stiffness to the structure. The 1st fore-aft natural frequency of the structure is mainly affected by the stiffness of the tower and turbine's mass which is constant in both FE models and as a result no significant discrepancy can be seen in the 1st mode shape. However, the 2nd and 3rd mode-shapes of the structure with Z braces are significantly smaller than the jacket with X braces.

Figure 5-29 shows comparatively snap shots taken from the time series of the deformation of the jacket structure with X and Z braces subject to the breaking wave LC-B2. The jacket structure with Z braces has asymmetric deformation under the weight of the turbine, transition piece and the structure (t=0). Immediately after the breaking and broken waves hit the front and rear faces of the jacket structure respectively at t=2.01 and t=2.66s, a large local deformation occurs in the braces at Elevation 2. This deformation is significantly smaller for the structure with X braces as the braces have lateral inhibition which reduces the effective length (l_e) of the member compared to Z braces.

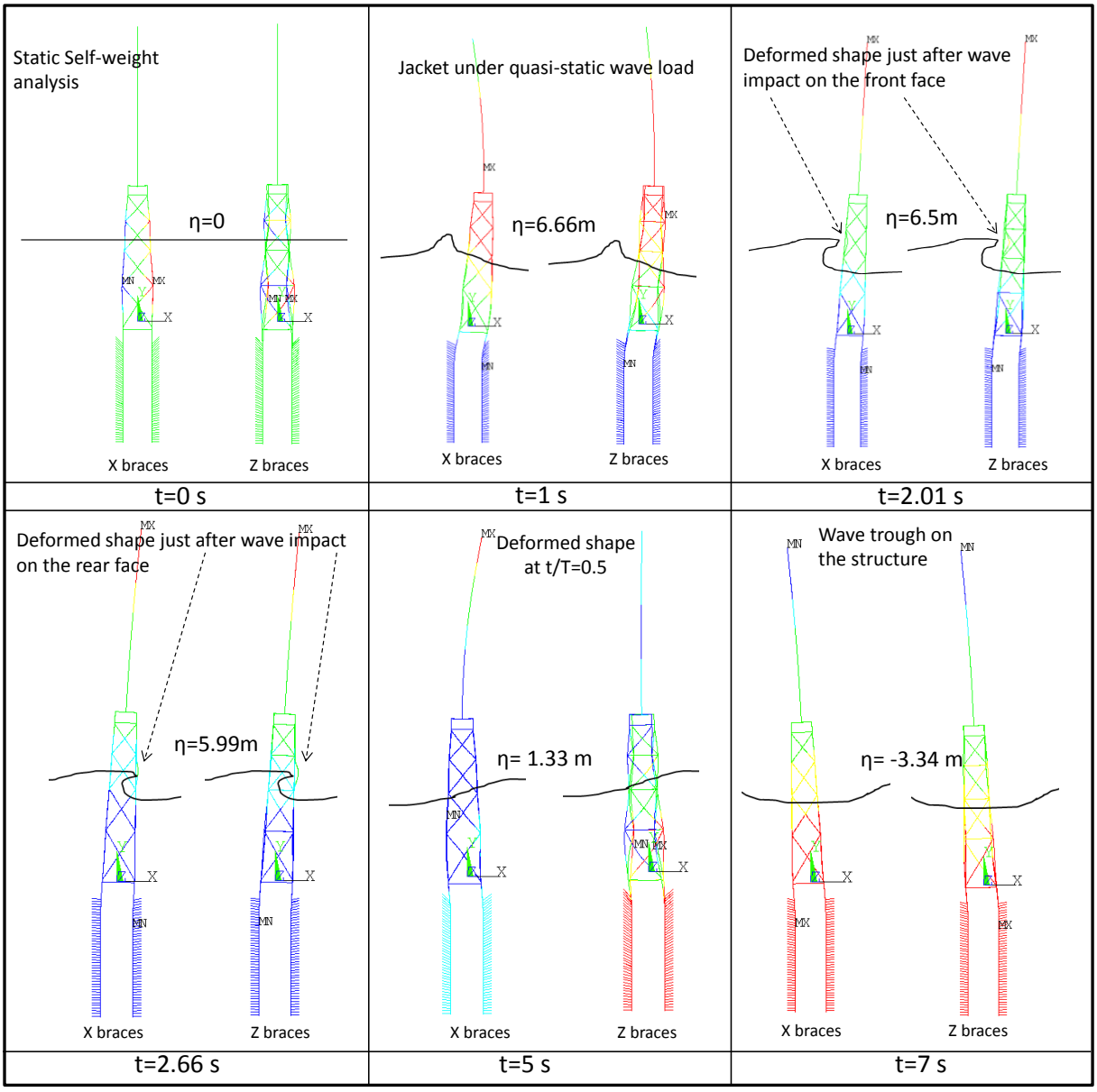

Figure 5-29. Deformed shape of the jacket structure with X and Z braces under different loads at different time steps

Figure 5-30 shows the torsion of the structure with X and Z braces. In general, when the eccentricity between the centres of mass and stiffness increases, torsion might occur. In order to restrict the probable torsion of the structure, the layout of the structure in plan and elevation must be designed carefully. The final objective of the design is to provide the structure with the greatest possible symmetry in terms of both stiffness and mass. As can be seen in Figure 5-30, modelling the jacket structure with Z braces reduces the symmetry of the structure and consequently, the eccentricity between the centres of mass and stiffness is increased. However, modelling the jacket structure with X braces provides a good distribution of the stiffness and mass and consequently enhances the rotational behaviour of the jacket structure (Figure 5-30).

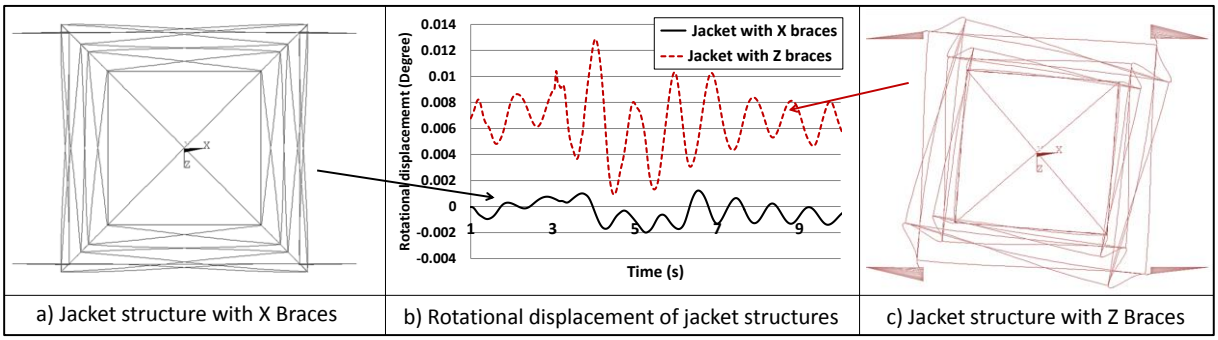

Figure 5-30. Rotational displacement of the jacket structure with X and Z braces

Figure 5-31 shows axial force in the side braces (SB4 & SB3) of the OC4 jacket structure considering X and Z braces. The axial force in braces of the jacket structure with Z braces is significantly higher than the structure with X braces (80%). The is due to the quantity of the braces withstanding the lateral forces caused by breaking waves which is double for the structure with X braces and therefore, lower forces are expected in each brace of the structure.

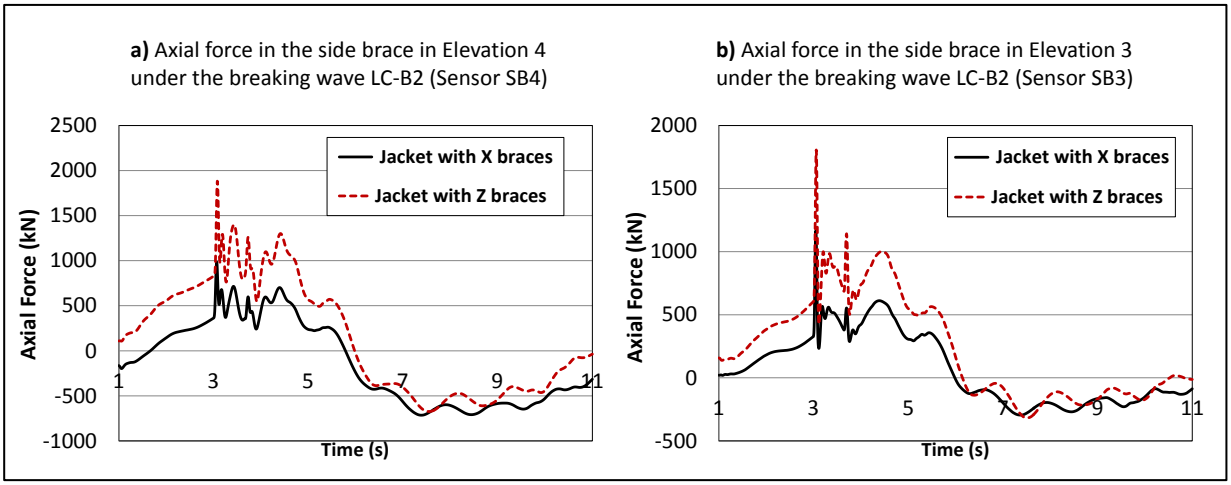

Figure 5-31. Axial force in side braces of the jacket structure with X & Z braces

In general, jacket structures with X braces are shown to perform better than those with Z braces because of the following reasons:

(i) The distribution of the stiffness around the mass of the structure is more symmetric which might reduce the torsion of the structure;

(ii) The axial and bending forces in the braces of the structure will be lower than the structure with Z braces;

(iii) The out-of-plane bending stiffness of X braces is higher than Z braces. Therefore, the local deformation of the braces is lower (Figure 5-29);

(iv) X braces have lateral inhibition and their bucking length is shorter than Z braces, implying that X braces are more resistant to buckling.

The numerical model of the OC4 jacket structure with pile foundation is applied to perform a systematic parameter study to identify the parameters affecting the dynamic response of jacket structures to breaking waves including: (i) *wave* parameters (ii) *pile and soil* parameters and (iii) *structure* parameters.

For *wave parameters*, the extreme loading case induced by breaking waves on jacket structures is identified LC2 and the applicability of different models to predict slamming force induced by breaking waves on jacket structures is assessed. It was revealed that the slamming force formulae initially developed for the impact force and duration on a single cylindrical pile cannot be used for jacket structures since they might underestimate the dynamic force response.

For *pile and soil parameters*, the accuracy of the current modelling techniques for pile foundation of jacket structures including the scour effects and linear and non-linear soil modelling is evaluated. It was shown that the pile foundation of jacket structures mainly behaves linearly and the slight non-linear effects in the pile foundation can be neglected. Moreover, scour will significantly affect the dynamic response of jacket structures (up to 25%) and therefore, should be considered in the design process.

For *structure parameters*, the relative structural parameters influencing the dynamic response as well as legs and braces diameters and geometry of the structure (jacket with X and Z braces) are analysed. The most appropriate geometry of the braces for jacket structures is identified X braces. The results of a parameter study with different member's diameters showed that decreasing the diameter of legs and braces might improve the dynamic response to hydrodynamic forces. However, this might increase the axial stresses in the legs of the structure due to the available static forces and consequently, it may reduce the resistance of the members to buckling.

It is expected that, the experience achieved from the conducted parameter study will be used to substantially improve the modelling techniques of jacket structures under breaking waves, and consequently to achieve a safer and more reliable design of jacket-type support structure of wind turbines or offshore platform under extreme loads induced by breaking waves, as well as by near-breaking and non-breaking waves

5.5 Summary of key results

Overall, his chapter study has contributed to substantially improve the understanding of the dynamic response of jacket structures with pile foundation to extreme load events induced by breaking waves, near-breaking and non-breaking waves. Important contributions are made with regards to the following research and development issues:

(i) Prediction formulae for quasi-static and impact forces caused by non-breaking to breaking waves on full-scale jacket structures;

(ii) Modelling and analysis of the effect of pile foundation on the dynamic response of jacket structures;

(iii) Performance of a systematic parameter study on a jacket structure with pile foundation to identify the parameters affecting the dynamic response, and accordingly the design optimization of the jacket structure under extreme wave loads;

(iv) Comparative analysis of different modelling approaches used in previous studies to calculate the dynamic response of jacket structures with pile foundation and identification of the most accurate and applicable approaches in order to improve the design.

For this purpose, a parameter study using a numerical model of a full-scale jacket structure called 'OC4 jacket' under non-breaking to breaking waves was performed. Overall, the results may be summarised as follows:

(i) The highest wave loads on the front face of the jacket structures is identified for load case 2 (LC-B2) in which the wave breaks (1.5~2.5)L_{Span} far in front of the structure. The highest wave load on the rear face however, is observed for load case 4 (LC-B4) in which the wave breaks within the structure. Moreover, the highest total force response TFR of the entire structure is also obtained for load case 2 (LC-B2), which might also result in the most extreme lateral forces on the pile foundation of jacket structures.

(ii) The slamming force formulae by Wienke (2005) and further similar formulae initially developed for the impact force and duration on a single cylindrical pile cannot be readily applied for jacket structures as they might underestimate significantly the dynamic force response DFR of the structure to breaking wave impact. The new slamming force formulae developed in this study predict much lower peaks of the slamming force than those predicted by other similar formulae, initially developed for a single pile. Nevertheless, the dynamic force response (DFR) of the structure using the new formulae is much higher (Figure 5-16), due to the much higher impact duration of breaking wave forces on jacket structures as predicted by the new formulae.

(iii) The deformation shape of the pile and the lateral displacement of the jacket structure are higher for the structure with clay foundation compared to the structure with sand foundation as the clay stiffness is significantly lower than sand stiffness. Moreover, the axial and bending forces in the braces of the jacket structure might increase when the soil foundation becomes less stiff, so that the displacements and deformations of the structure become higher (Figure 5-17 & Figure 5-18).

(iv) The non-linear behaviour of the soil under breaking waves in the upper soil layers for jacket support structures is less severe compared to mono-pile structures because jacket structures have significantly more restrained pile-head rotation and displacement. In general, except the top soil layer (first 2 meters) of the founda-

tion, the soil exhibits a linear behaviour even under the extreme wave loads induced by breaking waves (Figure 5-19).

(v) Scour might cause an increase of the natural frequency of jacket structures (up to 10%) and the lateral displacement of the structure (up to 25% at transition piece). This is due to the effect of scour on the bearing capacity of the soil and consequently the relative stiffness of soil and pile and to the reduction of the involved soil mass in the dynamic response of the system. Moreover, it also increases the height of the unbraced zone of the structure which decreases the bending stiffness of the structure.

(vi) It is crucial to account for the pile foundation in the modelling of the response to the entire structure, and thus in the design process of jacket structures. In fact, considering a rigid fixed-bottom jacket structure (as in the previous studies of the OC4 jacket structures) might overestimate the natural frequencies by up to 40%. Moreover, uncertainties in the pile-soil properties might significantly affect the natural frequency of the structure, thus highlighting the relevance of a good knowledge of these properties in the design process.

(vii) Decreasing the diameter of the legs and braces of the jacket structure might result in a decrease of the quasi-static and impact forces on the structure and concurrently in a decrease of the stiffness of the structure. Jacket structures benefit indeed from a braced structural system, which strictly restrains the lateral displacement by diagonal braces connected to the legs. Decreasing the diameter of the members may not significantly increase the horizontal displacements. However, 'buckling effect', which is very common in such a structural system, will be more probable. In general, decreasing the diameter of the members might result in much lower wave loads on the structure while it might also improve the dynamic response to hydrodynamic forces. However, this might negatively affects the structural integrity under static and self-weight forces.

(viii) Jacket structures with Z braces might reduce the fabrication and installation costs up to 10% as compared to structures with X braces. Nevertheless, the structural performance using X braces is significantly better due to the following reasons: the extreme forces in the braces of the structure are lower, the out of plane stiffness of the braces is higher, the brace resistance to buckling is higher and the occurrence probability of torsion in the structure is lower.

The parameter study performed in the present study and the unique large-scale experiments in the large wave flume (GWK) have significantly contributed (i) to improve the methods to calculate non-breaking and breaking wave induced loads on jacket structures and (ii) to enhance the modelling techniques of jacket structure to predict their dynamic response to breaking waves. Nevertheless, some uncertainties might be overcome in further studies in order to achieve safer and more reliable design of jacket structures under extreme wave loads. For instance, the approach implemented in the study for the prediction of the wave forces on jacket structures and the associated dynamic response neglect the interaction between the structural motions and the hydrodynamic force does not ac-

count for hydroelasic effects. ‘Hydro-elastic modelling” will allow the analysis to explicitly account for the mutual interaction between the hydrodynamic loading and the motions of the entire structure with its pile foundation. Although the recent application of such modelling approaches for monopile structure have revealed the importance of hydro-elasticity effects (i.e. Sagar et al, 2015 and; El Moctar & Ley, 2016) as addressed in Chapter 2, no study is yet available the implementation of hydro-elastic approaches for the calculation of wave loads on jacket structures.

6 Summary and outlook

Jacket support structures are among the most widely used offshore structures in wind energy and oil/gas industries. Wave-induced loading of such structures are among the most uncertain and challenging issues in the design of offshore jacket structures. Therefore, a proper estimation of the wave loading of the legs and braces of jacket structures is crucial for both safety and costs.

Unlike the case of slender pile under breaking waves, where a large number of diverse studies and formulae are available, together with the well-known Morison equation which is still widely applied for the calculation of non-breaking force, less attention have been paid to truss structures where the interactions between wave and closely spaced legs and braces is more obvious due to interference effects that may crucially affect the wave-induced flow around the structure members. In fact, no reliable wave load formula is yet available for the prediction of breaking wave-induced forces on the legs and braces of a jacket structure. Moreover, to the author's knowledge, no methodology or/and formulae yet exist to calculate the total wave load on the entire jacket structure.

The main objective of this PhD study was therefore (i) to develop new reliable formulae for the prediction of breaking wave induced loads on legs and braces of jacket structures; (ii) to develop a methodology and formulae for the prediction of total loads induced on an entire jacket structure by breaking, near-breaking and non-breaking waves (ii) to investigate the effect of the most relevant influencing wave parameters, soil parameters and structural parameters on the dynamic response of jacket structures subject to breaking wave loads.

Therefore, the key contributions of this thesis may be summarised as follows: (i) the generation of a knowledge base for an improved understanding of the processes involved in the interaction of waves and jacket structures for a broad range of wave conditions including breaking, near-breaking and non-breaking waves and (ii) the development of physically-based and thus more generic wave load formulae for the prediction of wave loads on the structure legs and braces as well as on the entire jacket structure as a function of the most significant wave and structural parameters. This was achieved by means of the following four major steps:

First, a comprehensive review and analysis of the current knowledge on breaking and non-breaking wave loads on jacket structure and their dynamic response with pile foundation was conducted. As a result the missing knowledge required to achieve the objectives of the PhD study were identified.

Second, the available large-scale tests carried out in the Large Wave Flume (GWK) on a jacket structure under breaking waves were analysed. Different types of incident breaking waves on the GWK truss structure were examined and classified by considering the distance of the incipient wave breaking location from the structure. Two Matlab codes were developed to recover the actual slamming forces on the front face of the GWK truss from the measured Total Force Response (TFR) using: (i) Duhamel's integral method (ii) Frequency Response Function FRF method. Both codes were validated against the experimental data and were ap-

plied to analyse the slamming forces on the front face, the side braces and the rear face of the GWK truss structure. Finally, new formulae for the prediction of wave slamming force and duration on the front face, side braces and rear face of jacket structures were developed considering the physical process involved in the interaction of breaking waves with different members of the jacket structure

Third, a numerical CFD model (in OpenFOAM) for waves and the new slamming formulae were applied to develop a methodology for the calculation of total forces induced by breaking, near-breaking and non-breaking waves on the entire jacket structure. Total wave forces on the entire GWK truss structure were calculated through superposition of (i) quasi-static force component obtained by means of the Morison equation using the parameters of the wave-induced flow obtained from the CFD model and (ii) the slamming force component calculated using the new prediction formulae proposed in chapter 3. The computed total wave forces were validated against the measured forces on the structure from the laboratory tests in GWK. Afterwards, the CFD model was applied to (i) reproduce the selected tests of the GWK tests; (ii) extend the hydrodynamic and structural conditions tested in the GWK, particularly for the CFD generation of further data for breaking wave induced loads on the rear face of the GWK truss which is missing in the physical model tests and (iii) specify more precisely and systematically the most relevant influencing wave and structural parameters on the wave loading of jacket structures.

Fourth, the methodological applied developed in Chapter 4 was applied on a full scale jacket structure called 'OC4 jacket'. The CSD model of the OC4 jacket structure with pile foundation was set up in ANSYS and the CFD model of non-breaking and breaking waves on the structure were simulated in OpenFOAM. The performance of both CFD and CSD models were examined by comparing the results with the results of other numerical models developed for the OC4 jacket. The plausible CSD model of the OC4 jacket structure with pile foundation is then applied to perform a systematic parameter study to identify the parameters related to waves, pile foundation and structure affecting the dynamic response.

Overall, the new slamming formulae for breaking waves on jacket structure and the developed methodology for the calculation of total forces induced by breaking, near-breaking and non-breaking waves on jacket structures are expected to be widely applied as prediction tools for wave loads on truss-type structures.

In the following sections, an attempt is made to summarise the key results of this study and to derive the priority tasks for further research.

6.1 Summary of key results

Re-analysis of the experiments previously performed in the large wave flume GWK

The large scale laboratory tests on a jacket structure under breaking and non-breaking waves performed in a previous study to improve the knowledge associated with wave-jacket structure interaction were re-analysed using (i) low filter analysis; (ii) Duhamel's integral method

and (ii) Frequency Response Function method. The key results may be summarised as follows:

(i) As expected, the response of the truss structure was not only affected by a breaking wave on the front face of the structure, but also by a broken wave on the rear face. This was obvious from the measured Total Force Response (TFR) of the GWK truss in which two distinct peaks were observed. The wave slamming force on the rear and front faces of jacket structures is significantly affected by the distance from the incipient wave breaking location to the structure.

(ii) The classification of the wave breakers was conducted in five load cases by considering the distance of the incipient wave breaking location to the structure front. The analysis of each load case revealed that the maximum measured slamming force on the front face of the GWK truss structure occurs for load case 2 where the wave breaks just in front of the structure and not far from the structure.

(iii) The calculated slamming force function for breaking waves on the front face of jacket structures based on the theoretical slamming models initially developed for mono-pile structures differs significantly from the slamming force function obtained by the analysis of the GWK tests of the truss structure. Therefore, the slamming models by Wienke and Oumeraci (2005), Goda (1966) and further similar formulae developed for the impact force and duration on single cylindrical piles cannot be readily applied for jacket structures.

New slamming formulae for breaking waves on jacket structures, applications and limitations

The implementation of the developed codes based on the Duhamel's integral and Frequency Response Function methods on the GWK experiments by considering the physical processes involved in the interaction of breaking waves with different members of the jacket structure resulted in a new set of wave slamming formulae for the prediction of slamming forces induced by breaking waves on the front face and rear face of jacket structures. These new formulae are summarized in Figure 6-1.

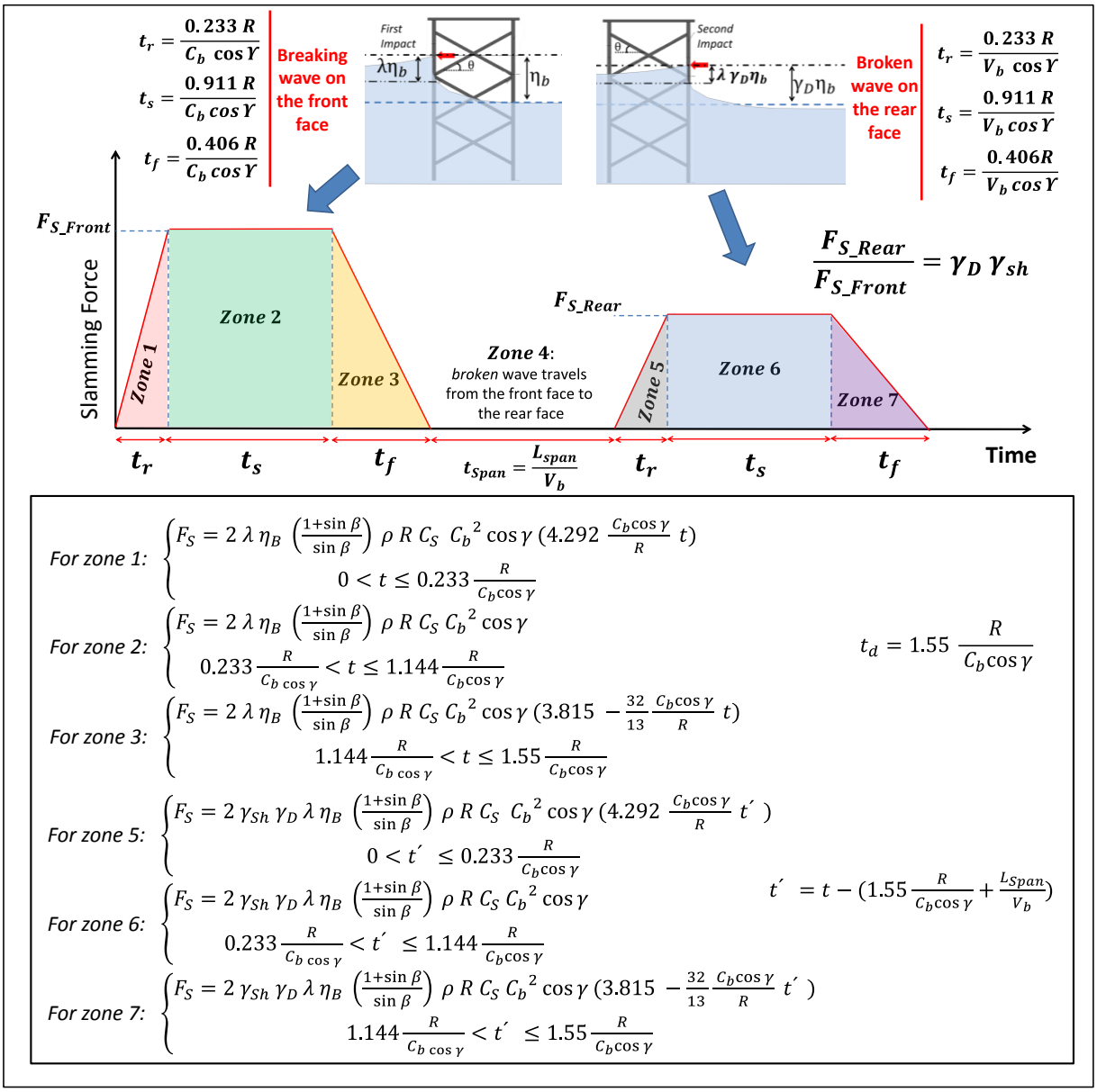

Figure 6-1. Overview of the new slamming formulae developed for breaking waves on truss structures

The concluding remarks drawn from the new slamming formulae are summarized as follows:

(iv) Considering the very small magnitude of the slamming forces on the side braces of the truss structure as compared to those on the front face (<10%) and in order to come up with simpler prediction formulae for slamming force on truss-type structures, the impact force on the side braces are neglected. Therefore, the wave slamming formulae for breaking waves on the entire truss structure were developed by considering only the wave impact forces on the front and rear faces.

(v) The new slamming model and formulae for breaking waves on the front and rear faces of jacket structures are relatively simple, compact, transparent and physically-based; they allows us to systematically predict the wave slamming forces depending on the dis-

tance between the incipient wave breaking location and the structure front, the characteristics of the incident wave and the geometry of the structure.

(vi) The high accuracy of the new formulae in predicting the wave slamming force and duration is examined by comparing the amplitude, signal-correlation and spectrum correlation of the measured DFR with those DFR induced by the slamming force function obtained from the proposed formulae.

(vii) The new slamming model is valid for jacket structures subject to depth-induced wave breaking on a sloped bottom (i.e plunging breaker) for the hydrodynamic conditions tested in the large wave flume GWK as described in Section 3.1, but may also be applied for wave breaking in larger water depths due to wave-wave interaction (i.e focused waves).

New methodology for prediction of total wave forces on jacket structures, applications and limitations

A new relatively simple and computationally less demanding approach is proposed to calculate the wave forces induced by non-breaking, near breaking and breaking waves on legs and braces of jacket structure as well as on the entire structure and to predict the associated dynamic response of the jacket structure by employing CFD modeling (in OpenFOAM) for the incident waves and CSD modelling (in ANSYS)for jacket structure as follows:

(i) The *quasi-static force component* is calculated using the Morison formula considering the velocity and acceleration obtained from the validated CFD model.

(ii) The *slamming force component* is predicted by applying the proposed wave slamming formulae in Chapter 3.

(iii) The total wave force induced by breaking waves on the entire structure is calculated by superposing the *quasi-static force component* and *slamming force component*

This approach was used to reproduce selected GWK tests and to generate more numerical data related to the wave loading of the front face, the side braces and the rear face of GWK truss structure. Application of the aforementioned approach leads to the following main conclusions:

(i) As expected, non-breaking waves may induce only quasi-static forces on jacket structures; therefore, the Morison can be applied for the prediction of non-breaking wave induced forces on the legs and braces of the jacket structure.

(ii) The total forces induced by near-breaking waves on jacket structures cannot be accurately predicted by the Morison equation. A tentative analysis of the GWK tests considering the affecting parameters of wave steepness H/L, breaker index H/h, and wave number k, revealed that the Morison formula underestimates the total forces up to 35 % and therefore, should not be applied to predict the total forces by near-breaking waves with the following non-linearity parameters waves $H/L > 0.059$ & $H/h > 0.53$.

(iii) Superposition of quasi-static force component by Morison equation and the slamming force component by the new developed wave slamming model, for the prediction of breaking wave-induced forces on the entire jacket structure, provided a high accuracy for total forces on the front face (less than 10% for peak-to-peak comparison) and a moderate accuracy for the total forces on the rear face of the structure (up to 25% for peak-to-peak comparison). In fact, even the advanced CFD model used in this study (OpenFOAM) is not capable to predict entirely the highly complicated shape of the wave front and the kinematics of the water particles associated with breaking and broken waves at and inside such highly complex structures.

(iv) The methodology used in this study neglects the interaction between the motions of the structure (assumed as rigid) and the hydrodynamic forces on the structure. In fact, the proposed approach can be used when the lateral displacement of the structure is relatively small. The threshold of the displacement beyond which the proposed methodology cannot be applied should be determined in further research studies.

Dynamic response of jacket structures to wave forces induced by breaking waves

The methodology and models developed in the present PhD study were applied on a full-scale jacket structure called 'OC4 jacket' to calculate the dynamic response of the structure. The results were compared to those obtained from other numerical models developed for the same jacket without pile foundation. The model for the dynamic response was then extended to consider pile foundation with appropriate clay and sand soil models. Using the extended model, a systematic parameter study of the dynamic response of the jacket structure to breaking waves was performed to identify the parameters of the incident *waves*, *pile foundation* and *structure* affecting the dynamic response. The key outcomes might be summarised as follows:

(i) *Breaking waves on jacket structures*: Breaking waves load cases 2 and load case 4 induce the highest wave loads on the front and rear faces of jacket structures, respectively. In order to design jacket structures under these forces, the theoretical slamming force formulae initially developed for the impact force and duration on a single cylindrical pile (e.g. Wienke & Oumeraci, 2005) cannot be readily applied for jacket structures since they might underestimate (up to 50%) the dynamic force response DFR of the structure to breaking wave loads. The new slamming force formulae developed in this study predict much lower peaks and much higher durations of the slamming force than those predicted by the formulae, initially developed for a single pile. Nevertheless, the dynamic force response (DFR) of the structure using the new formulae is much higher, due to the much higher impact duration of breaking wave forces on jacket structures as predicted by the new formulae.

(ii) *Pile foundation of jacket structures*: Pile foundation model significantly affects the dynamic performance of the entire jacket structure (40% for natural frequency),

and thus has to be considered in the design process of jacket structures. In general, the lower soil stiffness in the foundation, the higher are the displacements and deformations of the structure and consequently, the higher are the forces in the members of the jacket structure. Scour effect should be considered in the design of jacket structures as it might reduce the foundation bearing capacity and might increase the failure probability in terms of both serviceability and ultimate limit state. Moreover, scour may change the eigen-frequency of the entire jacket structure (up to 10%) embedded in the soil and as a result, affect the dynamic response. The investigations revealed that, the soil non-linear behaviour in the foundation of jacket structures is less severe as they have restrained pile-head rotation and displacement. In this study, even under the extreme wave forces induced by breaking waves the soil exhibited a linear behaviour.

(iii) *Structural model of jackets:* Comparative analysis of the dynamic response of jacket structures with X & Z Braces to breaking waves showed that, although considering jackets with Z braces may reduce the costs moderately (up to 10%), the structural performance of jackets with X braces is significantly better. It was found that decreasing the diameter of the legs and braces of jacket structures may result in lower quasi-static and slamming forces induced by breaking waves on the structure and therefore, may improve the dynamic response to hydrodynamic forces. Nevertheless, this might negatively affect the behaviour of the structure under static (e.g. self-weight) forces.

6.2 Limitations of the results and implications for further research

Although this PhD research contributed to substantially enhance the understanding of wave-jacket structure-pile foundation interaction which has led to the development of new more generic formulae for the prediction of wave slamming forces on legs and braces as well as on the entire jacket structure, considerable limitations of the results and uncertainties still remain which must be overcome in order to achieve a safer and more economic design of jacket support structure of wind turbines. Based on the knowledge gained from this PhD study, the following recommendations for further research may be drawn:

(i) So far, there are no reliable formulae for the prediction of the characteristics of the incident breaking, broken and post-breaking waves (i.e. water surface elevation and wave kinematics). Moreover, the application of available methods (e.g. Hilbert frequency, physical observation of the breaker tongue) for the identification of the incipient wave breaking location, which might significantly affect the resulting breaking force on the structure, is questionable.

(ii) The applicability and validity range of the Morison formula for jacket structures become questionable with increasing the lateral displacement of the structure. The threshold values of structure displacements considering the environmental condition at the structure should be identified, beyond which the application of the Morison formula may result in an underestimation/overestimation of the force induced

by non-linear and breaking waves. For this purpose, a systematic parameter study using fully coupled CFD and CSD models is recommended.

(iii) The available approaches for the prediction of the wave forces on jacket structures and the associated dynamic response neglect the interaction between structure motions and hydrodynamic forces. The hydro-elastic design practice incorporates this complex iteration and considers the mutual effects of hydrodynamic forces and the structure motions. The application of hydro-elastic approaches have not been considered so far for the wave loading of jacket structures, although the previous studies have highlighted the importance of these effects for monopile structures. Furthermore, the available wave slamming models including the models developed for single piles (e.g. Wienke & Oumeraci, 2005; Goda, 1966) and the new slamming model proposed in this study are developed with the assumption that the structure is rigid. Consideration of moveable/flexible slender piles for the structure might affect the process involved in the interaction of breaking wave and slender piles (e.g. pile-up process) and may consequently change the impact duration and forces on the structure. So far, no slamming model is proposed to predict the breaking wave induced impact duration and force on moveable/deformable slender cylinders.

(iv) The members of jacket structures are relatively closely spaced thus the wave load on a single slender member might be significantly affected by the neighbouring members. The effect of neighbouring members on the wave loading of a single member of the jacket structure can be investigated. For this purpose, the results from Bonakdar (2014) might be used as starting base. As it is not feasible economically and practically to deploy a myriad of measuring devices (e.g. pressure or force transducers) on legs and braces of a jacket structure to experimentally investigate the effect of neighbouring members, a well-validated CFD model might be used for the investigation of these interference effects.

(v) Further research is required to obtain the actual force history of breaking/broken waves on the side faces of jacket structures. This is also particularly important for oblique wave directions to the front face.

References

Aashamar, M., 2012. Wave slamming forces on truss support structures for wind turbines. Master thesis, Norwegian University of Science and Technology (NTNU), Department of Civil and Transport Engineering.

American Bureau of Shipping (ABS), 2010. Guide for Building and Classing Offshore Wind Turbine Installations.

American Bureau of Shipping (ABS), 2011. Design standards for offshore wind farms.

American Petroleum Institute (API), 2005. 2A–WSD Recommended practice for planning, designing and constructing fixed offshore platforms–Working stress design. In Twenty first.

American Petroleum Institute (API), 2007. API Bulletin 2INT-MET, Interim Guidance on Hurricane Conditions in the Gulf of Mexico.

Apelt, C. J., Piorewicz, J., 1986. Interference Effects on Breaking Wave Forces on Rows of Vertical Cylinders. Proceeding of 1st Australasian Port, Harbour and Offshore Engineering Conference, Sydney, Australia.

Armand, J.L., Cointe R., 1986. Hydrodynamic Impact Analysis of a Cylinder. The 5th Offshore Mechanics and Arctic Engineering (OMAE) Conference, Tokyo, Japan.

Arnsten, Ø., Gudmestad, O., 2013. Wave slam forces on truss structures in shallow water. Data Storage Report, Norwegian University of Science and Technology & University of Stavanger, Norway.

Azau, S. and Casey, Z., 2011. Wind in Our Sails—The Coming of Europe's Offshore Wind Energy Industry, Report by the European Wind Energy Association (EWEA).

Barahona, B., Jonkman, J. M., Damiani, R., Robertson, A., and Hayman, G., 2015. Verification of the new FAST v8 Capabilities for the Modeling of Fixed-Bottom Offshore Wind Turbines. In 33rd Wind Energy Symposium (p. 1205).

Barltrop, N. D., Adams, A. J., and Hallam, M. G., 1991. Dynamics of fixed marine structures (Vol. 8). Oxford: Butterworth-Heinemann.

Bonakdar, L., 2014. Pile group effect on the wave loading of a slender pile. PhD thesis, Technische Universität Braunschweig, Germany (ISBN 978-3-86948-383-2).

Burmester, S., de Ridder, E. J., Wehmeyer, C., Asp, E., Gujer, P. 2017. Comparing different approaches for calculating wave impacts on a monopile turbine foundation. Proc 36th OMAE 2017 V010T09A063.

Campbell, I., Weynberg, P. A., 1980. Measurement of Parameters Affecting Slamming. Technology Reports 440, Southampton University, Wolfson Unit for Marine Technology.

Chakrabarti, S. K., 1980. In-line forces on fixed vertical cylinders in waves. Journal of Waterways, Port, Coastal and Ocean Div., ASCE, 106, 145-155.

Chella, M., 2012. An overview of wave impact forces on offshore wind turbine structures. Energy Procedia. 20, 217 – 226.

Choi,S.J., Lee,K.H., Gudmestad O.T., 2013. The effect of dynamic amplification due to a structure's vibration on breaking wave impact. Ocean Engineering Journal. 96, 8-20.

Choi, S. J., 2014. Breaking wave impact forces on an offshore structure (Doctoral dissertation, PhD thesis (UiS No. 231), University of Stavanger, Norway, at the Department of Mechanical and Structural Engineering and Material Science).

Chopra, A, K., 1981. Dynamics of Structures, A Primer, Earthquake Engineering Research institute, Berkeley, CA.

Cordle, A., Kaufer, D., Vorpahl, F., Fischer, T., Sørensen, J., Schmidt, B., Matha, D., Lucas, J., McCowen, D., Pereira, R., and Argyriadis, K., 2011. Final report for WP4.3: Enhancement of design methods and standards, Deliverable D4.3.6, (WP4: Offshore Foundations and Support Structures).

Corte, C., and Grilli, S. T., 2006. Numerical modeling of extreme wave slamming on cylindrical offshore support structures. In The Sixteenth International Offshore and Polar Engineering Conference. International Society of Offshore and Polar Engineers.

Det Norske Veritas (DNV), 2010. DNV-RP-C205: Environmental conditions and environmental loads.

Det Norske Veritas (DNV), 2013. OS-J101: Design of Offshore Wind Turbine Structures.

Damiani, R., Song, H., Robertson, A., and Jonkman, J., 2013. Assessing the Importance of Nonlinear Structural Characteristics in the Development of a Jacket Model for the Wind Turbine CAE Tool FAST". In 32nd International Conference on Ocean, Offshore and Arctic Engineering (OMAE2013). pp. 9-14.

El Moctar, O. Ley, J., 2016. Computational Fluid and Structure Dynamics Methods to Assess Wave-induced Loads and Hydroelasticity Effects. Book Chapter in Maritime Technology and Engineering III, ISBN 9781138030008.

El Safti, H., Bonakdar, L., Oumeraci, H., 2014. A Hybrid 2D-3D CFD Model System for Offshore Pile Groups Subject to Wave Loading. 33rd International Conference on Ocean, Offshore and Arctic Engineering (OMAE), San Francisco, USA.

Faseela, A., Jayalekshmi, R., 2015. In-Place Strength Evaluation of Jacket Platforms and Optimization of Bracing Configurations. International Journal of Research in Advent Technology (E-ISSN: 2321-9637) Special Issue.

Fenech, L., Sant, T., Muscat, M., 2011. Design and cost evaluation of a deep water support structure for a wind turbine in central mediterranean waters. In Proceedings of the European Wind Energy Conference, Brussels, Belgium.

Fevåg, L. S., 2012. Influence of marine growth on support structure design for offshore wind turbines, Master Thesis, Norwegian University of Science and Technology, Norway.

Føreland. S., Rastad. M. O., Aas-Jakobsen. K., 2012. A parametric study on fixed-bottom wind turbines in the North Sea, Nordic steel construction conference.

Fuchs, V., Gundlach, J., and Wünsch, O., 2013. Simulation of multiregional wave-structure impact on damping elements on offshore structures. Journal of Marine Science and Technology, 18(3), 276-293.

Ghaderi, P., Dick, A. J., Foley, J. R., Falbo, G., 2012. Spectral Domain Force Identification of Impulsive Loading in Beam Structures. In Topics in Nonlinear Dynamics. Springer New York. 3, 157-165.

Gazetas, G., 1991. Foundation Vibrations, Foundation Engineering Handbook, 2nd Edition, Vas Nostrand Reinhold, Edited by Hsai-Yang Fang.

Germanischer Lloyd (GL), 2005. Guideline for the Certification of Offshore Wind Turbines.

Goda, Y., Haranaka, S., Kitahata, M., 1966. Study on impulsive breaking wave forces on piles. Report Port and Harbour Technical Research Institute, 6, 1-30.

Grabe, J., Mahutka, K. P., and Dührkop, J., 2005. Monopilegründungen von Offshore Windenergieanlagen–Zum Ansatz der Bettung. Bautechnik, 82(1), 1-10.

Grilli, S. T., Svendsen, I. A, and Subramanya, R. 1997. Breaking criterion and characteristics for solitary waves on slopes. Journal of Waterway, Port, Coastal and Ocean Engineering. 132(3), 102-112.

Gustavo E. Pacheco-Crosetti, 2007. Dynamic Lateral Response of Single Piles Considering Soil Inertia Contribution. A thesis submitted for the degree of Doctor Of Philosophy In Civil Engineering University Of Puerto Rico Mayagüez Campus, May 2007.

Haselbach, P., Natarajan, A., Jiwinangun, R. G., and Branner, K., 2013. Comparison of coupled and uncoupled load simulations on a jacket support structure. Energy Procedia, 35, 244-252.

Hazzar, L., Hussien, M. N., and Karray, M., 2016. Influence of vertical loads on lateral response of pile foundations in sands and clays. Journal of Rock Mechanics and Geotechnical Engineering.

HBM, 2001. Force transducer S9M, Hottinger Baldwin Messtechnik GmbH, Darmstadt, Germany.

Henderson, A. R., and Zaaijer, M. B., 2008. Hydrodynamic loading on offshore wind turbine support structures. Engineering integrity, 25, 24-31.

Hensel, J., Sharma, R. M. S., Baxter, C. D. P., and Hu, S.-L. J., 2012. Development of a Technical Type Factor for Jacket Structures for Offshore Wind Turbines in Rhode Island, Journal of Renewable and Sustainable Energy 4, Vol. 4, No. 6.

Hildebrandt, A., and Schlurmann, T., 2012. Breaking wave kinematics, local pressures, and forces on a tripod structure. Coastal Engineering Proceedings, 1(33), 71.

Hildebrandt, A., Sriram, V., Schlurmann, T., 2013. Simulation of Focusing Waves and Local Line Forces due to Wave Impacts on a Tripod Structure, Proceedings of the Twenty-third International Offshore and Polar Engineering Conference (ISOPE), ISBN 978-1-880653-99-9, ISSN 1098-6189, Anchorage, USA.

Higgins, P., and Foley, A., 2014. The evolution of offshore wind power in the United Kingdom. Renewable and sustainable energy reviews, 37, 599-612.

Horn, J. T. H., Krokstad, J. R., and Amdahl, J., 2016. Hydro-Elastic Contributions to Fatigue Damage on a Large Monopile. Energy Procedia, 94, 102-114.

International Electrotechnical Commission, 2009. IEC 61400-3. Ed.1: Wind Turbines—Part 3: Design Requirements for Offshore Wind Turbines.

International Organization for Standardization (ISO), 2007. ISO 19902: Petroleum and natural gas industries - Fixed Steel Offshore Structures. Geneva, Switzerland.

International Organization for Standardization (ISO), 2010. ISO 21650: Actions from Waves and Currents on Coastal Structures. Geneva, Switzerland.

Irschik, K., Sparboom, U., Oumeraci, H., 2004. Breaking Wave Loads on a Slender Pile in Shallow Water. Coastal engineering conference. ASCE American society of civil engineering. 29, 568.

Issa, R., 1986. Solution of the implicitly discretized fluid-flow equations by operator splitting. Journal of Computational Physics, 62, 40-65.

Kaufer, D., Fischer, T., Vorpahl, F., Popko, W., and Kühn, M., 2010. Different Approaches to Modelling Jacket Support Structures and Their Impact on Overall Wind Turbine Dynamics. Deutsche Windenergie-Konferenz (DEWEK). Endowed Chair of Wind Energy at the Institute of Aircraft Design Universität Stuttgart.

Khansari, A. and Oumeraci, H., 2015a. Wave Slamming Forces on Legs and Braces of Truss Structures, Progress Report 2, Leichtweiß Institute for Hydraulic Engineering and Water Resources, Braunschweig, Germany.

Khansari, A. and Oumeraci, H., 2015b. Calculation of Breaking and Non-breaking Wave Loads on Truss Structures, Progress Report 3, Leichtweiß Institute for Hydraulic Engineering and Water Resources, Braunschweig, Germany.

Khansari, A. and Oumeraci, H. 2016a. Dynamic Response of OC4 Jacket Structure to Breaking and Non-breaking Wave Loads- Progress Report 4_Part 1: Without the effect of pile foundation, Leichtweiß Institute for Hydraulic Engineering and Water Resources, Braunschweig, Germany.

Khansari, A. and Oumeraci, H. 2016b. PR4: Dynamic Response of OC4 Jacket Structure to Breaking and Non-breaking Wave Loads- Progress Report 4_Part 2: With the effect of pile foundation- Parameter and comparative studies, Leichtweiß Institute for Hydraulic Engineering and Water Resources, Braunschweig, Germany.

Khansari, A. and Oumeraci, H., 2017. Dynamic response of jacket structure to breaking and non-breaking wave loads, Progress Report 1: State of the Art Report, Leichtweiß Institute for Hydraulic Engineering and Water Resources, Braunschweig, Germany.

Kunho Kim, Tzu-Wei Lo and Qing Y., 2013. A Dynamic Analysis Method for an Offshore Wind Turbine with a Jacket Support Structure. SNAME Offshore Symposium.

Larsen, T. J., Kim, T., 2011. Comparison of wave kinematics models for an offshore wind turbine mounted on a jacket substructure. EWEA offshore.

Lin, Y. H., Chen, J. F., and Lu, P. Y., 2017. A CFD model for simulating wave run-ups and wave loads in case of different wind turbine foundations influenced by nonlinear waves. Ocean Engineering, 129, 428-440.

Lombardi, D., Bhattacharya, S., and Muir Wood, D., 2013. Dynamic soil–structure interaction of monopile supported wind turbines in cohesive soil. Soil Dynamics and Earthquake Engineering, 49, 165-180.

Jonkman, J., Butterfield, S., Musial, W., and Scott, G. 2009. Definition of a 5-MW Reference Wind Turbine for Offshore System Development. Technical Report NREL / TP-500-38060, National Renewable Energy Laboratory, Golden,CO.

Jonkman, J., Popko, W., Vorpahl, F., Zuga, A., Kohlmeier, M., Larsen, T. J., ... and Nichols, J., 2012. Offshore Code Comparison Collaboration Continuation (OC4), Phase I–Results of Coupled Simulations of an Offshore Wind Turbine with Jacket Support Structure.

Jose, J., and Choi, S. J., 2017. Estimation of slamming coefficients on local members of offshore wind turbine foundation (jacket type) under plunging breaker. International Journal of Naval Architecture and Ocean Engineering.

Jose, J., Podrazka, O., 2014. Progress report: Experimental analysis of slamming load for truss structures within the framework of WaveSlam project, University of Stavanger ,Norway.

Jose, N. M., and Mathai, A., 2016. A Study on Lateral Deformation of Monopile of Offshore Wind Turbine due to Environmental Loads. Procedia Technology, 24, 287-294.

Leschka, S., Oumeraci, H. and Larsen, O., 2014. Hydrodynamic Forces on a Group of Three Emerged Cylinders by Solitary Waves and Bores: Effect of Cylinder Arrangements and Distances. Journal of Earthquake and Tsunami, 8 (3), 144005, 1-36.

Li, C.W., Lin, P., 2001. A numerical study of three-dimensional wave interaction with a square cylinder. Ocean Engineering, 28, 1545–1555.

Lin, P., Li, C.W., 2003. Wave–current interaction with a vertical square cylinder. Ocean Engineering, 30, 855-876.

Määttanen, M., 1981. Laboratory tests for dynamic ice-structure interaction. Engineering Structures, 3(2), 111-116.

Matlock, H., 1970. Correlations for design of laterally loaded piles in soft clay. Offshore Technology in Civil Engineering's Hall of Fame Papers from the Early Years, 77-94.

Mindao, G., Lihua, H., Shaoshu, S., 1987. Experimental study for the wave forces on pile groups due to regular waves, Proc. 2nd International Conference on Coastal and Port Engineering in Developing Countries (COPEDEC), China Ocean Press, Beijing, pp. 1956 – 1965.

Modarresi, M., Rasouli, H., Ghalesari, A. T., and Baziar, M. H., 2016. Experimental and Numerical Study of Pile-to-Pile Interaction Factor in Sandy Soil. Procedia Engineering, 161, 1030-1036.

Moll, H., Vorpahl, F., and Busmann, H. G., 2010. Dynamics of support structures for offshore wind turbines in fully-coupled simulations-influence of water added mass on jacket mode shapes, natural frequencies and loads". In European Wind Energy Conference (EWEC). Fraunhofer Institute for Wind Energy and Energy Systems Technology IWES.

Morgan, G. C. J., Zang, J., 2010. Using the rasInterFoam CFD model for non-linear wave interaction with a cylinder. In the proceeding of the 20th International Offshore and Polar Engineering Conference (ISOPE), Beijing, China.

Morison, J. R., O'Brien, M. P., Johnson, J. W., Schaaf, S. A., 1950. The force exerted by surface waves on piles. Petroleum Transactions, AIME, 2(05), 149-154.

Muskulus, M., and Schafhirt, S., 2014. Design Optimization of Wind Turbine Support Structures—A Review, J Ocean Wind Energy, ISOPE, 1(1), 12–22.

National Iranian oil company (NIOC), 2009, SP17 WHP- Jacket inplace static analysis and foundations design calculation.

National Iranian oil company (NIOC), 2011, SPD 22 WHP- Jacket inplace static analysis and foundations design calculation.

Navaratnam, C., Tørum, A., Arntsen, Ø., 2013. Progress Report: Preliminary analysis of wave slamming force response data from tests on a truss structure in large wave flume, Hannover, Germany,. Department of Civil and Transport Engineering, NTNU, Trondheim, Norway.

Navaratnam, C., 2013. Wave slamming loads on truss structures for wind turbines. Master thesis, Norwegian University of Science and Technology (NTNU), Department of Civil and Transport Engineering.

Nygaard, T. A., De Vaal, J., Pierella, F., Oggiano, L., and Stenbro, R., 2016. Development, Verification and Validation of 3DFloat; Aero-Servo-Hydro-Elastic Computations of Offshore Structures. Energy Procedia, 94, 425-433.

Obhrai, C., 2014. Experimental Analysis of Slamming Loads for Truss Structures WaveSlam Project, Technical Lecture. University of Stavanger, Norway.

O'Neill, M.W. and Murchinson, J. M., 1983. An Evaluation of p-y Relationships in Sands. A Report to the American Petroleum Institute.

Oumeraci, H., 2008. Vertiefervorlesung Küsteningenieurwesen I. TU Braunschweig, Germany (in German).

Popko, W., Vorpahl, F., Zuga, A., Kohlmeier, M., Jonkman, J., Robertson, A., ... and Von Waaden, H., 2012. Offshore Code Comparison Collaboration Continuation (OC4), Phase I–Results of Coupled Simulations of an Offshore Wind Turbine with Jacket Support Structure. In 22nd International Society of Offshore and Polar Engineers Conference. Rhodes, Greece.

Peng, L., 2010. Analysis and Design of Offshore Jacket Wind Turbine (Master's thesis, Norges teknisk-naturvitenskapelige universitet, Fakultet for ingeniørvitenskap og teknologi, Institutt for marin teknikk).

Randolph, M.F., 1981. The Response of Flexible Piles to Lateral Loading, Géotechnique, Vol. 31, no. 2.

Rausa, H., 2014. Characterization of wave slamming forcers for a truss structure within in the framework of WaveSlam project. Master thesis, Norwegian University of Science and Technology (NTNU), Department of Civil and Transport Engineering.

Rausa, I. E., Muskulus, M., Arntsen, Ø. A., and Wåsjø, K., 2015. Characterization of wave slamming forces for a truss structure within the framework of the WaveSlam project. Energy Procedia, 80, 276-283.

Sadeghi, K., 2001. An overview of design, analysis, construction and installation of offshore petroleum platforms suitable for Cyprus oil/gas fields. GAU J. Soc. and Appl. Sci, 2(4), 1-16.

Sagar, H., Ley, J., and el Moctar, B., 2015. Hydroelasticity Effects of Wave Induced Loads on Offshore Monopile Structure. 7th International Conference on Hydroelasticity in Marine Technology. Split, Croatia

Sarpkaya, T. and Isaacson, M., 1981. Mechanics of Wave Forces on Offshore Structures. Number ISBN 0-442-25402-4. Van Nostrand Reinhold Company Inc., New York.

Shi, W., Park, H. C., Baek, J. H., Kim, C. W., Kim, Y. C., and Shin, H. K., 2012. Study on the marine growth effect on the dynamic response of offshore wind turbines. International Journal of Precision Engineering and Manufacturing, 13(7), 1167-1176.

Shi, W., Park, H., Han, J., Na, S., and Kim, C., 2013. A study on the effect of different modelling parameters on the dynamic response of a jacket-type offshore wind turbine in the Korean Southwest Sea. Renewable Energy, 58, 50-59.

Shi, W., Park, H. C., Chung, C. W., Shin, H. K., Kim, S. H., Lee, S. S., and Kim, C. W., 2015. Soil-structure interaction on the response of jacket-type offshore wind turbine. International Journal of Precision Engineering and Manufacturing-Green Technology, 2(2), 139-148.

Song, H., Damiani, R., Robertson, A., and Jonkman, J., 2013. A New Structural-Dynamics Module for Offshore Multimember Substructures within the Wind Turbine Computer-Aided Engineering Tool FAST. In The Twenty-third International Offshore and Polar Engineering Conference. International Society of Offshore and Polar Engineers.

Sumer B.M. and Fredsoe J., 2002. The mechanics of scour in the marine environment, World Scientific.

Tanimoto, K., Takahashi, S., Kaneco, T., Shiota, K., 1986. Impulsive breaking wave forces on an inclined pile exerted by random waves. Proceedings of the 20th International Conference on Coastal Engineering, 2288 - 2302.

Van Der Tempel, J., 2006. Design of support structures for offshore wind turbines. A thesis submitted for the degree of Doctor of Philosophy in Civil Engineering, University of technology Delft.

Verhaegh, M., 2014. Modelling the manufacturing and installation costs of offshore wind farm substructures for a micro sitting model. A thesis submitted for the degree of Master of Science in Aerospace Engineering, University of technology Delft.

Vemula, N. K., 2010. Design Solution for the UpWind Reference Offshore Support Structure-Deliverable D4.2.5 (WP4: Offshore Foundations and Support Structures). Technical report, Rambøll Wind Energy, Esbjerg.

von Karman, T., 1929. The impact on seaplane floats during landing. National Advisory Committee for Aeronautics.

Vorpahl, F., Popko, W., and Kaufer, D., 2013. Description of a basic model of the "UpWind reference jacket" for code comparison in the OC4 project under IEA Wind Annex 30, Fraunhofer Institute for Wind Energy and Energy System Technology (IWES), Germany.

Vorpahl, F., and Popko, W., 2013. Description of the Load Cases and Output Sensors to be Simulated in the OC4 Project under IEA Wind Annex 30. Fraunhofer Institute for Wind Energy and Energy System Technology IWES, Bremerhaven, Germany.

Whitehouse, R., 1998. Scour at marine structures: A manual for practical applications. Thomas Telford.

Wienke, J., 2001. Druckschlagbelastung auf schlanke zylandrische Bauwerke durch brechende Wellen, PhD thesis, Technischen Universität Carolo-Wilhelmina zu Braunschweig, Germany.

Wienke, J., Oumeraci, H., 2005. Breaking wave impact force on a vertical and inclined slender pile—theoretical and large-scale model investigations.Coastal engineering, 52(5), 435-462.

Wagner, H., 1932. Über Stoβ-und Gleitvorgänge an der Oberfläche von Flüssigkeiten. Zeitschrift für angewandte Mathematik und Mechanik 12 (4), 193–215.

Wiersma, F., Grassin, J., Crockford, A., Winkel, T., Ritzen, A., Folkerts, L., 2011. State of the Offshore Wind Industry in Northern Europe: Lessons Learnt in the First Decad, Ecofys Netherlands BV, Netherlands.

Zaaijer, M. B., 2002. Foundation models for the dynamic response of offshore wind turbines. In Proceedings of MAREC.

Zaaijer, M. B., 2006. Foundation modelling to assess dynamic behaviour of offshore wind turbines. Applied Ocean Research, 28(1), 45-57.

Zhang, Z., Matveev, A., Øvrebø, S., Nilssen, R., and Nysveen, A., 2011. State of the art in generator technology for offshore wind energy conversion systems. International Electric Machines and Drives Conference (IEMDC), Canada.

Zhou, J., 2010. Numerical investigation of breaking waves and their interactions with structures using MLPG_R method (Doctoral dissertation, City University London).